Title

Analysis and characterization of the biosynthetic pathway of Coenzyme Q in eukaryotes, and the role of ring precursors and key intermediates

Author

Nag, Anish

Publication Date

2019

Peer reviewed|Thesis/dissertation

UNIVERISTY OF CALIFORNIA

Los Angeles

Analysis and characterization of the biosynthetic pathway of Coenzyme Q in eukaryotes, and the role of ring precursors and key intermediates

A dissertation submitted in partial fulfillment for the degree of

Doctor of Philosophy in Chemistry

by

Anish Nag

2019

ABSTRACT OF THE DISSERTATION

Analysis and characterization of the biosynthetic pathway of Coenzyme Q in eukaryotes, and the role of ring precursors and key intermediates

by

Anish Nag
Doctor of Philosophy in Chemistry
University of California, Los Angeles, 2019
Professor Catherine F. Clarke, Chair

Coenzyme Q (known by various names that include ubiquinone, CoQ or simply Q) is a crucial redox-active lipid that consists of a fully substituted benzenoid head group and a polyisoprenoid tail. The benzenoid head group moiety that resembles a quinone, can undergo reversible redox reactions interconverting from the fully oxidized quinone through a radical semi-quinone intermediate to the fully reduced quinol. This structural feature aids in the essential role that Q plays in cellular respiration, wherein it transports electrons from NADH and succinate to cytochrome *c* (Respiratory complex I and II to III respectively in eukaryotes). Q also acts as a lipid soluble chain terminating anti-oxidant. Thus, complete lack of Q is embryonically fatal and sufficient de novo Q biosynthesis is crucial for proper health maintenance in humans. Q deficiency has been directly or indirectly linked to a wide spectrum of health disorders in humans, including kidney disease, neurodegenerative diseases, cerebellar ataxia, and cardiovascular complications. Additionally, decreased Q levels have been linked to aging. Current therapeutic strategies to treat Q deficiency related complications involve direct oral

supplementation of Q, which has its challenges due to the hydrophobicity and low bio-availability of Q. Therefore, our research is aimed at characterizing the biosynthesis and metabolism of Q in living cells, thereby potentially leading the way to novel therapeutic techniques.

Saccharomyces cerevisiae (yeast) serves as a highly useful model for research on Q, due to its widely studied molecular genetics and its close homology to human Q biosynthesis, metabolism and function. Q biosynthesis in *S. cerevisiae* (which makes Q_6 with six isoprene units, versus humans whose Q_{10} has ten isoprene units) takes place in the mitochondria. Chapter 1 highlights the currently known Q biosynthetic steps along with phenotypes observed from deletion and malfunction of Q biosynthesis in yeast and humans. The primary precursor molecule that is utilized by eukaryotes to biosynthesize Q is 4-hydroxybenzoic acid (4HB). The latter is in turn immediately preceded by 4-hydroxybenzaldehyde (4HBz) in the Q biosynthetic pathway. Fourteen known proteins that localize in the mitochondria are responsible for catalyzing different steps in this process—Coq1-Coq11, Yah1 (ferredoxin), Arh1 (ferredoxin reductase), and Hfd1 (aldehyde dehydrogenase). In yeast 4HBz is biosynthesized from the precursor amino acid Tyrosine (Tyr). However, this pathway lacks proper characterization and only the deaminases Aro8 and Aro9 and the aldehyde dehydrogenase Hfd1 have been identified. The human homolog of Hfd1 is *ALDH3A1* which can serve as a potential target when attempting to screen for Q deficiency in humans.

Chapter 2 investigates the role of key proteins and intermediates in the biosynthesis of Q in yeast. In addition to 4HB yeast is also capable of utilizing p-aminobenzoic acid (pABA) as a Q ring precursor. However, the exact steps by which the two pathways converge was not fully characterized. It was postulated that the deamination followed by hydroxylation of the pABA

phenyl ring occurs via Schiff base chemistry. Additionally, high performance liquid chromatography tandem mass spectrometry (HPLC-MS/MS) analysis of yeast mutants with deletions in selected Coq genes, showed accumulation of Q intermediates. These intermediates included 3-hexaprenyl-4-hydroxyphenol (4-HP), 3-hexaprenyl-4-aminophenol (4-AP), demethyl demethoxy Q_6 ($DDMQ_6$), imino demethyl demethoxy Q_6 ($IDDMQ_6$), demethoxy Q_6 (DMQ_6), and imino demethoxy Q_6 ($IDMQ_6$). In order to test the hypothesis of the Schiff base chemistry responsible for Q biosynthesis from pABA, and to investigate whether the above mentioned intermediates are actual productive Q intermediates or just dead-end intermediates, farnesylated analogs (wherein the hexaprenyl tail of Q intermediates is changed to a farnesyl tail consisting of three isoprene units) of 4-HP, $DDMQ_6$ and DMQ_6 along with the reduced intermediate $IDDMQ_6H_2$, were chemically synthesized. Thus 2-farnesyl-4-dyroxyphenol (4-HFP), demethyl demethoxy Q_3 ($DDMQ_3$), demethoxy Q_3 (DMQ_3) and reduced imino demethyl demethoxy Q_3 ($IDDMQ_3H_2$) were correspondingly obtained. These intermediates were fed to yeast in biochemical feeding assays and their corresponding potential transformation to Q_3 was analyzed via HPLC-MS/MS studies. DMQ_3 showed ready conversion to Q_3. However, $DDMQ_3$ showed very limited Q_3 generation, whereas, 4-HFP and $IDDMQ_3H_2$ failed to show detectable levels of Q_3. Thus the role of DMQ_6 as a Q biosynthetic intermediate was further elucidated.

It was demonstrated by Dr. Fabien Pierrel's research group that the Schiff base chemistry hypothesis for the convergence of the pABA and 4HB pathways leading to Q biosynthesis, was incorrect, and the deamination of the ring of pABA occurs further upstream than formerly postulated. Therefore efforts to further synthesize and investigate farnesylated analogs of Q intermediates were postponed and instead investigations were carried out to test the role of ring precursors in addition to 4HB and pABA in Q biosynthesis. Chapter 3 gives details of the studies

conducted on selected alternate Q ring precursors, and the discovery of kaempferol (a plant derived flavonol), as a novel Q ring precursor in mammalian cells. Mouse kidney proximal tubule epithelial (Tkpts) cells and human embryonic kidney cells 293 (HEK 293) were treated with several types of polyphenols, and kaempferol produced the largest increase in Q levels. Experiments with stable isotope ^{13}C-labeled kaempferol demonstrated a previously unrecognized role of kaempferol as an aromatic ring precursor in Q biosynthesis. Investigations of the structure-function relationship of related flavonols showed the importance of two hydroxyl groups, located at C3 of the C ring and C4′ of the B ring, both present in kaempferol, as important determinants of kaempferol as a Q biosynthetic precursor. Concurrently, through a mechanism not related to the enhancement of Q biosynthesis, kaempferol also augmented mitochondrial localization of Sirt3. The role of kaempferol as a precursor that increases Q levels, combined with its ability to upregulate Sirt3, identify kaempferol as a potential candidate in the design of interventions aimed on increasing endogenous Q biosynthesis, particularly in kidney.

In addition to kaempferol, other phenolic molecules were previously shown to act as Q ring precursors in yeast and mammalian cells. This included p-coumaric acid. Chapter 4 reports a detailed investigation into the role of p-coumaric acid as a Q ring precursor in yeast. Stable isotope labeled [$^{13}C_6$-ring]-p-coumaric acid was chemically synthesized. This was tested on BY4741 and W303 genetic backgrounds of wild type (WT) yeast to analyze corresponding [$^{13}C_6$-ring]-Q levels via HPLC-MS/MS. Different growth media conditions and times of incubation were utilized in order to fully assess the role of p-coumaric acid as an alternate Q ring precursor. It was discovered that the W303 genetic background of yeast has a much higher efficiency of p-coumaric acid uptake and subsequent conversion to Q. Furthmore, attempts were made to test the pathway by which p-coumaric acid is biosynthesized to Q. It was postulated that

this occurs via intermediary biosynthesis of the former to 4HB. To investigate this possibility the Hfd1 gene was knocked out in the W303 genetic background, and the corresponding *hfd1 null* strain was assayed with [$^{13}C_6$-ring]-p-coumaric acid.

Chapter 5 provides insight and perspectives into projects being currently pursued and potential experiments to be conducted in the future. In particular, we are probing further into the role of kaempferol as a Q ring precursor in mammalian cells. It was hypothesized that the B ring of kaempferol underwent cleavage from the rest of the molecule and was utilized to generate the ring of Q in mammalian cells. This explanation was further strengthened when Dr. Gilles Basset was able to confirm the utilization of the B ring of kaempferol to generate Q in *Arabidopsis thaliana*. Moreover, Dr. Bassett showed that this occurs through a peroxidative cleavage mechanism, whereby the B ring of kaempferol is converted to 4HB, which in turn is used to generate Q. Attempts are being made to probe into a similar potential peroxidative mechanism occurring in mammalian cells. An *in vitro* peroxidation assay similar to the one used by Dr. Bassett is in the process of being set up on mammalian cell extracts incubated with kaempferol. Methods have been generated to detect 4HB (synthesized by kaempferol peroxidation in the cell extracts) by HPLC-MS/MS via a derivatization strategy. In addition, mouse kidney cells grown in presence of kaempferol with the B ring selectively labeled with stable ^{13}C isotope (generated by Dr. Bassett), have shown production of ^{13}C stable isotope ring labeled Q.

Finally, the Appendix contains two additional publications. The first explores alternative splicing in yeast and the role it plays in Q biosynthesis. *PTC7* encodes the phosphatase responsible for the dephosphorylation of Coq7 undergoes alternative splicing, which is rare in yeast. The study also implicated *SNF2* as the gene that is responsible for this alternative splicing event and showed that deletion of *SNF2* leads to increased Q levels in yeast. The second

publication explores the rescue of the clinical phenotypes associated with Coq6 deletion in mice by supplementation with 2,4-dihydroxybenzoic acid. In particular it was shown that steroid resistance nephrotic syndrome which develops in mice with Coq6 deletion, can be ameliorated by treatment with 2,4-dihydroxybenzoic acid.

The dissertation of Anish Nag is approved.

Ohyun Kwon

Jing Huang

Catherine F. Clarke, Chair

University of California, Los Angeles

2019

Table of Contents

List of Tables and Figures		xi
Acknowledgements		xvi
Vita		xxii
Chapter 1	Coenzyme Q_{10} deficiencies: pathways in yeast and humans	1
	References	13
Chapter 2	Chemical synthesis and biochemical assays of farnesylated analogs of selected intermediates postulated to play a role in Coenzyme Q biosynthesis in *Saccharomyces cerevisiae*	18
	References	53
Chapter 3	Kaempferol increases levels of coenzyme Q in kidney cells and serves as a biosynthetic ring precursor	55
	References	66
Chapter 4	Investigation and characterization of the role of *p*-coumaric acid as a ring precursor in coenzyme Q biosynthesis in yeast	68
	References	95
Chapter 5	Discussion of ongoing project and future directions	97

References 115

Appendix I Chromatin-remodeling SWI/SNF complex regulates Coenzyme Q_6 synthesis and a metabolic shift to respiration in yeast 116

References 131

Appendix II Treatment with 2,4-dihydroxybenzoic acid prevents progression of FSGS and renal fibrosis in podocyte-specific Coq6 knockout mice 133

References 144

List of Tables and Figures

Chapter 1	Figure 1	CoQ biosynthetic pathways in the yeast *S. cerevisiae* and in humans	4
	Figure 2	A model of the CoQ Synthome in the yeast *S. cerevisiae*	5
Chapter 2	Figure 1	Reversible oxidation of Q	34
	Figure 2	Previously postulated Q_6 biosynthetic pathway in *S. cerevisiae*	35
	Figure 3	Chromatogram obtained from the HPLC-MS/MS analysis of $DDMQ_3$ standard	36
	Figure 4	Chromatogram obtained from the HPLC-MS/MS analysis of DMQ_3 standard	37
	Figure 5	Chromatogram obtained from the HPLC-MS/MS analysis of Q_3 standard	38
	Figure 6	Chromatogram obtained from the HPLC-MS/MS analysis of Q_6 standard	39
	Figure 7	Q_3 content measured in yeast treated with $DDMQ_3$ and DMQ_3	40
	Figure 8	$DDMQ_3$ and DMQ_3 content measured in yeast treated with $DDMQ_3$ and DMQ_3	41
	Figure 9	Q_6 content measured in yeast treated $DDMQ_3$ and DMQ_3	42
	Figure 10	$DDMQ_6$ and DMQ_6 content in yeast treated with EtOH	43
	Scheme 1	Attempted synthesis of 2-bromo-1,4-dihydroxyphenol **1**	44
	Scheme 2	Synthesis of 2-bromo-1,4-diacetoxybenzene **3**	45

	Scheme 3	Synthesis of tributyl farnesyl stannane **4**	46
	Scheme 4	Synthesis of 1,4-diacetoxy-2-farnesylbenzene **6**	47
	Scheme 5	Synthesis of 2-farnesyl-1,4-dihydroxyphenol **4-HFP**	48
	Scheme 6	Synthesis of 4-amino-3-bromo-5-methoxyphenol **7**	49
	Scheme 7	Synthesis of 4-amino-5-farnesyl-3-methoxyphenol **IDDMQ$_3$H$_2$**	50
	Scheme 8	Synthesis of 5-farnesyl-3-methoxybenzoquinone **DDMQ$_3$**	51
	Scheme 9	Synthesis of 5-farnesyl-3-methoxy-6-methylbenzoquinone **DMQ$_3$**	52
Chapter 3	Table 1	HPLC-MS-MS transitions for each analyte	58
	Figure 1	Kaempferol strongly increases Q levels in Tkpts cells	59
	Figure 2	The mitochondrial sirtuin Sirt3 does not participate in the regulation of Q levels	60
	Figure 3	Kaempferol augmentation of Q levels is related to the enhancement of Q biosynthesis	61
	Figure 4	Effect of curcumin, ferulic acid and vanillin on Q biosynthesis in Tkpts cells	62
	Figure 5	4HB is a limiting step in the biosynthesis of Q in kidney cells	63
	Figure 6	Kidney-derived Tkpts cells display increased levels of Q and Coq2 in comparison with hepatic Hepa1.6 cells	64
	Figure 7	Kaempferol, ferulic acid, vanillin and curcumin are not utilized as Q ring precursors as efficiently as 4HB in yeast	64
Chapter 4	Table 1	Genotypes and sources of yeast strains	82
	Figure 1	Yeast growth curves in YPD and YPG	83
	Figure 2	Yeast growth curves in SD-complete and DOD	84

	Figure 3	Endogenous unlabeled and *de novo* ^{13}C-labeled Q content in YPD	85
	Figure 4	Endogenous unlabeled and *de novo* ^{13}C-labeled Q content in YPG	86
	Figure 5	Endogenous unlabeled and *de novo* ^{13}C-labeled Q content in SD-complete	87
	Figure 6	Endogenous unlabeled and *de novo* ^{13}C-labeled Q content in DOD	88
	Figure 7	Q content comparison in WT and *Coq nulls* grown in DOD	89
	Figure 8	DMQ_6 content comparison in WT and *Coq nulls* grown in DOD	90
	Figure 9	HHB content comparison in WT and *Coq nulls* grown in DOD	91
	Figure 10	Q content comparison in W303 WT yeast grown in DOD	92
	Figure 11	*De novo* stable isotope labeled Q content comparison in WT and *hfd1 null* yeast labeled with different Q precursors	93
	Scheme 1	Synthesis of [$^{13}C_6$-ring]-p-coumaric acid **^{13}C-P**	94
Chapter 5	Table 1	Summary of all the Q analytes and the precursor-product ion masses detected during the HPLC-MS/MS analysis of cellular lipid extracts	106
	Figure 1	Possible routes for conversion of kaempferol to Q	107
	Figure 2	Effect of [$^{13}C_6$-B-ring]-kaempferol treatment on mouse Tkpts cells	108
	Figure 3	Precursor ion chromatogram of dansyl-4HB	109
	Figure 4	Product ion chromatogram of dansyl-4HB	110
	Figure 5	Representative chromatogram of dansyl-Cl standard sample with concentration 1 ng/mL	111

	Figure 6	Dansyl-Cl standard calibration curve 1	112
	Figure 7	Dansyl-Cl standard calibration curve 2	113
	Scheme 1	Synthesis of dansyl-4-hydroxybenzoic acid **dansyl-4HB**	114
Appendix I	Figure 1	Deletion of *SNF2* enhances splicing of *PTC7* and the steady-state levels of the short Ptc7 protein isoform	119
	Figure 2	CoQ_6 biosynthetic pathway in *S. cerevisiae* and role of $Ptc7_s$ isoform on Coq7 phosphorylation and function	120
	Figure 3	Deletion of *SNF2* leads to increased steady state levels and *de novo* CoQ_6 biosynthesis in yeast and improves the flux from DMQ_6 to CoQ	121
	Figure 4	Snf2 levels decrease during batch growth, coinciding with increased *PTC7* splicing and increased CoQ_6 synthesis	122
	Figure 5	The decrease in Snf2 levels over time in batch cultures of WT yeast correlates with enhanced splicing of *PTC7* RNA	123
	Figure 6	Overall conversion efficiency of the CoQ_6 biosynthetic pathway increases upon depletion of Snf2, with increased conversions of both DMQ_6 to Q_6 and HHB to Q_6	124
	Figure 7	RPG down-regulation and redistribution of spliceosomes result in increased *PTC7* splicing	125
	Figure 8	Structural predictions of mitochondrial $Ptc7_s$ and nuclear membrane traversing $Ptc7_{ns}$	126
	Figure 9	Ptc7 isoforms have differing and opposing effects on CoQ_6 synthesis	127
	Figure 10	Exclusive expression of Ptc7 isoforms dramatically alters levels of CoQ_6 biosynthetic pathway intermediates DMQ_6 and HHB, yet overall conversion efficiency between both isoforms is comparable	128
	Figure 11	Model for a novel role for Snf2 in respiration, and in the transition from a primarily fermentative mode of metabolism	

		to a primarily respiratory mode of metabolism	129
	Table 1	Genotype and sources of yeast strains	130
Appendix II	Figure 1	Nphs2.Cre^{+};Coq6$^{flox/flox}$ mice develop severe progressive proteinuria and consecutive death in adulthood. Treatment with 2,4-diHB prevents disease progression, resulting in normal survival range	137
	Figure 2	Development of FSGS is abrogated by treatment with 2,4-diHB in Nphs2.Cre^{+};Coq6$^{flox/flox}$ mutant mice	139
	Figure 3	Glomerular structure is disrupted in Nphs2.Cre^{+};Coq6$^{flox/flox}$ mutant mice and is preserved by 2,4-diHB treatment	140
	Figure 4	Severely impaired podocyte foot process (FP) structure of Nphs2.Cre^{+};Coq6$^{flox/flox}$ mutant mice can be preserved by 2,4-diHB administration	141
	Figure 5	Nphs2.Cre^{+};Coq6$^{flox/flox}$ mutant mice show reduced expression of podocyte-specific proteins	143
	Figure 6	COQ6 localizes to mitochondria and its loss from glomerular podocytes causes mitochondrial intumescence	144

Acknowledgments

As I reach the threshold of completing my PhD in Chemistry, I can't help but feel a sense of accomplishment on successfully finishing such a time and labor intensive feat. However, at the same time I am overwhelmed by a sense of humility and gratitude for all the scores of institutions, places and people that have made a crucial and invaluable contribution towards my personal and professional success. So many individuals have played so many different roles, no matter how small, in my overall development, all of which has culminated today in me fortuitously completing my PhD. I will try my utmost best to acknowledge every single person and institution that have helped and enriched me along my path. However, I am also aware that it would be impossible to list all of the several names that have guided me on my journey, and I sincerely apologize for any omissions. I am truly forever grateful and indebted to anybody and everybody who have made a positive impact in my life over the years.

First and foremost, I wish to express my deepest and wholehearted gratitude for my thesis committee chair and advisor Dr. Catherine F. Clarke (Cathy). I simply cannot thank her enough for all the indispensable help, guidance, and counsel that she has extended towards me over the last six years. I can assert without a shadow of a doubt in my mind that Cathy is the greatest mentor I could have had as a graduate student. Her intelligence, her passion for chemistry and biochemistry, her kind nature and her forever cheerful demeanor, are just few of the countless qualities that make Cathy such an incredible researcher, teacher, mentor, and above all a truly wonderful human being. It was a pleasure and honor to have been able to work with her and grow and flourish academically under her tutelage. She never ceases to amaze me with the

amount of care and nurture she provides towards every single person that works for her and has always gone beyond and out of her way to offer help to me whenever I needed it. I consider myself absolutely privileged to have been able to enjoy her irreplaceable supervision over the last few years, all of which has been critical for my success here at UCLA.

In addition to Cathy, I also wish to express my deepest and most sincere gratitude for my thesis committee members at UCLA namely Dr. William M. Gelbart (Bill), Dr. Ohyun Kwon (Ohyun) and Dr. Jing Huang. Bill has always been a constant and an invaluable source of guidance and inspiration to me during my tenure as a graduate student at UCLA. I have always been awe-inspired by his innovative research into viruses, intertwining the multidisciplinary realms of physical, organic, biophysical and biological chemistry. My fascination for his exemplary research into unlocking the role of viruses and virus like particles in novel therapeutics, led me to choose him as my future research mentor as I transition into my future position of Assistant Adjunct Professor at the Department of Chemistry and Biochemistry in UCLA. I am also deeply thankful to Bill for willing to serve as my mentor as I further continue to fulfil my ultimate career goals and aspirations as a scientist. Ohyun has also been exceptional as a source of advice and guidance in my research, academic and other non-academic activities as a graduate student. I am especially thankful to her for letting me utilize her lab space to conduct all of the experiments that required resources that were beyond the scope of Cathy's lab. Such experiments included all of the work pertaining to synthetic organic chemistry, which have been absolutely critical to my development as a graduate student and for the completion of this thesis. I am also wholeheartedly grateful for the pertinent counsel that Dr. Jing Huang provided to me that contributed directly to success in my research and career choice after the completion of my PhD.

Several other faculty members at UCLA and beyond have also been instrumental in scripting the path I followed over the last six years to reach the pinnacle where I am at right now, and I will forever be grateful to them. Foremost amongst them, is Dr. Neil K. Garg (Neil), without whom I would probably not even be pursuing a PhD in Chemistry at UCLA. He was kind and generous enough to accept me into his research group during my first summer at UCLA, and I will always cherish my experience in his lab. Working with him was one of the most enriching and endearing professional experiences I have ever had, and I am ever thankful for all the crucial advice and mentorship that Neil provided to me both during and after my time working in his lab. Dr. Tracy L. Johnson (Tracy) is another faculty member at UCLA whose guidance has proven to be of great positive influence and benefit for my career. It has been an utmost pleasure and honor to have worked together with Tracy on the HHMI-CURL workshops for meritorious undergraduate students from underrepresented backgrounds. I wish to thank Tracy with all my heart for selecting me as one of her first workshop leaders, an experience that helped me immensely in developing and enhancing my skills at teaching college chemistry. I am also immeasurably grateful for all the help, guidance, and counsel I received from Dr. Steven G. Clarke and Dr. Maher M. Henary. I had the absolute privilege of serving as a Teaching Assistant for their respective classes, which has been essential for helping me further improve my teaching skills. I have also had the pleasure of working with several collaborators during the course of my PhD career that include Dr. Cuiwen He, Dr. Michael Corsello and Dr. Jesus Moreno, and Dr. Yu Chen at UCLA, Dr. Jennifer N. Shepherd at Gonzaga University, Dr. Jose M. Villalba at University of Cordoba, and Dr. Gilles J. Basset at University of Florida. I am deeply thankful to all of them for the exceptional collaborations that we were able to achieve, all of which led

directly or indirectly to the positive progress and success of my work at UCLA as a graduate student.

I would also like to take this opportunity to thank all of the faculty members and teachers who played a vital and precipitous role in nurturing my instincts as a scientist during my days in high school and college. I wish to express my earnest and most sincere gratitude to Dr. Dipakranjan Mal, who served as my undergraduate research advisor at the Indian Institute of Technology, Kharagpur (IITKGP). Dr. Mal is perhaps one of the most incredibly talented exceptionally kind person that I have ever come across, and his help and contribution towards my academic success are invaluable and irreplaceable. I am equally indebted to several other faculty members at IITKGP that include Dr. Narayn D. P. Singh, Dr. Anoop Ayappan, and Dr. Amita Mahanty. I would also like to thank Dr. Michael Hall (Newcastle University), Dr. David Churchill (Korea Advanced Institute of Science and Technology), and Dr. Dennis Gillingham, all three of whom generously hosted me as an undergraduate researcher in their respective research groups. I cannot stress enough on how incredibly important and effective these experiences had been in shaping, molding and motivating my future aspirations to pursue chemistry as a scientific career. I am also wholeheartedly grateful for the exceptional teachers who provided me their tutelage and guidance at my alma-mater South Point High School. Teachers that include Sharmila Datta Bose, Amartya Mukherjee, and Dr. Narayan Chakrabarti, whose pedagogical efforts created a positive and essential impact in my path to success as a scientist.

I have been extremely fortunate to have been able to enjoy the company of a group of exemplarily smart, talented, diligent and benevolent colleagues in Cathy's research group. I will be forever thankful to Dr. Chris Allan, Dr. Theresa Nguyen, Dr. Hui (Su) Tsui, Dr. Lucia

Fernandez-del-rio, Michelle Bradley, and Nguyen Pham for providing me the pleasure of working with them and learning from them over the last six years. However, I will always be indebted to the most wonderful colleague and human being that I have ever had the fortune of being acquainted with, Dr. Agape Awad (Agape). She has always been a constant and everlasting source of inspiration and support to me both professionally and personally over the last few years. I truly cannot conceive of the notion of being where I am at right now, without her invaluable and irreplaceable contribution. I came over to the great city of Los Angeles six years ago to pursue my PhD. I arrived on these shores as a foreigner, with no friends or family whom I could turn to for help and support. However, I managed to find more than that in my truest and dearest friend Agape, and along with her family, she has been there to support me through all the thick and thin of my struggles as a PhD student at UCLA. Therefore, I wish to endlessly thank Agape, her husband Beshoy, her parents Mr. and Mrs. Awad and her godmother Ms. Eddy, who gave me a family half a world away from my own. I pray that I will always be able to have her support and for her and her family's health, happiness, success, and well-being. In addition to Agape and her family, I was successful in forging several other friendships that proved to be extremely meaningful and endearing to me. I would like to express my thanks for several people people whose friendships have shaped my life for the better of the last few years, and they include Nicole Lima, Ashley Hong, Gabbi Navarro, Gregory Tsafos, among several others.

Last and by far not the least, I wish to put forth my most heartfelt gratitude towards my family which includes my parents, my aunts and cousins, and our family help. I cannot possibly even begin to express in words, the contribution that my parents made in my life and my career. My mother Mrs. Pushpita Nag and my father Mr. Dilip Nag, are the two greatest human beings

that I know of, and I truly consider myself to be blessed to have been born as their son in their household. I owe them a debt that can never be repaid, and the best I can do is what they have always expected from me, which is to strive to be a better human being and a better version of myself every single day. I can go on and on about all the tiny yet poignant ways by which my parents always supported me and stood up for me, all the incredible efforts that they devoted towards me that were critical in my success, but that would require entire novels to be written. I can only attempt to encapsulate a fraction of the sacrifices and struggles that my parents undertook with a smile on their faces just to ensure my happiness and prosperity, by dedicating this thesis to them. I pray that I will continue to enjoy their company, their good health, their happiness and fortitude, and their blessings for as long as I can. I also wish to thank wholeheartedly our family help Sumitra didi, who has remained the cornerstone of our family ever since I was 3 years old. Her contributions and hard work in ensuring the happiness and prosperity of our family, is truly immeasurable. She truly helped me thrive throughout my childhood and adolescence, and I pray for her health and happiness as well.

Finally, I would like to end this acknowledgement by expressing my gratitude towards the University of California, Los Angeles, the city of Los Angeles, the state of California and the great county of the United States of America. There are a myriad opportunities available here for everybody who has a dream and a passion to seek success in life. Opportunities that I might not have had access to anywhere else in the world, and I am truly thankful for that. I would continue to seek excellence in my personal and professional life here, and undertake the betterment of human society through my work to the very best of my abilities.

VITA

2013	B.S. and M.S. (hons.) in Industrial Chemistry Indian Institute of Technology, Kharagpur Kharagpur, West Bengal, India
2013-2019	Graduate Student Researcher Department of Chemistry and Biochemistry University of California, Los Angeles Los Angeles, CA
2013-2019	Teaching Assistant, Teaching Associate, Teaching Fellow Department of Chemistry and Biochemistry University of California, Los Angeles Los Angeles, CA
2016	Hanson-Dow Teaching Assistant Award University of California, Los Angeles Los Angeles, CA
2018	John Stauffer Fellowship Research Award University of California, Los Angeles Los Angeles, CA
2018	Graduate Student Poster Award, Seaborg Symposium, UCLA University of California, Los Angeles Los Angeles, CA

PUBLICATIONS

"**Treatment with 2,4-Dihydroxybenzoic Acid Prevents FSGS Progression and Renal Fibrosis in PodocyteSpecific Coq6 Knockout Mice".** Eugen Widmeier, Merlin Airik, Hannah Hugo, David Schapiro, Johannes Wedel, Chandra C. Ghosh, Makiko Nakayama, Ronen Schneider, Agape M. Awad, **Anish Nag**, Jang Cho, Markus Schueler, Catherine F. Clarke, Rannar Airik, and Friedhelm Hildebrandt. *J. Am. Soc. Nephrol.*, **2019**, *30*, 393-405.

"Coenzyme Q_{10} deficiencies: pathways in yeast and humans". *Agape M. Awad, *Michelle C. Bradley, *Lucía Fernández-del-Rio, ***Anish Nag**, *Hui Tsui, and Catherine F. Clarke. *Essays in Biochemistry*, **2018**, July.

"Chromatin-remodeling SWI/SNF complex regulates coenzyme Q6 synthesis and a metabolic shift to respiration in yeast". ***Agape M. Awad, *Srivats Venkataramanan, **Anish Nag, Anoop Raj Galivanche, Michelle C. Bradley, Lauren Neves, Stephen Douglass, Catherine F. Clarke, and Tracy L. Johnson. *J. Biol. Chem*., **2017**, *292*, 14851.

"Kaempferol increases levels of coenzyme Q in kidney cells and serves as a biosynthetic ring precursor". ***Lucía Fernández-del-Río, **Anish Nag, Elena Gutiérrez Casado, Julia Ariza, Agape M. Awad, Akil I. Joseph, Ohyun Kwon, Eric Verdin, Rafael de Cabo, Claus Schneider, Jorge Z. Torres, María I. Burón, Catherine F. Clarke, and José M. Villalba. *Free Radical Biology and Medicine,* **2017**, *110*, 176.

PRESENTATIONS

Nag, A., Basset, G. J., Kwon, O., and Clarke, C. F. **Seaborg Medal Symposium 2018.**

Nag, A., Basset, G. J., Kwon, O., and Clarke, C. F. **The 9th conference of the International Coenzyme $Q1_0$ Association, 2018.**

Nag, A., Basset. G. J., and Clarke, C. F. *FASEB J*, **2018** 32:*1*. **Experimental Biology 2018.**

Nag, A., Li, Y., Kwon, O., Basset, G. J., and Clarke, C. F. **UCLA Mitochondria Symposium 2017. Seaborg Medal Symosium 2017.**

Nag, A., Fernandez, L., Villalba, J. M., Shepherd, J. N., Kwon, O., and Clarke, C. F. *FASEB J*, **2017** 31:*766*.17. **Experimental Biology 2017.**

Nag, A., He, C., Shepherd, J. N., Fernandez, L., Clarke, C. F., and Villalba, J. M.

FASEB J, **2016** 30:*661*.7. **Experimental Biology 2016. Seaborg Medal Symposium 2016.**

Nag, A., He, C., Shepherd, J., Clarke, C. *FASEB J*, **2015**: *568*.30. **Experimental Biology 2015**.

CHAPTER 1

Coenzyme Q_{10} deficiencies: pathways in yeast and humans

Author contributions: The author contributions are listed on page 13.

Essays in Biochemistry (2018) **62** 361–376
https://doi.org/10.1042/EBC20170106

PORTLAND PRESS

Review Article

Coenzyme Q_{10} deficiencies: pathways in yeast and humans

Agape M. Awad, Michelle C. Bradley, Lucía Fernández-del-Río, Anish Nag, Hui S. Tsui and Catherine F. Clarke

Department of Chemistry and Biochemistry, Molecular Biology Institute, UCLA, Los Angeles, CA 90095, U.S.A.

Correspondence: Catherine F. Clarke (cathy@chem.ucla.edu)

Coenzyme Q (ubiquinone or CoQ) is an essential lipid that plays a role in mitochondrial respiratory electron transport and serves as an important antioxidant. In human and yeast cells, CoQ synthesis derives from aromatic ring precursors and the isoprene biosynthetic pathway. *Saccharomyces cerevisiae coq* mutants provide a powerful model for our understanding of CoQ biosynthesis. This review focusses on the biosynthesis of CoQ in yeast and the relevance of this model to CoQ biosynthesis in human cells. The *COQ1–COQ11* yeast genes are required for efficient biosynthesis of yeast CoQ. Expression of human homologs of yeast *COQ1–COQ10* genes restore CoQ biosynthesis in the corresponding yeast *coq* mutants, indicating profound functional conservation. Thus, yeast provides a simple yet effective model to investigate and define the function and possible pathology of human *COQ* (yeast or human gene involved in CoQ biosynthesis) gene polymorphisms and mutations. Biosynthesis of CoQ in yeast and human cells depends on high molecular mass multisubunit complexes consisting of several of the *COQ* gene products, as well as CoQ itself and CoQ intermediates. The CoQ synthome in yeast or Complex Q in human cells, is essential for *de novo* biosynthesis of CoQ. Although some human CoQ deficiencies respond to dietary supplementation with CoQ, in general the uptake and assimilation of this very hydrophobic lipid is inefficient. Simple natural products may serve as alternate ring precursors in CoQ biosynthesis in both yeast and human cells, and these compounds may act to enhance biosynthesis of CoQ or may bypass certain deficient steps in the CoQ biosynthetic pathway.

Introduction

Coenzyme Q (ubiquinone or CoQ) is a vital lipid component in mitochondrial energy metabolism. It is a two-part molecule containing a long polyisoprenyl tail of *n* isoprene units positioning the molecule in the mid-plane of membrane bilayer, and a fully substituted benzoquinone ring that undergoes reversible reduction and oxidation. The redox chemistry of CoQ and $CoQH_2$ (ubiquinol, a hydroquinone) allows it to play its best-known role in mitochondrial respiration, accepting electrons and protons from Complex I or Complex II and donating them to Complex III, thereby establishing a proton gradient across the mitochondrial inner membrane. CoQ also serves as an essential electron and proton acceptor in other aspects of metabolism including fatty acid β-oxidation, uridine biosynthesis, and oxidation of sulphide, proline, glycerol-3-phosphate, choline, dimethylglycine, and sarcosine [1,2]. $CoQH_2$ also serves a crucial antioxidant function, protecting membranes as a chain terminator of lipid peroxidation reactions, and in the maintenance of reduced forms of vitamin E [1,3]. $CoQ/CoQH_2$ is a component of lipoproteins and is present in all cellular membranes including the plasma membrane where it functions in cellular redox regulation as part of the plasma membrane oxidoreductase system [1].

The focus of this review is on the biosynthesis of CoQ_6 in the yeast *Saccharomyces cerevisiae* and the relevance of this model to the biosynthesis of CoQ_{10} in human cells. Readers are directed to other

Received: 26 February 2018
Revised: 08 April 2018
Accepted: 14 May 2018

Version of Record published: 06 July 2018

Essays in Biochemistry (2018) **62** 361–376
https://doi.org/10.1042/EBC20170106

recent reviews that discuss the biosynthesis of CoQ in prokaryotes such as *Escherichia coli* [4], and in eukaryotes including *Schizosaccharomyces pombe*, plants, *Caenorhabditis elegans*, *Mus musculus*, and humans [5-7]. For an in-depth discussion of the effects of CoQ_{10} deficiencies and the clinical syndromes associated with these deficiencies, readers are directed to the article by Brea-Calvo and colleagues [8] in this issue of *Essays in Biochemistry*.

Overview of CoQ biosynthesis

S. cerevisiae is an extraordinarily useful model for understanding the biosynthesis of CoQ. Early yeast classic and molecular genetics combined with subcellular fractionation, biochemical assays, and lipid chemistry have helped to identify many of the steps required for CoQ biosynthesis. In particular, the collection of respiratory deficient *coq* mutants identified by Tzagoloff [9,10] set the stage for isolation and characterization of the yeast *COQ* genes. A particular advantage is that the CoQ-less *coq* mutants are viable when cultured on growth medium containing a fermentable carbon source, but are incapable of growth on medium containing a non-fermentable carbon source. In most cases, expression of the human COQ (human polypeptide involved in CoQ_{10} biosynthesis) homolog restores function in the corresponding yeast *coq* mutant. This rescue of yeast *coq* mutants by human *COQ* genes is a powerful and simple functional assay still being used to ascertain the effects of human mutations or polymorphisms on human *COQ* gene function. Thus, what we have learned about the biosynthesis of CoQ_6 in the yeast model is highly relevant to the biosynthesis of CoQ_{10} in humans (Figure 1).

The yeast model also provided early evidence that the eukaryotic CoQ biosynthetic pathway was localized to mitochondria. The Coq (denotes *S. cerevisiae* polypeptide involved in CoQ_6 biosynthesis) polypeptides are nuclear encoded, and amino-terminal mitochondrial targetting sequences are needed to direct their transport to the mitochondrial matrix (Coq1, Coq3–Coq11) or to the inner mitochondrial membrane (Coq2). Assembly of Coq3–Coq9 plus Coq11 polypeptides into a high molecular mass complex termed the CoQ synthome in yeast (Figure 2) and Complex Q in human cells is another conserved feature of CoQ biosynthesis [7,11]. These complexes are essential for the biosynthesis of CoQ in yeast and human cells, and may serve to enhance catalytic efficiency and to minimize the escape of intermediates that may be toxic due to their redox or electrophilic properties. The CoQ-intermediates are quite hydrophobic and at least some of them appear to be essential partners in the assembly of the membrane-bound CoQ synthome [12] and Complex Q [7,13].

Ring precursors utilized in biosynthesis of CoQ

Origin of 4-hydroxybenzoic acid

In yeast and human cells, the primary precursor molecule that leads to the biosynthesis of CoQ is 4-hydroxybenzoic acid (4HB). Yeast cells generate 4HB via the shikimate pathway, but also utilize tyrosine as a ring precursor [14]. Unlike yeast, human cells contain phenylalanine hydroxylase, and so either phenylalanine or tyrosine may be utilized as precursors for the biosynthesis of 4HB. Many steps involved in the generation of 4HB from tyrosine are yet to be characterized [15,16]. However, two recent studies have shed light on the first and the last steps involved in yeast 4HB biosynthesis [17,18]. The first step involves the deamination of tyrosine to 4-hydroxyphenylpyruvate (4-HPP), catalyzed by either of the aminotransferases Aro8 or Aro9 [17]. Payet et al. [17] also identified 4-hydroxybenzaldehyde (4HBz) as the final intermediate leading to the biosynthesis of 4HB. The oxidation of 4HBz to 4HB is catalyzed by the aldehyde dehydrogenase Hfd1. Hfd1 is a mitochondrial outer membrane protein [19] indicating that 4HB is synthesized in the cytosol, and must be imported into the mitochondrial matrix, where it is incorporated into CoQ. Hence, there should be a mitochondrial transporter for 4HB that remains to be identified [7], and is responsible for use of exogenously added 4HB. Inactivation of *HFD1* results in CoQ_6 deficiency that may be complemented by the addition of exogenous 4HB. Expression of the human homolog ALDH3A1 restored CoQ_6 biosynthesis in the *hfd1* yeast mutant, and was shown to oxidize 4HBz to 4HB [17]. In an independent study Stefely et al. [18] confirmed these findings; MS was used to characterize the proteomes, lipidomes, and metabolomes of a large selection of yeast strains, each lacking a distinct gene related to mitochondrial biology. This multi-omic approach revealed that yeast Hfd1 and human ALDH3A1 serve as the aldehyde dehydrogenases responsible for the oxidation of 4HBz to 4HB. It will be important to determine whether human *ALDH3A1* is required for CoQ_{10} biosynthesis in human cells; if so, it may be a potential target gene that should be considered when screening for CoQ_{10} deficiencies in patients.

Other aromatic ring precursors of CoQ

In addition to 4HB, yeast utilize *para*-aminobenzoic acid (pABA) as a ring precursor of CoQ_6 [20,21]. Yeast Coq6 and Coq9 polypeptides are required for this metabolism. Yeast Coq6 is required for the oxidative deamination of

Essays in Biochemistry (2018) **62** 361–376
https://doi.org/10.1042/EBC20170106

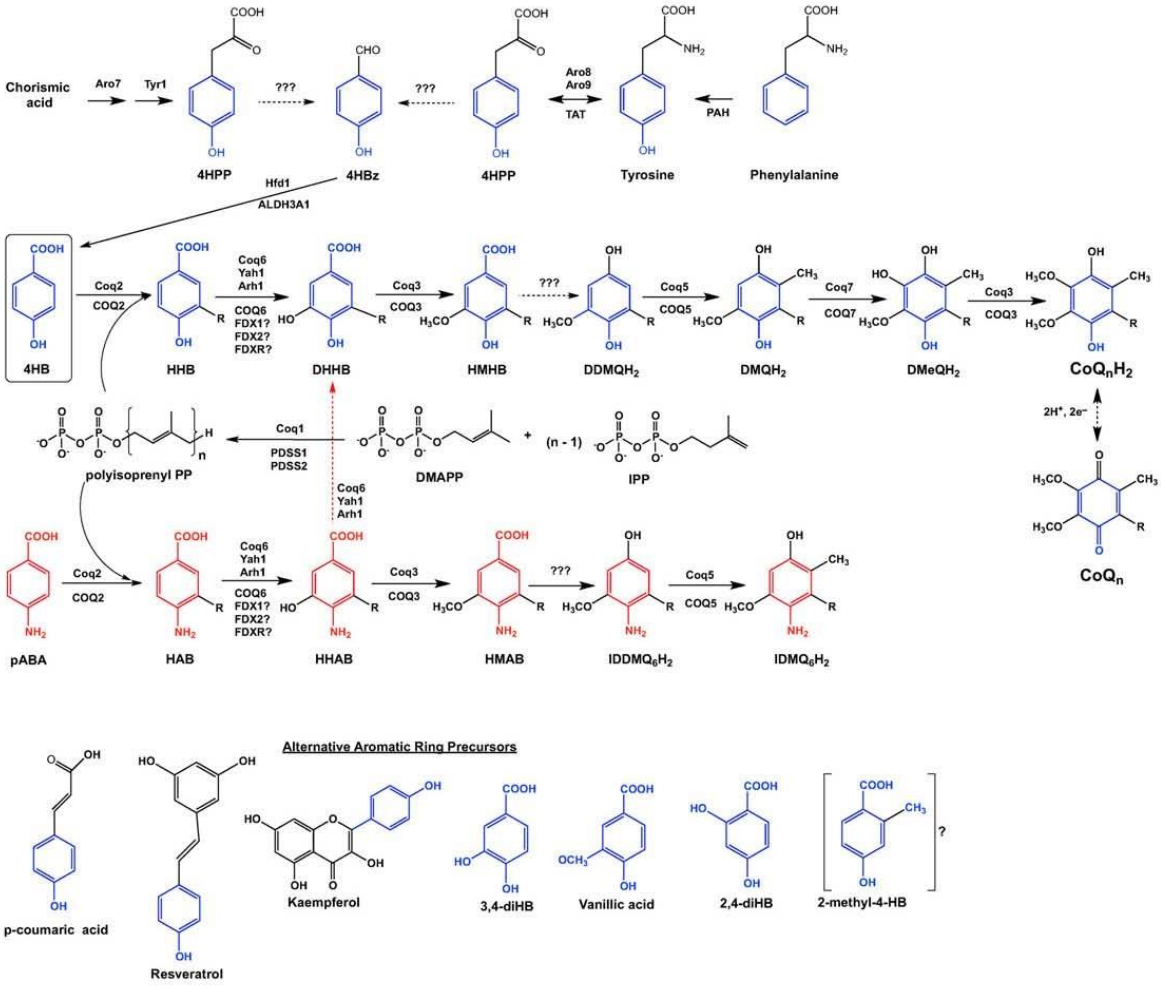

Figure 1. CoQ biosynthetic pathways in the yeast *S. cerevisiae* and in humans

The CoQ biosynthetic pathway has been shown to involve at least 14 nuclear-encoded proteins that are necessary for mitochondrial CoQ biosynthesis in *S. cerevisiae*. Black dotted arrows denote more than one step. Solid arrows denote a single step attributed to the corresponding yeast polypeptide named above each arrow. The corresponding human homologs are named below each arrow. The main ring precursor used by both yeast and humans is 4-hydroxybenzoic acid (4HB). Yeasts synthesize 4HB *de novo* from chorismate or may obtain it from the metabolism of tyrosine. Humans rely on tyrosine to produce 4HB (or on phenylalanine and phenylalanine hydroxylase to produce tyrosine). Yeast and human cells produce isopentenyl pyrophosphate (IPP) and dimethylally pyrophosphate (DMAPP) as precursors to form hexaprenyl diphosphate (n=6) via Coq1 in yeast or decaprenyl diphosphate (n=10) via PDSS1/PDSS2 in humans. Yeast Coq2 and human COQ2 attach the polyisoprenyl tail to 4HB. Subsequent to this step, the next three intermediates are identified as yeast hexaprenyl-intermediates: HHB, 3-hexaprenyl-4HB; DHHB, 3-hexaprenyl-4,5-dihydroxybenzoic acid; HMHB, 3-hexaprenyl-4-hydroxy-5-methoxybenzoic acid. The next three intermediates are hydroquinones: $DDMQH_2$, 2-hexaprenyl-6-methoxy-1,4-benzenediol; $DMQH_2$, 2-hexaprenyl-3-methyl-6-methoxy-1,4-benzenediol; $DMeQH_2$, 2-hexaprenyl- 3-methyl-6-methoxy-1,4,5-benzenetriol; to ultimately produce the final reduced product (CoQ_nH_2). Red text identifies *para*-aminobenzoic acid (pABA) as an alternate ring precursor utilized by yeast (but not by humans). The next three intermediates are identified as yeast hexaprenyl-intermediates: HAB, 4-amino-3-hexaprenylbenzoic acid; HHAB, 4-amino-3-hexaprenyl-5-hydroxybenzoic acid; HMAB, 4-amino-3-hexaprenyl-5-methoxybenzoic acid. The next two intermediates are: $IDDMQH_2$, 4-amino-3-hexaprenyl-5-methoxyphenol; $IDMQH_2$, 4-amino-3-hexaprenyl-2-methyl-5-methoxyphenol. The step denoted by the red dotted arrow depends on yeast Coq6 and converts HHAB into DHHB. Interconversion of (CoQ_nH_2) and (CoQ_n) is shown via a reversible two-electron reduction and oxidation. Steps indicated by '???' are catalyzed by as yet unknown enzymes. Alternative compounds that may serve as ring precursors in CoQ biosynthesis are shown at the bottom of the

Essays in Biochemistry (2018) **62** 361–376
https://doi.org/10.1042/EBC20170106

panel: *p*-coumaric acid, resveratrol, and kaempferol. Analogs of 4HB that can function to bypass certain deficiencies in the CoQ biosynthetic pathway include: 3,4-dihydroxybenzoic acid (3,4-diHB), vanillic acid and 2,4-dihydroxybenzoic acid (2,4-diHB). It is not yet known whether 2-methyl-4HB (2-methyl-4HB) may also serve a bypass function.

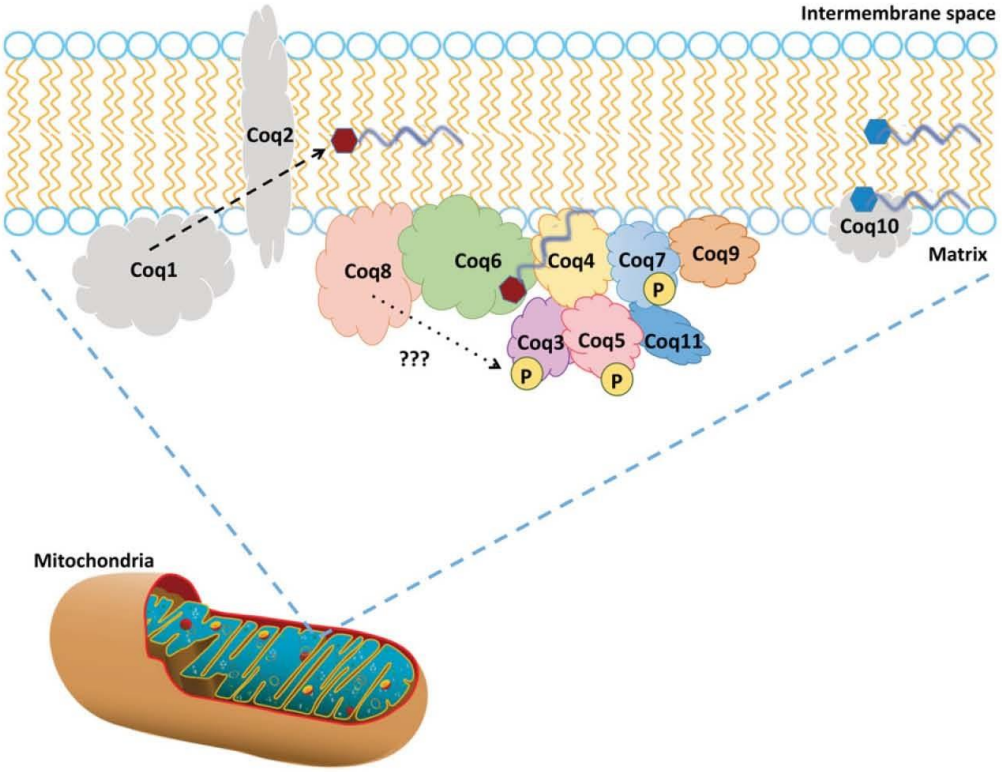

Figure 2. A model of the CoQ Synthome in the yeast *S. cerevisiae*

Studies in *S. cerevisiae* have provided evidence for a high-molecular mass multisubunit protein and lipid complex, the CoQ synthome (see text for references). The Coq3–Coq9 and Coq11 polypeptides, designated in color, co-purify, and are members of this complex that is peripherally associated with the matrix-side of the inner mitochondrial membrane. Coq1, Coq2, and Coq10 are individual polypeptides that do not associate with the complex (indicated in gray). Coq1 and Coq2 synthesize the early intermediates HHB and HAB (denoted by red hexagon with a gray hexaprenyl tail). Coq10 binds CoQ (and also late-stage CoQ-intermediates denoted as blue hexagons with a gray tail), and functions as a chaperone for this hydrophobic lipid that normally resides at the mid-plane of the membrane bilayer. The Coq3, Coq5, and Coq7 polypeptides are phosphorylated in a Coq8-dependent manner (shown by '???'). The function of Coq8 is still under investigation; although part of a family of atypical kinases, Coq8 has been shown to autophosphorylate, but not yet shown to phosphorylate any other proteins, *in vitro* or *in vivo*. It is speculated to have ATPase function and potentially has the ability to phosphorylate lipids or other small molecules. Hence the phosphorylation of Coq3, Coq5, and Coq7 may be from Coq8 or be produced via another kinase that is recruited to the CoQ synthome to act upon those particular polypeptides. In yeast, it has been shown that the phosphatase that dephosphorylates Coq7 is $Ptc7_S$, the product of the spliced form of *PTC7* (not shown).

the ring nitrogen substituent [22]. Coq9 is also required for Coq6 activity, including the Coq6-mediated deamination function [23,24]. Analogs of 4HB, including 2,4-dihydroxybenzoic acid (2,4-diHB), 3,4-dihydroxybenzoic acid (3,4-diHB) and vanillic acid may be incorporated into CoQ_6 [16] (Figure 1). These analogs may allow for the bypass of CoQ_6 biosynthetic defects in certain yeast *coq6* and *coq7* mutants [16,24,25], as discussed in 'Yeast and human

genes essential for CoQ biosynthesis'. Additional aromatic ring precursors incorporated into CoQ_6 in yeast include *p*-coumarate and the polyphenols resveratrol and kaempferol [26,27] (Figure 1), although the use of kaempferol by yeast is very marginal.

In contrast, pABA is not utilized for CoQ synthesis by human or mouse cells [26], and instead it acts to inhibit the incorporation of 4HB into CoQ [16,28,29]. In mammalian cells, *p*-coumarate, vanillic acid, 3,4-diHB, resveratrol, and kaempferol also serve as CoQ ring precursors, with the difference that in this case kaempferol is a very efficient precursor that is even able to up-regulate CoQ_9 and CoQ_{10} levels in human and mouse kidney cells [27]. While the mechanism underlying the use of polyphenols is still unknown, it is clear that a highly specific process occurs because other polyphenols with similar structures, such as piceatannol or apigenin, are not used for CoQ synthesis in mammalian cells [27].

A hypothesis for the use of *p*-coumarate, resveratrol, and kaempferol as ring precursors of CoQ is that they are metabolized to produce 4HB. The set of reactions that allow this conversion is not yet identified but, independent of the metabolic route involved, an increase in alternative CoQ ring precursors in cells will only turn into higher CoQ levels if cells have a low availability of endogenous 4HB, which is the primary precursor of CoQ. The fact that the availability of 4HB is a rate-limiting step in the CoQ biosynthetic pathway has been previously described in yeast and in mammalian kidney cells [21,27]. Supplementing mammalian kidney cells with exogenous 4HB resulted in an increase in CoQ levels four- to six-fold higher as compared with the non-supplemented control [27]. This observation led the authors to propose the possibility that increasing the availability of CoQ precursors in cells could move the metabolic flux in favor of the biosynthesis of CoQ, helping to ameliorate the phenotype associated with certain Q deficiencies.

Yeast and human genes essential for CoQ biosynthesis

Yeast *COQ1*; human *PDSS1* and *PDSS2*

In yeast and human cells, the synthesis of the polyisoprenyl diphosphate tail derives from a non-sterol branch of the mevalonate pathway [7]. Yeast Coq1 is responsible for the synthesis of the hexaprenyl diphosphate tail moiety from the precursors dimethylallyl diphosphate and isopentenyl diphosphate [30]. The Coq1 polypeptide is peripherally associated with the matrix side of the inner mitochondrial membrane [31]. The analogous polyprenyl diphosphate synthases in other species determine the tail length (*n*) of the CoQ_n (ubiquinone-n or coenzyme Q_n (refers to a specific isoform, where n is number of isoprenyl units in the tail of CoQ_n, e.g. CoQ_{10} in humans, CoQ_6 in *S. cerevisiae*)) produced [32], and when expressed in yeast direct the synthesis of corresponding isoforms of CoQ_n [33]. The yeast Coq1 polypeptide is not associated with the CoQ synthome, but its lipid product is essential for the formation and/or stabilization of this complex [31,34].

PDSS1 and PDSS2 form a heterotetramer responsible for the synthesis of the decaprenyl-diphosphate tail precursor used to synthesize CoQ_{10} in human cells [35]. Patients with partial deficiencies in PDSS1 [36] and PDSS2 [37] show severe disruptions in multiple organ systems. As reviewed in this volume [8], the complexity of phenotypes is a hallmark of mitochondrial deficiency diseases.

Yeast *COQ2*; human *COQ2*

The yeast Coq2 polypeptide is required for the attachment of the polyisoprenyl 'tail' to 4HB [38]. In yeast, Coq2 generates 3-hexaprenyl-4-hydroxy benzoic acid (HHB; Figure 1), the first polyisoprenylated ring CoQ-intermediate in the biosynthetic pathway. This early hydrophobic CoQ-intermediate was found to accumulate in many of the yeast *coq* null mutants, including the *coq3-coq9* null mutants [39,40]. Coq2 is imported into mitochondria via the Tim23 pathway [41], and is an integral membrane protein of the inner mitochondrial membrane [34]. It was originally hypothesized that Coq2 might serve to anchor the CoQ-synthome to the inner mitochondrial membrane [11], however there is no evidence that Coq2 is associated with the other Coq polypeptides that assemble into the CoQ-synthome [12]. Instead it appears that polyisoprenylated CoQ-intermediates produced by Coq1 and Coq2 are important for the stabilization of the CoQ synthome [34] (Figure 2).

Forsgren et al. [42] isolated human *COQ2* cDNA and showed its expression in a yeast *coq2* null mutant restored CoQ_6 biosynthesis. Recently, Desbats et al. [43] have defined the 5′ transcription start sites of the human *COQ2* transcript, indicating that of four potential upstream ATG translation initiation codons, the first two are rarely (if ever) used and that it is the fourth ATG that is in fact predominant. All isoforms of COQ2 were shown to co-localize to mitochondria. This finding argues against the previous hypothesis that the shorter COQ2 isoforms may represent non-mitochondrial polypeptides that may mediate cytoplasmic prenylation of 4HB [42]. The predominant use of the fourth ATG results in a shorter COQ2 polypeptide and the authors suggest new numbering that should be used to

Essays in Biochemistry (2018) **62** 361–376
https://doi.org/10.1042/EBC20170106

designate mutations of human COQ2 [43]. Desbats et al. [43] found a good correlation between disease severity in patients and the effect of *COQ2* mutations on the decreased production of CoQ_6 in a yeast complementation assay. Patients who harbored two alleles that markedly impair CoQ biosynthesis manifested multisystem severe clinical symptoms at birth or infancy, while patients who had a least one allele with residual CoQ biosynthesis manifested isolated steroid resistant nephrotic syndrome (SRNS) or adult onset encephalopathy [43].

Based on two structures determined for prokaryotic homologs of COQ2 (UbiA family aromatic prenyltransferases), human COQ2 is proposed to contain nine transmembrane helices [43]. The C-terminus of human COQ2 resides in the intermembrane space in mitochondria of HEK293 cells [43]. A recent structural model is compatible with this suggestion and predicts that the active site of human COQ2 faces the matrix [44]. Two of the disease-related mutations (given in the old nomenclature) are posited to interfere with the binding of the polyisoprenyl diphosphate (R197H) or to clash with the Mg^{2+} ions that participate in catalysis (A302V) [44].

A recent study by Herebian et al. [45] demonstrated that supplementation with 4HB fully restores endogenous CoQ_{10} biosynthesis in partially deficient COQ2 human fibroblasts harboring homozygous mutant alleles, including the A302V severe allele. Based on an *in silico* model of human COQ2, the authors identified several binding sites for 4HB and posited a channel for 4HB transport across the inner mitochondrial membrane. The authors proposed that the rescue of CoQ_{10} synthesis in fibroblasts from COQ2-deficient patients by treatment with 4HB may represent amelioration of a 4HB transport deficit and/or an enhancement of activity by increased supply of the ring substrate [45]. It will be important to experimentally determine whether the COQ2 polypeptide also functions as a 4HB transporter. In addition to restoring CoQ_{10} levels, the 4HB treatment also increased the steady state levels of COQ4 and COQ7 proteins involved in CoQ biosynthesis, and enhanced cell viability in response to stress conditions. This finding makes sense in light of the important role that CoQ and CoQ-intermediates play in stabilizing the CoQ-synthome in yeast and Complex Q in human cells [7,12,34]. This rescue of COQ2-deficient cells by 4HB treatment is quite striking and deserves further testing as a potential therapy. Even a small enhancement in the biosynthesis of CoQ is able to restore a wide array of phenotypes associated with CoQ deficiency [46].

Yeast *COQ3*; human *COQ3*

Yeast Coq3 is an *S*-adenosylmethionine (AdoMet)-dependent methyltransferase required for the two *O*-methylation steps of CoQ biosynthesis [47-49]. Coq3 is peripherally associated with the matrix-side of the mitochondrial inner membrane [49]. Recent studies reveal that *E. coli* UbiG, a functional homolog of Coq3, binds to liposomes containing cardiolipin [50]. Structural determination of UbiG identifies it as a seven β-strand AdoMet-dependent methyltransferase that contains an unusual insertion sequence that mediates UbiG binding to membranes, and is required for CoQ biosynthesis [50].

Assays with farnesylated analogs of CoQ-intermediates provided early evidence that a complex of yeast Coq polypeptides is required to observe the Coq3 *O*-methyltransferase activity and hence CoQ biosynthesis [39,51]. Recovery of the yeast Coq3-consecutive non-denaturing affinity purification (CNAP) tagged polypeptide from digitonin-solubilized mitochondrial extracts showed that it co-purified with Coq4, Coq5, Coq6, Coq7, Coq9, and Coq11 polypeptides, in a high molecular mass complex that contained CoQ_6 and several CoQ_6-intermediates [12]. Thus Coq3 is an integral member of the CoQ synthome in yeast. The phosphorylation state of Coq3 may modulate the stability of the Coq3 polypeptide and that of the CoQ synthome [52,53]. Overexpression of Coq8, an atypical putative protein kinase, has been shown to stabilize several Coq polypeptides and the CoQ synthome in certain yeast *coq* null mutants [24,34]. Indeed, overexpression of Coq8 in the yeast *coq3* null mutant increased steady state levels of the Coq4, Coq6, Coq7, and Coq9 polypeptides, and stabilized the CoQ synthome. Treatment of *coq3* null mutants overexpressing Coq8 with vanillic acid (a 4HB analog that should bypass the first hydroxylation and first methylation steps) resulted in the production of the late stage CoQ-intermediate DMQ_6 [24] (Figure 1). This finding indicates the potential difficulties in using analogs of 4HB to bypass deficiencies in Coq3, due to its involvement in two *O*-methylation steps, and to the apparent absence of Coq7 hydroxylase activity. It is tempting to speculate that treatment with 2,3-dimethoxy-4HB might serve to bypass both *O*-methyltransferase deficient steps in the *coq3* null mutant. Such bypass would require that this analog could still be prenylated by Coq2, and subjected to decarboxylation, hydroxylation and *C*-methylation steps.

Expression of human COQ3 in yeast *coq3* null mutants rescued growth on a non-fermentable source and partially restored the biosynthesis of CoQ_6 [54]. Assays with farnesylated analogs of CoQ-intermediates showed that mitochondria prepared from *coq3* null mutant yeast expressing human COQ3 performed both *O*-methylation steps [54]. Many lines of evidence indicate a similar Complex Q containing the COQ3–COQ9 polypeptides is involved in

human CoQ_{10} biosynthesis [7]. So far, no mutations causing primary CoQ_{10} deficiency have been reported for the human *COQ3* gene.

Yeast *COQ4*; human *COQ4*

Yeast Coq4 is required for CoQ_6 biosynthesis in yeast, and is peripherally associated with the inner mitochondrial membrane on the matrix side [55]. It is thought to serve as a scaffold or organizer for the CoQ synthome [34,56], as it is associated with Coq3, Coq6, and Coq9 [12,51,57]. No enzyme activity or exact function has been associated with the Coq4 polypeptide. A known crystal structure of the Coq4 domain, determined as part of the structural genomics effort (PDB: 3KB4, Northeastern structural genomics program) identified long hydrophobic α helices bound to a geranylgeranyl monophosphate lipid. A conserved $HDxxHx_{10-13}E$ motif [56] chelated a magnesium ion (Mg^{2+}) near to the phosphate head group [57]. From this structure, the function of Coq4 is speculated to bind the long polyisoprenyl tail of CoQ-intermediates and/or CoQ and to organize the enzymes that perform the ring modifications [34,57] (Figure 2).

Human COQ4 was shown to be a functional ortholog of yeast Coq4, and is capable of restoring CoQ_6 biosynthesis in the yeast *coq4* null mutant [58]. Distinct *COQ4* RNA transcripts indicated the potential for two different isoforms of the human COQ4 polypeptide; the longest isoform was shown to possess a mitochondrial targetting sequence, was localized to mitochondria in HeLa cells, and restored CoQ_6 biosynthesis in the yeast *coq4* null mutant. The functional significance of the shorter isoform is not known; it lacks the mitochondrial targetting sequence and failed to rescue *coq4* mutant yeast.

Patients who harbor two recessive *COQ4* mutant alleles exhibit a broad spectrum of mitochondrial disorders associated with CoQ_{10} deficiencies [59]. Intriguingly, haploinsufficiency of *COQ4* also causes CoQ_{10} deficiency in both human and yeast diploid cells [60]. Recently a heterozygous missense E161D mutation in *COQ4* was reported in a patient with lethal rhabdomyolysis; introduction of the missense mutation was introduced to iPSCs, and recapitulated the muscle-specific CoQ_{10} deficiency [61].

Yeast *COQ5*; human *COQ5*

The yeast Coq5 polypeptide is an AdoMet-dependent methyltransferase required for the *C*-methylation step of CoQ biosynthesis [62,63]. It is peripherally associated with the matrix-side of the mitochondrial inner membrane [64]. Dai et al. [65] determined the structure of yeast Coq5; it has a typical seven β-strand AdoMet methyltransferase structure, and the protein was crystallized both in the presence and absence of AdoMet. The catalytic mechanism is yet to be determined; based on modeling the authors proposed an active site highly conserved Arg^{201} or Tyr^{78} act to deprotonate a water molecule that then acts as the base to deprotonate the C5-ring H from $DDMQ_6H_2$ [65]. Yeast *coq5* point mutants that harbor mutations in the Class I methyltransferase motifs result in a loss of *C*-methyltransferase function, but retain steady state levels of the Coq5 polypeptide, and of the Coq polypeptide partner proteins of the CoQ synthome. In contrast, these CoQ synthome partner proteins are destabilized in the *coq5* null mutant [64]. Overexpression of Coq8 in the *coq5* null yeast mutant results in the increased steady-state levels of the Coq4, Coq7, Coq9 polypeptides, the stabilization of the CoQ synthome, and the accumulation of $DDMQ_6H_2$, the substrate of Coq5 [24,34] (Figure 1). It is possible that the 4HB analog 2-methyl-4-BH might function to bypass the defect in *coq5* point mutants with stable Coq5 polypeptide, however, this has not yet been tested.

Regulated expression of yeast Coq5 is necessary for the correct assembly of the CoQ synthome. Recently, two mechanisms of COQ5 post-transcriptional regulation have been elucidated. The RNA binding protein Puf3 regulates the translation of appropriate amounts of Coq5 so the CoQ synthome can be assembled [66]. Oct1 is a mitochondrial matrix-localized protease that removes eight residues from the amino-terminal mitochondrial targetting sequence of Coq5 and is essential for formation of the mature amino-terminus of Coq5 and its stability [67]. There is also evidence that yeast Coq5 is phosphorylated in a Coq8-dependent manner [53].

Expression of the human COQ5 polypeptide was found to rescue the CoQ_6 biosynthetic defect of the *coq5* point mutants or in a *coq5* null mutant overexpressing Coq8, but not a *coq5* null mutant [68]. Thus, human COQ5 is an ortholog of yeast Coq5, but can rescue yeast only when the other yeast Coq partner proteins are present and the CoQ synthome is assembled. Primary CoQ_{10} deficiency has been recently diagnosed due to a partial loss of function of COQ5 [69]. The deficiency is shown to be due to a duplication of the *COQ5* gene, and that due to alternative splicing appears to generate an unstable *COQ5* mRNA with a long 3′-UTR. Steady state levels of the COQ5 polypeptide were dramatically decreased in fibroblasts from the affected homozygous patients as compared with controls. The affected patients had variable degrees of cerebellar ataxia, and showed a modest decrease in the levels of CoQ_{10} in peripheral blood leukocytes, and a more dramatic decrease in CoQ_{10} levels in a skeletal muscle biopsy [69]. The reduction in

Essays in Biochemistry (2018) **62** 361–376
https://doi.org/10.1042/EBC20170106

CoQ_{10} levels is consistent with the observation that decreases in COQ5-containing mitochondrial protein complex impairs the production of CoQ_{10} [70].

Yeast *COQ6*; human *COQ6*

The yeast Coq6 polypeptide is characterized as a flavin-dependent monooxygenase [71]. Conserved catalytic regions in Coq6 include the ADP binding fingerprint, the NAD(P)H/FAD binding motif, and the ribityl binding region [71]. Yeast Coq6 co-purifies with a tightly bound FAD, and modeling studies are consistent with its proposed activity as a ring hydroxylase [72]. Yeast Coq6 is responsible for the first hydroxylation step (ring C5) in CoQ biosynthesis [73]. It is also necessary for the deamination of ring C4 in *S. cerevisiae* when pABA is used an aromatic ring precursor [22]. The yeast Coq6 polypeptide is peripherally associated with inner mitochondrial membrane on the matrix side [71], and associates with Coq4, Coq5, Coq7, Coq8, and Coq9 polypeptides of the CoQ synthome [12]. Recent investigations discovered a physical association of Coq6 with Coq8 [12]. Yeast *coq6* point mutants that affect the active site but preserve steady state levels of the Coq6 polypeptide and assembly of the CoQ synthome may be rescued by providing alternate ring precursors such as 3,4-diHB and vanillic acid (Figure 1). These alternate ring precursors, once prenylated by Coq2, allow the defective *coq6* step to be bypassed [73]. Such bypass is also effective in *coq6* null yeast mutants provided yeast *COQ8* is overexpressed [24].

The human homolog COQ6, is able to rescue a yeast *coq6* null mutant [25,74], and interacts with human COQ8B (ADCK4) and COQ7 [75]. Yeast *coq6* null mutants expressing certain hypomorphic mutations of human *COQ6* are rescued by treatment with either 3,4-diHB or vanillic acid [25]. The effectiveness of such bypass therapies as treatments for patients with mutations in *COQ6* remains to be explored. It seems possible that these alternate ring precursors might serve to restore endogenous CoQ_{10} biosynthesis in patients with *COQ6* deficiencies.

Mutations in human *COQ6* have been implicated in an autosomal recessive disease characterized by severe progressive nephrotic syndrome and deafness [74]. It has been suggested that kidney biopsy should be performed on young children present with SRNS and sensorineural hearing loss [76]. The rationale for this suggestion is that the abnormal mitochondria in podocytes may provide an early diagnostic clue of mutations in CoQ biosynthetic genes. Supplementation with high doses of CoQ_{10} can stop the progression of kidney disease, and this therapy should be started immediately at first suspicion of CoQ_{10} deficiency [76,77].

Yeast *YAH1* and *ARH1*; human *FDX1*, *FDX2*, and *FDXR*

Unlike most flavin-dependent monooxygenases that utilize NAD(P)H directly as a source of electrons, the electrons from NAD(P)H are funneled indirectly to yeast Coq6 via the coupled system of ferredoxin (Yah1) an iron–sulphur protein, and ferredoxin reductase (Arh1) [73]. Yeast engineered to be transiently depleted in Yah1 or Arh1 were shown to be defective in the same C5 ring-hydroxylation step, and to accumulate the same polyisoprenylated ring-intermediates as yeast mutants harboring inactive *coq6* alleles [21,73]. *YAH1* and *ARH1* are essential genes in yeast, and in addition to CoQ biosynthesis, are also required for iron–sulphur cluster biosynthesis [78].

There are two human homologs of yeast Yah1 – FDX1 and FDX2. Human FDX2 was shown to complement the iron–sulphur cluster biosynthetic defect of Yah1 depleted yeast [79]. However, neither human FDX1 nor FDX2 were able to complement the CoQ_6 biosynthetic defect of Yah1 depleted yeast [73]. The human homolog of Arh1 is termed as FDXR, which functions as an electron transfer protein in cholesterol biosynthesis and overall steroid metabolism, as well as iron–sulphur cluster biosynthesis [78]. Whether FDX1, FDX2, or FDXR function to assist human COQ6 catalytic activity in the biosynthesis of CoQ_{10} is not yet known.

Yeast *COQ7 (CAT5)* and *PTC7*; human *COQ7* (*CAT5*, *CLK-1*) and *PPTC7*

Yeast Coq7 is a hydroxylase responsible for catalyzing the penultimate step of the CoQ biosynthetic pathway [80-82]. The hydroxylase activity depends on a carboxylate-bridged diiron binding motif, first identified as a highly conserved sequence across a wide array of organisms, and predicted to mediate hydroxylation similar to other members of the carboxylate-bridged diiron protein family, such as methane monoxygenase, ribonucleotide reductase, and phenol-hydroxylase [82]. Modeling predicted Coq7 to be a four-helix bundle protein with an additional helix mediating an interfacial association with the membrane [82]. Experiments with isolated mitochondria and mitoplasts show yeast Coq7 polypeptide is peripherally associated with inner mitochondrial membrane on the matrix side [34].

Expression of human COQ7 rescues the CoQ_6 deficiency of yeast *coq7* null mutants [83], indicating profound conservation of function. Overexpression of a soluble fusion protein containing human COQ7 polypeptide fused to an immunoglobulin-binding domain of protein G was purified (termed as GB1-hCLK-1) and spectroscopic and kinetic methods provided evidence for the presence of the diiron center [84]. Binding of the substrate analogs DMQ_0 or

DMQ_2 to GB1-hCLK1 mediated the reduction in the diiron site by NADH and in the presence of O_2 the hydroxylation step was catalyzed [84].

Yeast *coq7* null mutants accumulate the early CoQ-intermediates HHB and HAB, while *coq7* point mutants [80] and *coq7* null mutants overexpressing Coq8 accumulate DMQ_6 the penultimate intermediate in the pathway [24,85]. Expression of the unrelated *E. coli* UbiF hydroxylase rescued a *coq7* point mutant, but failed to rescue the *coq7* null mutant [86]. These findings indicated Coq7 is an important polypeptide partner of the CoQ synthome; indeed, Coq7 co-purifies with tagged forms of Coq3, Coq6, and Coq9 polypeptides [12].

A mutation in the human *COQ7* gene is associated with a primary ubiquinone deficiency, and results in multiple organ involvement [87]. Interestingly, the deficiencies in CoQ_{10} content and mitochondrial respiratory activities in fibroblasts isolated from this patient were improved following treatment with 2,4-diHB, a 4HB analog that bypasses the COQ7-dependent hydroxylase step [87]. The effectiveness of treatment with 2,4-diHB depends on the type of *COQ7* mutation(s) present in patients [88]. It is likely that the success of these bypass therapies will depend on the stable presence of other COQ polypeptides and their ability to form the CoQ synthome (or complex Q) [16,24]. Regulated expression of COQ7 has been shown to impact the rates of CoQ_{10} biosynthesis, both at the level of NF-κB transcriptional up-regulation of *COQ7* gene expression [89], and at the level of RNA binding proteins that mediate stability of *COQ7* mRNA [90]. The regulated expression of COQ7 and the other component polypeptides of the CoQ synthome seem likely to influence its assembly and function, and so impact biosynthesis of CoQ_{10}.

Yeast Coq7 is modified by phosphorylation [12,53]. Predictive algorithms suggested that the phosphorylation status of Coq7 was regulatory for CoQ_6 biosynthesis, with at least three predicted phosphorylation sites on Ser^{20}, Ser^{28}, and Thr^{32} [91]. When these residues are replaced with alanine, phosphorylation was abolished and CoQ_6 levels were significantly increased in yeast expressing Coq7 with the triple-Alanine substitution. In contrast, yeast expressing the Coq7 with substitution of acidic residues at these residues (Asp^{20}, Glu^{28}, and Asp^{32}) had decreased levels of CoQ_6 and accumulated DMQ_6, indicating that the non-phosphorylatable form of Coq7 is the active form that catalyzes the penultimate pathway step [91]. Other sites of phosphorylation may also influence Coq7 activity; yeast expressing Coq7 harboring the phosphomimetic $Ser^{114}Glu$ substitution also produced lower amounts of CoQ_6 and accumulated DMQ_6 [92].

The phosphatase responsible for Coq7 dephosphorylation is Ptc7, a *bona fide* mitochondrial serine/threonine protein phosphatase belonging to the PPM family of phosphatases [93]. It was recently discovered that two distinct forms of *PTC7* RNA exist, spliced and non-spliced forms, displaying a rare case of alternative splicing in yeast that results in two viable isoforms of a spliced protein [94,95]. The previously reported Ptc7 phosphatase was shown to be the spliced form ($Ptc7_s$) that resides in the mitochondria, while the non-spliced form ($Ptc7_{ns}$) is a nuclear membrane localized protein that contains a transmembrane helix that anchors it to the nuclear membrane [94]. Exclusive expression of $Ptc7_s$ showed significantly higher *de novo* CoQ biosynthesis, as compared with $Ptc7_{ns}$. These findings suggest that the mitochondrial targetting of the Ptc7s results in Coq7 dephosphorylation, and allows Coq7 to catalyze the penultimate step of the CoQ biosynthetic pathway [95]. Ptc7s acts to dephosphorylate other mitochondrial proteins, and deletion of *ptc7* perturbs mitochondrial function [96]. PPTC7 is the human serine/threonine phosphatase homolog of yeast Ptc7, however it is not known whether phosphorylation regulates human COQ7, and if so, whether PPTC7 recognizes it as a substrate.

Yeast *COQ8*; human *COQ8A* (*ADCK3*) and *COQ8B* (*ADCK4*)

The *S. cerevisiae* Coq8 polypeptide is identified as a putative kinase in the biosynthetic pathway of CoQ_6. Coq8 harbors six of twelve motifs present in protein kinases and is required to observe the presence of phosphorylated forms of Coq3, Coq5, and Coq7 polypeptides [53]. Coq8 co-purifies with the CoQ synthome [12]. Further, overexpression of Coq8 in certain of the *coq* null strains restores steady state levels of Coq4, Coq7, and Coq9, and stabilizes the formation of the CoQ synthome [24,34].

Expression of human COQ8A (ADCK3) in yeast *coq8* mutant strains restored CoQ_6 biosynthesis and the phosphorylation state of several of the yeast Coq polypeptides, indicating a profound conservation of function [53]. Rescue of yeast *coq8* mutants by human COQ8A depended on fusion to a yeast mitochondrial targetting sequence [53]. Yeast Coq8 and human COQ8A are homologs of atypical protein kinases. These proteins are able to autophosphorylate and show a surprising affinity and selectivity for ADP, as opposed to ATP [97]. Human COQ8A lacks *in vitro* protein kinase activity and instead shows ATPase activity that is essential for CoQ biosynthesis [98]. The ATPase activity is strongly activated by cardiolipin and small molecule mimics of CoQ intermediates [99]. Thus, the ATPase function of yeast Coq8 and human COQ8A is proposed to function in a chaperone-like activity to facilitate the assembly of the CoQ synthome and *de novo* [65] biosynthesis of CoQ [99].

Essays in Biochemistry (2018) **62** 361–376
https://doi.org/10.1042/EBC20170106

Expression of human COQ8B (ADCK4) also rescues CoQ_6 biosynthesis in yeast *coq8* mutants [100]. Although the amino terminus of COQ8B has a typical mitochondrial matrix targetting sequence, rescue of *coq8* mutant yeast by COQ8B depends on the addition of a yeast mitochondrial targetting sequence [100]. The effect of a *COQ8B* polymorphism present in 50% of the European population (COQ8B-H174R) was tested in the yeast expression model. Yeast *coq8* mutants expressing the human COQ8B-His^{174} polypeptide had decreased steady state levels of the COQ8B polypeptide, decreased growth on medium containing a non-fermentable carbon source, and decreased CII + CIII activity as compared with mutants expressing the COQ8B-Arg^{174} polypeptide [100]. Thus, it is possible that this common COQ8B polymorphism may represent a risk factor for secondary CoQ_{10} deficiencies. Various human diseases are directly associated with mutations in the *COQ8A* and *COQ8B* genes. Most prevalent are recessive ataxia and childhood-onset cerebellar ataxia associated with mutated *COQ8A* [101,102], and a steroid-resistant nephrotic disease related to mutated *COQ8B* [75,100].

Yeast *COQ9*; human *COQ9*

In *S. cerevisiae,* Coq9 is required for CoQ biosynthesis, is a member of the CoQ synthome, and is peripherally associated with the inner mitochondrial membrane, on the matrix side [34,103]. A temperature-sensitive *coq9* mutant (*coq9-ts19*) shifted to the non-permissive temperature results in the disassembling of the CoQ synthome, demonstrating that Coq9 is essential for the formation and stabilization of the high-molecular mass complex [23]. Coq9 is required for the deamination of Carbon 4 on CoQ-intermediates when pABA is utilized as the ring precursor in yeast [23]. The removal of the ring nitrogen substituent depends on the function of Coq6, and yeast with *coq9* mutations accumulate 3-hexaprenyl-4-aminophenol (4-AP), an intermediate that has also been shown to build up in a *coq6* null mutant overexpressing *COQ8* [24]. It is therefore likely that both Coq6 and Coq9 are needed for the 5-hydroxylation and 4-deamination steps of CoQ-intermediates. Additionally, an accumulation of late-stage intermediates suggests Coq7 is not active in the absence of Coq9 [6,24]. In summary, the yeast Coq9 polypeptide is required for both Coq6 and Coq7 hydroxylation steps, via an indirect or supportive role.

Attempts to rescue yeast *coq9* null mutants by expression of human COQ9 have so far failed [104-106]. However, expression of human COQ9 rescued the yeast *coq9-ts19* mutant [106]. Under these conditions, a small amount of the human COQ9 polypeptide enhanced the synthesis of CoQ_6 from 4HB (but not from pABA) and co-purified with the yeast Coq6-CNAP tagged polypeptide, indicating that human COQ9 is able to interact with the yeast CoQ synthome.

The presence of both human COQ9 and human COQ7 are needed for the hydroxylation step catalyzed by COQ7, and the two polypeptides interact [13]. Human cells with deficiencies in COQ9 accumulate DMQ_{10}, the same intermediate that accumulates in COQ7 deficient cells [107]. Both COQ7 and COQ9 deficient cell lines respond to treatment with 2,4-diHB, another example of bypass therapy [108,109]. In fact, human fibroblasts with mutations in COQ9 show decreased steady state levels of the COQ7 polypeptide [109]. Interestingly, treatment with vanillic acid also restored function in the COQ9 deficient cells, but not the COQ7 deficient cells [108]. Perhaps human COQ9 and COQ6 function may also be linked, similar to the situation in yeast. In humans, *COQ9* mutations result in various disease states, including predominant encephalomyopathy and an autosomal-recessive neonatal-onset CoQ deficiency [104,107].

Yeast and human genes required for efficient CoQ biosynthesis

Yeast *COQ10*; human *COQ10A, COQ10B*

Unlike the completely CoQ-less *coq1–coq9* null mutants, the yeast *coq10* null mutant produces near wild-type levels of CoQ at stationary phase, but synthesizes CoQ less efficiently during log phase growth [110,111]. While CoQ is eventually produced at near normal levels, the *coq10* null mutant still has severe defects in respiratory electron transport and is sensitive to treatment with polyunsaturated fatty acids, phenotypes that are hallmarks of the *coq1–coq9* null mutants [110]. Thus, even though CoQ_6 content is similar to that of wild-type yeast, Coq10 is required for efficient function and biosynthesis of CoQ_6. The Coq10 polypeptide contains a steroidogenic acute regulatory (StAR)-related lipid transfer (StART) domain, and binds CoQ and late-stage CoQ-intermediates both *in vitro* and *in vivo*, suggesting Coq10 may function as a lipid chaperone involving delivery of CoQ from site of synthesis to sites of function [110-114].

Humans have two homologs of yeast *COQ10*, namely *COQ10A* and *COQ10B*. Each isoform has several transcript variants as a result of alternative transcription initiation and/or alternative splicing [6]. The function of the COQ10 polypeptide is widely conserved across different organisms; expression of homologs from either *Caulobacter crescentus* or human COQ10A rescue the impaired growth of yeast *coq10Δ* mutant yeast [110]. Currently, there is no

known disease phenotype associated with mutations in human *COQ10A* or *COQ10B*. However, the postulated lipid chaperone function of COQ10A and COQ10B makes these polypeptides intriguing targets for study of the movement of CoQ between mitochondrial membranes and the respiratory complexes.

Yeast *COQ11*; human *NDUFA9*

COQ11 (*YLR290C*) was recently identified to be required for efficient *de novo* CoQ biosynthesis in *S. cerevisiae*. Affinity purification of CNAP-tagged Coq11 showed Coq11-CNAP co-purified with Coq4, Coq5, and Coq7 – members of the high molecular mass CoQ synthome [12]. A separate high throughput study also identified Coq11 as a mitochondrial protein, confirming its localization to the portion of the cell where CoQ is synthesized [115]. Due to its novelty, the functional roles, organization, and stoichiometry of Coq11 within the CoQ-synthome are not yet fully understood. However, numerous features of Coq11 and its homologs solidify its link to CoQ biosynthesis. In five fungal genomes, the existence of Coq11-Coq10 fusion proteins suggests these proteins may have a functional relationship [12]. High throughput studies found *COQ11* to have a genetic correlation with both *COQ2* and *COQ10*, which further supports this hypothesis [115]. Sequence analyses establish Coq11 as a member of the atypical short-chain dehydrogenase/reductase superfamily of oxidoreductases (SDR). SDR superfamily proteins contain a conserved Rossmann fold, a protein structural motif used to bind nucleotide co-factors such as FAD, FMN, and NAD(P) [116]. This bound co-factor is then used to assist the protein in its catalysis of different chemical reactions including isomerization, decarboxylation, epimerization, imine reduction, and carbonyl-alcohol oxidoreduction [116,117]. It is therefore tempting to speculate that Coq11 may use its Rossmann fold to perform enzymatic reactions within the CoQ biosynthetic pathway.

Interestingly, a protein similarity network analysis reveals that the taxonomy of YLR290C-like proteins includes the SDR subfamily protein NDUFA9, an auxiliary subunit of Complex I in humans important for complex stability [12,118-120]. Patients with decreased levels of NDUFA9 are unable to assemble Complex I properly and may develop a degenerative infancy respiratory disorder known as Leigh syndrome, which is often fatal in the first years of life [121,122]. Differences in *NDUFA9* deficiency produce phenotypic variations in patients [46]. It will be challenging to evaluate whether NDUFA9 deficiencies impact CoQ biosynthesis directly, because the deficiencies resulting from Complex I defects (and other mitochondrial defects) may secondarily influence CoQ biosynthesis [123,124]. Further exploration of Coq11 homology with NDUFA9 will help define their functional relationship.

Summary

- The *COQ1–COQ11* genes identified in the *S. cerevisiae* yeast model are required for efficient biosynthesis of CoQ_6.
- Expression of human homologs of yeast *COQ1–COQ10* genes restore CoQ biosynthesis in the corresponding yeast *coq* mutants, indicating profound functional conservation.
- Yeast provides a simple yet powerful model to investigate and define the function and possible pathology of human *COQ* gene polymorphisms and mutations.
- Simple natural products may serve as alternate ring precursors in CoQ biosynthesis, and these compounds may act to enhance biosynthesis of CoQ or may bypass select deficient steps.
- Biosynthesis of CoQ in yeast and human cells depends on high molecular mass multi-subunit complexes consisting of several of the *COQ* gene products, as well as CoQ itself and CoQ-intermediates.
- Thus the CoQ synthome in yeast, or Complex Q in human cells is essential for *de novo* biosynthesis of CoQ.

Acknowledgements

We thank Dr A. Tzagoloff (Columbia University) for the original yeast *coq* mutant strains. We also thank the UCLA Molecular Instrumentation Core for the use of the QTRAP 4000.

Essays in Biochemistry (2018) **62** 361–376
https://doi.org/10.1042/EBC20170106

Competing interests

The authors declare that there are no competing interests associated with this manuscript.

Funding

This work was supported in part by the National Science Foundation [grant number MCB-1330803 (to C.F.C.)]; and the National Institutes of Health [grant number T32 GM 008496 (to M.C.B. and H.T.)].

Author contribution

A.M.A., M.C.B., L.F.-d.-R., A.N., H.T., and C.F.C. contributed to drafting this review, revising it for intellectual content and approved the final version. A.M.A., A.N., L.F.-d.R., and C.F.C. contributed to preparation of the figures.

Abbreviations

AdoMet, *S*-adenosylmethionine; CNAP, consecutive non-denaturing affinity purification; CoQ, ubiquinone or coenzyme Q; $CoQH_2$, ubiquinol or CoQ hydroquinone; CoQ_n, ubiquinone-n or coenzyme Q_n (refers to a specific isoform, where n is number of isoprenyl units in the tail of CoQ_n, e.g. CoQ_{10} in humans, CoQ_6 in *Saccharomyces cerevisiae*); Coq, *Saccharomyces cerevisiae* polypeptide involved in CoQ_6 biosynthesis; COQ, human polypeptide involved in CoQ_{10} biosynthesis; *COQ*, yeast or human gene involved in CoQ biosynthesis; pABA, *para*-aminobenzoic acid; SDR, short-chain dehydrogenase/reductase superfamily of oxidoreductases; SRNS, steroid resistant nephrotic syndrome; 2,4-diHB, 2,4-dihydroxybenzoic acid; 3,4-diHB, 3,4-dihydroxybenzoic acid; 4HB, 4-hydroxybenzoic acid; 4HBz, 4-hydroxybenzaldehyde.

References

1 Turunen, M., Olsson, J. and Dallner, G. (2004) Metabolism and function of coenzyme Q. *Biochim. Biophys. Act.* **1660**, 171–199, https://doi.org/10.1016/j.bbamem.2003.11.012
2 Crane, F.L. (2001) Biochemical functions of coenzyme Q_{10}. *J. Am. Coll. Nutr.* **20**, 591–598, https://doi.org/10.1080/07315724.2001.10719063
3 Bentinger, M., Brismar, K. and Dallner, G. (2007) The antioxidant role of coenzyme Q. *Mitochondrion* **7S**, S41–S50, https://doi.org/10.1016/j.mito.2007.02.006
4 Aussel, L., Pierrel, F., Loiseau, L., Lombard, M., Fontecave, M. and Barras, F. (2014) Biosynthesis and physiology of coenzyme Q in bacteria. *Biochim. Biophys. Acta* **1837**, 1004–1011, https://doi.org/10.1016/j.bbabio.2014.01.015
5 Hayashi, K., Ogiyama, Y., Yokomi, K., Nakagawa, T., Kaino, T. and Kawamukai, M. (2014) Functional conservation of coenzyme Q biosynthetic genes among yeasts, plants, and humans. *PLoS ONE* **9**, 14, https://doi.org/10.1371/journal.pone.0099038
6 Wang, Y. and Hekimi, S. (2013) Molecular genetics of ubiquinone biosynthesis in animals. *Crit. Rev. Biochem. Mol. Biol.* **48**, 69–88, https://doi.org/10.3109/10409238.2012.741564
7 Stefely, J.A. and Pagliarini, D.J. (2017) Biochemistry of mitochondrial coenzyme Q biosynthesis. *Trends Biochem. Sci.* **42**, 824–843, https://doi.org/10.1016/j.tibs.2017.06.008
8 Alcázar-Fabra, M., Trevisson, E. and Brea-Calvo, G. (2018) Clinical syndromes associated with Coenzyme Q_{10} deficiency. *Essays Biochem.* **62**, 377–398, https://doi.org/10.1042/EBC20170107
9 Tzagoloff, A., Akai, A. and Needleman, R.B. (1975) Assembly of the mitochondrial membrane system. Characterization of nuclear mutants of *Saccharomyces cerevisiae* with defects in mitochondrial ATPase and respiratory enzymes. *J. Biol. Chem.* **250**, 8228–8235
10 Tzagoloff, A. and Dieckmann, C.L. (1990) *PET* genes of *Saccharomyces cerevisiae*. *Microbiol. Rev.* **54**, 211–225
11 Tran, U.C. and Clarke, C.F. (2007) Endogenous synthesis of coenzyme Q in eukaryotes. *Mitochondrion* **7S**, S62–S71, https://doi.org/10.1016/j.mito.2007.03.007
12 Allan, C.M., Awad, A.M., Johnson, J.S., Shirasaki, D.I., Wang, C., Blaby-Haas, C.E. et al. (2015) Identification of Coq11, a new coenzyme Q biosynthetic protein in the CoQ-Synthome in *Saccharomyces cerevisiae*. *J. Biol. Chem.* **290**, 7517–7534, https://doi.org/10.1074/jbc.M114.633131
13 Lohman, D.C., Forouhar, F., Beebe, E.T., Stefely, M.S., Minogue, C.E., Ulbrich, A. et al. (2014) Mitochondrial COQ9 is a lipid-binding protein that associates with COQ7 to enable coenzyme Q biosynthesis. *Proc. Natl. Acad. Sci. U.S.A.* **111**, E4697–E4705, https://doi.org/10.1073/pnas.1413128111
14 Clarke, C.F. (2000) New advances in coenzyme Q biosynthesis. *Protoplasma* **213**, 134–147, https://doi.org/10.1007/BF01282151
15 Kawamukai, M. (2016) Biosynthesis of coenzyme Q in eukaryotes. *Biosci. Biotechnol. Biochem.* **80**, 23–33, https://doi.org/10.1080/09168451.2015.1065172
16 Pierrel, F. (2017) Impact of chemical analogs of 4-hydroxybenzoic acid on coenzyme Q biosynthesis: from inhibition to bypass of coenzyme Q deficiency. *Front. Physiol.* **8**, 436, https://doi.org/10.3389/fphys.2017.00436
17 Payet, L.A., Leroux, M., Willison, J.C., Kihara, A., Pelosi, L. and Pierrel, F. (2016) Mechanistic details of early steps in coenzyme Q biosynthesis pathway in yeast. *Cell Chem. Biol.* **23**, 1241–1250, https://doi.org/10.1016/j.chembiol.2016.08.008
18 Stefely, J.A., Kwiecien, N.W., Freiberger, E.C., Richards, A.L., Jochem, A., Rush, M. J.P. et al. (2016) Mitochondrial protein functions elucidated by multi-omic mass spectrometry profiling. *Nat. Biotechnol.* **34**, 1191–1197, https://doi.org/10.1038/nbt.3683
19 Zahedi, R.P., Sickmann, A., Boehm, A.M., Winkler, C., Zufall, N., Schonfisch, B. et al. (2006) Proteomic analysis of the yeast mitochondrial outer membrane reveals accumulation of a subclass of preproteins. *Mol. Biol. Cell* **17**, 1436–1450, https://doi.org/10.1091/mbc.e05-08-0740

20 Marbois, B., Xie, L.X., Choi, S., Hirano, K., Hyman, K. and Clarke, C.F. (2010) para-Aminobenzoic acid is a precursor in coenzyme Q_6 biosynthesis in *Saccharomyces cerevisiae*. *J. Biol. Chem.* **285**, 27827–27838, https://doi.org/10.1074/jbc.M110.151894
21 Pierrel, F., Hamelin, O., Douki, T., Kieffer-Jaquinod, S., Muhlenhoff, U., Ozeir, M. et al. (2010) Involvement of mitochondrial ferredoxin and para-aminobenzoic acid in yeast coenzyme Q biosynthesis. *Chem. Biol.* **17**, 449–459, https://doi.org/10.1016/j.chembiol.2010.03.014
22 Ozeir, M., Pelosi, L., Ismail, A., Mellot-Draznieks, C., Fontecave, M. and Pierrel, F. (2015) Coq6 is responsible for the C4-deamination reaction in coenzyme Q biosynthesis in *Saccharomyces cerevisiae*. *J. Biol. Chem.* **290**, 24140–24151, https://doi.org/10.1074/jbc.M115.675744
23 He, C.H., Black, D.S., Nguyen, T.P., Wang, C., Srinivasan, C. and Clarke, C.F. (2015) Yeast Coq9 controls deamination of coenzyme Q intermediates that derive from para-aminobenzoic acid. *Biochim. Biophys. Acta* **1851**, 1227–1239, https://doi.org/10.1016/j.bbalip.2015.05.003
24 Xie, L.X., Ozeir, M., Tang, J.Y., Chen, J.Y., Jaquinod, S.K., Fontecave, M. et al. (2012) Overexpression of the Coq8 kinase in *Saccharomyces cerevisiae coq* null mutants allows for accumulation of diagnostic intermediates of the coenzyme Q_6 biosynthetic pathway. *J. Biol. Chem.* **287**, 23571–23581, https://doi.org/10.1074/jbc.M112.360354
25 Doimo, M., Trevisson, E., Airik, R., Bergdoll, M., Santos-Ocana, C., Hildebrandt, F. et al. (2014) Effect of vanillic acid on *COQ6* mutants identified in patients with coenzyme Q_{10} deficiency. *Biochim. Biophys. Acta* **1842**, 1–6, https://doi.org/10.1016/j.bbadis.2013.10.007
26 Xie, L.X., Williams, K.J., He, C.H., Weng, E., Khong, S., Rose, T.E. et al. (2015) Resveratrol and para-coumarate serve as ring precursors for coenzyme Q biosynthesis. *J. Lipid Res.* **56**, 909–919, https://doi.org/10.1194/jlr.M057919
27 Fernandez-Del-Rio, L., Nag, A., Gutierrez Casado, E., Ariza, J., Awad, A.M., Joseph, A.I. et al. (2017) Kaempferol increases levels of coenzyme Q in kidney cells and serves as a biosynthetic ring precursor. *Free Radic. Biol. Med.* **110**, 176–187, https://doi.org/10.1016/j.freeradbiomed.2017.06.006
28 Alam, S.S., Nambudiri, A.M. and Rudney, H. (1975) J-Hydroxybenzoate: polyprenyl transferase and the prenylation of 4-aminobenzoate in mammalian tissues. *Arch. Biochem. Biophys.* **171**, 183–190, https://doi.org/10.1016/0003-9861(75)90022-3
29 Gonzalez-Aragon, D., Buron, M.I., Lopez-Lluch, G., Herman, M.D., Gomez-Diaz, C., Navas, P. et al. (2005) Coenzyme Q and the regulation of intracellular steady-state levels of superoxide in HL-60 cells. *Biofactors* **25**, 31–41, https://doi.org/10.1002/biof.5520250105
30 Ashby, M.N. and Edwards, P.A. (1990) Elucidation of the deficiency in two yeast coenzyme Q mutants. Characterization of the structural gene encoding hexaprenyl pyrophosphate synthetase. *J. Biol. Chem.* **265**, 13157–13164
31 Gin, P. and Clarke, C.F. (2005) Genetic evidence for a multi-subunit complex in coenzyme Q biosynthesis in yeast and the role of the Coq1 hexaprenyl diphosphate synthase. *J. Biol. Chem.* **280**, 2676–2681, https://doi.org/10.1074/jbc.M411527200
32 Okada, K., Suzuki, K., Kamiya, Y., Zhu, X., Fujisaki, S., Nishimura, Y. et al. (1996) Polyprenyl diphosphate synthase essentially defines the length of the side chain of ubiquinone. *Biochim. Biophys. Acta* **1302**, 217–223, https://doi.org/10.1016/0005-2760(96)00064-1
33 Okada, K., Kainou, T., Matsuda, H. and Kawamukai, M. (1998) Biological significance of the side chain length of ubiquinone in *Saccharomyces cerevisiae*. *FEBS Lett.* **431**, 241–244, https://doi.org/10.1016/S0014-5793(98)00753-4
34 He, C.H., Xie, L.X., Allan, C.M., Tran, U.C. and Clarke, C.F. (2014) Coenzyme Q supplementation or over-expression of the yeast Coq8 putative kinase stabilizes multi-subunit Coq polypeptide complexes in yeast *coq* null mutants. *Biochim. Biophys. Acta* **1841**, 630–644, https://doi.org/10.1016/j.bbalip.2013.12.017
35 Saiki, R., Nagata, A., Kainou, T., Matsuda, H. and Kawamukai, M. (2005) Characterization of solanesyl and decaprenyl diphosphate synthases in mice and humans. *FEBS J.* **272**, 5606–5622, https://doi.org/10.1111/j.1742-4658.2005.04956.x
36 Mollet, J., Giurgea, I., Schlemmer, D., Dallner, G., Chretien, D., Delahodde, A. et al. (2007) Prenyldiphosphate synthase, subunit 1 (*PDSS1*) and OH-benzoate polyprenyltransferase (*COQ2*) mutations in ubiquinone deficiency and oxidative phosphorylation disorders. *J. Clin. Invest.* **117**, 765–772, https://doi.org/10.1172/JCI29089
37 Lopez, L.C., Schuelke, M., Quinzii, C.M., Kanki, T., Rodenburg, R.J., Naini, A. et al. (2006) Leigh syndrome with nephropathy and CoQ_{10} deficiency due to decaprenyl diphosphate synthase subunit 2 (*PDSS2*) mutations. *Am. J. Hum. Genet.* **79**, 1125–1129, https://doi.org/10.1086/510023
38 Ashby, M.N., Kutsunai, S.Y., Ackerman, S., Tzagoloff, A. and Edwards, P.A. (1992) *COQ2* is a candidate for the structural gene encoding para-hydroxybenzoate:polyprenyltransferase. *J. Biol. Chem.* **267**, 4128–4136
39 Hsu, A.Y., Do, T.Q., Lee, P.T. and Clarke, C.F. (2000) Genetic evidence for a multi-subunit complex in the O-methyltransferase steps of coenzyme Q biosynthesis. *Biochim. Biophys. Acta* **1484**, 287–297, https://doi.org/10.1016/S1388-1981(00)00019-6
40 Johnson, A., Gin, P., Marbois, B.N., Hsieh, E.J., Wu, M., Barros, M.H. et al. (2005) *COQ9*, a new gene required for the biosynthesis of coenzyme Q in *Saccharomyces cerevisiae*. *J. Biol. Chem.* **280**, 31397–31404, https://doi.org/10.1074/jbc.M503277200
41 Leuenberger, D., Bally, N.A., Schatz, G. and Koehler, C.M. (1999) Different import pathways through the mitochondrial intermembrane space for inner membrane proteins. *EMBO J.* **18**, 4816–4822, https://doi.org/10.1093/emboj/18.17.4816
42 Forsgren, M., Attersand, A., Lake, S., Grunler, J., Swiezewska, E., Dallner, G. et al. (2004) Isolation and functional expression of human *COQ2*, a gene encoding a polyprenyl transferase involved in the synthesis of CoQ. *Biochem. J.* **382**, 519–526, https://doi.org/10.1042/BJ20040261
43 Desbats, M.A., Morbidoni, V., Silic-Benussi, M., Doimo, M., Ciminale, V., Cassina, M. et al. (2016) The *COQ2* genotype predicts the severity of coenzyme Q_{10} deficiency. *Hum. Mol. Genet.* **25**, 4256–4265, https://doi.org/10.1093/hmg/ddw257
44 Li, W. (2016) Bringing bioactive compounds into membranes: the UbiA superfamily of intramembrane aromatic prenyltransferases. *Trends Biochem. Sci.* **41**, 356–370, https://doi.org/10.1016/j.tibs.2016.01.007
45 Herebian, D., Seibt, A., Smits, S. H.J., Rodenburg, R.J., Mayatepek, E. and Distelmaier, F. (2017) 4-Hydroxybenzoic acid restores CoQ_{10} biosynthesis in human COQ2 deficiency. *Ann. Clin. Transl. Neurol.* **4**, 902–908, https://doi.org/10.1002/acn3.486
46 Baertling, F., Sanchez-Caballero, L., van den Brand, M. A.M., Fung, C.W., Chan, S.H., Wong, V.C. et al. (2018) *NDUFA9* point mutations cause a variable mitochondrial complex I assembly defect. *Clin. Genet.* **93**, 111–118, https://doi.org/10.1111/cge.13089
47 Clarke, C.F., Williams, W. and Teruya, J.H. (1991) Ubiquinone biosynthesis in *Saccharomyces cerevisiae*. Isolation and sequence of *COQ3*, the 3,4-dihydroxy-5-hexaprenylbenzoate methyltransferase gene. *J. Biol. Chem.* **266**, 16636–16644

48 Hsu, A.Y., Poon, W.W., Shepherd, J.A., Myles, D.C. and Clarke, C.F. (1996) Complementation of *coq3* mutant yeast by mitochondrial targeting of the *Escherichia coli* UbiG polypeptide: evidence that UbiG catalyzes both O-methylation steps in ubiquinone biosynthesis. *Biochemistry* **35**, 9797–9806, https://doi.org/10.1021/bi9602932

49 Poon, W.W., Barkovich, R.J., Hsu, A.Y., Frankel, A., Lee, P.T., Shepherd, J.N. et al. (1999) Yeast and rat Coq3 and *Escherichia coli* UbiG polypeptides catalyze both *O*-methyltransferase steps in coenzyme Q biosynthesis. *J. Biol. Chem.* **274**, 21665–21672, https://doi.org/10.1074/jbc.274.31.21665

50 Zhu, Y., Wu, B., Zhang, X., Fan, X., Niu, L., Li, X. et al. (2015) Structural and biochemical studies reveal UbiG/Coq3 as a class of novel membrane-binding proteins. *Biochem. J.* **470**, 105–114, https://doi.org/10.1042/BJ20150329

51 Marbois, B., Gin, P., Faull, K.F., Poon, W.W., Lee, P.T., Strahan, J. et al. (2005) Coq3 and Coq4 define a polypeptide complex in yeast mitochondria for the biosynthesis of coenzyme Q. *J. Biol. Chem.* **280**, 20231–20238, https://doi.org/10.1074/jbc.M501315200

52 Tauche, A., Krause-Buchholz, U. and Rodel, G. (2008) Ubiquinone biosynthesis in *Saccharomyces cerevisiae*: the molecular organization of *O*-methylase Coq3p depends on Abc1p/Coq8p. *FEMS Yeast Res.* **8**, 1263–1275, https://doi.org/10.1111/j.1567-1364.2008.00436.x

53 Xie, L.X., Hsieh, E.J., Watanabe, S., Allan, C.M., Chen, J.Y., Tran, U.C. et al. (2011) Expression of the human atypical kinase ADCK3 rescues coenzyme Q biosynthesis and phosphorylation of Coq polypeptides in yeast *coq8* mutants. *Biochim. Biophys. Acta* **1811**, 348–360, https://doi.org/10.1016/j.bbalip.2011.01.009

54 Jonassen, T. and Clarke, C.F. (2000) Isolation and functional expression of human *COQ3*, a gene encoding a methyltransferase required for ubiquinone biosynthesis. *J. Biol. Chem.* **275**, 12381–12387, https://doi.org/10.1074/jbc.275.17.12381

55 Belogrudov, G.I., Lee, P.T., Jonassen, T., Hsu, A.Y., Gin, P. and Clarke, C.F. (2001) Yeast *COQ4* encodes a mitochondrial protein required for coenzyme Q synthesis. *Arch. Biochem. Biophys.* **392**, 48–58, https://doi.org/10.1006/abbi.2001.2448

56 Marbois, B., Gin, P., Gulmezian, M. and Clarke, C.F. (2009) The yeast Coq4 polypeptide organizes a mitochondrial protein complex essential for coenzyme Q biosynthesis. *Biochim. Biophys. Acta* **1791**, 69–75, https://doi.org/10.1016/j.bbalip.2008.10.006

57 Rea, S.L., Graham, B.H., Nakamaru-Ogiso, E., Kar, A. and Falk, M.J. (2010) Bacteria, yeast, worms, and flies: exploiting simple model organisms to investigate human mitochondrial diseases. *Dev. Disabil. Res. Rev.* **16**, 200–218, https://doi.org/10.1002/ddrr.114

58 Casarin, A., Jimenez-Ortega, J.C., Trevisson, E., Pertegato, V., Doimo, M., Ferrero-Gomez, M.L. et al. (2008) Functional characterization of human *COQ4*, a gene required for Coenzyme Q_{10} biosynthesis. *Biochem. Biophys. Res. Commun.* **372**, 35–39, https://doi.org/10.1016/j.bbrc.2008.04.172

59 Brea-Calvo, G., Haack, T.B., Karall, D., Ohtake, A., Invernizzi, F., Carrozzo, R. et al. (2015) *COQ4* mutations cause a broad spectrum of mitochondrial disorders associated with CoQ_{10} deficiency. *Am. J. Hum. Genet.* **96**, 309–317, https://doi.org/10.1016/j.ajhg.2014.12.023

60 Salviati, L., Trevisson, E., Rodriguez Hernandez, M.A., Casarin, A., Pertegato, V., Doimo, M. et al. (2012) Haploinsufficiency of *COQ4* causes coenzyme Q_{10} deficiency. *J. Med. Genet.* **49**, 187–191, https://doi.org/10.1136/jmedgenet-2011-100394

61 Romero-Moya, D., Santos-Ocana, C., Castano, J., Garrabou, G., Rodriguez-Gomez, J.A., Ruiz-Bonilla, V. et al. (2017) Genetic rescue of mitochondrial and skeletal muscle impairment in an induced pluripotent stem cells model of coenzyme Q_{10} deficiency. *Stem Cells* **35**, 1687–1703, https://doi.org/10.1002/stem.2634

62 Barkovich, R.J., Shtanko, A., Shepherd, J.A., Lee, P.T., Myles, D.C., Tzagoloff, A. et al. (1997) Characterization of the *COQ5* gene from *Saccharomyces cerevisiae*. Evidence for a C-methyltransferase in ubiquinone biosynthesis. *J. Biol. Chem.* **272**, 9182–9188, https://doi.org/10.1074/jbc.272.14.9182

63 Dibrov, E., Robinson, K.M. and Lemire, B.D. (1997) The *COQ5* gene encodes a yeast mitochondrial protein necessary for ubiquinone biosynthesis and the assembly of the respiratory chain. *J. Biol. Chem.* **272**, 9175–9181, https://doi.org/10.1074/jbc.272.14.9175

64 Baba, S.W., Belogrudov, G.I., Lee, J.C., Lee, P.T., Strahan, J., Shepherd, J.N. et al. (2004) Yeast Coq5 C-methyltransferase is required for stability of other polypeptides involved in coenzyme Q biosynthesis. *J. Biol. Chem.* **279**, 10052–10059, https://doi.org/10.1074/jbc.M313712200

65 Dai, Y.N., Zhou, K., Cao, D.D., Jiang, Y.L., Meng, F., Chi, C.B. et al. (2014) Crystal structures and catalytic mechanism of the C-methyltransferase Coq5 provide insights into a key step of the yeast coenzyme Q synthesis pathway. *Acta Crystallogr. Sec. D Biol. Crystallogr.* **70**, 2085–2092, https://doi.org/10.1107/S1399004714011559

66 Lapointe, C.P., Stefely, J.A., Jochem, A., Hutchins, P.D., Wilson, G.M., Kwiecien, N.W. et al. (2018) Multi-omics reveal specific targets of the RNA-binding protein Puf3p and its orchestration of mitochondrial biogenesis. *Cell Syst.* **6**, 125–135.e126

67 Veling, M.T., Reidenbach, A.G., Freiberger, E.C., Kwiecien, N.W., Hutchins, P.D., Drahnak, M.J. et al. (2017) Multi-omic mitoprotease profiling defines a role for Oct1p in coenzyme Q production. *Mol. Cell* **68**, 970–977.e911, https://doi.org/10.1016/j.molcel.2017.11.023

68 Nguyen, T.P., Casarin, A., Desbats, M.A., Doimo, M., Trevisson, E., Santos-Ocana, C. et al. (2014) Molecular characterization of the human COQ5 C-methyltransferase in Coenzyme Q biosynthesis. *Biochim. Biophys. Acta*, https://doi.org/10.1016/j.bbalip.2014.08.007

69 Malicdan, M. C.V., Vilboux, T., Ben-Zeev, B., Guo, J., Eliyahu, A., Pode-Shakked, B. et al. (2018) A novel inborn error of the coenzyme Q_{10} biosynthesis pathway: cerebellar ataxia and static encephalomyopathy due to COQ5 C-methyltransferase deficiency. *Hum. Mutat.* **39**, 69–79, https://doi.org/10.1002/humu.23345

70 Yen, H.C., Liu, Y.C., Kan, C.C., Wei, H.J., Lee, S.H., Wei, Y.H. et al. (2016) Disruption of the human COQ5-containing protein complex is associated with diminished coenzyme Q_{10} levels under two different conditions of mitochondrial energy deficiency. *Biochim. Biophys. Acta* **1860**, 1864–1876, https://doi.org/10.1016/j.bbagen.2016.05.005

71 Gin, P., Hsu, A.Y., Rothman, S.C., Jonassen, T., Lee, P.T., Tzagoloff, A. et al. (2003) The *Saccharomyces cerevisiae COQ6* gene encodes a mitochondrial flavin-dependent monooxygenase required for coenzyme Q biosynthesis. *J. Biol. Chem.* **278**, 25308–25316, https://doi.org/10.1074/jbc.M303234200

72 Ismail, A., Leroux, V., Smadja, M., Gonzalez, L., Lombard, M., Pierrel, F. et al. (2016) Coenzyme Q biosynthesis: evidence for a substrate access channel in the FAD-dependent monooxygenase Coq6. *PLoS Comput. Biol.* **12**, e1004690, https://doi.org/10.1371/journal.pcbi.1004690

73 Ozeir, M., Muhlenhoff, U., Webert, H., Lill, R., Fontecave, M. and Pierrel, F. (2011) Coenzyme Q biosynthesis: Coq6 is required for the C5-hydroxylation reaction and substrate analogs rescue Coq6 deficiency. *Chem. Biol.* **18**, 1134–1142, https://doi.org/10.1016/j.chembiol.2011.07.008

74 Heeringa, S.F., Chernin, G., Chaki, M., Zhou, W., Sloan, A.J., Ji, Z. et al. (2011) *COQ6* mutations in human patients produce nephrotic syndrome with sensorineural deafness. *J. Clin. Invest.* **121**, 2013–2024, https://doi.org/10.1172/JCI45693
75 Ashraf, S., Gee, H.Y., Woerner, S., Xie, L.X., Vega-Warner, V., Lovric, S. et al. (2013) *ADCK4* mutations promote steroid-resistant nephrotic syndrome through CoQ_{10} biosynthesis disruption. *J. Clin. Invest.* **123**, 5179–5189, https://doi.org/10.1172/JCI69000
76 Park, E., Ahn, Y.H., Kang, H.G., Yoo, K.H., Won, N.H., Lee, K.B. et al. (2017) *COQ6* mutations in children with steroid-resistant focal segmental glomerulosclerosis and sensorineural hearing loss. *Am. J. Kidney Dis.* **70**, 139–144, https://doi.org/10.1053/j.ajkd.2016.10.040
77 Gigante, M., Diella, S., Santangelo, L., Trevisson, E., Acosta, M.J., Amatruda, M. et al. (2017) Further phenotypic heterogeneity of CoQ_{10} deficiency associated with steroid resistant nephrotic syndrome and novel *COQ2* and *COQ6* variants. *Clin. Genet.* **92**, 224–226, https://doi.org/10.1111/cge.12960
78 Sheftel, A., Stehling, O. and Lill, R. (2010) Iron-sulfur proteins in health and disease. *Trends Endocrinol. Metab.* **21**, 302–314, https://doi.org/10.1016/j.tem.2009.12.006
79 Sheftel, A.D., Stehling, O., Pierik, A.J., Elsasser, H.P., Muhlenhoff, U., Webert, H. et al. (2010) Humans possess two mitochondrial ferredoxins, Fdx1 and Fdx2, with distinct roles in steroidogenesis, heme, and Fe/S cluster biosynthesis. *Proc. Natl. Acad. Sci. U.S.A.* **107**, 11775–11780, https://doi.org/10.1073/pnas.1004250107
80 Marbois, B.N. and Clarke, C.F. (1996) The *COQ7* gene encodes a protein in *Saccharomyces cerevisiae* necessary for ubiquinone biosynthesis. *J. Biol. Chem.* **271**, 2995–3004, https://doi.org/10.1074/jbc.271.6.2995
81 Jonassen, T., Proft, M., Randez-Gil, F., Schultz, J.R., Marbois, B.N., Entian, K.D. et al. (1998) Yeast Clk-1 homologue (Coq7/Cat5) is a mitochondrial protein in coenzyme Q synthesis. *J. Biol. Chem.* **273**, 3351–3357, https://doi.org/10.1074/jbc.273.6.3351
82 Stenmark, P., Grunler, J., Mattsson, J., Sindelar, P.J., Nordlund, P. and Berthold, D.A. (2001) A new member of the family of di-iron carboxylate proteins. Coq7 (clk-1), a membrane-bound hydroxylase involved in ubiquinone biosynthesis. *J. Biol. Chem.* **276**, 33297–33300, https://doi.org/10.1074/jbc.C100346200
83 Vajo, Z., King, L.M., Jonassen, T., Wilkin, D.J., Ho, N., Munnich, A. et al. (1999) Conservation of the *Caenorhabditis elegans* timing gene *clk-1* from yeast to human: a gene required for ubiquinone biosynthesis with potential implications for aging. *Mamm. Genome* **10**, 1000–1004, https://doi.org/10.1007/s003359901147
84 Lu, T.T., Lee, S.J., Apfel, U.P. and Lippard, S.J. (2013) Aging-associated enzyme human clock-1: substrate-mediated reduction of the diiron center for 5-demethoxyubiquinone hydroxylation. *Biochemistry* **52**, 2236–2244, https://doi.org/10.1021/bi301674p
85 Padilla, S., Tran, U.C., Jimenez-Hidalgo, M., Lopez-Martin, J.M., Martin-Montalvo, A., Clarke, C.F. et al. (2009) Hydroxylation of demethoxy-Q_6 constitutes a control point in yeast coenzyme Q_6 biosynthesis. *Cell. Mol. Life Sci.* **66**, 173–186, https://doi.org/10.1007/s00018-008-8547-7
86 Tran, U.C., Marbois, B., Gin, P., Gulmezian, M., Jonassen, T. and Clarke, C.F. (2006) Complementation of *Saccharomyces cerevisiae coq7* mutants by mitochondrial targeting of the *Escherichia coli* UbiF polypeptide. Two functions of yeast Coq7 polypeptide in coenzyme Q biosynthesis. *J. Biol. Chem.* **281**, 16401–16409, https://doi.org/10.1074/jbc.M513267200
87 Freyer, C., Stranneheim, H., Naess, K., Mourier, A., Felser, A., Maffezzini, C. et al. (2015) Rescue of primary ubiquinone deficiency due to a novel *COQ7* defect using 2,4-dihydroxybensoic acid. *J. Med. Genet.* **52**, 779–783, https://doi.org/10.1136/jmedgenet-2015-102986
88 Wang, Y., Smith, C., Parboosingh, J.S., Khan, A., Innes, M. and Hekimi, S. (2017) Pathogenicity of two *COQ7* mutations and responses to 2,4-dihydroxybenzoate bypass treatment. *J. Cell. Mol. Med.* **21**, 2329–2343, https://doi.org/10.1111/jcmm.13154
89 Brea-Calvo, G., Siendones, E., Sanchez-Alcazar, J.A., de Cabo, R. and Navas, P. (2009) Cell survival from chemotherapy depends on NF-kappaB transcriptional up-regulation of coenzyme Q biosynthesis. *PLoS ONE* **4**, e5301, https://doi.org/10.1371/journal.pone.0005301
90 Cascajo, M.V., Abdelmohsen, K., Noh, J.H., Fernandez-Ayala, D.J., Willers, I.M., Brea, G. et al. (2016) RNA-binding proteins regulate cell respiration and coenzyme Q biosynthesis by post-transcriptional regulation of COQ7. *RNA Biol.* **13**, 622–634, https://doi.org/10.1080/15476286.2015.1119366
91 Martin-Montalvo, A., Gonzalez-Mariscal, I., Padilla, S., Ballesteros, M., Brautigan, D.L., Navas, P. et al. (2011) Respiratory-induced coenzyme Q biosynthesis is regulated by a phosphorylation cycle of Cat5p/Coq7p. *Biochem. J.* **440**, 107–114, https://doi.org/10.1042/BJ20101422
92 Busso, C., Ferreira-Junior, J.R., Paulela, J.A., Bleicher, L., Demasi, M. and Barros, M.H. (2015) Coq7p relevant residues for protein activity and stability. *Biochimie* **119**, 92–102, https://doi.org/10.1016/j.biochi.2015.10.016
93 Martin-Montalvo, A., Gonzalez-Mariscal, I., Pomares-Viciana, T., Padilla-Lopez, S., Ballesteros, M., Vazquez-Fonseca, L. et al. (2013) The phosphatase Ptc7 induces coenzyme Q Biosynthesis by activating the hydroxylase Coq7 in yeast. *J. Biol. Chem.* **288**, 28126–28137, https://doi.org/10.1074/jbc.M113.474494
94 Juneau, K., Nislow, C. and Davis, R.W. (2009) Alternative splicing of *PTC7* in *Saccharomyces cerevisiae* determines protein localization. *Genetics* **183**, 185–194, https://doi.org/10.1534/genetics.109.105155
95 Awad, A.M., Venkataramanan, S., Nag, A., Galivanche, A.R., Bradley, M.C., Neves, L.T. et al. (2017) Chromatin-remodeling SWI/SNF complex regulates coenzyme Q_6 synthesis and a metabolic shift to respiration in yeast. *J. Biol. Chem.* **292**, 14851–14866, https://doi.org/10.1074/jbc.M117.798397
96 Guo, X., Niemi, N.M., Hutchins, P.D., Condon, S.G., Jochem, A., Ulbrich, A. et al. (2017) Ptc7p dephosphorylates select mitochondrial proteins to enhance metabolic function. *Cell Rep.* **18**, 307–313, https://doi.org/10.1016/j.celrep.2016.12.049
97 Stefely, J.A., Reidenbach, A.G., Ulbrich, A., Oruganty, K., Floyd, B.J., Jochem, A. et al. (2015) Mitochondrial ADCK3 employs an atypical protein kinase-like fold to enable coenzyme Q biosynthesis. *Mol. Cell* **57**, 83–94, https://doi.org/10.1016/j.molcel.2014.11.002
98 Stefely, J.A., Licitra, F., Laredj, L., Reidenbach, A.G., Kemmerer, Z.A., Grangeray, A. et al. (2016) Cerebellar ataxia and coenzyme Q deficiency through loss of unorthodox kinase activity. *Mol. Cell* **63**, 608–620, https://doi.org/10.1016/j.molcel.2016.06.030
99 Reidenbach, A.G., Kemmerer, Z.A., Aydin, D., Jochem, A., McDevitt, M.T., Hutchins, P.D. et al. (2018) Conserved lipid and small-molecule modulation of COQ8 reveals regulation of the ancient kinase-like UbiB family. *Cell Chem. Biol.* **25**, 154–165.e111, https://doi.org/10.1016/j.chembiol.2017.11.001

100 Vazquez Fonseca, L., Doimo, M., Calderan, C., Desbats, M.A., Acosta, M.J., Cerqua, C. et al. (2018) Mutations in *COQ8B* (*ADCK4*) found in patients with steroid-resistant nephrotic syndrome alter COQ8B function. *Hum. Mutat.* **39**, 406–414, https://doi.org/10.1002/humu.23376
101 Lagier-Tourenne, C., Tazir, M., Lopez, L.C., Quinzii, C.M., Assoum, M., Drouot, N. et al. (2008) ADCK3, an ancestral kinase, is mutated in a form of recessive ataxia associated with coenzyme Q_{10} deficiency. *Am. J. Hum. Genet.* **82**, 661–672, https://doi.org/10.1016/j.ajhg.2007.12.024
102 Mollet, J., Delahodde, A., Serre, V., Chretien, D., Schlemmer, D., Lombes, A. et al. (2008) *CABC1* gene mutations cause ubiquinone deficiency with cerebellar ataxia and seizures. *Am. J. Hum. Genet.* **82**, 623–630, https://doi.org/10.1016/j.ajhg.2007.12.022
103 Hsieh, E.J., Gin, P., Gulmezian, M., Tran, U.C., Saiki, R., Marbois, B.N. et al. (2007) *Saccharomyces cerevisiae* Coq9 polypeptide is a subunit of the mitochondrial coenzyme Q biosynthetic complex. *Arch. Biochem. Biophys.* **463**, 19–26, https://doi.org/10.1016/j.abb.2007.02.016
104 Duncan, A.J., Bitner-Glindzicz, M., Meunier, B., Costello, H., Hargreaves, I.P., Lopez, L.C. et al. (2009) A nonsense mutation in *COQ9* causes autosomal-recessive neonatal-onset primary coenzyme Q_{10} deficiency: a potentially treatable form of mitochondrial disease. *Am. J. Hum. Genet.* **84**, 558–566, https://doi.org/10.1016/j.ajhg.2009.03.018
105 Hayashi, K., Ogiyama, Y., Yokomi, K., Nakagawa, T., Kaino, T. and Kawamukai, M. (2014) Functional conservation of coenzyme Q biosynthetic genes among yeasts, plants, and humans. *PLoS ONE* **9**, e99038, https://doi.org/10.1371/journal.pone.0099038
106 He, C.H., Black, D.S., Allan, C.M., Meunier, B., Rahman, S. and Clarke, C.F. (2017) Human COQ9 rescues a *coq9* yeast mutant by enhancing coenzyme Q biosynthesis from 4-hydroxybenzoic acid and stabilizing the CoQ-synthome. *Front. Physiol.* **8**, 463, https://doi.org/10.3389/fphys.2017.00463
107 Danhauser, K., Herebian, D., Haack, T.B., Rodenburg, R.J., Strom, T.M., Meitinger, T. et al. (2016) Fatal neonatal encephalopathy and lactic acidosis caused by a homozygous loss-of-function variant in COQ9. *Eur. J. Hum. Genet.* **24**, 450–454, https://doi.org/10.1038/ejhg.2015.133
108 Herebian, D., Seibt, A., Smits, S. H.J., Bunning, G., Freyer, C., Prokisch, H. et al. (2017) Detection of 6-demethoxyubiquinone in CoQ_{10} deficiency disorders: Insights into enzyme interactions and identification of potential therapeutics. *Mol. Genet. Metab.* **121**, 216–223, https://doi.org/10.1016/j.ymgme.2017.05.012
109 Luna-Sanchez, M., Diaz-Casado, E., Barca, E., Tejada, M.A., Montilla-Garcia, A., Cobos, E.J. et al. (2015) The clinical heterogeneity of coenzyme Q_{10} deficiency results from genotypic differences in the *Coq9* gene. *EMBO Mol. Med.* **7**, 670–687, https://doi.org/10.15252/emmm.201404632
110 Allan, C.M., Hill, S., Morvaridi, S., Saiki, R., Johnson, J.S., Liau, W.S. et al. (2013) A conserved START domain coenzyme Q-binding polypeptide is required for efficient Q biosynthesis, respiratory electron transport, and antioxidant function in *Saccharomyces cerevisiae*. *Biochim. Biophys. Acta* **1831**, 776–791, https://doi.org/10.1016/j.bbalip.2012.12.007
111 Barros, M.H., Johnson, A., Gin, P., Marbois, B.N., Clarke, C.F. and Tzagoloff, A. (2005) The *Saccharomyces cerevisiae COQ10* gene encodes a START domain protein required for function of coenzyme Q in respiration. *J. Biol. Chem.* **280**, 42627–42635, https://doi.org/10.1074/jbc.M510768200
112 Busso, C., Bleicher, L., Ferreira, J.R. and Barros, M.H. (2010) Site-directed mutagenesis and structural modeling of Coq10p indicate the presence of a tunnel for coenzyme Q_6 binding. *FEBS Lett.* **584**, 1609–1614, https://doi.org/10.1016/j.febslet.2010.03.024
113 Cui, T.Z. and Kawamukai, M. (2009) Coq10, a mitochondrial coenzyme Q binding protein, is required for proper respiration in *Schizosaccharomyces pombe*. *FEBS J.* **276**, 748–759, https://doi.org/10.1111/j.1742-4658.2008.06821.x
114 Shen, Y., Goldsmith-Fischman, S., Atreya, H.S., Acton, T., Ma, L., Xiao, R. et al. (2005) NMR structure of the 18 kDa protein CC1736 from *Caulobacter crescentus* identifies a member of the START domain superfamily and suggests residues mediating substrate specificity. *Proteins* **58**, 747–750, https://doi.org/10.1002/prot.20365
115 Perocchi, F., Jensen, L.J., Gagneur, J., Ahting, U., von Mering, C., Bork, P. et al. (2006) Assessing systems properties of yeast mitochondria through an interaction map of the organelle. *PLoS Genet.* **2**, e170, https://doi.org/10.1371/journal.pgen.0020170
116 Marchler-Bauer, A., Zheng, C., Chitsaz, F., Derbyshire, M.K., Geer, L.Y., Geer, R.C. et al. (2013) CDD: conserved domains and protein three-dimensional structure. *Nucleic Acids Res.* **41**, D348–D352, https://doi.org/10.1093/nar/gks1243
117 Rossmann, M.G., Moras, D. and Olsen, K.W. (1974) Chemical and biological evolution of nucleotide-binding protein. *Nature* **250**, 194–199, https://doi.org/10.1038/250194a0
118 Pagliarini, D.J., Calvo, S.E., Chang, B., Sheth, S.A., Vafai, S.B., Ong, S.E. et al. (2008) A mitochondrial protein compendium elucidates complex I disease biology. *Cell* **134**, 112–123, https://doi.org/10.1016/j.cell.2008.06.016
119 Hirst, J. (2011) Why does mitochondrial complex I have so many subunits? *Biochem. J.* **437**, e1–e3, https://doi.org/10.1042/BJ20110918
120 Stroud, D.A., Formosa, L.E., Wijeyeratne, X.W., Nguyen, T.N. and Ryan, M.T. (2013) Gene knockout using transcription activator-like effector nucleases (TALENs) reveals that human NDUFA9 protein is essential for stabilizing the junction between membrane and matrix arms of complex I. *J. Biol. Chem.* **288**, 1685–1690, https://doi.org/10.1074/jbc.C112.436766
121 Leshinsky-Silver, E., Lev, D., Tzofi-Berman, Z., Cohen, S., Saada, A., Yanoov-Sharav, M. et al. (2005) Fulminant neurological deterioration in a neonate with Leigh syndrome due to a maternally transmitted missense mutation in the mitochondrial ND3 gene. *Biochem. Biophys. Res. Commun.* **334**, 582–587, https://doi.org/10.1016/j.bbrc.2005.06.134
122 van den Bosch, B.J., Gerards, M., Sluiter, W., Stegmann, A.P., Jongen, E.L., Hellebrekers, D.M. et al. (2012) Defective NDUFA9 as a novel cause of neonatally fatal complex I disease. *J. Med. Genet.* **49**, 10–15, https://doi.org/10.1136/jmedgenet-2011-100466
123 Kuhl, I., Miranda, M., Atanassov, I., Kuznetsova, I., Hinze, Y., Mourier, A. et al. (2017) Transcriptomic and proteomic landscape of mitochondrial dysfunction reveals secondary coenzyme Q deficiency in mammals. *Elife* **6**, https://doi.org/10.7554/eLife.30952
124 Yubero, D., Montero, R., Martin, M.A., Montoya, J., Ribes, A., Grazina, M. et al. (2016) Secondary coenzyme Q_{10} deficiencies in oxidative phosphorylation (OXPHOS) and non-OXPHOS disorders. *Mitochondrion* **30**, 51–58, https://doi.org/10.1016/j.mito.2016.06.007

CHAPTER 2

Chemical synthesis and biochemical assays of farnesylated analogs of selected intermediates postulated to play a role in Coenzyme Q biosynthesis in *Saccharomyces cerevisiae*

Author contributions: Anish Nag, Jennifer N. Shepherd, Ohyun Kwon, and Catherine F. Clarke contributed to the intellectual development of the project described and the chemical synthesis of compounds. Anish Nag, Cuiwen He, and Catherine F. Clarke contributed to the studies involving yeast and the HPLC-MS/MS analysis. Anish Nag contributed to the data acquisition, characterization, and error analysis. Anish Nag and Catherine F. Clarke contributed to the writing and revision of the chapter.

Introduction:

Ubiquinone, (also known as Coenzyme Q, CoQ or simply Q), is a lipid with an essential role in the mitochondrial electron transport chain of eukaryotes as well as cellular respiration in the plasma membrane of prokaryotes (1). The structure of Q consists of a benzenoid head group moiety that resembles a fully substituted quinone, and a hydrophobic isoprenoid tail that can vary in length and the number of isoprene units constituting it, depending on the species in which it is found. The quinone group undergoes reversible electron transfers, and can interchange between the fully oxidized quinone and the fully reduced quinol (Figure 1). At the same time, the isoprenoid lipophilic tail functions to anchor Q in the membrane. In eukaryotes, Q performs the critical role of shuttling electrons from either Complex I or Complex II to Complex III/*bc*1 complex. The transfer of electrons from Q to the bc_1 complex is coupled to a proton gradient that is set up across the membrane via the Q cycle mechanism that was first proposed by Mitchell (2).

The redox properties of Q also allow it to function as a lipid soluble chain terminating antioxidant. Q functions either directly, by scavenging lipid peroxyl radicals (4), or indirectly, by discarding α-tocopherol radicals to regenerate α-tocopherol (5, 6). Additionally, Q protects cell and cell organelles from damage caused by the autoxidation of polyunsaturated fatty acids and other oxidative stress (7). Q is present in many eukaryotic intracellular membranes, which include the plasma membrane, wherein it is capable of scavenging ascorbate free radicals in conjunction with the plasma membrane electron transport chain (8, 9). In the plasma membrane of prokaryotes, Q participates in the maintenance and function of the catalytic activity of

DsbA/DsbB disulfide bond forming proteins and enzymes (10), and Q-deficient *Escherichia coli* (*E. coli*) strains are hypersensitive to thiol exposure.

The biosynthesis of Q (Figure 2) as hypothesized in 2010, involved a series of intermediates, starting from either 4-hydroxy benzoic acid (4HB) or para amino benzoic acid (pABA), in the case of yeast (3). The pathway was conceived from the characterization of accumulating Q biosynthetic intermediates in studies with *Saccharomyces cerevisiae* (12) and *E. coli* (13) Q-deficient mutants (17). Coq8 over-expression (*hcCOQ8*) in certain *coq null* strains led to the accumulation of novel intermediates, which suggested the existence of branches in the Q biosynthetic pathway. For example, in the presence of hcCOQ8, *coq6* or *coq9 null* mutants accumulated 4-AP (derived from pABA), and 4-HP (derived from 4HB), indicating that in some cases decarboxylation and hydroxylation at position 1 of the ring might occur before the Coq6 hydroxylation step. Other intermediates that were found to accumulate were demethyl demethoxy Q_6 ($DDMQ_6$), imino demethyl demethoxy Q_6 ($IDDMQ_6$), demethoxy Q_6 (DMQ_6), and imino demethoxy Q_6 ($IDMQ_6$). The exact mechanism by which the pathway deriving from pABA converges with that deriving from 4HB is unknown. It was postulated and previously published that a potential Schiff base mechanism chemistry is responsible for the deamination and hydroxylation of the phenyl ring of pABA as shown by the purple dotted lines in Figure 2 (18). Moreover the exact role of some of the aforementioned intermediates in overall Q biosynthesis was unknown. Two such intermediates are 4-HP and 4-AP. An approach to gather further insight into the role of these intermediates as well as the convergence of the pathway originating from pABA with that originating from 4HB, involves generation of farnesylated analogs of these intermediates. Farnesylated analogs where the isoprenoid tail is substituted for a

farnesyl tail instead of a hexaprenyl one, have previously been used for various tests studies (14, 15). In particular, it has been demonstrated that farnesylated analogs of Q intermediates are converted to Q_3 in *R. rubrum* (16). In this current study, the intermediates 2-farnesyl-4-hydroxyphenol (4-HFP), demethyl demethoxy Q_3 ($DDMQ_3$), demethoxy Q_3 (DMQ_3) and imino demethyl demethoxy Q_3H_2 ($IDDMQ_3H_2$) were chemically synthesized and used in biochemical feeding assays on *Saccharomyces cerevisiae* wild type strains. Thus we are trying to further characterize the pathway of Q biosynthesis in yeast, by analyzing whether these intermediates are converted to Q_3 by wild type yeast strains via subsequent HPLC-MS/MS analysis.

Results:

Based on the previously investigated approach to synthesize the farnesylated analogs of Q intermediates (14, 15), a Stille coupling reaction to attach the farnesyl "tail" on the corresponding brominated substrates was devised. Attempts made to synthesize 2-bromo-4-hydroxyphenol **1,** the corresponding brominated starting material through Stille coupling for 4-HFP, by direct bromination of hydroquinone **2** (Scheme 1**)**, was unsuccessful and **1** could not be isolated.

Therefore **1** was commercially obtained and was subjected to an acetylation reaction (Scheme 2**)**. It was treated with acetic anhydride, triethyl amine and catalytic amounts of N,N-dimethyl aminopyridine to give the acetylated product **3**.

The tributyl farnesyl stannane **4** required for the Stille coupling was prepared by treating commercially available trans,trans- farnesyl chloride **5**, with tributyltin hydride and LDA (11), (Scheme 3). The Stille coupling was then carried out on **3**, using tetrakis triphenylphosphine palladium (0) catalyst, to give the farnesylated product **6** (Scheme 4).

Compound **6** was then deacetylated by basic hydrolysis with potassium carbonate, to give the required 4-HFP (Scheme 5**)**. Stronger basic hydrolysis conditions involving lithium hydroxide under reflux, seemed to decompose the starting material **6**. The 4-HFP thus synthesized was stored under argon at -20 ^{o}C and was found to be susceptible to auto-oxidation to the corresponding quinone. However, either the hydroquinone or the quinone is a suitable substrate for testing in feeding assays with yeast, so steps were not taken to prevent the auto-oxidation of 4-HFP.

Simultaneously a strategy was designed to synthesize 4-amino-3-bromo-6-methoxyphenol **7** that would serve as the brominated starting material for coupling with tributyl farnesyl stannane to give IDDMQ$_3$H$_2$ (19) (Scheme 6). Commercially available 3,5-difluorophenol **8** was treated with concentrated nitric acid to give the nitrated product **9**. The phenol was then treated with chloromethyl methyl ether, in presence of N,N-diisopropylethylamine, to give the acetal protected product **10**. This was then treated with ammonia solution in methanol to give the amine **11**, which on treatment with t-butyl nitrite and copper (I) bromide, undergoes a Sandmeyer type reaction to give the brominated product **12**. This when treated with sodium methoxide solution (25 wt% in methanol), gives the methoxy benzene product **13**. Subsequent deprotection with trifluoroacetic acid gives the phenol **14**, which on reduction gives our required product **7**. The

bromobenzene **7** was then directly subjected to the Stille coupling with tributyl farnesyl stannane, without acetylating it first, in order to minimize the total number of steps required and also to reduce possible losses in yield (Scheme 7). Coupling of **7** with tributyl farnesyl stannane, catalyzed by tetrakis triphenylphosphine palladium (0) yielded the required $IDDMQ_3H_2$. The final product was stored under argon at -20 ^oC. However, it was found to be extremely prone to decomposition and the overall synthesis had to be reattempted a second time in order to use fresh stocks of $IDDMQ_3H_2$ in the subsequent yeast feeding studies.

A scheme was also set up for synthesizing $DDMQ_3$ starting from vanillin **15** (Scheme 8) (14). Vanilin **18**, was brominated to give **19**, which was oxidized through a Dakin type oxidation approach into **20**. This was then acetylated to give **21**, which was subjected to the Stille coupling step with tributyl farnesyl stannane to give **22**, which yielded **$DDMQ_3$** on deacytalion and basic work up with 1M NaOH.

DMQ_3 was synthesized from the commercially available compound **23** (Scheme 9) (14). Oxidation of **23** was carried out using Fremy's salt to yield the quinone **24**. Subsequent condensation of the quinone **24** in presence of boron trifluoride etherate and farnesol yielded the required product **DMQ3**.

Subsequently tests were carried out using the four synthetic farnesylated analogs 4-HFP, $DDMQ_3$, DMQ_3, and $IDDMQ_3H_2$ on WT yeast in order to assess the conversion of the analogs into Q_3. BY4741 WT and W303 WT were fed EtOH solutions of the analogs at a final concentration of 10 µM. The samples were collected at periodic time points after addition of

treatment and subsequently the lipid content of the samples were extracted. The lipid extracts were prepared for reverse phase analysis by HPLC-MS/MS and were injected into a 4000 Qtrap. Standards of the analogs $DDMQ_3$ (Figure 3) and DMQ_3 (Figure 4), and the Q species Q_3 (Figure 5) and Q_6 (Figure 6) produced characteristic chromatograms when analyzed via reverse phase HPLC-MS/MS. Subsequent Q content analysis of the yeast samples showed almost 1000-fold higher Q_3 levels in both the BY4741 and W303 strains that were treated with DMQ_3 versus those treated with $DDMQ_3$ (Figure 7, A and B). There was also a time dependent increase in Q_3 levels with the samples collected at 48 hour time point showing the highest values of Q_3. The total $DDMQ_3$ and DMQ_3 contents in the samples were also analyzed and it was observed that both the yeast strains had almost 100-fold higher DMQ_3 levels when treated with DMQ_3 compared to $DDMQ_3$ levels when treated with $DDMQ_3$ (Figure 8, A and B). There was also a steady decrease in the levels of both the intermediate analogs during the later time points. Q_3 was not detected in both BY4741 WT and W303 WT yeast treated with 4-HFP and $IDDMQ_3H_2$ separately (data not shown). Q_3 was also not detected in the EtOH treated vehicle control samples (data not shown). Steady state endogenous Q_6 content was also measured and intriguingly it was observed that the $DDMQ_3$ treated samples had lower Q_6 content compared with the DMQ_3 treated samples (Figure 9, A and B). This effect was especially pronounced in the W303 WT compared to the BY4741 WT yeast. The Q_6 content was seen to decrease over time in both the yeast strains and both treatment conditions. The levels for DMQ_6 and $DDMQ_6$ were not significantly different in the yeast treated with EtOH serving as vehicle control (Figure 10, A and B).

Discussion:

In order to further characterize the biosynthetic pathway of Q in yeast, a number of intermediates that were previously shown to accumulate in *coq* null strains were targeted. Farnesylated analogs of these intermediates were chemically synthesized. These synthetic analogs thus obtained were 4-HFP, $DDMQ_3$, DMQ_3 and $IDDMQ_3H_2$. The primary synthetic route employed to achieve the final compounds, involved modifications and derivatizations of phenyl rings to obtain the required substituents in the correct positions on the ring. The penultimate step generally involved a Stille coupling reaction that was employed to attach the farnesyl tail in the right position replacing a bromine on the ring. In the case of 4-HFP synthesis, direct bromination of hydroquinone was unsuccessful, possibly due to auto-oxidation of hydroquinone into the fully oxidized quinone which would in turn not support the Friedel-Craft's bromination of the aryl ring and also is prone to polymerization. The synthesis of DMQ_3 differed from the rest of the analogs, because of the absence of the Stille coupling reaction. Instead a boron trifluoride mediated enone condensation reaction was utilized to attach the farnesyl tail at the required position on the ring.

4-HFP was highly prone to aerial auto-oxidation. However, measures were not taken to prevent oxidation since yeast is capable of uptaking and utilizing both the oxidized and reduced intermediates of Q. All the intermediate analogs thus synthesized, were stored under argon at -20 ^{o}C. However, despite these measures $IDDMQ_3H_2$ was found to be extremely susceptible to decomposition. Hence, fresh synthesis was required for immediate use in yeast feeding assays.

BY4741 WT and W303 WT yeast strains were selected for the feeding assays with the synthetic intermediate analogs. The analogs were dissolved in EtOH and were added to the yeast samples at a final concentration of 10 µM such that the final volume of EtOH that was added remained consistent in all the samples. The same volume of EtOH was added in the samples serving as vehicle control. Q_3 levels detected in the yeast treated with both DMQ_3 and DDMQ3 increased consistently with time. This is expected since Q_3 is not the naturally occurring Q in yeast, and therefore the cells would be more efficient at producing Q_6 instead at earlier periods of growth. Q_3 contents were also observed to be 1000-fold higher in the yeast treated with DMQ_3 than those treated with $DDMQ_3$. One possibility for explaining this observation is the electrophilic stress that can be created by $DDMQ_3$ on the yeast, due to the potential role that $DDMQ_3$ can play as an electrophile in Michael addition type reactions with cellular nucleophiles. This assumption can be further supported by the much higher uptake of DMQ_3 by both the WT yeast strains compared with $DDMQ_3$. In addition, Q_6 levels were also observed to be lower in the $DDMQ_3$ treated samples, further supporting the potential toxicity of this particular molecule. No Q_3 was observed in the cells treated with 4-HFP and $IDDMQ_3H_2$. This result can also be explained by the possible toxicity and electrophilic stress created by these two molecules. Additionally, there is the possibility that these molecules are not viable intermediates that get converted to Q, and are instead merely dead-end intermediates along the Q biosynthetic pathway branch points. The Q_6 content was observed to decrease with time. This result has been previously observed as well, however, there aren't any clear explanation to explain this observation. One possibility is that the yeast cell walls become more rigid and impermeable with time, which would make the cells harder to lyse during the lipid extraction step. This can consequently decrease the cellular lipids

that are actually extracted. Possible solutions to avoid this would be to use beads when lysing the cells with methanol and to use longer and more vigorous vortex conditions.

A concurrent and independent study led by Dr. Fabien Pierrel showed that the deamination of the phenyl ring of pABA occurs further upstream than our original postulate (21). They utilized stable isotope labeled $H_2{}^{18}O$ to demonstrate that water plays a nucleophilic role in the deamination and hydroxylation of the C-4 position on the ring of pABA, a process which in turn is catalyzed by Coq6. Thus at that point there wasn't enough evidence supporting the theory that the deamination of pABA occurs via a Schiff base mediated chemistry. Further efforts to verify this premise can be undertaken in the future by utilizing intermediate analogs that can potentially avoid causing electrophilic stress and toxicity on the yeast.

Materials and methods:

Chemical synthesis of Q intermediates

All reagents for organic synthesis were purchased from Aldrich and used as received unless otherwise stated. Dichloromethane, hexamethylphosphoric triamide, and triethylamine were distilled from calcium hydride. Unless specified as dry, the solvents were of unpurified reagent grade. All air- or water-sensitive reactions were carried out under positive pressure of argon in oven-dried glassware. Reactions were followed by TLC using Whatman precoated plates of silica gel 60 with fluorescent indicator (0.25 mm). Reactions forming quinones were followed by leucomethylene blue stain. Flash chromatography was performed on Davisil Grade 643 silica gel (230–400 mesh). NMR spectra were measured on a Bruker AM360, ARX400, or ARX500

spectrometer and were recorded in ppm using the solvent signal as an internal standard. Mass spectra and high resolution mass spectra were recorded on a VG Autospec and are reported in units of mass to charge (*m*/*z*). High resolution mass spectra were re-corded with an EI source. Yeast media and supplies were obtained from Thermo Fischer Scientific.

*Synthesis of 1,4-diacetoxy-2-bromobenzene **3***: The synthesis of **3** was carried out using methods similar to those highlighted in (14). Briefly 2-Bromo-4-hydroxyphenol (216 mg, 1.15 mmol) was suspended in CH_2Cl_2 (2.5 ml). Triethylamine (0.56 ml, 4.12 mmol) and acetic anhydride (0.33 ml, 3.44 mmol) were then added, followed by 4-(dimethylamino) pyridine (15 mg). The reaction was allowed to proceed for 7 hours at room temperature. The reaction was quenched with NH_4Cl, and the CH_2Cl_2 was removed *in vacuo*. The residue was extracted with ethyl acetate (2 X 5 ml), and the combined extracts were washed with brine (5 ml), dried over $MgSO_4$, filtered, and concentrated. Flash chromatography (*R* factor = 0.3, 8:2 hexanes/ethyl acetate) was performed to obtain 255 mg (94% yield) colorless oil **3**. ^{1}H NMR ($CDCl_3$, 360 MHz) δ: 2.22 (s, 3H); 2.28 (s, 3H); 6.58 (m, 2H); 6.95 (s, 1H). ^{13}C NMR ($CDCl_3$, 90 MHz)
δ: 20.21; 20.82; 105.65; 116.73; 117.19; 135.56; 148.66; 152.48; 167.65; 168.73. HRMS Calcd for $[C_{10}H_9BrO_4]^+$: 271.97. Found: 271.98.

*Synthesis of tributyl farnesyl stannane **4***: The synthesis of **4** was carried out using commercially available **5** as the starting material according to (11).

Synthesis of 1,4-diacetoxy-2-farnesylbenzene ***6***: The synthesis of **6** was carried out using methods similar to those highlighted in (14). Briefly, Tetrakis(triphenylphosphine) palladium (0) ($(Pd(PPh_3)_4$; 23 mg, 0.020 mmol) was dissolved in hexamethylphosphoric triamide (HMPA; 1.0 ml), in a Schlenk tube under argon in a glove box. Compound **3** (273 mg, 1.00 mmol) was dissolved in HMPA (1.0 ml), and the resulting solution was added via syringe to the solution

containing $Pd(PPh_3)_4$. A solution of **4** (743 mg, 1.5 mmol) dissolved in HMPA (1.5 ml) was then added to this reaction mixture. The reaction vessel was sealed under argon, removed from the glove box, and heated at 65 °C in a sand bath for 48 h. The reaction was then quenched with saturated NH_4Cl (3 ml) and extracted with ether (3 X 5 ml). The ethereal layers were washed with H_2O (5 ml) and brine (5 ml), dried over $MgSO_4$, filtered, and concentrated. Flash chromatography was performed (*R* factor = 0.5, 9:1 hexanes/ethyl acetate) to give 118 mg (45% yield) of pale yellow oil 1,4-diacetoxy-2-farnesyl-benzene **6**. ^{1}H NMR ($CDCl_3$, 360 MHz) δ: 1.57 (s, 6H); 2.01 (m, 8H); 2.22 (s, 3H); 2.28 (s, 3H); 3.20 (d, 2H, *J* = 7.2 Hz); 5.05 (m, 2H); 5.15 (m, 1H); 6.45 (m, 2H); 6.50 (s, 1H). ^{13}C NMR ($CDCl_3$, 90 MHz) δ: 13.45; 15.83; 16.10; 17.11; 17.42; 20.59; 21.01; 25.41; 26.32; 26.37; 26.69; 27.49; 28.51; 39.53; 39.64; 104.00; 113.69; 120.21; 123.57; 124.23; 131.11; 135.05; 135.49; 135.60; 137.32; 148.47; 151.49; 168.63; 169.32. HRMS Calcd for $[C_{25}H_{34}O_4]^+$: 398.2563. Found: 398.2571.

*Synthesis of 2-farnesyl-4-hydroxyphenol **4-HFP***: The synthesis of 4-HFP was carried out using methods similar to those highlighted in (14). Briefly $LiAlH_4$ (67 mg, 1.75 mmol) was suspended in ether (5 ml) and cooled to 0 °C. 1,4-diacetoxy-2-farnesylbenzene (130 mg, 0.350 mmol) was dissolved in ether (10 ml) and added dropwise to the suspension. The resulting reaction mixture was stirred for 1 hour. The reaction was quenched with water (5 ml) and then 1 M NaOH (5 ml), followed by water (5 ml) and allowed to warm to room temperature. A colorless precipitate formed and was extracted with ether (2 X 15 ml), and the combined ethereal extracts were washed with brine (30 ml), dried over $MgSO_4$, filtered, and concentrated. The expected hydroquinone was oxidized during basic work-up, and a brown oil **4-HFP** was obtained (82 mg, 80% yield). ^{1}H NMR ($CDCl_3$, 360 MHz) δ: 1.55 (s, 6H); 1.58 (s, 3H); 1.63 (s, 3H); 2.00 (m, 8H); 3.08 (d, 2H, *J* = 7.2 Hz); 5.06 (m, 2H); 5.13 (m, 1H); 5.85 (m, 2H); 6.22 (s, 1H). ^{13}C NMR

($CDCl_3$, 90 MHz) δ: 15.96; 16.08; 17.60; 25.63; 26.32; 26.61; 27.07; 39.56; 39.61; 101.01; 117.62; 123.67; 124.27; 131.18; 132.73; 135.33; 140.05; 146.34; 158.80; 182.11; 187.64. HRMS Calcd for $[C_{21}H_{28}O_2]^+$: 312.219. Found: 312.218.

Synthesis of 4-amino-5-farnesyl-3-methoxyphenol ***IDDMQ$_3$H$_2$***: First **7** was synthesized according to (19) with no modifications. **7** was then subjected to Stille coupling similar to the synthesis of **6** to obtain **IDDMQ$_3$H$_2$** as a brown oil (65 mg, 39% yield). ^{1}H NMR ($CDCl_3$, 360 MHz) δ: 1.66 (s, 6H); 1.78 (s, 3H); 2.03 (s, 3H); 2.15 (m, 8H); 3.18 (d, 2H, J = 7.2 Hz); 3.75 (s, 3H); 5.26 (m, 2H); 5.33 (m, 1H); 6.15 (s, 1H); 6.32 (s, 1H). ^{13}C NMR ($CDCl_3$, 90 MHz) δ: 17.96; 18.08; 18.60; 25.69; 26.72; 27.61; 28.07; 40.56; 40.61; 62.69; 111.01; 119.62; 124.67; 126.27; 132.18; 133.73; 137.33; 142.05; 148.34; 168.80; 172.11; 188.64. HRMS Calcd for $[C_{22}H_{31}O_2]^+$: 297.212. Found: 297.212.

Synthesis of 2-methoxy-6-farnesyl-1,4-benzoquinone ***DDMQ$_3$***: The synthesis of $DDMQ_3$ was carried out according to (14) without any modification.

Synthesis of 2-methoxy-6-farnesyl-5-methyl-1,4-benzoquinone ***DMQ$_3$***: The synthesis of DMQ_3 was carried out according to (14) without any modification.

Yeast strains and growth media

Sachharomyces cerevisiae wild type strains from two different genetic backgrounds were used: BY4741 (MAT a *his3Δ0 leu2Δ0 met15Δ0 ura3Δ0*) and W3031B (MAT α *ade2-1 his3-1,15 leu2-3,112 trp1-1 ura3-1*). YPD medium (2% dextrose, 1% yeast extract and 2% peptone) was prepared as described (20). Solid plate medium included the stated components plus 2% Bacto agar.

Preparation of stock solutions for compounds added

The synthetic analogs 4-HFP, $DDMQ_3$, DMQ_3 and $IDDMQ_3H_2$ were freshly dissolved in absolute EtOH. The concentration of each stock solution thus obtained were adjusted so that addition of 9 µL of each corresponding EtOH stock solution in 6 mL YPD liquid media would result in a final concentration of 10 µM for each compound.

Farnesylated analogs feeding assay

Yeast colonies from YPD plate medium were first inoculated into 125 mL Erlenmeyer flasks containing 30 mL YPD liquid medium. Following overnight incubation with shaking (250 rpm) at 30 ^oC, the yeast cells were inoculated into fresh 6mL liquid YPD medium in 18x150 mm borosilicate test tubes. The inoculation was performed so that the final OD_{600} of the yeast cells in 6mL liquid YPD medium in each test tube is 0.1. The tubes with the yeast were further incubated by shaking (250 rpm) at 30 ^oC slanted at a 45^o angle. The OD_{600} the yeast cultures in the test tubes were monitored till an OD_{600} of 0.5 was reached. At that time point 9 µL of the EtOH stock solutions of the compounds of interest were added to the tubes. The tubes with the yeast were incubated with shaking under the same conditions as mentioned previously. At 4, 8, 12, 24, and 48 hours after addition of the treatments, the tubes were removed from the incubator. The OD_{600} at each time point for each yeast sample was measured, 5mL of the vortexed liquid yeast culture was withdrawn into fresh 10mL centrifuge tubes. The tubes were centrifuged at 3000xg rpm for 5 minutes, and the liquid media was aspirated out to obtain yeast cell pellets. The pellets thus obtained were stored at -20 ^oC. The experiment was conducted in triplicates for each time point, yeast strain and treatment added.

Lipid extraction of yeast cell pellets

Lipid extractions of the yeast cell pellets were performed similar to the description in (17). Briefly the cell pellets were thawed on ice and then suspended in 2 ml of methanol Q_4 was added as an internal standard for the determination of Q_6 content in the lipid extracts. The tubes were vortexed at maximum intensity for 30 seconds followed by addition of 2 mL of petroleum ether. This was followed by another round of vortex as before, after which the upper petroleum ether layer was removed from the phase boundary and transferred to a fresh tube. The petroleum ether addition, vortex, and removal of the upper petroleum ether layer was repeated for a total of two cycles. The petroleum ether solutions were consolidated for each sample, and the solvent was evaporated under a stream of nitrogen gas.

HPLC-MS/MS analysis to measure Q and Q intermediates

The HPLC-MS/MS analysis to quantify Q from the yeast lipid extracts previously obtained was carried out as described in (17). Briefly, the dry lipid extracts were first resuspended in 200 µL benzoquinone solution (0.1 mg/mL in EtOH). This was done to ensure complete oxidation of all the lipids which simplifies the subsequent detection and quantification process. a 4000 QTRAP linear MS/MS spectrometer from Applied Biosystems (Foster City, CA) was used. Applied Biosystem software, Analyst version 1.4.2, was used for data acquisition and processing. A binary HPLC solvent delivery system was used with a Luna phenyl-hexyl column (particle size 5 µm, 100 × 4.60 mm; Phenomenex) for yeast cell lipid extracts. The mobile phase consisted of solvent A (methanol:isopropanol, 95:5, with 2.5 mM ammonium formate) and solvent B (isopropanol, 2.5 mM ammonium formate). For separation of yeast quinones, the percentage of solvent B increased linearly from 0 to 5% over 6 min, and the flow rate increased from 600 to 800 µL/ min. The flow rate and mobile phase were linearly changed back to initial condition by

7 min. All samples were analyzed in multiple reaction monitoring mode; multiple reaction monitoring transitions were as follows: *m/z* 591/197.1 (Q_6); *m/z* 608/197.1 (Q_6 with ammonium adduct); *m/z* 387/197.1 (Q_3); *m/z* 404/197 (Q_3 with ammonium adduct); *m/z* 357/167.1 (DMQ_3); *m/z* 174/167.1 (DMQ_3 with ammonium adduct); *m/z* 342.2/153.1 ($DDMQ_3$); *m/z* 359.2/153.1 ($DDMQ_3$ with ammonium adduct).

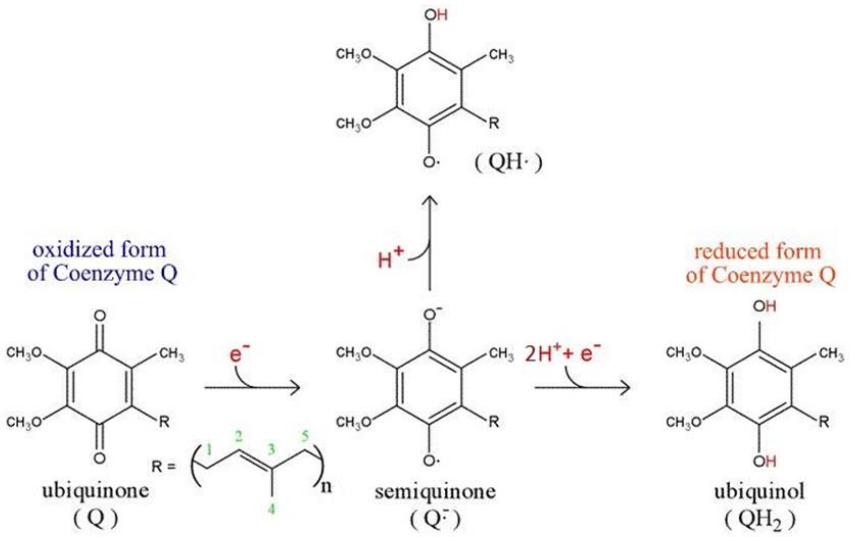

Figure 1. Reversible oxidation of Q. Coenzyme Q can undergo transformation from the fully oxidized ubiquinone form to the fully reduced ubiquinol form via a semi-oxidized semiquinone radical intermediate. The polyisoprenoid tail is represented by R, where the value of *n* specifies the number of isoprene units and can range from 6 to 10 in living species.

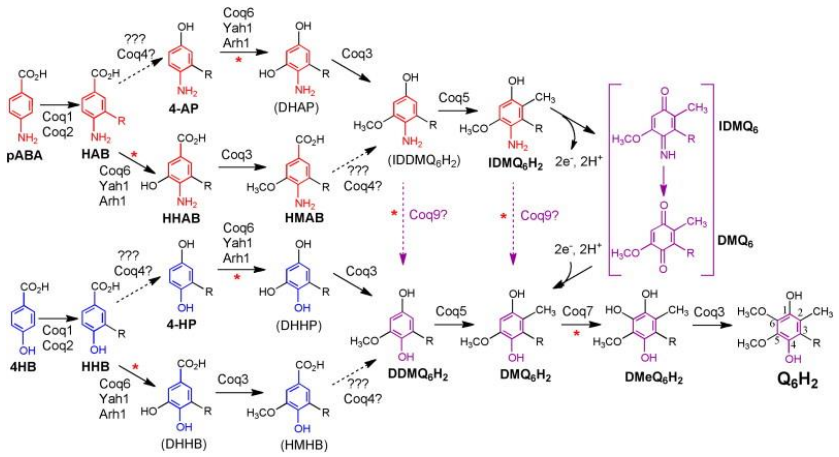

Figure 2. Previously postulated Q_6 biosynthetic pathway in *S. cerevisiae*. The Q biosynthetic pathway is shown in *blue* oroginating from 4HB (4-hydroxybenzoic acid). Alternatively, the *red* pathway indicates that pABA (*para*-aminobenzoic acid) is utilized as the ring precursor for Q. In the presence of hcCOQ8, *coq6* or *coq9* null mutants accumulate 4-AP (deriving from pABA), and 4-HP (deriving from 4HB). *Purple dotted arrows* illustrate the replacement of the C4-amine with a C4-hydroxyl and correspond to a proposed C4-deamination/deimination reaction, resulting in the convergence of the 4HB and pABA pathways. A possible mechanism to replace the C4-imino group with the C4-hydroxy group is shown in *purple brackets* for $IDMQ_6$ but could also occur on $IDDMQ_6$ (*not shown*). Several steps defective in the *coq9 null* strain are designated with *red asterisks*. Intermediates previously detected are shown in bold: 4-AP (3-hexaprenyl-4-aminophenol); $DDMQ_6H_2$, the reduced form of demethyl-demethoxy-Q_6; DMQ_6, demethoxy-Q_6; DMQ_6H_2, demethoxy-Q_6H_2 (the reduced form of DMQ_6); HHAB, 3-hexaprenyl-5-hydroxy-4-aminobenzoic acid; HMAB, 3-hexaprenyl-5-methoxy-4-aminobenzoic acid; 4-HP (3-hexaprenyl-4-hydroxyphenol); $IDMQ_6$, (4-imino-demethoxy-Q_6); $IDMQ_6H_2$, 4-amino demethoxy-Q_6H_2 (the reduced form of $IDMQ_6$). Parentheses designate intermediates that have not been detected yet (18).

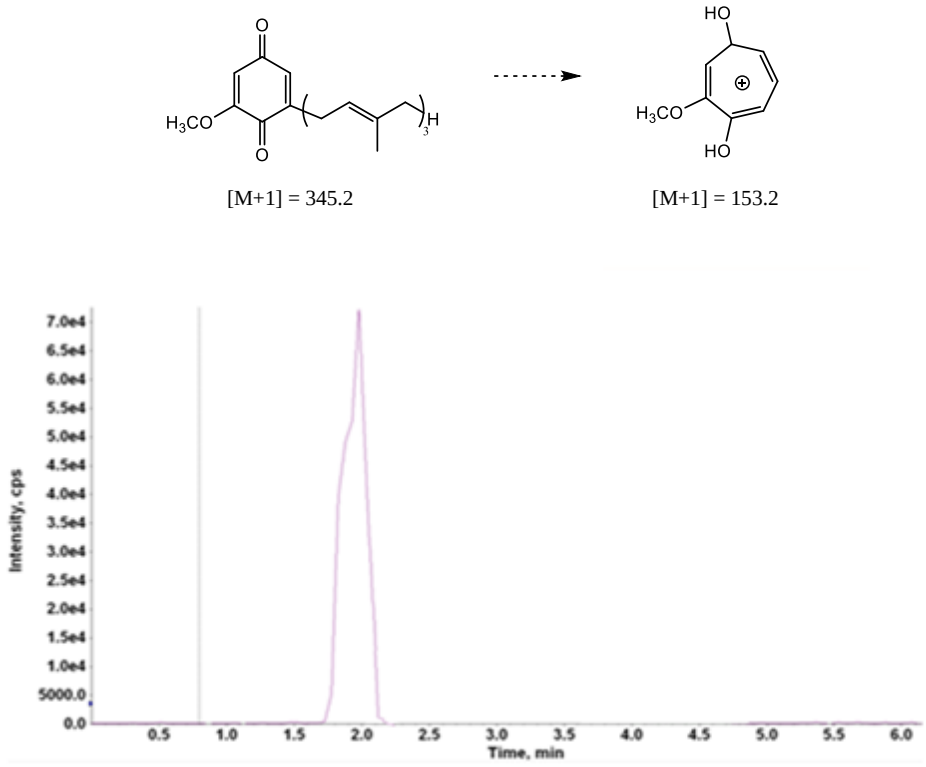

Figure 3. Chromatogram obtained from the HPLC-MS/MS analysis of DDMQ$_3$ standard.

The transition detected between the precursor and the product tropylium cation is shown.

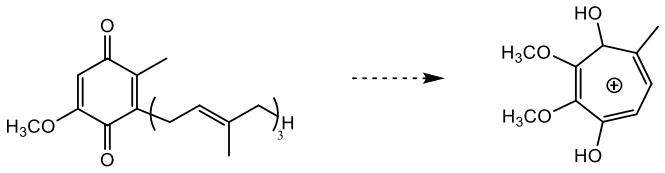

[M+1] = 357.2 [M+1] = 167.2

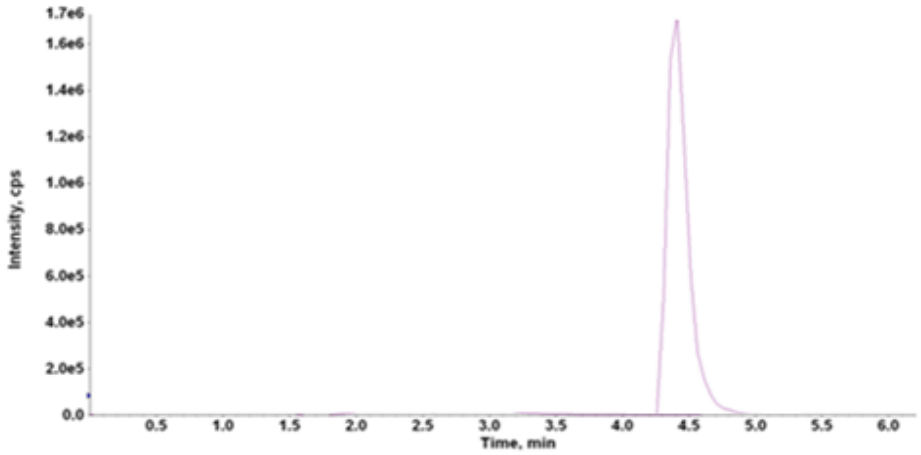

Figure 4. Chromatogram obtained from the HPLC-MS/MS analysis of DMQ_3 standard.

The transition detected between the precursor and the product tropylium cation is shown.

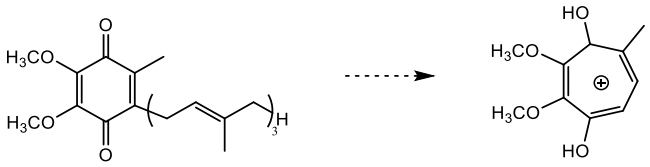

[M+1] = 387.2 [M+1] = 197.1

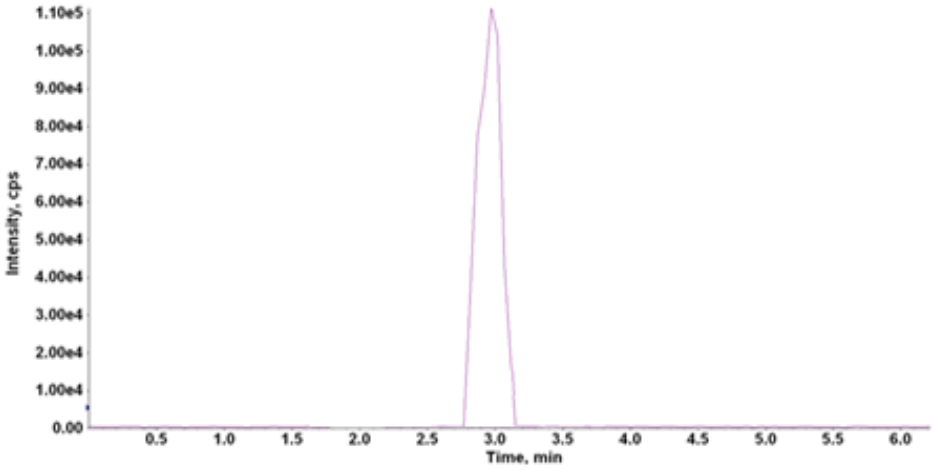

Figure 5. Chromatogram obtained from the HPLC-MS/MS analysis of Q_3 standard. The transition detected between the precursor and the product tropylium cation is shown.

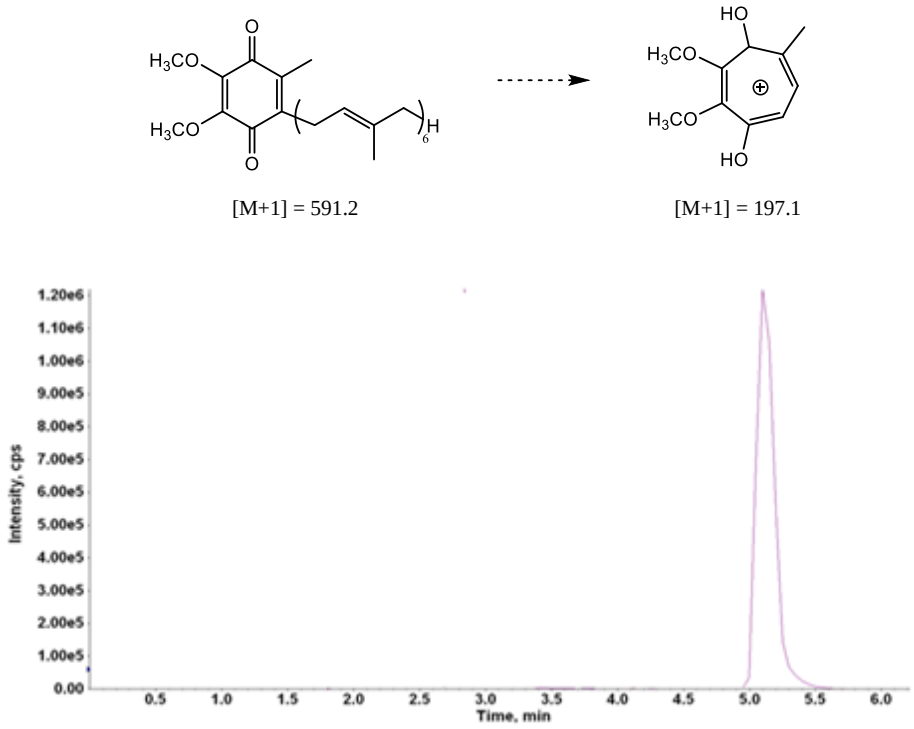

Figure 6. Chromatogram obtained from the HPLC-MS/MS analysis of Q_6 standard. The transition detected between the precursor and the product tropylium cation is shown.

A

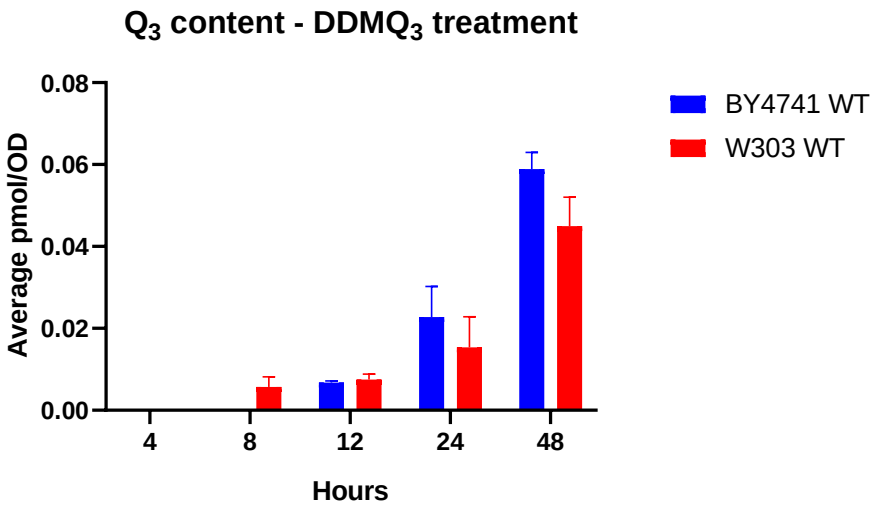

B

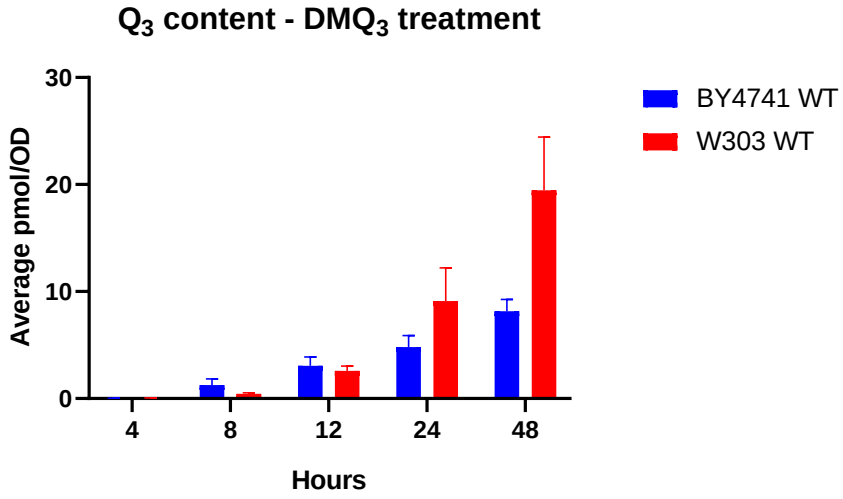

Figure 7. Q_3 content measured in yeast treated with $DDMQ_3$ and DMQ_3. (A) Q_3 levels observed in BY4741 WT (blue) and W303 WT (red) treated with $DDMQ_3$ (B) Q_3 levels observed in BY4741 WT (blue) and W303 WT (red) treated with DMQ_3. Error bars represent S.D. (n = 3).

A

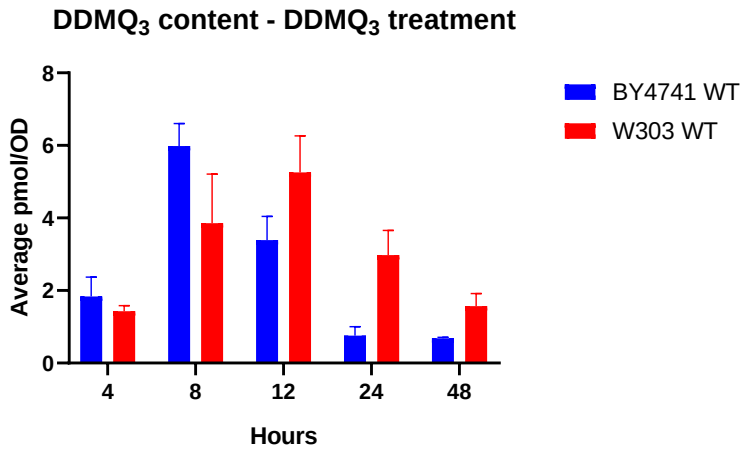

B

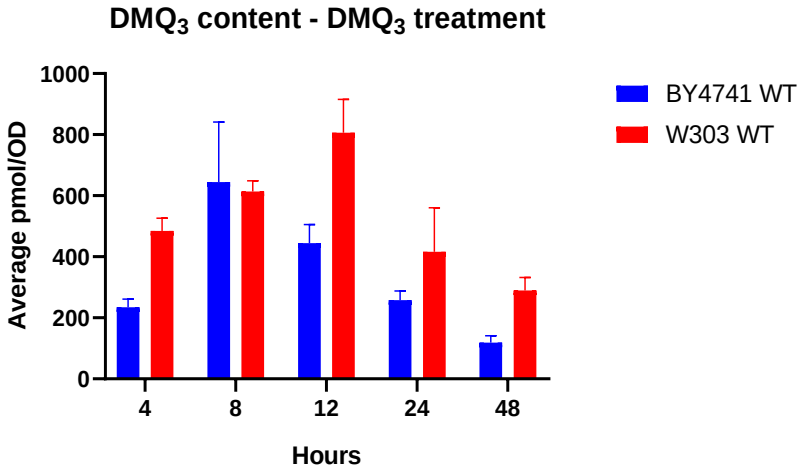

Figure 8. $DDMQ_3$ and DMQ_3 content measured in yeast treated with $DDMQ_3$ and DMQ_3 respectively. (A) $DDMQ_3$ levels observed in BY4741 WT (blue) and W303 WT (red) treated with $DDMQ_3$ (B) DMQ_3 levels observed in BY4741 WT (blue) and W303 WT (red) treated with DMQ_3. Error bars represent S.D. (n = 3).

A

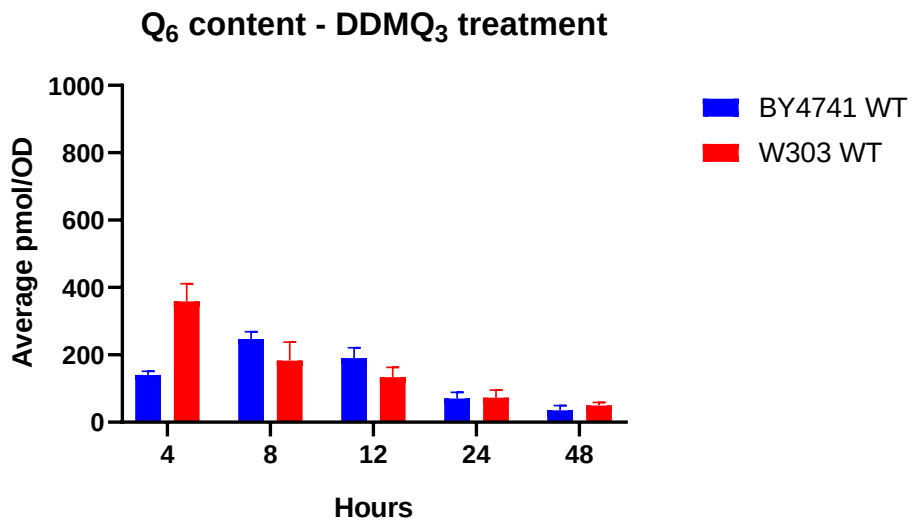

B

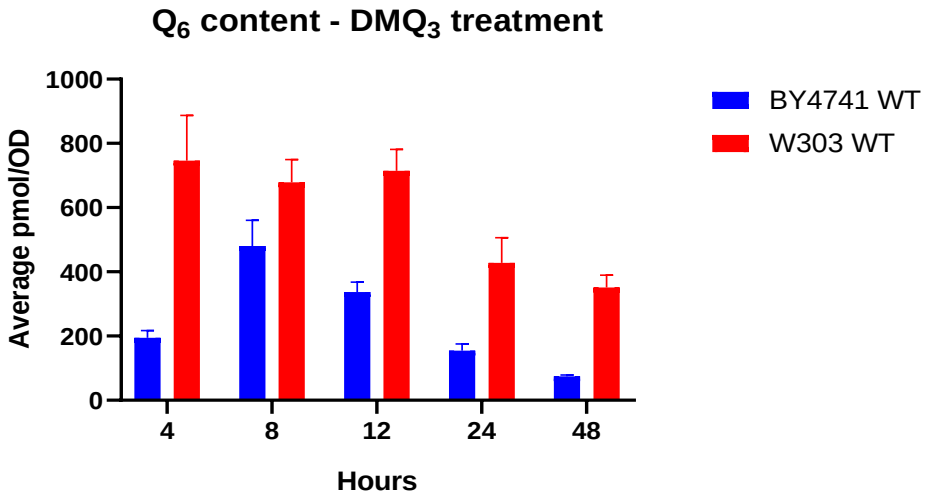

Figure 9. Q_6 content measured in yeast treated with and $DDMQ_3$ and DMQ_3. (A) Q_6 levels observed in BY4741 WT (blue) and W303 WT (red) treated with $DDMQ_3$ (B) Q_6 levels observed in BY4741 WT (blue) and W303 WT (red) treated with DMQ_3. Error bars represent S.D. (n = 3).

A

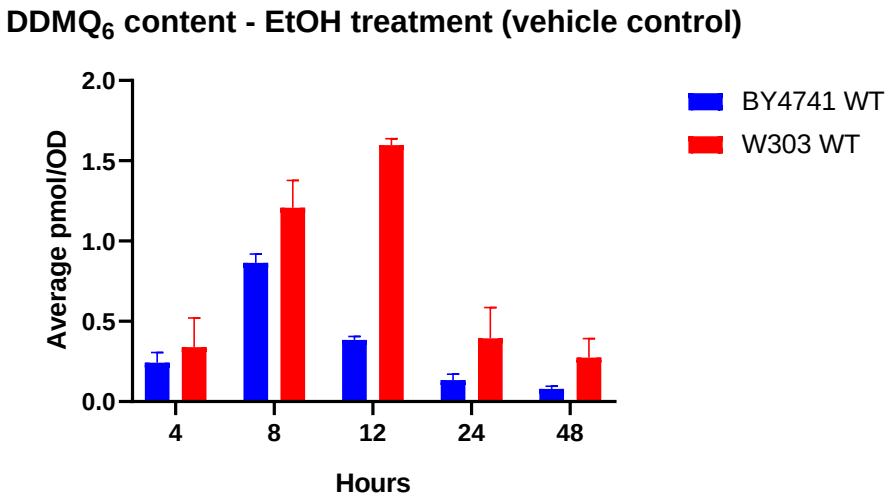

B

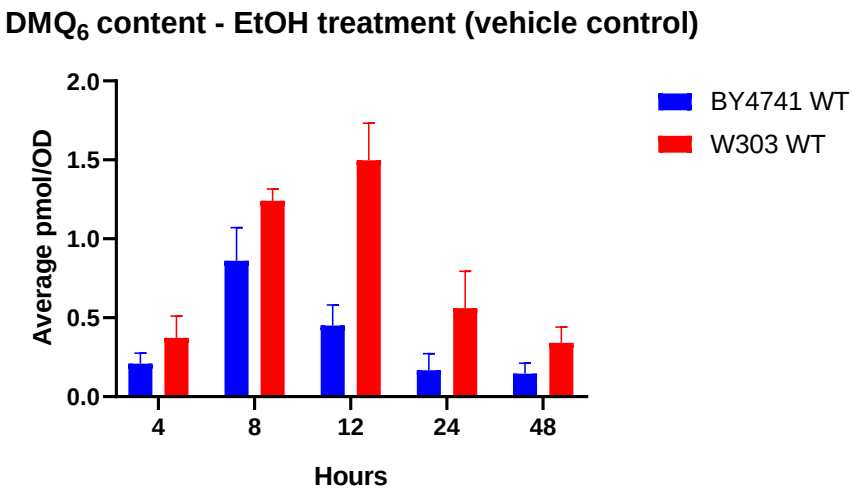

Figure 10. $DDMQ_6$ and DMQ_6 content measured in yeast treated with EtOH. (A) $DDMQ_3$ levels observed in BY4741 WT (blue) and W303 WT (red) treated with EtOH (B) DMQ_3 levels

observed in BY4741 WT (blue) and W303 WT (red) treated with EtOH. Error bars represent S.D. (n = 3).

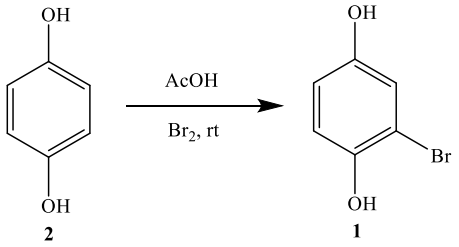

Scheme 1: Attempted synthesis of 2-bromo-1,4-dihydroxyphenol **1**

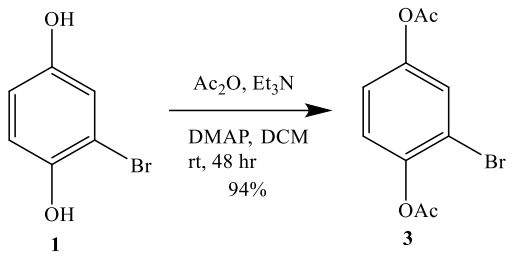

Scheme 2: Synthesis of 2-bromo-1,4-diacetoxybenzene **3**

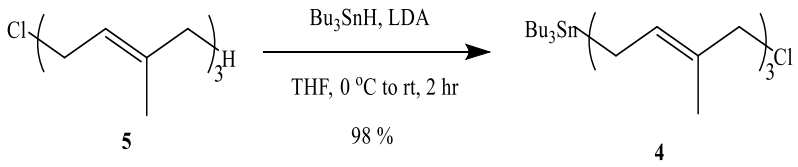

Scheme 3: Synthesis of tributyl farnesyl stannane **4**

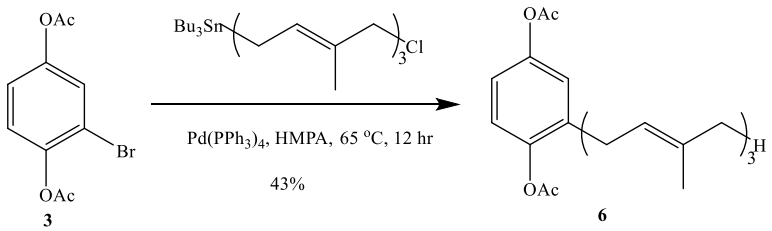

Scheme 4: Synthesis of 1,4-diacetoxy-2-farnesylbenzene **6**

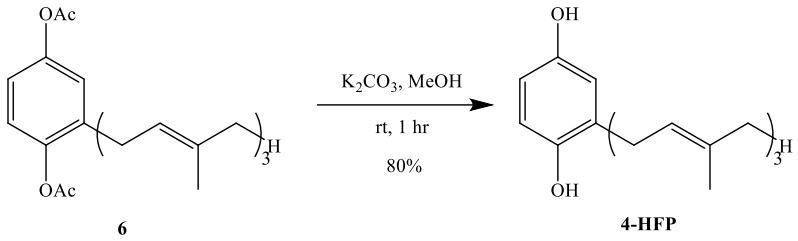

Scheme 5: Synthesis of 2-farnesyl-1,4-dihydroxyphenol **4-HFP**

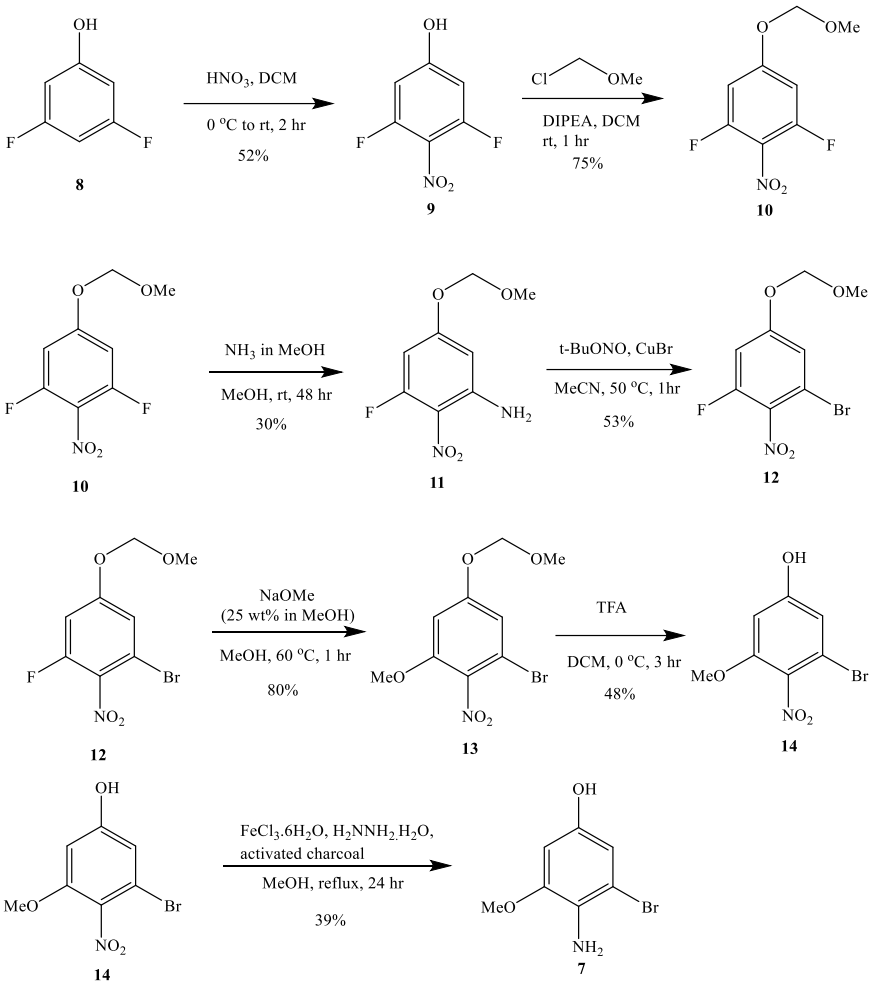

Scheme 6: Synthesis of 4-amino-3-bromo-5-methoxyphenol **7**

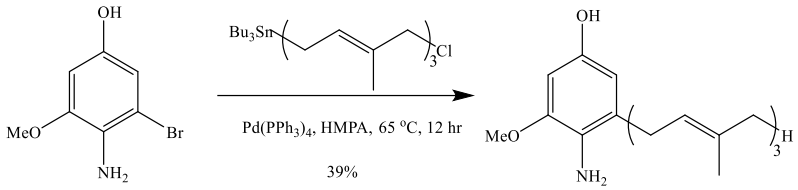

7 **IDDMQ$_3$H$_2$**

Scheme 7: Synthesis of 4-amino-5-farnesyl-3-methoxyphenol **IDDMQ$_3$H$_2$**

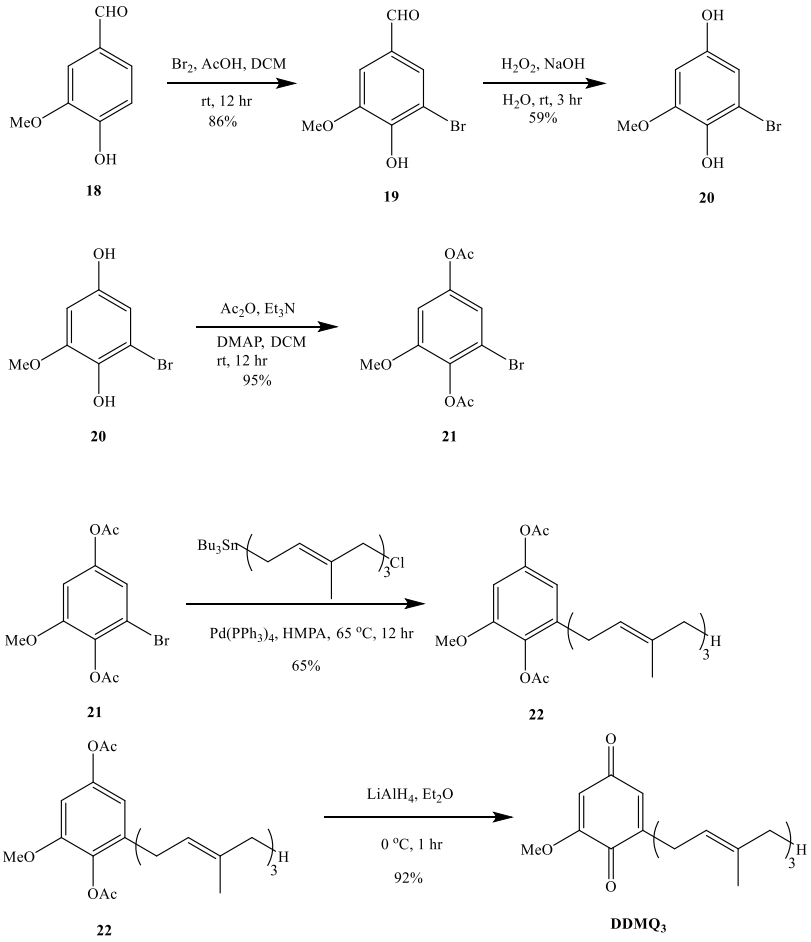

Scheme 8: Synthesis of 5-farnesyl-3-methoxybenzoquinone **$DDMQ_3$**

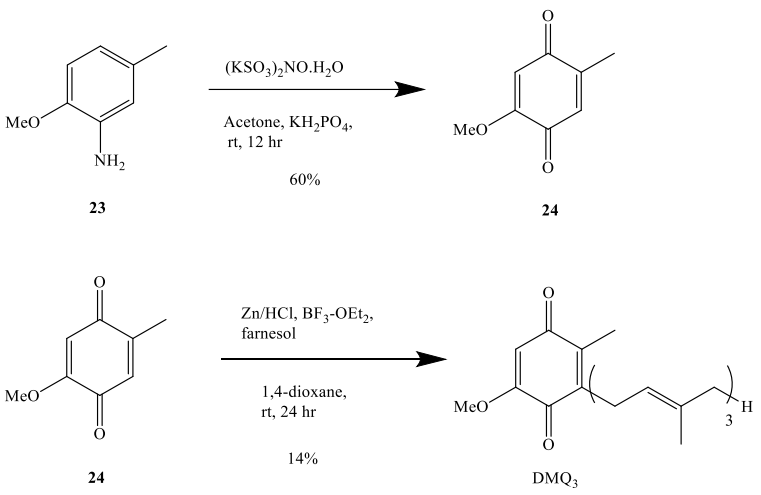

Scheme 9: Synthesis of 5-farnesyl-3-methoxy-6-methylbenzoquinone **DMQ_3**

References:

1. Brandt, U., and Trumpower, B. (**1994**). *Crit. Rev. Biochem. Mol. Biol.* **29**, 165

2. Mitchell, P. (**1976**). *J. Theor. Biol*., **62**, 327

3. Marbois, B., Xie, L. X., Choi, S., Hirano, K., Hyman, K., and Clarke, C. F. (**2010**). *J. Biol. Chem*., **285**, 27827

4. Ernster, L., and Forsmark-Amdree, P. (**1993**). *Clin. Invest.*, **71**, 560

5. Kagan, V., Serbinova, E., and Packer, L., (**1990**). *Biochem. Biophys. Res. Commun.*, **169**, 851

6. Bowry, V. W., Mohr, D., Cleary, J., and Stocker, R. (**1995**). *J. Biol. Chem.*, **270**, 5756

7. Do, T., Schultz, J. R., and Clarke, C. F. (**1996**). *Proc. Natl. Acad. Sci. U. S. A.*, **93**, 7534

8. Santos-Ocana, C., Cordoba, F., Crane, F. L., Clarke, C. F., and Navas, P. (**1998**). *J. Biol. Chem.*, **273**, 8099

9. Santos-Ocana, C., Villalba, J. M., Cordoba, F., Padilla, S., Crane, F. L., Clarke, C. F., and Navas, P. (**1998**). *J. Bioenerg. Biomembr.*, **30**, 465

10. Kobayashi, T., Kishigami, S., Sone, M., Inokuchi, H., and Mogi, T. (**1997**). *Proc. Natl. Acad. Sci. U. S. A.*, **94**, 11857

11. Still, W. C. (**1978**). *J. Am. Chem. Soc.*, **100,** 1481

12. Olson, R. E., and Rudney, H. (**1983**). *Vitam. Horm*., **40**, 1499

13. Gibson, F. (**1973**). *Biochem. Soc. Trans*., **1**, 317

14. Barkovich, R. J., Shtanko, A., Shepherd, J., Lee, P. T., Myles, D. C., Tzagoloff, A., Clarke, C. F. (**1997**). *J. Biol. Chem.*, **272**, 9182

15. Poon, W. W., Barkovich, R. J., Hsu, A. Y., Frankel, A., Lee, P. T., Shepherd, J. N., Myles, D. C., Clarke, C. F. (**1999**). *J. Biol. Chem.*, **274**, 21665

16. Brajcich, B. C., Iarocci, A. L., Johnstone, L. A. G., Morgan, R. K., Lonjers, Z. T., Hotchko, M. J., Muhs, J. D., Kieffer, A., Reynolds, B. J., Mandel, S. M., Marbois, B. N., Clarke, C. F., and Shepherd, J. N., (**2010**). *J. Bacteriology*, **192**, 436

17. Xie, L. X., Ozeir, M., Tang, J. Y., Chen, J. Y., Jaquinod, S-K., Fontecave, M., Clarke, C. F., and Pierrel. F. (**2012**). *J. Biol. Chem.*, **287**, 23571

18. He, C. H., Xie, L. X., Allan, C. M., Tran, U. P.C., and Clarke, C. F. (**2014**). *Biochim. Biophys. Acta.*, **1841**, 630

19. Lim, K. S., Lee, H., Kim, E. S., Ha, T-H., Ann, J., Son, K., Choi, S., Sun, W., Pearce, L. V., DeAndrea-Lazarus, I. A., Blumberg, P. M., and Lee, J. (**2013**). *European Journal of Medicinal Chemistry*, **68**, 233

20. Burke, D. J., D. C. Amberg, and J. N. Strathern. (**2005**). "Methods in Yeast Genetics: A Cold Spring Harbor Laboratory Course Manual". *Cold Spring Harbor Laboratory Press, Plainview, NY*

21. Ozeir, M., Pelosi, L., Ismail, A., Mellot-Draznieks, C., Fontecave, M., and Pierrel, F. (**2015**). *J. Biol. Chem.*, **290**, 24140

Chapter 3

Kaempferol increases levels of coenzyme Q in kidney cells and serves as a biosynthetic ring precursor

Author contributions: Lucía Fernández-del-Río, María I. Burón, Catherine F. Clarke, and José M. Villalba contributed to the intellectual development of the project. Lucía Fernández-del-Río, Anish Nag, Elena Gutiérrez Casado, Julia Ariza, Agape M. Awad, Akil I. Joseph, Ohyun Kwon, Eric Verdin, Rafael de Cabo, Claus Schneider, Jorge Z. Torres, María I. Burón, Catherine F. Clarke, and José M. Villalba contributed to the mammalian cell culture studies**.** Lucía Fernández-del-Río and Anish Nag contributed to the HPLC-MS/MS analysis, data acquisition, and statistical analysis. Anish Nag and Agape M. Awad contributed to the yeast studies. Anish Nag and Ohyun Kwon contributed to the chemical synthesis. Lucía Fernández-del-Río, Anish Nag, María I. Burón, Catherine F. Clarke, and José M. Villalba contributed to the writing and revision of the manuscript.

Free Radical Biology and Medicine 110 (2017) 176–187

Contents lists available at ScienceDirect

Free Radical Biology and Medicine

journal homepage: www.elsevier.com/locate/freeradbiomed

Original article

Kaempferol increases levels of coenzyme Q in kidney cells and serves as a biosynthetic ring precursor

Lucía Fernández-del-Río[a], Anish Nag[b], Elena Gutiérrez Casado[a], Julia Ariza[a], Agape M. Awad[b], Akil I. Joseph[c], Ohyun Kwon[b], Eric Verdin[d], Rafael de Cabo[e], Claus Schneider[c], Jorge Z. Torres[b], María I. Burón[a], Catherine F. Clarke[b], José M. Villalba[a,*]

[a] Departamento de Biología Celular, Fisiología e Inmunología, Universidad de Córdoba, Campus de Excelencia Internacional Agroalimentario, ceiA3, Spain
[b] Department of Chemistry and Biochemistry and the Molecular Biology Institute, UCLA, Los Angeles, CA, USA
[c] Department of Pharmacology, and the Vanderbilt Institute of Chemical Biology, Vanderbilt University Medical School, Nashville, TN, USA
[d] Buck Institute for Research on Aging, Novato, CA, USA
[e] Translational Gerontology Branch, National Institute on Aging, National Institutes of Health, Baltimore, MD, USA

ARTICLE INFO

Keywords:
Coenzyme Q
Plant polyphenols
Flavonols
Kaempferol
Antioxidants
Sirt3
4-hydroxybenzoic acid
Kidney cells

ABSTRACT

Coenzyme Q (Q) is a lipid-soluble antioxidant essential in cellular physiology. Patients with Q deficiencies, with few exceptions, seldom respond to treatment. Current therapies rely on dietary supplementation with Q_{10}, but due to its highly lipophilic nature, Q_{10} is difficult to absorb by tissues and cells. Plant polyphenols, present in the human diet, are redox active and modulate numerous cellular pathways. In the present study, we tested whether treatment with polyphenols affected the content or biosynthesis of Q. Mouse kidney proximal tubule epithelial (Tkpts) cells and human embryonic kidney cells 293 (HEK 293) were treated with several types of polyphenols, and kaempferol produced the largest increase in Q levels. Experiments with stable isotope ^{13}C-labeled kaempferol demonstrated a previously unrecognized role of kaempferol as an aromatic ring precursor in Q biosynthesis. Investigations of the structure-function relationship of related flavonols showed the importance of two hydroxyl groups, located at C3 of the C ring and C4′ of the B ring, both present in kaempferol, as important determinants of kaempferol as a Q biosynthetic precursor. Concurrently, through a mechanism not related to the enhancement of Q biosynthesis, kaempferol also augmented mitochondrial localization of Sirt3. The role of kaempferol as a precursor that increases Q levels, combined with its ability to upregulate Sirt3, identify kaempferol as a potential candidate in the design of interventions aimed on increasing endogenous Q biosynthesis, particularly in kidney.

1. Introduction

Coenzyme Q (Q) is the only lipid-soluble antioxidant synthesized endogenously and present in all cellular membranes. It plays an important role in cellular metabolism and protects membranes and lipoproteins from protein oxidation and lipid peroxidation [1]. The biosynthesis of Q is still not completely characterized. Its biosynthesis is divided into three steps: the synthesis of the polyisoprenoid tail, the attachment of the tail to the benzoquinone ring precursor, followed by subsequent modifications of the ring. In higher eukaryotes, synthesis of the polyisoprenoid tail depends on the cytosolic mevalonate pathway and on polyisoprenyl-diphosphate synthases located within the mitochondria [2,3]. The number of isoprene units (designated as the subscript *n*, Q_n) in the polyisoprenyl tail varies in different organisms. While *Saccharomyces cerevisiae* synthesize Q_6 and humans mainly Q_{10}, mice have two major isoforms, Q_9 and Q_{10} [4]. The polyprenyltransferase Coq2 joins the quinone ring precursor to the polyisoprenoid tail inside mitochondria, and then the ring is modified by distinct enzymes encoded by several *COQ* genes [5]. These modifications include three hydroxylations, one decarboxylation, two *O*-methylations and one *C*-methylation.

4-Hydroxybenzoic acid (4HB) was considered to function as the only confirmed ring precursor of Q for more than 40 years. In 2010 Marbois et al. and Pierrel et al. characterized *p*-aminobenzoic acid (PABA) as a novel Q precursor in yeasts [6,7]. In 2014, Block et al. showed that *Arabidopsis* is able to use *p*-coumarate, but not PABA, as another ring precursor in Q biosynthesis [8]. Recently, in 2015, Xie et al. have described that human and *E. coli* cells do not utilize PABA as

Abbreviations: Q, Coenzyme Q; 2,4-DHB, 2,4-dihydroxybenzoic acid; DOD, drop-out-dextrose medium; FBS, fetal bovine serum; 4HB, 4-Hydroxybenzoic acid; 4HPAA, 4-hydroxyphenylacetic acid; MEF, mouse embryonic fibroblast; MTT, 3-(4,5-dimethylthiazol-2-yl)-2,5-diphenyltetrazolium bromide; NAM, nicotinamide; PABA, p-aminobenzoic acid; YPD, yeast extract peptone dextrose; TCA, trichlocoacetic acid

* Corresponding author.

http://dx.doi.org/10.1016/j.freeradbiomed.2017.06.006
Received 17 March 2017; Received in revised form 29 May 2017; Accepted 6 June 2017
Available online 09 June 2017
0891-5849/

precursor in the biosynthesis of Q while both *p*-coumarate and resveratrol, another polyphenol structurally similar to *p*-coumarate, can serve as a ring precursors of Q biosynthesis in *E. coli*, yeasts and human cells [9].

A decrease of Q biosynthesis and total Q levels correlates with physiological aging in some tissues [10]. Q_{10} deficiencies related to distinct diseases are observed in patients, and fortunately some patients with Q deficiencies respond to treatment with dietary supplementation of Q_{10} [5,11]. However, the long polyisoprenoid chain renders Q_{10} highly lipophilic and difficult to absorb by cells. Thus, the poor bioavailability of exogenous Q_{10} often results in treatments that are ineffective [12]. To develop more successful strategies, efforts should also focus on identifying molecules that enhance the endogenous synthesis of Q.

A traditional view is that plant polyphenols constitute a principal source of antioxidants in human diet. However, polyphenols are redox active compounds that elicit cellular signaling and modulate pathways that determine activity of the mitochondrial electron transport chain, membrane potential and biogenesis, intra-mitochondrial oxidative status and, ultimately, mitochondria-triggered cell death [13]. The more than 5000 polyphenol molecules identified have been classified into five major chemical families, namely flavonoids, phenolic acids, stilbenes, lignans and curcuminoids [14]. Studies reveal that their specific chemical structure affects their biological properties [14,15], and some of them can act as Q ring precursors [9].

In the present study, we determined the effect of several polyphenols on Q content and biosynthesis. Among the several polyphenols tested, kaempferol produced the strongest increase in Q content and acted as a novel ring precursor of Q biosynthesis in mammalian cells. The effect of kaempferol on Q biosynthesis may be linked to the numerous beneficial effects attributed to flavonoids. Our studies indicate a novel potential biosynthetic pathway leading to aromatic ring precursors of Q and also suggest new strategies that can help to alleviate the symptoms associated with Q deficiency in aging or disease states.

2. Material and methods

2.1. Chemicals and reagents

Non-labeled kaempferol, resveratrol, quercetin, piceatannol, apigenin, luteolin, naringenin, curcumin, and ferulic acid were obtained from Santa Cruz Biotechnology, Inc. All these compounds were checked in the Mass Spectrometry & Chromatography Service of the University of Córdoba and contamination with 4HB, vanillic or protocatechuic acid was not detected at levels higher than 0.01% of solid material. PABA, 4HB, vanillin, nicotinamide (NAM), 4-hydroxyphenylacetic acid and *p*-cresol were purchased from Sigma-Aldrich. ^{13}C-kaempferol was obtained from IsoLife and D_6-curcumin and D_3-ferulic acid were purchased from SynInnova. $^{13}C_{12}$-curcumin was synthesized from $^{13}C_6$-vanillin (Cambridge Isotopes Laboratories Inc) following a published procedure [16]. Standards of Q_4, Q_6, Q_9 and Q_{10} were purchased from Sigma-Aldrich. Dipropoxy-Q_{10} was synthesized essentially as described by Edlund [17] for diethoxy-Q_{10}, except 1-propanol was substituted for ethanol while maintaining the other reagents and conditions.

2.2. Cell cultures

Mouse kidney proximal tubule epithelial (Tkpts) cells [18], were provided by Dr. Elsa Bello-Reuss (Texas Tech University Health Science Center) and Dr. Judit K. Magyesi (University of Arkansas for Medical Sciences, Little Rock, AR). Human embryonic kidney cells 293 (HEK 293), human liver hepatoma cells (Hep G2), human promyelocytic leukemia cells (HL-60), mouse liver hepatoma cells (Hepa 1.6) and mouse embryonic fibroblast (MEFs) were also used in some studies. These cell lines were obtained from ATCC, whereas MEFs were obtained in our own laboratory by repeated subculture of cells derived from mouse embryos following a standard 3T3 immortalization protocol [19]. Tkpts and Hepa 1.6 cells were grown in DMEM/F12 with 4.5 g/L glucose supplemented with 10% FBS, 2 mM L-glutamine, and gentamicin-amphotericin B (125 µg/ml and 5 mg/ml, respectively). The same media but containing 1 g/L of glucose was used to culture HEK 293 cells. MEFs were cultured in DMEM with 2 g/L glucose supplemented with 10% fetal bovine serum (FBS, Sigma-Aldrich), 2 mM L-glutamine and gentamicin. Hep G2 cells were maintained in MEM containing 1 g/L glucose and supplemented with 10% FBS, 1% sodium pyruvate, 1% L-glutamine and gentamicin-amphotericin B. HL-60 cells were grown in RPMI-1640 supplemented with 10% FBS, 2 mM L-glutamine and gentamicin-amphotericin B. All cultures were maintained at 37 °C in a humidified atmosphere with 5% CO_2.

Saccharomyces cerevisiae BY4741, with genotype MAT **a** *his3Δ1 leu2Δ0 met15Δ0 ura3Δ0* [20] was used in all the determinations involving yeasts. Cells were grown in drop-out-dextrose medium (DOD) composed of 2% dextrose, 6.8 g/L Bio101 yeast nitrogen base minus pABA minus folate with ammonium sulfate and 5.83 mM sodium monophosphate (pH adjusted to 6.0 with NaOH). The yeast colonies were maintained in solid plate yeast extract peptone dextrose (YPD) medium composed of 1% Bacto-Yeast extract, 2% Bacto-Peptone, 2% Dextrose and 2% Bacto agar.

2.3. Treatments of human and mouse cells with polyphenols, and viability assays

The same experimental conditions were used for all compounds when tested in mouse and human cells. Assays were performed in six-well plates with an initial amount of 50,000–100,000 cells/well. Cells were incubated with the tested compounds for 48 h under standard culture conditions (37 °C, 5% CO_2). Once the treatment was completed, cells were detached from culture plates and pelleted by low-speed centrifugation (approximately 1000g). Cell pellets were collected and stored at −80 °C until use. Final concentrations of each polyphenol in assays to determine Q content and biosynthesis were selected from the results of viability assays to ensure that experimental conditions did not jeopardize cell viability. To perform these assays, 50 µl/ml of a 5 mg/ml stock of 3-(4,5-dimethylthiazol-2-yl)-2,5-diphenyltetrazolium bromide (MTT, Sigma) was added to the cell cultures (previously plated in 24 well-plates). After 2 h of incubation at 37 °C in 5% CO_2, the medium was removed, the formazan solubilized with 0.04 M HCl in absolute isopropanol, and the absorbance measured at 590 nm in a plate reader (Optic Ivymen System 2000-C).

2.4. Growth and treatment of yeast cells with polyphenols

BY4741 yeast were grown in 50 ml precultures in DOD medium overnight in a shaking incubator (30 °C, 250 rpm). A sample of the yeast preculture was inoculated in 18 × 150 mm borosilicate test tubes containing 5 ml of DOD medium to give an initial cell density of 0.2 A_{600}. Incubations continued at 30 °C and 250 rpm until a cell density of 0.5 A_{600}. At that point, designated polyphenol compounds were added to attain a final concentration of 10 µM and incubation resumed. The tubes were removed from the shaker at 3 h. The A_{600} values were measured and the cell pellets were collected and stored at −20 °C.

2.5. Preparation of cell and tissue extracts

Whole lysates were prepared from cells as described by Ariza et al. [21] and steady state protein levels were determined by Western blot (see below). Tissues were obtained from Sirt3 knockout mice and their corresponding genetic background-matched controls bred at the Gladstone Institute (San Francisco, CA, USA). Extracts from these tissues were prepared as described by Ariza et al. [21].

2.6. Lipid extractions

2.6.1. Lipid extractions for HPLC-electrochemical detection measurements

Mouse and human cell pellets (approx. 10^6 cells) from the different treatments or 20 mg of the tissue homogenate were collected and re-suspended in 90 µl of Hanks' balanced salt solution. Samples were then solubilized using 10 µl of 10% SDS followed by 200 µl of 95:5 ethanol-isopropanol. After vigorous vortexing, 500 µl of hexane were added and the samples were centrifuged for 5 min at 12,500 rpm in an Eppendorf Minispin. Lipids were recovered within the upper hexane phase, and this extraction step was repeated twice. Hexane phases were combined and the solvent evaporated under vacuum. Lipid extracts were stored frozen at −80 °C until use.

2.6.2. Lipid extractions for HPLC-MS/MS measurements

Di-propoxy-Q_{10} was added to the pellets as internal standard in mouse and human samples while Q_4 was used in yeast samples. Cell pellets were vortexed in 1 ml of methanol and 1 ml of petroleum ether. The organic upper layer was transferred to a new tube. Another 1 ml of petroleum ether was added to the original methanol layer, and samples were vortexed again. The organic phase was removed, and the combined organic phase was dried under a stream of nitrogen gas.

2.7. Measurements of Q levels by HPLC

HPLC analysis was carried out with a Beckman Gold System (Beckman Coulter, USA) connected to a Coulochem II electrochemical detector (ESA, Chemsfold, MA, USA). The chromatographic separation was performed with a C18 reverse phase analytical column (4.6 mm × 25 cm, Ultrasphere ODS, 5 µm particle). The mobile phase was composed of methanol/isopropanol/1 M ammonium acetate, pH 4.4, (53:45:2), and a flow rate of 1 ml/min. The analytical cell (ESA, Model 5010) was set at potentials of −500 mV and +300 mV in electrodes 1 and 2, respectively. The entire procedure was performed at room temperature. Lipid extracts were dissolved in 30 µl of methanol, and the sample was subjected then to a reduction step by adding 1 µl of freshly prepared 50 mM sodium borohydride just before injection into the system. This procedure results in the reduction of the quinones (Q) to their corresponding hydroquinones (QH_2), which are detected at the second electrode with maximal sensitivity, and allows for a shorter chromatography time. Retention times were 10–11 min for reduced Q_9H_2 and 14–15 min for reduced $Q_{10}H_2$. The area units of hydroquinone peaks were integrated and referred to the reduced $Q_{10}H_2$ standard. Normalized values were obtained by referring to the amount of protein of each sample, calculated previously with a Bradford assay [22].

2.8. Assays of Q biosynthesis

2.8.1. Assays with a radiolabeled precursor

Q biosynthesis was measured with the radiolabeled precursor 4-hydroxy-(U-^{14}C) benzoate (^{14}C-4HB) synthesized from (U-^{14}C)-tyrosine (Amersham) essentially as described by Clarke et al. [23] with a minor modification: aqueous tyrosine was dissolved in 25 µl of 10 M KOH and 12.5 µl of 10 M NaOH before blown to near dryness under nitrogen. ^{14}C-4HB (100,000 CPM) was added to the cells during the 48 h incubation with the treatment. Samples were processed as described previously by Córdoba-Pedregosa et al. [24]. Briefly, cells were rinsed twice with Hanks' balanced salt solution and fixed for 15 min in 1 ml of 5% trichlocoacetic acid (TCA). After thoroughly washing with TCA to remove the non-incorporated precursor, the radioactivity from the TCA-insoluble Q-containing fraction was directly extracted with 1 ml of 1 M NaOH for 2 h at room temperature with gentle stirring. Radioactivity was quantified in a Beckman scintillation counter by mixing 900 µl of each sample with 4 ml of scintillation liquid. The CPM values so obtained were then referred to the total amount of protein in each sample.

Table 1
HPLC-MS-MS transitions for each analyte. We summarize here the transitions used for each molecule in the HPLC-MS/MS. We monitored both the protonated and the ammoniated transitions.

Molecule	*m/z* (+ H)	*m/z* (+ NH_3)
Q_4	455.3/197.08	472.3/197.08
Q_6	591.4/197.08	608.4/197.08
$^{13}C_6$-Q_6	597.4/203.08	614.4/203.08
Q_9	795.6/197.08	812.6/197.08
D_3-Q_9	798.6/200.08	815.6/200.08
$^{13}C_6$-Q_9	801.6/203.08	818.6/203.08
Q_{10}	863.6/197.08	880.6/197.08
D_3-Q_{10}	866.6/200.08	883.6/200.08
$^{13}C_6$-Q_{10}	869.6/203.08	886.6/203.08
Dipropoxy-Q_{10}	919.7/253.1	936.7/253.1

2.8.2. Assays with stable isotope-labeled compounds

Lipid extracts were measured by HPLC-tandem mass spectrometry (MS/MS) analyses as previously described by Xie et al. [9] with minor modifications. Samples were resuspended in 200 µl of ethanol containing 1 mg/ml benzoquinone in order to oxidize all the lipids prior to chromatographic separation with a mobile phase composed of 90% solvent A (95:5 mixture of methanol:isopropanol containing 2.5 mM ammonium formate) and 10% solvent B (isopropanol containing 2.5 mM ammonium formate) at a constant flow rate of 1 ml/min. Transitions monitored are described in Table 1. The area value of each peak, normalized with the correspondent standard curve and internal standard, was referred either to the initial amount of protein in the case of determinations carried out in murine and human cells, or to the total OD present in the yeast cell pellet (as determined by measurements of A_{600}).

2.9. Polyacrylamide gel electrophoresis and Western blot immunodetection

The procedure was performed as described by Ariza et al. [21] with samples of whole cell extracts (50 µg of protein) applied per gel lane. The following primary antibodies were used: Anti-Sirt3 (Santa Cruz Biotechnology, Inc) at 1:1000 dilution, anti-acetyl lysine (Cell Signaling) at 1:1000 dilution, and anti-Coq2 [25] at 1:1000 dilution. In all cases, horseradish peroxidase-conjugated secondary antibodies were used to reveal immunoreactivity by enhanced chemiluminescence. An anti-rabbit secondary antibody (at 1:2000 dilution, Santa Cruz Biotechnology, Inc) was used for Sirt3 and acetyl lysine, while an anti-chicken secondary antibody (at 1:5000 dilution, Sigma-Aldrich) was used for Coq2.

2.10. Statistical analyses

Statistical analyses were performed using GraphPad Prism 5.03 (GraphPad Software Inc., San Diego, CA, USA). All the data shown are mean ± standard error (SEM) from at least five replicates. Normality of data was checked by Kolmogorov-Smirnov test with the Dallal-Wilkinson-Lilliefor corrected p value. Means were compared using either the parametric two-tail Student's *t*-test or non-parametric Mann-Whitney test depending on the results of the normality test. Significant differences were referred as *$p < 0.05$, **$p < 0.01$ and ***$p < 0.001$.

3. Results

3.1. Kaempferol increases Q in cultured kidney cells

We determined the effect of several polyphenols on Q content and biosynthesis. Each compound used in this study was first added to cells at concentrations ranging from 5 nM to 100 µM over a period of 48 h, and tested with the MTT assay to determine effects on cellular viability (see Supplementary Fig. S1). Based on these data, we chose to test

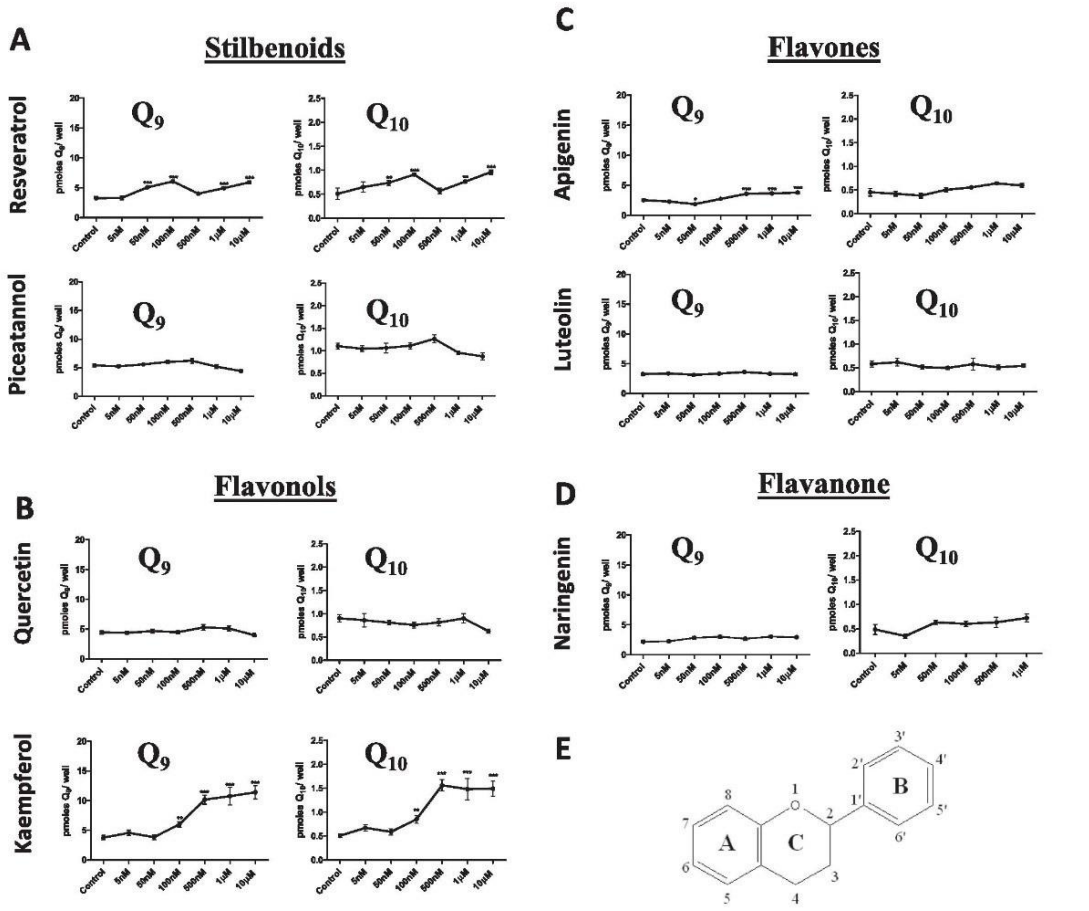

Fig. 1. Kaempferol strongly increases Q levels in Tkpts cells. Q_9 and Q_{10} levels were determined in Tkpts cells treated with different polyphenols at the given concentrations for 48 h. After the incubation period, lipids were extracted and Q levels quantified. **(A)** Stilbenoids. Resveratrol, but not piceatannol, produced a modest increase of Q_9 and Q_{10} levels. **(B)** Flavonols. Quercetin did not affect Q levels, but kaempferol produced a dramatic increase of both Q_9 and Q_{10}. **(C-D)** Flavones and a flavanone. Apigenin, but not luteolin or naringenin, slightly increased Q_9 and Q_{10} levels. **(E)** Basic chemical skeleton of flavonoids. Statistically significant differences between control and treatments are represented by $^*p < 0.05$, $^{**}p < 0.01$ and $^{***}p < 0.001$.

phenolic compounds at concentrations ranging from 5 nM to 10 μM to detect possible effects on Q content. Within this range, none of the polyphenols under study decreased viability significantly, and only a small increase in viability was observed at 1 μM piceatannol.

Next, we tested how two stilbenoids (resveratrol and piceatannol) and two flavonols (quercetin and kaempferol) affected Q levels in Tkpts cells. As shown in Fig. 1A, resveratrol produced a slight increase of Q_9 and Q_{10} levels at most concentrations above 50 nM, whereas the other stilbenoid tested, piceatannol, and the flavonol quercetin had no effect on Q levels (either Q_9 or Q_{10}) at any of the concentrations tested. In contrast, kaempferol produced a dramatic increase of both Q_9 and Q_{10} at 100 nM and higher concentrations, producing a plateau at concentrations between 500 nM and 10 μM (Fig. 1B). We also confirmed a substantial increase of Q_9 and Q_{10} levels in Tkpts cells treated with kaempferol at concentrations above 100 nM when specific values were calculated on a protein basis (Supplementary Fig. S2).

Given the differential effects of kaempferol and quercetin (which differ only in one hydroxyl group), we hypothesized that the chemical structure of the flavonoids could influence their effect on Q content (see chemical structures of the compounds used in Supplementary Fig. S1 and the basic chemical skeleton of flavonoids in Fig. 1E). Thus, we tested how additional polyphenols of the flavonoid group affected Q levels in Tkpts cells. For these experiments, we chose two flavones: apigenin, luteolin (Fig. 1C), and one flavanone: naringenin (Fig. 1D). Among these three flavonoids, only apigenin produced a slight increase in Q at concentrations between 500 nM and 10 μM, although a concentration of 50 nM was found inhibitory and statistically significant differences were observed for Q_9 but not for the Q_{10} isoform (Fig. 1C).

The following experiments, aimed to elucidate how flavonoids function to increase Q levels, were focused on kaempferol, as this polyphenol was by far the most efficient in augmenting the amounts of cellular Q.

3.2. Kaempferol activation of the mitochondrial sirtuin Sirt3 is unrelated with the increased Q levels

Kaempferol has been reported to up-regulate Sirt3 [26,27], a mitochondrial sirtuin that plays an important role in regulating cellular processes like homeostasis, oxidative stress and aging [28]. Up-regulation of mitochondrial Sirt3 optimizes redox processes linked to the

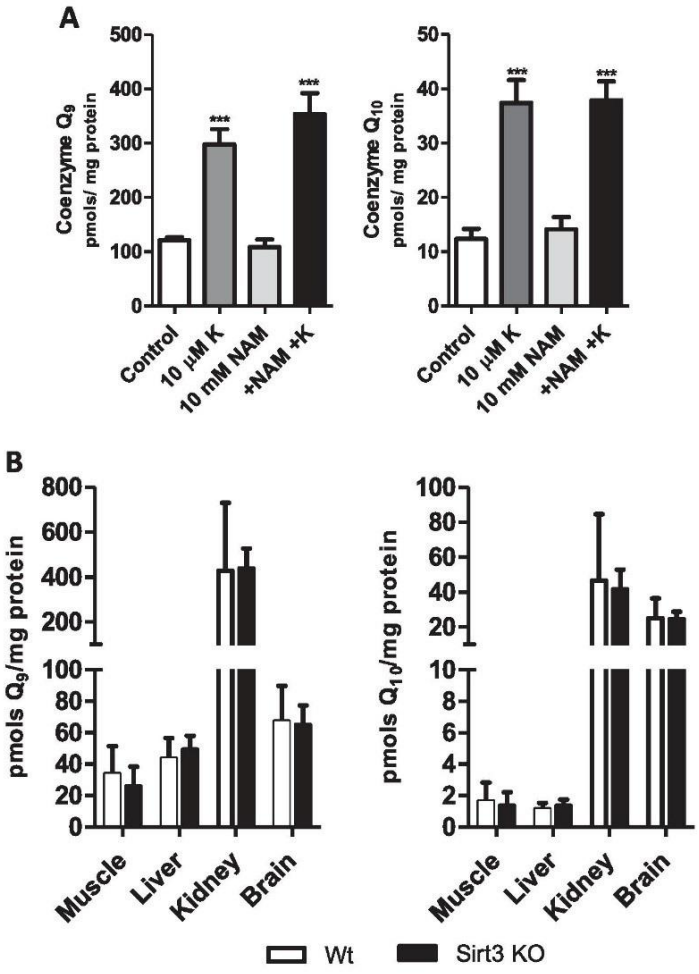

Fig. 2. The mitochondrial sirtuin Sirt3 does not participate in the regulation of Q levels. (A) General inhibition of sirtuin deacetylases by nicotinamide (NAM) at 10 mM did not prevent the increase of Q levels in Tkpts cells treated kaempferol (K) at 10 μM. **(B)** Q levels are not altered in tissues (skeletal muscle, liver, kidney and brain) obtained from Sirt3 knockout mice in comparison with age-matched controls. Asterisks denote statistically significant differences (***$p < 0.001$).

electron transport chain and boosts antioxidant defense in this organelle by activating ROS-scavenging systems [29]. Thus, it seemed possible that Sirt3-mediated changes might affect Q levels by providing an antioxidant environment that would diminish oxidative Q degradation. To investigate this, Tkpts cells were treated with kaempferol and the up-regulation of mitochondrial Sirt3 was then assessed. As depicted in Supplementary Fig. S3A, treatment of Tkpts cells with kaempferol increased significantly the levels of the mitochondrially-targeted (cleaved) form of Sirt3 at concentrations that also increased Q_9 and Q_{10} levels. We next proceeded to verify whether this up-regulation of Sirt3 mediated the increase in Q levels or, on the contrary, it was an independent event. To this purpose, we tested whether simultaneous treatment with NAM, a well-known inhibitor of sirtuin deacetylase activity [27], impacted Q levels in Tkpts cells treated with kaempferol. As shown in Fig. 2A, treatment with 10 mM NAM did not alter basal levels of Q in Tkpts cells, and the kaempferol-mediated increase of Q_9 and Q_{10} was completely unaffected by NAM. A western-blot using an anti-acetyl lysine antibody confirmed that, under our experimental conditions, deacetylase activity was significantly inhibited by 10 mM NAM since this treatment produced a substantial increase of protein acetylation (Supplementary Fig. S3B). Furthermore, we also determined Q levels in several tissues obtained from Sirt3 knockout mice. In each tissue examined, including muscle, liver, kidney, and brain, Q levels from Sirt3 knockout mice were not significantly different from their background-matched controls (Fig. 2B). Thus, although similar concentrations of kaempferol can indeed up-regulate Sirt3-dependent mitochondrial functions and increase amounts of Q, the increase in Q content does not appear to be related to the upregulation of Sirt3 activity.

3.3. Kaempferol activates endogenous Q biosynthesis by acting as a ring precursor in mouse and human kidney cells

We considered the possibility that the increase of Q levels caused by kaempferol could be a consequence of a higher Q biosynthetic rate. To test this possibility, we followed two different approaches. First, we studied how PABA, a well-characterized inhibitor of Coq2 activity in animal cells [30,31], affected Q levels in control and in Tkpts cells that had been treated simultaneously with kaempferol. As expected, PABA decreased Q levels in the control cells. Moreover, PABA abolished the increase of Q in response to kaempferol treatment, indicating a direct link between kaempferol and Q biosynthesis (Fig. 3A).

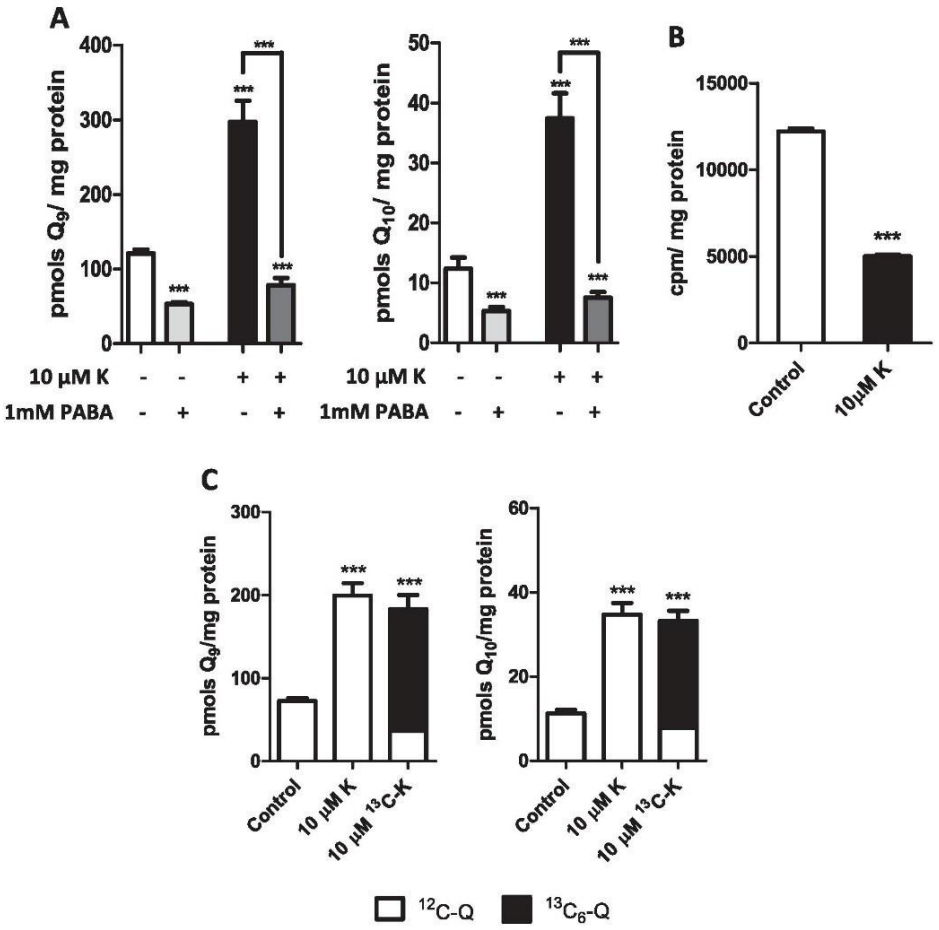

Fig. 3. Kaempferol augmentation of Q levels is related to the enhancement of Q biosynthesis. (A) Inhibition of the Coq2 polyprenyltransferase with PABA decreased Q levels in control Tkpts cells and abolished the increase of Q_9 and Q_{10} in cells treated with kaempferol (K). Cells were cultured for 48 h in the presence of kaempferol at 10 µM and /or PABA at 1 mM. Lipids were then extracted for quantification of Q by HPLC. **(B)** Competition assay of ^{14}C-4HB incorporation into Q. Treatment of cells with 10 µM kaempferol (K) inhibited the incorporation of ^{14}C-4HB into Q, which indicates competition of kaempferol and 4HB as Q ring precursors. **(C)** Demonstration of the role played by kaempferol as a Q ring precursor in Tkpts cells. Cells were cultured for 48 h in the presence of unlabeled (K) or ^{13}C-labeled kaempferol (^{13}C-K) at 10 µM. Unlabeled (^{12}C, *open bars*) and $^{13}C_6$-labeled (*closed bars*) Q were then measured with HPLC-MS/MS. The majority of Q measured in cells treated with ^{13}C-kaempferol was $^{13}C_6$-Q, demonstrating a role for kaempferol as a novel Q ring precursor. Asterisks denote statistically significant differences (***$p < 0.001$).

Secondly, we measured Q biosynthesis with an assay based on the incorporation of exogenous ^{14}C-labeled 4HB as Q ring precursor. Our results showed that kaempferol produced a substantial decrease in the incorporation of ^{14}C-4HB (Fig. 3B). The simultaneous increase of Q levels and decrease of ^{14}C-4HB incorporation into Q by kaempferol, implies that this compound competes with the substrate 4HB to behave as a ring precursor for Q biosynthesis. To confirm this possibility, we cultured Tkpts cells in the presence of ^{13}C-labeled kaempferol and then measured the levels of ^{12}C-Q and $^{13}C_6$-Q with HPLC-MS-MS. This technique allows the simultaneous measurement of the amount of cellular Q derived from endogenous 4HB (^{12}C-Q) and the amount of newly synthesized Q derived from ^{13}C-kaempferol ($^{13}C_6$-Q). Total levels of Q obtained in the presence of ^{13}C-kaempferol were also compared with those obtained when cells were grown in the presence of the non-labeled polyphenol. We found that Q_9 and Q_{10} levels increased equally with both non-labeled and ^{13}C-kaempferol. Of note, when the ^{13}C-labeled precursor was used, nearly all the Q present in Tkpts cells was $^{13}C_6$-Q, identifying kaempferol as an efficient novel Q ring precursor (Fig. 3C). Similar experiments were carried out to test the effects of kaempferol in human HEK 293 cells, another kidney cell line and, as observed for Tkpts cells, Q levels were also increased by kaempferol treatment. Furthermore, when ^{13}C-kaempferol was used, almost all the Q present in HEK 293 cells was $^{13}C_6$-Q (Supplementary Fig. S4A). In sum, our results demonstrate a role for kaempferol as a Q ring precursor both in murine and human kidney cell lines.

Colonic microflora metabolize kaempferol to 4-hydroxyphenylacetic acid (4HPAA) and 4-methyphenol (or *p*-cresol) [32,33]. Moreover, Serra et al. [34] have detected 4HB derived from the metabolic pathway of kaempferol in rat microflora, possibly as a result of further 4HPAA processing. To investigate if kidney cells could directly transform kaempferol in a similar way, we tested whether 4HPAA or p-cresol could serve as Q ring precursors. A MTT assay ruled out any toxicity of these compounds in concentrations ranging from 5 nM to 100 µM (data not shown). Thus, we used both 4HPAA and *p*-cresol at a

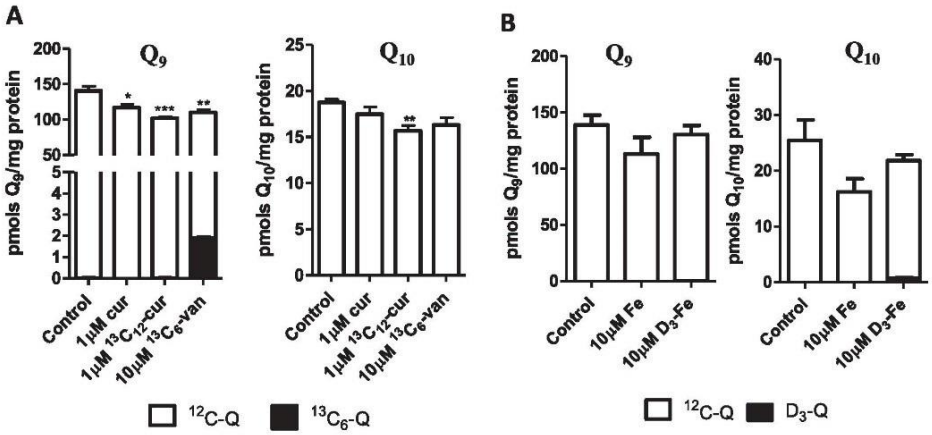

Fig. 4. Effect of curcumin, ferulic acid and vanillin on Q biosynthesis in Tkpts cells. (A) Q levels were slightly decreased in Tkpts cells treated with curcumin and vanillin. A small amount of $^{13}C_6$-Q was detected when Tkpts cells were treated with $^{13}C_6$-vanillin, but not when treated with $^{13}C_{12}$-curcumin, indicating that curcumin does not act as a Q ring precursor. **(B)** Ferulic acid did not alter Q levels and no deuterated signal was recovered after the treatment with D_3-ferulic acid, indicating that ferulic acid does not serve as a Q ring precursor. Statistically significant differences in total Q_9 or Q_{10} between control and treatments are represented by *$p < 0.05$, **$p < 0.01$ and ***$p < 0.001$.

similar concentration as that used in our previous experiments with kaempferol (10 μM). Our results showed that neither 4HPAA nor *p*-cresol increased Q levels, and they were also unable to compete with ^{14}C-4HB in a Q biosynthesis competition assay (Supplementary Fig. S5). Together, these results argue against 4HPAA and *p*-cresol as metabolites mediating the effect of kaempferol on Q biosynthesis in kidney cells.

3.4. Role of other phenolic compounds as Q ring precursors

To further study the ability of other dietary phenolic substances to act as precursors in Q biosynthesis we tested curcumin and ferulic acid, which have a quite different structure in comparison with the stilbenoids and flavonoids we already tested. We also analyzed vanillin, a simpler molecule that shares the same ring structure as curcumin, and ferulic acid (see Supplementary Fig. S1). Vanillic acid, which also bears hydroxyl and methoxy groups in the same position of the ring, has been previously described as a Q ring precursor in mammals [35]. As shown in Fig. 4A, total Q_9 levels were decreased when Tkpts cells were treated with both unlabeled or $^{13}C_{12}$-labeled curcumin, with no $^{13}C_6$-Q being detected in the latter case. The same trend was observed for Q_{10} levels, although a statistically significant decrease was observed only in the case of $^{13}C_{12}$-labeled curcumin. Similar results were obtained using D_6-curcumin in Tkpts cells (data not shown). Vanillin also produced a decrease of Q_9 levels, and the same trend was observed for Q_{10} although without statistical significance. Strikingly, even when total Q levels were decreased, we were able to detect a signal for $^{13}C_6$-Q_9 although not for $^{13}C_6$-Q_{10} in lipid extracts obtained from cells cultured in the presence of $^{13}C_6$-vanillin (Fig. 4A). However, the proportion of $^{13}C_6$-Q_9 present in cells treated with $^{13}C_6$-vanillin was only about 2%, which is much lower than that produced by ^{13}C-kaempferol (see Fig. 3C). Ferulic acid did not produce any significant change of total Q levels, and deuterated forms of Q_9 or Q_{10} only accounted for a minor portion of total Q after treatment of Tkpts cells with D_3-ferulic acid (Fig. 4B).

Treatments were also carried out in human HEK 293 cells and, in this case, we found that both curcumin and vanillin increased Q levels. We were unable to detect any $^{13}C_6$-Q_{10} in cells cultured for 48 h in the presence of $^{13}C_{12}$-labeled curcumin (Supplementary Fig. S4B), which indicated that the increase of Q levels is not related to augmented Q biosynthesis. Total amounts of Q were also increased in HEK 293 cells cultured in the presence of $^{13}C_6$-labeled vanillin, but $^{13}C_6$-Q_{10} was only about 1% of total Q (Supplementary Fig. S4B), making it unlikely that augmented Q biosynthesis plays a prominent role for the increase of Q levels observed in this cell type. Treatment with ferulic acid did not alter Q levels and the deuterated form of Q_{10} (D_3-Q_{10}) was not detected. In summary, we demonstrate that neither curcumin nor ferulic acid serve as ring precursor for the Q biosynthetic pathway in mouse or human kidney cells, whereas vanillin plays only a minor role in comparison with kaempferol or with the endogenous substrate 4HB.

3.5. 4HB availability is a limiting step for Q biosynthesis in kidney cells

The efficient utilization of kaempferol by kidney cells as a Q ring precursor could be linked to a limited availability of endogenous ring precursors in these cells. In accordance, Pierrel et al. [7] described that availability of the ring precursor (4HB or PABA) was a rate-limiting step for the biosynthesis of Q_6 in yeasts cultured in PABA-free medium. To test whether the effect of kaempferol-mediated increase in Q levels in mammalian cells resulted from limiting amounts of endogenous ring precursors, we measured Q levels in cells that had been treated with exogenous 4HB. For these determinations, we compared the response of the two kidney-derived cell types (mouse Tkpts and human HEK 293) with that of non-kidney cell lines, including mouse liver hepatoma Hepa 1.6, MEFs, human liver hepatoma Hep G2, and human promyelocytic leukemia HL-60 cells. As depicted in Fig. 5, Q levels were dramatically increased in the two kidney-derived cell lines when cultured in the presence of 4HB, and attained levels four- to six-fold higher as compared to the corresponding no addition control. HEK 293 cells were particularly sensitive to supplementation of culture medium with 4HB, with a close to maximal response being already achieved at concentrations as low as 5 nM 4HB. In the mouse Hepa 1.6 cell line, Q levels were increased two-fold by 4HB concentrations between 5 nM and 1 μM but, strikingly, this response was lost at concentration of 10 μM and higher. In the case of MEFs, a slight increase was obtained for the Q_9 isoform at concentrations of 4HB between 50 nM and 1 μM, but no significant changes were observed for Q_{10}. Except for a slight increase of Q_{10} levels at 50 nM 4HB in Hep G2 cells, no further alteration of Q levels by exogenous 4HB supplementation was observed in this cell line or in HL-60 cells at any concentration.

Taken together, these results indicate that availability of endogenous 4HB is a limiting step for Q biosynthesis in kidney cells, and that incorporation of exogenously applied ring precursors, such as kaempferol is favored. This could be due to a rapid flow of metabolites towards Q biosynthesis, which maintains very low levels of upstream substrates such as endogenous 4HB in kidney cells. This interpretation

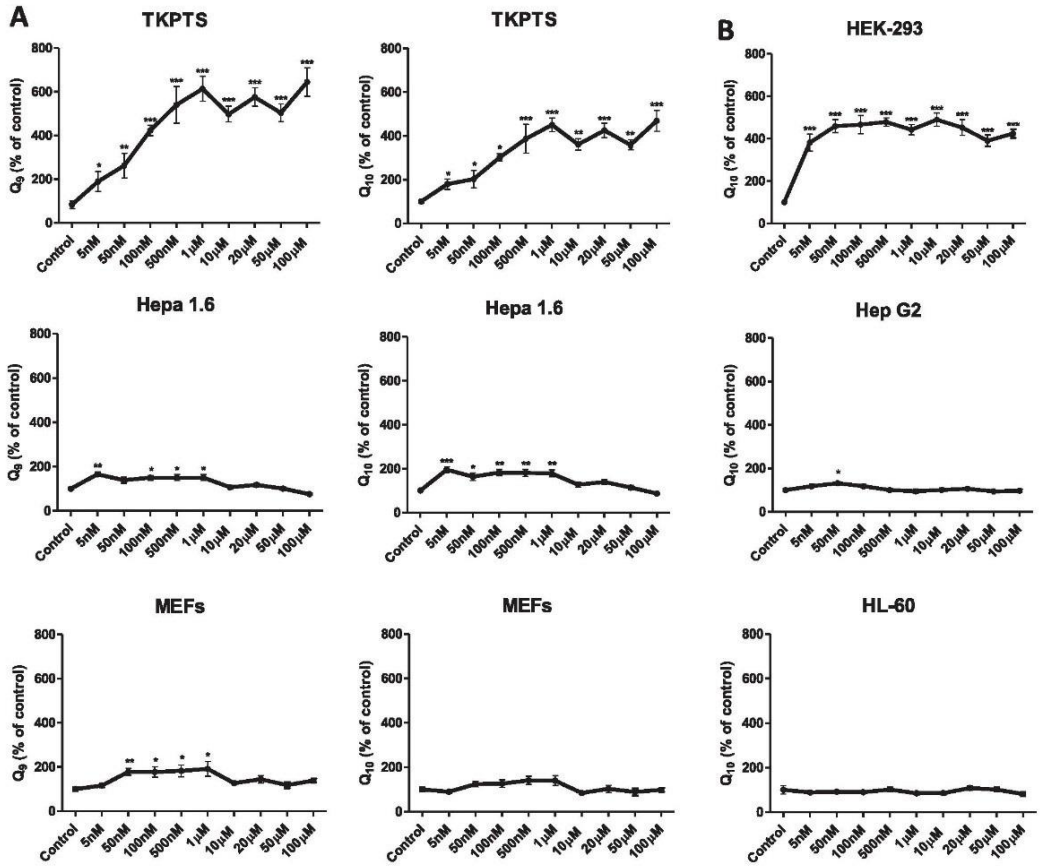

Fig. 5. 4HB is a limiting step in the biosynthesis of Q in kidney cells. (A) Different types of murine cells were treated with increasing concentrations of 4HB. Tpkts cells exhibited a dramatic increase in Q_9 and Q_{10} levels. However, only a slight increase at some concentrations of 4HB was observed for Hepa 1.6 and MEFs. **(B)** Similar experiments were performed in human cell lines. Human kidney-derived cells (HEK 293) displayed a significant increase of Q_{10} levels, but this effect was not found in human lines from another origin, such as Hep G2 or HL-60. The dramatic increase of Q levels in Tkpts and HEK 293 supports that availability of 4HB is a limiting step for the Q biosynthetic pathway in kidney cells. Statistically significant differences in total Q_9 or Q_{10} between control and treatments are represented by $^*p < 0.05$, $^{**}p < 0.01$ and $^{***}p < 0.001$.

was further supported by the comparison of Q levels in Tkpts and Hepa 1.6 cells, the former containing much higher amounts of Q, particularly Q_{10} (Fig. 6A), and of the polyprenyltransferase Coq2, the enzyme that catalyzes the condensation reaction between ring and hydrophobic tail precursors, which was found also significantly enriched in Tkpts in comparison with Hepa 1.6 cells (Fig. 6B). This situation resembles that of kidney and liver tissues in the mouse [25].

3.6. Kaempferol is not utilized as a Q ring precursor by yeast cells as efficiently as 4HB

Since yeast utilize several ring precursors alternative to 4HB for Q biosynthesis, such as PABA [6,7], *p*-coumarate and resveratrol [9], we investigated whether kaempferol might also serve as a biosynthetic Q precursor in *S. cerevisiae*. In this study, we also investigated the effects of ferulic acid, vanillin, and curcumin, which had not been tested previously as putative Q biosynthetic ring precursors. As stated above, all of these compounds share the same ring structure as vanillic acid. Results obtained with these compounds were compared with those obtained with the endogenous substrate 4HB. Importantly, for these experiments yeast cells were cultured in minus PABA medium, since the presence of PABA in the medium could mask a role for the phenolics as putative Q biosynthetic precursors [6,7]. Yeast cells were grown for 3 h in the presence of each compound at 10 μM concentration, and lipids were extracted for Q_6 quantification. As depicted in Fig. 7A, no significant differences could be observed in the Q_6 levels between cells treated with the unlabeled compounds compared to the control cells.

We next cultured yeast cells in the presence of ^{13}C-labeled kaempferol to test whether kaempferol might still serve as a ring precursor of Q_6 in yeast. Although $^{13}C_6$-Q_6 was detected, it comprised only two to four percent of the total Q content (Fig. 7B). In contrast, $^{13}C_6$-4HB was readily incorporated into $^{13}C_6$-Q_6, and also significantly enhanced the total Q content (Fig. 7B) indicating that, compared to kaempferol, yeast can utilize 4HB as a Q ring precursor with a substantially higher efficacy. As we previously observed in kidney cells, despite the decrease of Q_6 levels produced by vanillin, some $^{13}C_6$-labeled Q_6 could be detected when yeast cells were grown in the presence of $^{13}C_6$-labeled vanillin. Finally, as also found previously for kidney cells, no $^{13}C_6$-labeled Q_6 was detected when yeast cells were cultured in the presence of $^{13}C_{12}$-curcumin, suggesting this compound does not serve as a Q ring precursor.

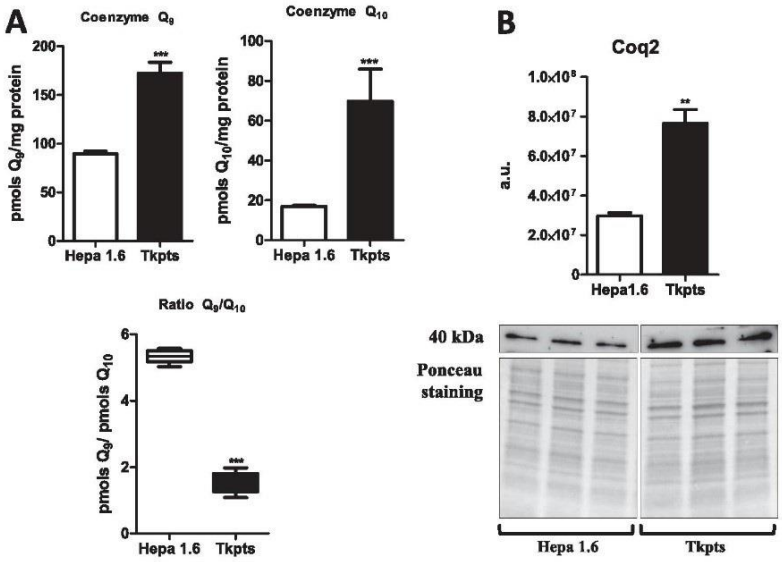

Fig. 6. Kidney-derived Tkpts cells display increased levels of Q and Coq2 in comparison with hepatic Hepa1.6 cells. (A) Q levels and Q_9/Q_{10} ratio. Q levels were higher and Q_9/Q_{10} ratio lower in Tkpts than in Hepa 1.6 cells. **(B)** Coq2 prenyltransferase levels. Arbitrary units depicted in the graph relate directly to the immunoblots shown underneath, which derive from the same film. Statistically significant differences between both cell types are represented by $^{**}p < 0.01$ and $^{***}p < 0.001$.

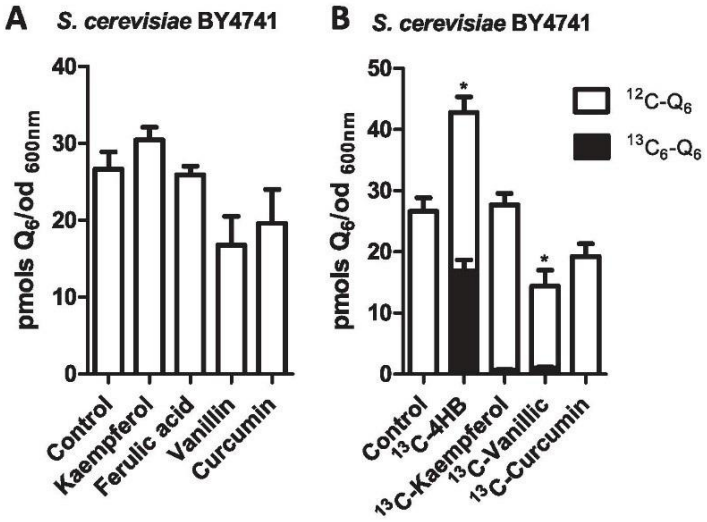

Fig. 7. Kaempferol, ferulic acid, vanillin and curcumin are not utilized as Q ring precursors as efficiently as 4HB in yeast. (A) Effect of kaempferol, ferulic acid, vanillin and curcumin on Q_6 levels. BY4741 yeast cells were treated with these compounds at 10 μM concentrations each, or with EtOH to establish the vehicle control. Yeast were subsequently grown for 3 h in PABA-minus folate-minus medium. **(B)** Effect of ^{13}C-ring-labeled compounds on *de novo* Q_6 biosynthesis. BY4741 yeast cells were treated with $^{13}C_6$-4HB, ^{13}C-kaempferol, $^{13}C_6$-vanilin, $^{13}C_{12}$-curcumin, or with EtOH to establish the vehicle control. Significant differences refer to the control condition and are represented by $^{*}p < 0.05$.

4. Discussion

Polyphenols, which are widely present in foods and beverages of plant origin, have received great interest during the last years due to their positive effects on human health. Several studies have strongly supported a role for polyphenols in the prevention of important diseases such as cancer, cardiovascular disease, chronic inflammation and neurodegenerative disease [36]. The beneficial properties of polyphenols have been partially attributed to a role as antioxidants as well as to their ability to modulate molecular targets and signaling pathways. Their antioxidant capacity is widely linked to their ability to reduce free radical formation and to scavenge free radicals, but other mechanisms of action serving to elevate endogenous antioxidants are also important. For example, polyphenols can induce antioxidant enzymes such as glutathione peroxidase, catalase and superoxide dismutase and inhibit the expression of enzymes such as xanthine oxidase [37]. Another important factor is the molecular structure of these compounds, which can modulate their properties and functions. Of note, the 3-hydroxyl group in flavonols is considered especially important for their antioxidant activities [38].

As a lipid-soluble antioxidant that can be endogenously synthesized by all organisms, Q plays a major role in antioxidant defense [30]. Resveratrol and *p*-coumarate have been described as Q ring precursors in *E. coli*, *S. cerevisiae* and human cells, but the possibility that polyphenols could actually increase the levels of this lipid antioxidant in cells has not been explored. A capacity to increase endogenous Q levels could be a very important finding to palliate Q deficiencies associated with aging or disease. Kidney cells are especially sensitive to a decrease of Q levels, and a nephrotic syndrome is a major clinical phenotype in Q deficiencies [39]. For this reason, we selected two kidney-derived lines,

murine Tkpts and human HEK 293 cells, to study the capacity of different polyphenols to increase Q levels.

Two stilbenes, (resveratrol and piceatannol), and two flavonols, (quercetin and kaempferol), were selected in the first phase of our studies. Resveratrol has been the subject of intense research due to its purported cardiovascular protective, antiplatelet, antioxidant, anti-inflammatory, blood-glucose-lowering and anti-cancer activities (reviewed in [40]). Piceatannol is a hydroxylated analogue of resveratrol and shares the structural motif and biological activities, being even more potent in some studies [41]. Apart from the beneficial effects of stilbenes, the regular consumption of flavonoids is related to reduced risk of a number of chronic diseases, including cancer, cardiovascular disease and neurodegenerative disorders (reviewed in [42]). Flavonoids are divided into several groups, with flavonols being those containing the 3-hydroxy group, which has been considered very important for antioxidant activity. For our determinations, we chose quercetin and kaempferol, the two most common compounds in this group. Among these four compounds, only kaempferol efficiently increased Q levels in kidney cells and, interestingly, the effects were observed at concentrations that can be attainable physiologically both by consumption of flavonoids-containing food and by oral supplementation [15,43,44]. Since this ability may derive from its chemical structure, we also tested additional structurally related flavonoids. We chose two flavones, apigenin and luteolin, and one flavanone, naringenin. Of these, only apigenin caused a slight increase in Q_9 and Q_{10} at select concentrations, although its effects were extremely limited in comparison with kaempferol and a slight inhibition was also observed for one of the concentrations tested.

The increase in Q levels by kaempferol in kidney cells depends directly on the stimulation of Q biosynthesis. The kaempferol-mediated increase in Q was blocked by the Q biosynthesis inhibitor PABA; conversely addition of kaempferol competed with incorporation of ^{14}C-4HB into ^{14}C-labeled Q. Cells treated with ^{13}C-kaempferol generated newly synthesized $^{13}C_6$-Q, and demonstrated that kaempferol behaves as a novel Q ring precursor in mammalian cells. The metabolism of kaempferol responsible for its incorporation into the Q biosynthetic pathway remains to be established, although two possibilities can be proposed: (1) kaempferol could act directly as a Q precursor being itself a substrate for the Coq2 transferase and would be subsequently metabolized and modified by different Coq proteins until it reaches the final structure of Q; or alternatively (2) kaempferol could be cleaved in the cell to yield potential ring precursors which would be then integrated into this pathway. Indeed, previous studies have shown that flavonoids can be transformed by colonic microflora into phenolic acids. However, the type of metabolic products depends on what phenolic compound is metabolized and its specific structure [34]. Cleavage of kaempferol by colonic microflora occurs between C-3 and C-4 carbons of ring C, forming 4HPAA [32,33] derived from the B ring, 4HPAA is then rapidly decarboxylated to form *p*-cresol [45]. If kidney cells were able to perform a biochemical transformation of kaempferol similar to that described for colonic microflora, this would provide an efficient source of Q precursors. However, neither 4HPAA nor *p*-cresol increased Q levels nor competed with ^{14}C-4HB, demonstrating that these compounds do not act as Q ring precursors. Therefore, even if kaempferol is cleaved in renal cells before entering the Q biosynthetic pathway, these known metabolites are not involved in augmenting Q levels.

Whatever the metabolic route involved, an increase of alternative Q ring precursors in cells will only result in higher Q levels if cells have low availability of endogenous 4HB. Pierrel et al. [7] described 4HB as a limiting step in the biosynthesis of Q in *S. cerevisiae* cells and, as we have demonstrated here, this also holds true for kidney cells, although not for other cell lines such as MEFs, Hep G2 and HL-60. The increase of Q observed after a treatment with nanomolar concentrations of 4HB or kaempferol confirms that the availability of endogenous ring precursors is very low in kidney cells of both mouse and human origin. The fact that many cell types do not show increased Q levels in response to exogenous 4HB is in agreement with the early demonstration that 4HB may be present at saturating concentrations in liver, as determined by *in vitro* assays with liver tissue slices [46]. Tissue-specificity regarding the effect of supplementation with ring precursors on Q biosynthesis is further supported by the observations of Wang et al. [47], who demonstrated that adding the ring precursor 2,4-dihydroxybenzoic acid (2,4-DHB) to the drinking water of Q-deficient Mclk1 KO mice resulted in a healthier phenotype, an increase in Q levels and an improvement of the mitochondrial respiratory capacity in heart, kidney and skeletal muscle, although no statistically significant differences were observed in small intestine. Moreover, when 2,4-DHB was given to wild-type mice an increase of Q_9 levels was still detected in kidney mitochondria, but no increase was observed in mitochondria isolated from heart, liver, skeletal muscle or intestine, which agrees with the idea that, even under normal (non deficient) conditions, availability of Q ring precursors is a limiting step in kidney.

In a previous report [25], we demonstrated maximal levels of Coq2 polypeptide in those organs displaying the highest Q concentrations, such as kidney and heart. In accordance, the murine kidney-derived Tkpts cells also showed significantly higher levels of both Q and Coq2 polypeptide than murine hepatic Hepa 1.6 cells. Higher levels of the Coq2 transferase might maintain low cellular concentrations of the ring precursor 4-HB due to its rapid use *via* the Coq2 prenyltransferase activity. Higher Coq2 levels could also account for making these cells particularly responsive to ring precursors as 4HB or kaempferol, leading to a significant increase of Q levels upon supplementation. Further experiments will be needed to fully understand how kaempferol is metabolized to take part directly in the biosynthesis of Q.

Experiments carried out with *S. cerevisiae* demonstrated that kaempferol is not effective in increasing Q_6 levels or acting as a Q ring precursor in this eukaryotic cell model, even when ring precursors are limiting the biosynthesis of Q. Previous studies indicate that yeast cultured under PABA limiting conditions show increased Q_6 content when supplemented with either 4HB or PABA (6). The lack of an effect of kaempferol indicates that yeast cannot utilize flavonoids in the same manner as mammalian cells.

The non-flavonoid compound curcumin, which contains two ferulic acid moieties linked *via* a methylene bridge at the carbonyl group C atoms, undergoes metabolism in animals, possesses antioxidant capacity and produces beneficial effects on diabetes, inflammation and neurodegenerative disease by modulating multiple signal molecules (transcription factors, enzymes, *etc.*) and controlling gene expression [48]. Structure of curcumin and ferulic acid differs substantially from that of flavonoids and stilbenoids, so testing their effect on Q system was of considerable interest. However, our data indicate that neither curcumin nor ferulic acid increase Q levels, and only ferulic produced a small but detectable signal of D_3-labeled Q in kidney cells. Similar results were obtained in yeast cells. Chemical structure is a key factor that define the functions and the effect of the different polyphenols. In our study, flavonoids were more efficient used in Q biosynthesis than other non-flavonoid compounds like stilbenoids and curcuminoids. Moreover, one member of the flanovol group (kaempferol) and one member from the flavone group (apigenin) were the ones that displayed the strongest effect increasing Q_9 and Q_{10} levels in renal cells.

The difference between flavonols and flavones is distinguished by the presence of a hydroxyl group in the C3 position. This group seems to be critical because kaempferol (that possesses this group) is much more efficient in increasing Q levels than apigenin and, interestingly, this specific OH group has been linked to an increase of antioxidant activity [38]. However, kaempferol and apigenin have a common characteristic that also seems to be an important determinant for their effect on Q biosynthesis: both compounds possess one hydroxyl group in the B ring. The presence of two hydroxyl groups in this ring, as is the case for quercetin and luteolin, abolishes the effect of these flavonoids on Q biosynthesis. One study that compared the anxiolytic effect of different flavonols noted that this activity decreased with an increasing number

of hydroxyl groups in the B ring: kaempferol revealed again the strongest effect, whereas myricetin (which possesses three hydroxyl groups) did not have any effect [49].

In addition, kaempferol has been previously described as a Sirt3 activator. This mitochondrial sirtuin mediates the adaptation of increased energy demand during adverse conditions to increase the production of energy equivalents, and also deacetylates and activates mitochondrial enzymes involved in fatty acid β-oxidation, amino acid metabolism, the electron transport chain, and antioxidant defense [28]. Our results have shown that mitochondrial levels of Sirt3 were indeed increased after kaempferol treatment, confirming these effects also take place in renal cells. However, treatment of kidney cells with NAM, a general inhibitor of sirtuin activity, did not affect the kaempferol-induced increase of Q levels, indicating that Sirt3 activation does not mediate kaempferol effects on Q biosynthesis. Furthermore, Q levels measured in different tissues obtained from Sirt3 knockout mice did not differ from those measured in their wild-type littermates, indicating that Sirt3 does not modulate Q biosynthesis.

Further experimentation is warranted to elucidate whether dietary kaempferol supplementation also increases Q levels in animals, both under normal and Q-deficient conditions. Extensive metabolism of kaempferol when administered with the diet results in very low levels of circulating kaempferol in mice [50], which could hamper potential beneficial effects on Q biosynthesis. However, given the specific response of kidney to small amounts of ring precursors, it is still possible that dietary kaempferol could lead to increased Q levels in this organ, as previously observed for 2,4-DHB [47]. Increasing the availability of Q precursors in cells could move the metabolic flux in favor of the synthesis of Q, helping to ameliorate the phenotype associated with certain Q deficiencies, at least for some organs such as kidney.

In conclusion, we demonstrate that some components of a healthy diet can influence the levels of Q in renal cells. The flavonol kaempferol is identified here as having the strongest effect on increased Q levels due to its action as a novel ring precursor in Q biosynthesis. The ability of kaempferol to simultaneously increase Q and Sirt3 levels, link several of the beneficial effects previously described for this molecule. Further experiments, both *in vitro* and *in vivo*, will be needed to elucidate the exact metabolic pathway by which kaempferol participates in Q biosynthesis, as well as to test its potential beneficial effects *in vivo*.

Acknowledgements

Supported by the Spanish Ministerio de Economía y Competitividad Grants (BFU2011-23578 and BFU2015-64630-R) cofinanced with EU FEDER funds, Junta de Andalucía (BIO-276) and Universidad de Córdoba. JA, LFR and EGC were supported by FPU fellowships from the Spanish Ministerio de Educación, Cultura y Deporte (reference AP2009-1491, FPU12/03398 and FPU13/04188, respectively) and BIO-276. C.S. and A.I.J. were supported by award AT006896 from NCCIH of the NIH to C.S., O.K. was supported by GM071779 from NIGMS of the NIH, and A.N. and A.A. were supported by a grant from the National Science Foundation (MCB-1330803) to C.F.C. Dr. Elsa Bello-Reuss and Dr. Judit Magyesi (University Medical Center, Lubbock, TX, USA) kindly provided the mouse kidney proximal tubule epithelial (Tkpts) cells. The authors thank the personnel from the Servicio Centralizado de Apoyo a la Investigación (SCAI; Universidad de Córdoba) for technical support.

Appendix A. Supplementary material

Supplementary data associated with this article can be found in the online version at http://dx.doi.org/10.1016/j.freeradbiomed.2017.06.006.

References

[1] J.M. Villalba, C. Parrado, M. Santos-Gónzalez, F.J. Alcaín, Therapeutic use of coenzyme Q10 and coenzyme Q10-related compounds and formulations, Expert Opin. Investig. Drugs 19 (4) (2010) 1–20.
[2] J. Ericsson, G. Dallner, Distribution, biosynthesis, and function of mevalonate pathway lipids, Sub-Cell. Biochem. 21 (1993) 229–272.
[3] M.A. Desbats, G. Lunardi, M. Doimo, E. Trevisson, L. Salviati, Genetic bases and clinical manifestations of coenzyme Q10 (CoQ 10) deficiency, J. Inherit. Metab. Dis. 38 (1) (2015) 145–156.
[4] K. Hayashi, Y. Ogiyama, K. Yokomi, T. Nakagawa, T. Kaino, M. Kawamukai, Functional conservation of coenzyme Q biosynthetic genes among yeasts, plants, and humans, PLoS One 9 (6) (2014) e99038.
[5] M.J. Acosta, L. Vazquez Fonseca, M.A. Desbats, C. Cerqua, R. Zordan, E. Trevisson, L. Salviati, Coenzyme Q biosynthesis in health and disease, Biochim. Et. Biophys. Acta 1857 (8) (2016) 1079–1085.
[6] B. Marbois, L.X. Xie, S. Choi, K. Hirano, K. Hyman, C.F. Clarke, para-Aminobenzoic acid is a precursor in coenzyme Q6 biosynthesis in Saccharomyces cerevisiae, J. Biol. Chem. 285 (36) (2010) 27827–27838.
[7] F. Pierrel, O. Hamelin, T. Douki, S. Kieffer-Jaquinod, U. Muhlenhoff, M. Ozeir, R. Lill, M. Fontecave, Involvement of mitochondrial ferredoxin and para-aminobenzoic acid in yeast coenzyme Q biosynthesis, Chem. Biol. 17 (5) (2010) 449–459.
[8] A. Block, J.R. Widhalm, A. Fatihi, R.E. Cahoon, Y. Wamboldt, C. Elowsky, S.A. Mackenzie, E.B. Cahoon, C. Chapple, N. Dudareva, G.J. Basset, The Origin and Biosynthesis of the Benzenoid Moiety of Ubiquinone (Coenzyme Q) in Arabidopsis, Plant Cell 26 (5) (2014) 1938–1948.
[9] L.X. Xie, K.J. Williams, C.H. He, E. Weng, S. Khong, T.E. Rose, O. Kwon, S.J. Bensinger, B.N. Marbois, C.F. Clarke, Resveratrol and para-coumarate serve as ring precursors for coenzyme Q biosynthesis, J. Lipid Res. 56 (4) (2015) 909–919.
[10] R.S. Sohal, M.J. Forster, Coenzyme Q, oxidative stress and aging, Mitochondrion 7 (Suppl) (2007) S103–S111.
[11] F. Ozaltin, Primary coenzyme Q10 (CoQ 10) deficiencies and related nephropathies, Pediatr. Nephrol. 29 (6) (2014) 961–969.
[12] Y. Wang, S. Hekimi, Understanding Ubiquinone, Trends Cell Biol. 26 (5) (2016) 367–378.
[13] C. Sandoval-Acuna, J. Ferreira, H. Speisky, Polyphenols and mitochondria: an update on their increasingly emerging ROS-scavenging independent actions, Arch. Biochem. Biophys. 559 (2014) 75–90.
[14] S. Hatia, A. Septembre-Malaterre, F. Le Sage, A. Badiou-Beneteau, P. Baret, B. Payet, C. Lefebvre d'hellencourt, M.P. Gonthier, Evaluation of antioxidant properties of major dietary polyphenols and their protective effect on 3T3-L1 preadipocytes and red blood cells exposed to oxidative stress, Free Radic. Res. 48 (4) (2014) 387–401.
[15] A. Scalbert, G. Williamson, Dietary intake and bioavailability of polyphenols, J. Nutr. 130 (8S Suppl) (2000) 2073s–2085ss.
[16] O.N. Gordon, L.A. Graham, C. Schneider, Facile synthesis of deuterated and [(14) C] labeled analogs of vanillin and curcumin for use as mechanistic and analytical tools, J. Label. Compd. Radiopharm. 56 (14) (2013) 696–699.
[17] P.O. Edlund, Determination of coenzyme Q10, alpha-tocopherol and cholesterol in biological samples by coupled-column liquid chromatography with coulometric and ultraviolet detection, J. Chromatogr. 425 (1) (1988) 87–97.
[18] S. Ernest, E. Bello-Reuss, Expression and function of P-glycoprotein in a mouse kidney cell line, Am. J. Physiol. 269 (2 Pt 1) (1995) C323–C333.
[19] G.J. Todaro, H. Green, Quantitative studies of the growth of mouse embryo cells in culture and their development into established lines, J. Cell Biol. 17 (1963) 299–313.
[20] C.B. Brachmann, A. Davies, G.J. Cost, E. Caputo, J. Li, P. Hieter, J.D. Boeke, Designer deletion strains derived from Saccharomyces cerevisiae S288C: a useful set of strains and plasmids for PCR-mediated gene disruption and other applications, Yeast 14 (2) (1998) 115–132.
[21] J. Ariza, J.A. Gonzalez-Reyes, L. Jodar, A. Diaz-Ruiz, R. de Cabo, J.M. Villalba, Mitochondrial permeabilization without caspase activation mediates the increase of basal apoptosis in cells lacking Nrf2, Free Radic. Biol. Med. 95 (2016) 82–95.
[22] M.M. Bradford, A rapid and sensitive method for the quantitation of microgram quantities of protein utilizing the principle of protein-dye binding, Anal. Biochem. 72 (1–2) (1976) 248–254.
[23] C.F. Clarke, W. Williams, J.H. Teruya, Ubiquinone Biosynthesis in Saccharomyces cerevisiae, J. Biol. Chem. 266 (25) (1991) 16636–16644.
[24] C. Cordoba-Pedregosa Mdel, J.M. Villalba, F.J. Alcain, Determination of coenzyme Q biosynthesis in cultured cells without the necessity for lipid extraction, Anal. Biochem. 336 (1) (2005) 60–63.
[25] C. Parrado-Fernandez, G. Lopez-Lluch, E. Rodriguez-Bies, S. Santa-Cruz, P. Navas, J.J. Ramsey, J.M. Villalba, Calorie restriction modifies ubiquinone and COQ transcript levels in mouse tissues, Free Radic. Biol. Med. 50 (12) (2011) 1728–1736.
[26] G. Marfe, M. Tafani, M. Indelicato, P. Sinibaldi-Salimei, V. Reali, B. Pucci, M. Fini, M.A. Russo, Kaempferol induces apoptosis in two different cell lines via Akt inactivation, Bax and SIRT3 activation, and mitochondrial dysfunction, J. Cell. Biochem. 106 (4) (2009) 643–650.
[27] H. Cimen, M.J. Han, Y. Yang, Q. Tong, H. Koc, E.C. Koc, Regulation of succinate dehydrogenase activity by SIRT3 in mammalian mitochondria, Biochemistry 49 (2) (2010) 304–311.
[28] B. Kincaid, E. Bossy-Wetzel, Forever young: SIRT3 a shield against mitochondrial meltdown, aging, and neurodegeneration, Front. Aging Neurosci. 5 (2013) 48.
[29] H.J. Weir, J.D. Lane, N. Balthasar, SIRT3: a central regulator of mitochondrial adaptation in health and disease, Genes Cancer 4 (3–4) (2013) 118–124.
[30] M. Turunen, J. Olsson, G. Dallner, Metabolism and function of coenzyme Q, Biochim. Et. Biophys. Acta (BBA) - Biomembr. 1660 (1–2) (2004) 171–199.
[31] D. Gonzalez-Aragon, M.I. Buron, G. Lopez-Lluch, M.D. Herman, C. Gomez-Diaz, P. Navas, J.M. Villalba, Coenzyme Q and the regulation of intracellular steady-state levels of superoxide in HL-60 cells, BioFactors 25 (1–4) (2005) 31–41.

[32] J. Winter, L.H. Moore, V.R. Dowell Jr., V.D. Bokkenheuser, C-ring cleavage of flavonoids by human intestinal bacteria, Appl. Environ. Microbiol. 55 (5) (1989) 1203–1208.
[33] F. Moradi-Afrapoli, M. Oufir, F.R. Walter, M.A. Deli, M. Smiesko, V. Zabela, V. Butterweck, M. Hamburger, Validation of UHPLC-MS/MS methods for the determination of kaempferol and its metabolite 4-hydroxyphenyl acetic acid, and application to in vitro blood-brain barrier and intestinal drug permeability studies, J. Pharm. Biomed. Anal. 128 (2016) 264–274.
[34] A. Serra, A. Macià, M.P. Romero, J. Reguant, N. Ortega, M.J. Motilva, Metabolic pathways of the colonic metabolism of flavonoids (flavonols, flavones and flavanones) and phenolic acids, Food Chem. 130 (2) (2012) 383–393.
[35] A.M. Nambudiri, D. Brockman, S.S. Alam, H. Rudney, Alternate routes for ubiquinone biosynthesis in rats, Biochem. Biophys. Res. Commun. 76 (2) (1976) 282–288.
[36] D. Del Rio, A. Rodriguez-Mateos, J.P. Spencer, M. Tognolini, G. Borges, A. Crozier, Dietary (poly)phenolics in human health: structures, bioavailability, and evidence of protective effects against chronic diseases, Antioxid. Redox Signal. 18 (14) (2013) 1818–1892.
[37] Y. Du, H. Guo, H. Lou, Grape seed polyphenols protect cardiac cells from apoptosis via induction of endogenous antioxidant enzymes, J. Agric. Food Chem. 55 (5) (2007) 1695–1701.
[38] R. Tsao, Chemistry and biochemistry of dietary polyphenols, Nutrients 2 (12) (2010) 1231–1246.
[39] C.M. Quinzii, M. Hirano, Primary and secondary CoQ(10) deficiencies in humans, BioFactors 37 (5) (2011) 361–365.
[40] L. Kursvietiene, I. Staneviciene, A. Mongirdiene, J. Bernatoniene, Multiplicity of effects and health benefits of resveratrol, Medicina 52 (3) (2016) 148–155.
[41] D. Arai, R. Kataoka, S. Otsuka, M. Kawamura, H. Maruki-Uchida, M. Sai, T. Ito, Y. Nakao, Piceatannol is superior to resveratrol in promoting neural stem cell differentiation into astrocytes, Food Funct. 7 (10) (2016) 4432–4441.
[42] A. Kozlowska, D. Szostak-Wegierek, Flavonoids–food sources and health benefits, Rocz. Panstw. Zakl. Hig. 65 (2) (2014) 79–85.
[43] C. Manach, A. Scalbert, C. Morand, C. Remesy, L. Jimenez, Polyphenols: food sources and bioavailability, Am. J. Clin. Nutr. 79 (5) (2004) 727–747.
[44] J.M. Calderon-Montano, E. Burgos-Moron, C. Perez-Guerrero, M. Lopez-Lazaro, A review on the dietary flavonoid kaempferol, Mini Rev. Med. Chem. 11 (4) (2011) 298–344.
[45] S. Labib, S. Hummel, E. Richling, H.U. Humpf, P. Schreier, Use of the pig caecum model to mimic the human intestinal metabolism of hispidulin and related compounds, Mol. Nutr. Food Res. 50 (1) (2006) 78–86.
[46] S. Ranganathan, T. Ramasarma, The regulation of the biosynthesis of ubiquinone in the rat, Biochem. J. 148 (1) (1975) 35–39.
[47] Y. Wang, D. Oxer, S. Hekimi, Mitochondrial function and lifespan of mice with controlled ubiquinone biosynthesis, Nat. Commun. 6 (2015) 6393.
[48] S. Ghosh, S. Banerjee, P.C. Sil, The beneficial role of curcumin on inflammation, diabetes and neurodegenerative disease: a recent update, Food Chem. Toxicol.: Int. J. Publ. Br. Ind. Biol. Res. Assoc. 83 (2015) 111–124.
[49] C. Vissiennon, K. Nieber, O. Kelber, V. Butterweck, Route of administration determines the anxiolytic activity of the flavonols kaempferol, quercetin and myricetin–are they prodrugs? J. Nutr. Biochem. 23 (7) (2012) 733–740.
[50] V. Zabela, C. Sampath, M. Oufir, F. Moradi-Afrapoli, V. Butterweck, M. Hamburger, Pharmacokinetics of dietary kaempferol and its metabolite 4-hydroxyphenylacetic acid in rats, Fitoterapia 115 (2016) 189–197.

CHAPTER 4

Investigation and characterization of the role of *p*-coumaric acid as a ring precursor in coenzyme Q biosynthesis in yeast

Author contributions: Anish Nag and Catherine F. Clarke contributed to the intellectual development of the project. Anish Nag, Ding Hui, and Ohyun Kwon contributed to the chemical synthesis of the stable isotope labeled compound. Anish Nag conducted the yeast assays and the HPLC-MS/MS studies. Anish Nag contributed to the data acquisition, characterization, and statistical analyses. Anish Nag and Catherine F. Clarke contributed to the writing and revision of the chapter.

Introduction:

Coenzyme Q (Q or ubiquinone) is an essential lipid composed of a fully substituted benzoquinone ring moiety and a polyisoprenoid tail that plays a critical role as an electron transporter in the mitochondrial respiratory chain and in the plasma membrane of *Escherichia coli* (1, 2). The polyisoprenoid tail of Q is made up of a variable number of isoprenyl units depending on the species (six for *Saccharomyces cerevisiae*, eight for *E. coli*, nine for mouse, and ten for human, hence Q_{10}). Coenzyme Q is generally biosynthesized from 4-hydroxybenzoic acid (4HB) in *S. cerevisiae* (yeast) (3). However, yeast can also use p-aminobenzoic acid (pABA) as another primary precursor of Q (4, 5). As reported in Chapter 3, Kaempferol can act as an alternate Q ring precursor in mammalian cells but not in yeast. However, in the quest for alternate ring precursors of Q in yeast, studies were able to identify two other phenolic compounds, resveratrol and p-coumaric acid that can be utilized to produce Q in yeast (6).

Between resveratrol and p-coumaric acid, the latter turned out to be of considerably more interest as an alternate Q ring precursor since it was identified as an intermediate in the biosynthesis of 4HB in *Arabidopsis thaliana* (7). Plant peroxisomes contain thiolases and CoA thioesterases that are capable of ultimately producing 4HB from 4-hydroxybenzoyl-CoA (7, 8). Tyrosine (Tyr) can also successfully supply the ring of Q in *Arabidopsis*; but it is surmised that this occurs through a parallel pathway, because *Arabidopsis* mutants that are unable to utilize phenylalanine (Phe) are still capable of utilizing Tyr in the biosynthesis of Q. Yeast is not able to hydroxylate Phe to form Tyr, and it therefore it was inferred that the conversion of tyrosine to 4HB occurs via its metabolism to p-coumaric acid (9, 10). However, 4HB biosynthesis in yeast and the exact role p-

coumaric acid plays as a Q ring precursor still remain largely obscure. Only recently were studies able to identify the first and penultimate steps involved in the conversion of tyrosine to 4HB in yeast (11, 12). These reports identified the penultimate step in the biosynthesis of 4HB to be the oxidation of 4-hydroxybenzaldehyde (4HBz) catalyzed by the alcohol dehydrogenase Hfd1. The formation of 4HBz, however, could not be related to p-coumaric acid.

Therefore, more detailed studies were made on the exact role p-coumaric acid plays in Q biosynthesis in yeast. Particularly, further insight was required regarding the uptake of exogenously added p-coumaric acid and its subsequent conversion to Q. Attempts were also made to delve into the possibility of p-coumaric acid acting as an intermediate in the 4HB pathway, and to investigate multiple potential pathways involving p-coumaric acid as a Q precursor with or without 4HBz and/or 4HB acting as an intermediate.

Results:

In order to study the uptake of p-coumaric acid and its conversion to Q in yeast, [$^{13}C_6$-ring]-p-coumaric acid (**^{13}C-P)** was chemically synthesized (Scheme 1). The synthesis was achieved by a Perkin type reaction using commercial [$^{13}C_6$-ring]-4-hydroxybenzaldehyde (^{13}C-4HBz**)** and malonic acid (**2)** as the starting reactants. BY4741 WT and W303 WT yeast strains were then grown in four different types of media: YP-Dextrose (YPD), YP-Glycerol (YPG), Synthetic dextrose-complete (SD-complete) and Drop out dextrose with ammonium sulfate without pABA without folate (DOD). Initially the rates of growth of the two different WT yeast strains were tested in the four media types to ascertain the best time points for subsequent labeling with **^{13}C-P**

in order to measure its conversion to Q. The yeast strains were inoculated in the corresponding media at an initial optical density of 0.2 and the subsequently optical densities were measured in 2 hour increments after the strains were allowed to finish one doubling period and reach an optical density of 0.4-0.5. The corresponding growth curve observed in YPD (Figure 1A) showed logarithmic rate of growth initially which eventually slowed down and reached late logarithmic growth phase between the 8 and 10 hour time points in YPD. However, in YPG (Figure 1B) the logarithmic growth phase was observed to continue without a marked reduction in growth rate even up to the 10 hour time point. The growth curves observed in SD-complete and DOD (Figure 2, A and B) were similar to that in YPD. It was however seen that the W303 WT strain had vastly lower optical densities when growing in the DOD media compared to the BY4741 WT, even though the growth trend were similar between the two strains (Figure 2B).

The previous growth assays showed that adding the label **^{13}C-P** when the cells are at an optical density of 0.4-0.5 and subsequently collecting and pelleting the labeled samples over a 10 hour time period in increments of 2 hours would fit optimally within the logarithmic range of growth. Therefore, fresh yeast stocks of both the BY4741 WT and W303 WT strains were inoculated in fresh YPD, YPG, SD-complete and DOD media at a starting optical density of 0.2. Once the yeast had reached an optical density of 0.4-0.5, the label **^{13}C-P** was added and the the samples were collected and pelleted at 2, 4, 6, 8 and 10 hour times points after labeling. The samples were then subjected to lipid extraction and the Q content was analyzed by HPLC-MS/MS methods. It was seen that the W303 WT not only had greater endogenous unlabeled Q, but was also able to uptake and create *de novo* [$^{13}C_6$-ring]-Q_6 (^{13}C-Q) from the added label P with much higher efficiency than the BY4741 WT in all 4 media tested (Figures 3B, 4B, 5B, 6B). This was

a novel result since most previous studies involving p-coumaric acid acting as a Q ring precursor in yeast were conducted in BY4741 WT. The *de novo* ^{13}C-Q content was 10-20 fold lower than the endogenous unlabeled Q content in most of the media (Figure 3-6). However, in DOD the labeled Q content observed in the W303 WT was almost 25% of the total Q content, proving that DOD and W303 WT are the most ideal media and yeast strain, respectively, to study the role of p-coumaric acid as a Q ring precursor.

The next goal was to test whether p-coumaric acid is utilized as a Q ring precursor via some unknown biosynthetic mechanism that bypasses one or more of the steps catalyzed by the Coq proteins. To test this possibility, W303 WT and *coq 1-coq11* nulls in the W303 yeast background were labeled separately with **^{13}C-P** and [$^{13}C_6$-ring]-4-hydroxybenzoic acid (^{13}C-4HB) and the Q levels were quantified after collecting the cells 6 hours after labeling. It was observed that *coq10Δ* and *coq11Δ* were the only null mutants that produced endogenous unlabeled Q and was capable of generating *de novo* labeled ^{13}C-Q when labeled with both ^{13}C-4HB and **^{13}C-P** (Figure 7, A and B). Furthermore, both the unlabeled and labeled Q contents observed in *coq10Δ* and *coq11Δ* were comparable to the Q levels in WT (Figure 7). The trends were similar when unlabeled and labeled quantities of the late stage Q biosynthetic intermediate demethoxy Q (DMQ_6) were measured, with the *coq10Δ* and *coq11Δ* yeast strains showing similar levels to WT (Figure 8, A and B). However, *coq7Δ* also showed high levels of endogenous and *de novo* DMQ_6 as well, since DMQ_6 is the substrate of Coq7 which is responsible for the ring hydroxylation of DMQ. In addition *coq10Δ* showed some accumulation of both the species of DMQ_6.

Unsurprisingly most of the *coq* null strains showed relatively high quantities of the early stage Q biosynthetic intermediate 2-hexaprenyl-4-hydroxyphenol (HHB), whereas WT, *coq1Δ*, *coq2Δ*, *coq10Δ*, and *coq11Δ* had no HHB (Figure 9, A and B).

We also wanted to investigate whether p-coumaric acid is capable of increasing total Q levels similar to the effect that 4HB treatment has. To test this theory, W303 WT yeast was treated with **^{13}C-P**, ^{13}C-4HB, 4HB, p-coumaric acid and EtOH to serve as vehicle control. When the Q content in the cells were subsequently analyzed after harvesting the cells 6 hours post-treatment, it was seen that both ^{13}C-4HB and 4HB increases the total Q content compared with EtOH treatment (Figure 10). However, treatment with **^{13}C-P** and p-coumaric acid does not have the same effect and the total Q levels are similar to the vehicle control samples.

Finally, we wanted to determine whether p-coumaric acid is somehow involved in the biosynthesis of 4HB via the Hfd1 catalyzed 4Hbz oxidation. To test this possibility the HFD1 gene was silenced and *hfd1Δ* was created in the W303 yeast genetic background. The latter was labeled separately with ^{13}C-4HB, ^{13}C-4HBz and **^{13}C-P**, and the samples were collected 5, 10, and 24 hours after addition of the label. The corresponding *de novo* Q contents were compared with W303 WT treated under similar conditions (Figure 11). Upon quantification of the labeled [$^{13}C_6$-ring]-Q_6 content in the cells via HPLC-MS/MS, no significant differences were seen between the two strains when they were labeled with ^{13}C-4HB. Unsurprisingly, the *hfd1Δ* mutant had significantly lower [$^{13}C_6$-ring]-Q_6 than the WT when labeled with ^{13}C-4HBz. In particular it was intriguing that the *hfd1Δ* mutant also had a significantly lower value of [$^{13}C_6$-ring]-Q_6 content

than the WT at the 5 hour time point when both strains were labeled with **^{13}C-P**. However, at the 10 and 24 hour time points, the [$^{13}C_6$-ring]-Q_6 levels are not significantly different between the WT and the mutant.

Discussion:

P-coumaric acid had been previously identified as a Q ring precursor in yeast (6). It had also been identified as an intermediate in the biosynthesis of 4HB in plants, where it was shown to be an intermediate in the biosynthesis of 4HB from Tyr that occurs in the peroxisome via a beta-oxidative pathway (7). However, such a correlation has not been successfully made in yeast so far. The exact mechanism by which p-coumaric acid acts as a Q ring precursor in yeast is still unknown. Previous to this study, a comprehensive time and media dependent assay with p-coumaric acid had not been conducted in yeast. First we were able to show that the ideal time of growth during which to conduct a labeling study would be 10 hours post-labeling to capture the yeast within the logarithmic growth phase. We then grew WT yeast from the two different genetic backgrounds – BY4741 and W303, in four different types of media – YPD, YPG, SD-complete and DOD. Both the WT strains showed generation of ^{13}C-Q in all four media types across all the five time points chosen. However, we were able to come to the novel conclusion that the W303 genetic background of yeast is much more efficient at uptaking and converting p-coumaric acid into Q. A potential reason for this observation is the fact that the W303 genetic background of yeast is more efficient at cellular respiration, as corroborated by the higher overall Q levels compared to BY4741. Therefore, the former is possibly more efficient at utilizing substrates and intermediates that aid in cellular respiration, which potentially includes p-

coumaric acid. We were also able to conclude that generation of ^{13}C-Q from **^{13}C-P** is the most efficient in DOD media and 6-8 hours after addition of the label.

Questions still remain regarding the mechanistic details through which the aforementioned conversion occurs. It was postulated that p-coumaric acid gets converted to Q via intermediary conversion to 4HB through a beta-oxidative pathway. However, the biosynthesis of 4HB in yeast is still largely uncharacterized and only recently the alcohol dehydrogenase Hfd1 was identified as one of the enzymes involved. However, the beta-oxidation pathway studied in plants that involves p-coumaric acid as a 4HB intermediate, does not involve Hfd1 homologs or 4HBz the substrate of Hfd1. We conducted a number of experiments to determine whether p-coumaric acid is involved in 4HB biosynthesis. First, we labeled *coq null* mutants in the W303 background with **^{13}C-P** and observed no uptake of the label for any of the inherently Q-less *coq null* mutants. Therefore, it can be concluded that p-coumaric acid is not able to bypass the Q biosynthesis pathway deriving from 4HB. We also showed that unlike 4HB which is able to increase total Q levels in yeast compared to vehicle control, p-coumaric acid does not produce any such enhancement of Q content. All of these observations potentially strengthen the hypothesis that p-coumaric acid is indeed metabolized into 4HB in yeast by some unknown mechanism.

Since Hfd1 is one of the few enzymes that have actually been illustrated to be directly linked to 4HB biosynthesis in yeast, we decided to silence the *HFD1* gene in the W303 yeast genetic background. The *hfd1Δ* strain thus created was tested alongside W303 WT to compare and contrast the relative production of unlabeled Q and *de novo* stable isotope labeled ^{13}C-Q upon

treatment with ^{13}C-4HB, ^{13}C-4HBz, and **^{13}C-P**. The unlabeled Q content was discovered to be similar between the WT and the mutant at all time points when treated with ^{13}C-4HB or ^{13}C-P. However, labeling the cells with ^{13}C-4HBz resulted in significantly lower endogenous unlabeled Q in the *hfd1Δ* compared to the WT. This is possibly due to the fact that Hfd1 catalyzes the oxidation of 4HBz to 4HB, and therefore treatment with isotope labeled 4HBz, is unable to restore endogenous Q levels to the same extent as treatment with stable isotope labeled 4HB or p-coumaric acid. Unsurprisingly, the *de novo* labeled ^{13}C-Q content was significantly reduced in the *hfd1Δ* across all the time points (5, 10 and 24 hour post addition of the label) compared to the WT when both were labeled with ^{13}C-4HBz, since the mutation is deleterious for the conversion of ^{13}C-4HBz to ^{13}C-4HB and in turn ^{13}C-Q. Conversely, labeling with ^{13}C-4HB produced no significant differences in ^{13}C-Q levels between the WT and the mutant.

Interestingly, upon **^{13}C-P** treatment there was a significant reduction of ^{13}C-Q content in the *hfd1Δ* mutant compared to the WT at the 5 hour time point, an affect that gets ameliorated at the later time points. This could potentially further add weight to the proposition that p-coumaric acid serves as a Q ring precursor via the 4HBz pathway as well as other alternate pathways that may lead to 4HB. The former predominantly occurs at the early periods of yeast growth that may include the early to mid-log phase, whereas during late-log or stationary phase of growth the yeast might switch to some alternate unknown pathway of converting p-coumaric acid to 4HB and in turn to Q. In the future, potential yeast homologs of the plant enzymes identified to play a role in the conversion of p-coumaric acid to Q via beta oxidation, can be identified and deleted. The *null* strains thus created can be tested via similar labeling assays to shed further light into the role of p-coumaric acid as a Q ring precursor in yeast.

Materials and methods:

Chemicals and reagents

[$^{13}C_6$-ring]-4-hydroxybenzaldehyde (^{13}C-4Hbz) and [$^{13}C_6$-ring]-4-hydroxybenzoic acid (^{13}C-4HB) were ordered from Cambridge Isotopes Inc. All other reagents and solvents required for organic synthesis were obtained from Sigma-Aldrich. All yeast media and supplies were obtained from Thermo Fischer Scientific. Primers for PCR reactions required for Hfd1 gene silencing were ordered from Eurofins Genomics.

Synthesis of [$^{13}C_6$-ring]-p-coumaric acid

The synthesis of [$^{13}C_6$-ring]-p-coumaric acid **^{13}C-P** was carried out as described in (6) with minor modifications. Briefly, to a flame dried round bottom flask (50 ml) was added [$^{13}C_6$-ring]-4-hydroxybenzaldehyde (^{13}C-4HBz, 300 mg, 2.5 mmol), malonic acid (450 mg, 4.3 mmol), piperidine (30 µl), and pyridine (6 ml). The reaction mixture was stirred under nitrogen at 92°C. The reaction was monitored through thin layer chromatography on 0.25 mm SiliCycle silica gel plates and visualized under UV light and with permanganate or 2,4-dinitrophenylhydrazine staining. Upon completion (48 hours), the mixture was sequentially added to 20 ml water, neutralized to pH 7–8, and then washed with dichloromethane. The aqueous solution was acidified to pH 1 and then extracted twice using 20mL ethyl acetate. The combined organic extract was concentrated *in vacuo* and purified through flash column chromatography. Flash column chromatography was performed with SiliCycle Silica-P Flash silica gel (60 Å pore size, 40–63 µm) and 50% ethyl acetate in hexanes as mobile phase, to furnish an off-white solid (328 mg, 82% yield). The product was further purified by preparatory HPLC in an Agilent 1200 LC

system, using a Waters Sunfire C18 Column (19 mm x 250 mm). The elution gradient used: 40-55% Acetonitrile +0.1% Trifluoroacetic acid, 2-7 min; Flow rate: 20 mL/min; Monitored at 254 nm. Fractions were pooled, concentrated in vacuo, and the aqueous remainder was lyophilized to give a white powder (291 mg, 73% final yield). NMR spectra were recorded using a Bruker Avance-400 spectrometer, calibrated to residual acetone-d_6 as the internal reference (2.05 ppm for ^{1}H NMR; 29.9 and 206.7 ppm for ^{13}C NMR. ^{1}H NMR (400 MHz, acetone-d6) δ: 9.40 (br s, 1H), 7.70–7.65 (m, 1H), 7.63–7.57 (m, 1H), 7.39–7.34 (m, 1H), 7.05–7.02 (m, 1H), 6.71–6.69 (m, 1H), 6.32 (dd, J = 5.2, 16.1 Hz, 1H); ^{13}C NMR (90 MHz, acetone-d_6) δ: 159.5, 129.9, 125.9, 115.6. GC-MS data were recorded using an Agilent 6890-5975 GC mass spectrometer equipped with an auto-sampler and an HP5 column; the sample was dissolved in ethanol. GC-MS (EI+) calcd for $[^{13}C_6{}^{12}C_3H_8O_3]^+$, *m/z* 170.1, found 170.1.

Strains and growth media

Sachharomyces cerevisiae strains used in this study are listed in Table 1. Liquid media was prepared as described in (13) and included: YPD (2% glucose, 1% yeast extract, 2% peptone), YPG (3% glycerol, 1% yeast extract, 2% peptone), Synthetic dextrose with all components added (SD-complete), and drop out dextrose (DOD) (2% dextrose, 6.8 g/l yeast nitrogen base minus pABA minus folate with ammonium sulfate (MP Biomedicals), 5.83 mM sodium monophosphate (pH adjusted to 6.0 with NaOH), amino acids and nucleotides added as described). Solid plate medium included the stated components plus 2% Bacto agar. The pRS303 plasmid was obtained in *Escherechia coli* strain DH5α.

***HFD1 null* strain construction**

The HFD1 deletion was introduced in W303-1A WT yeast using a PCR based deletion strategy (14) and primers:

5’ATCTAAAAGGAATATTCTAAAACCATAGCCATAGTAATTTATCACCAACTCTATTA CTCTTGGCCTCCTCTAG3’ (Forward)

5’ACGAAAGGTTACTTATACATCAAATAATTAATTAACCTTAAACATTACGTTCGGTG TCACTACATAAGAACACC3’ (Reverse)

The Phusion High-Fidelity DNA Polymerase and HF buffer (Thermo Scientific, USA) was used to perform the PCR reactions using conditions described in (14). The PCR fragment obtained from the selected plasmid was transformed into W303-1A WT yeast and corresponding colonies were plated on selective plate media. The final *HFD1* deletion and integration of the plasmid was verified by PCR and genomic sequencing.

Preparation of stock solutions for labels added

The stable isotope labeled compounds ^{13}C-4HB and ^{13}C-P, along with the unlabeled compounds 4HB and p-coumaric acid were freshly dissolved in EtOH. The concentration of each stock solution thus obtained were adjusted so that addition of 9 µL of each corresponding EtOH stock solution in 6 mL YPD liquid media would result in a final concentration of 50 mg/L for each compound.

Yeast labeling assay

Yeast colonies from YPD plate medium were first inoculated into 125 mL Erlenmeyer flasks containing 30 mL YPD, YPG, SD-complete, or DOD liquid media. Following overnight incubation with shaking (250 rpm) at 30 ^{o}C, the yeast cells were added into 18x150 mm borosilicate test tubes, containing fresh 6mL liquid media of the same type that the overnight pre-culture was incubated in. The inoculation during this step was performed so that the final OD_{600} of the yeast cells in 6mL liquid media in each test tube is 0.2. These tubes were further incubated by shaking (250 rpm) at 30 ^{o}C slanted at a 45^{o} angle. The OD_{600} of the yeast cultures

in the test tubes were monitored till an OD_{600} of 0.4-0.5 was reached. At that time point 9 µL of the EtOH stock solutions of the compounds of interest were added to the tubes so that the final concentrations of the compounds in 6 mL liquid media was achieved to be 50 mg/L. The tubes with the yeast were incubated with shaking under the same conditions as mentioned previously. At the selected time after addition of the treatments, the tubes were removed from the incubator. The OD_{600} at each time point for each yeast sample was measured, 5mL of the vortexed liquid yeast culture was withdrawn into fresh 10mL centrifuge tubes. The tubes were centrifuged at 3000xg rpm for 5 minutes, and the liquid media was aspirated out to obtain yeast cell pellets. The pellets thus obtained were stored at -20 ^{o}C. The experiment was conducted in triplicates for each time point, yeast strain and treatment added.

Lipid extraction of yeast cell pellets

Lipid extractions of the yeast cell pellets were performed similar to the description in (13). Briefly the cell pellets were thawed on ice and then suspended in 2 mL of methanol. Q_4 was added as an internal standard for the determination of Q_6 content in the lipid extracts. The tubes were vortexed at maximum intensity for 30 seconds followed by addition of 2 mL of petroleum ether. This was followed by another round of vortex as before, after which the upper petroleum ether layer was removed from the phase boundary and transferred to a fresh tube. The petroleum ether addition, vortex, and removal of the upper petroleum ether layer was repeated for a total of two cycles. The petroleum ether solutions were consolidated for each sample, and the solvent was evaporated under a stream of nitrogen gas.

HPLC-MS/MS analysis to measure Q and Q intermediates

The HPLC-MS/MS analysis to quantify Q from the yeast lipid extracts previously obtained was carried out as described in (13) with minor modifications. Briefly, the dry lipid extracts were first

resuspended in 200 µL benzoquinone solution (0.1 mg/mL in EtOH). This was done to ensure complete oxidation of all the lipids which simplifies the subsequent detection and quantification process. A 4000 QTRAP linear MS/MS spectrometer from Applied Biosystems (Foster City, CA) was used. Applied Biosystem software, Analyst version 1.4.2, was used for data acquisition and processing. A binary HPLC solvent delivery system was used with a Luna phenyl-hexyl column (particle size 5 µm, 100 × 4.60 mm; Phenomenex) for yeast cell lipid extracts. The mobile phase consisted of solvent A (methanol:isopropanol, 95:5, with 2.5 mM ammonium formate) and solvent B (isopropanol, 2.5 mM ammonium formate). For separation of yeast quinones, the percentage of solvent B increased linearly from 0 to 5% over 6 min, and the flow rate increased from 600 to 800 µL/ min. The flow rate and mobile phase were linearly changed back to initial condition by 7 min. All samples were analyzed in multiple reaction monitoring mode; multiple reaction monitoring transitions were as follows: *m/z* 591/197.1 (Q_6); *m/z* 608/197.1 (Q_6 with ammonium adduct); *m/z* 597/203.1 (^{13}C-Q_6); *m/z* 614/203.1 (^{13}C-Q_6 with ammonium adduct); *m/z* 561.6/167 (DMQ_6); *m/z* 578.6/167 (DMQ_6 with ammonium adduct); *m/z* 567.6/173 (^{13}C-DMQ_6); *m/z* 584.6/173 (^{13}C-DMQ_6 with ammonium adduct); *m/z* 547.2/151 (HHB); *m/z* 564.2/151 (HHB with ammonium adduct); *m/z* 553.2/157 (^{13}C-HHB); *m/z* 570.2/157 (^{13}C-HHB with ammonium adduct).

Table 1. Genotypes and sources of yeast strains

Strain	Genotype	Source
BY4741	MAT a *his3Δ1 leu2Δ0 met15Δ0 ura3Δ0*	(15)
W303-1A	MAT a *ade2-1 his3-1,15 leu2-3,112 trp1-1 ura3-1*	*R. Rothstein*
W303*Δcoq1*	MAT a *ade2-1 his3-1,15 leu2-3,112 trp1-1 ura3-1 coq1*::*LEU2*	(16)
W303*Δcoq2*	MAT a *ade2-1 his3-1,15 leu2-3,112 trp1-1 ura3-1 coq2*::*HIS3*	(17)
W303*Δcoq3*	MAT α *ade2-1 his3-1,15 leu2-3,112 trp1-1 ura3-1 coq3*::*LEU2*	(18)
W303*Δcoq4*	MAT a *ade2-1 his3-1,15 leu2-3,112 trp1-1 ura3-1 coq4*::*TRP1*	(19)
W303*Δcoq5*	MAT a *ade2-1 his3-1,15 leu2-3,112 trp1-1 ura3-1 coq5*::*HIS3*	(20)
W303*Δcoq6*	MAT a *ade2-1 his3-1,15 leu2-3,112 trp1-1 ura3-1 coq6*::*LEU2*	(21)
W303*Δcoq7*	MAT α *ade2-1 his3-1,15 leu2-3,112 trp1-1 ura3-1 coq7*::*LEU2*	(22)
W303*Δcoq8*	MAT a *ade2-1 his3-1,15 leu2-3,112 trp1-1 ura3-1 abc1/coq8*::*HIS3*	(19)
W303*Δcoq9*	MAT a *ade2-1 his3-1,15 leu2-3,112 trp1-1 ura3-1 coq9*::*URA3*	(23)
W303*Δcoq10*	MAT a *ade2-1 his3-1,15 leu2-3,112 trp1-1 ura3-1 coq10*::*HIS3*	(24)
W303*Δcoq11*	MAT a *ade2-1 his3-1,15 leu2-3,112 trp1-1 ura3-1 coq10*::*HIS3*	(13)
W303*Δhfd1*	MAT a *ade2-1 his3-1,15 leu2-3,112 trp1-1 ura3-1 coq10*::*HIS3*	This study

A

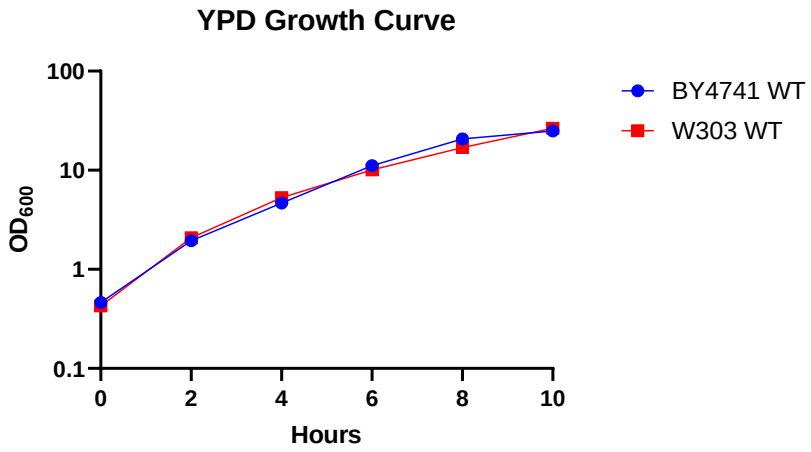

B

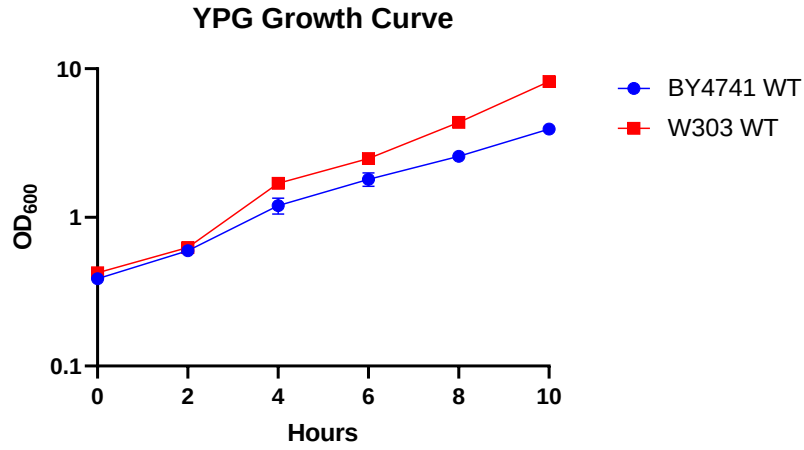

Figure 1. Yeast growth curves in YPD and YPG. (A) The growth of BY4741 WT (blue dots) and W303 WT (red squares) yeast as observed in YPD (B) The growth of BY4741 WT (blue dots) and W303 WT (red squares) yeast as observed in YPD. Error bars represent S.D. (n = 3).

A

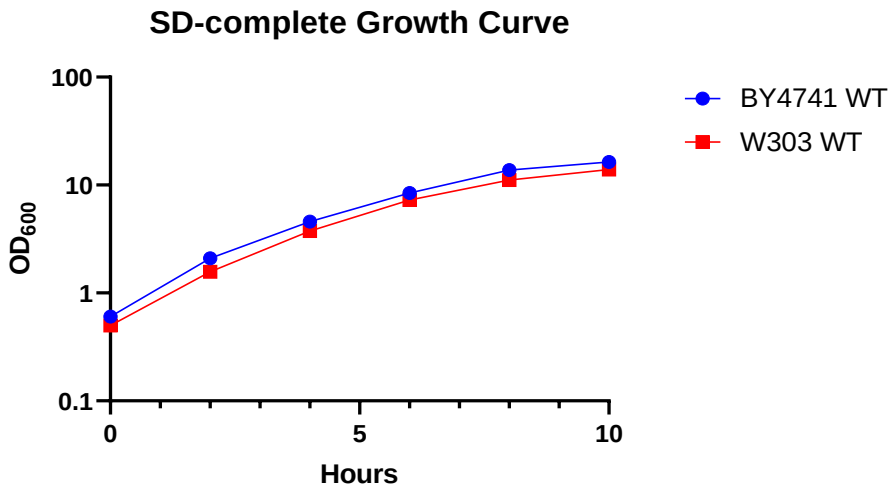

B

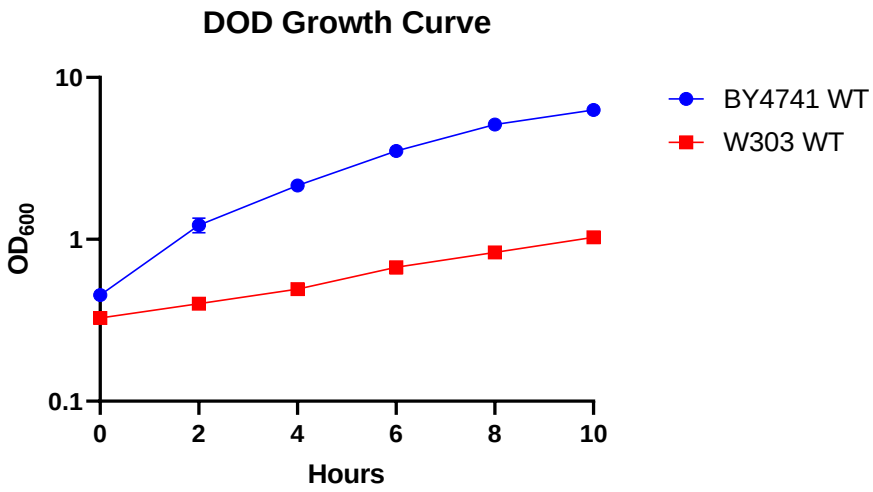

Figure 2. Yeast growth curves in SD-complete and DOD. (A) The growth of BY4741 WT (blue dots) and W303 WT (red squares) yeast as observed in SD-complete (B) The growth of BY4741 WT (blue dots) and W303 WT (red squares) yeast as observed in DOD. Error bars represent S.D. (n = 3).

A

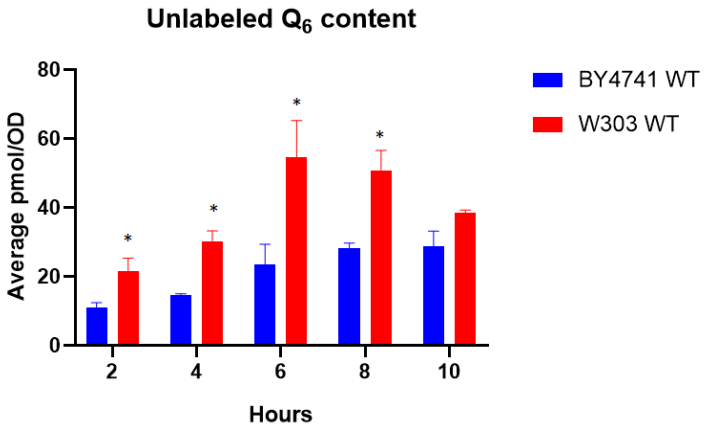

B

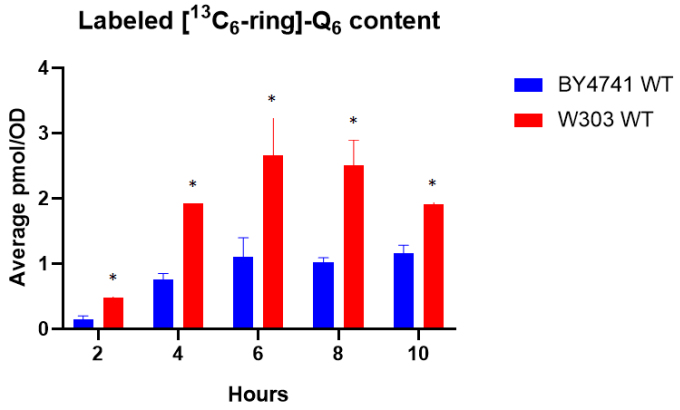

Figure 3. Endogenous unlabeled and *de novo* ^{13}C-labeled Q content in YPD. Q content comparison in the yeast samples labeled with [$^{13}C_6$-ring]-p-coumaric acid and grown in YPD. (A) Unlabeled Q6 in BY4741 WT (blue) and W303 WT (red). (B) Labeled [$^{13}C_6$-ring]-Q6 in BY4741 WT (blue) and W303 WT (red). Statistical significance was calculated by Student's T-test (two tailed unequal variance) between red and blue bars for each time point, single asterisk represents p value < 0.05. Error bars represent S.D. (n = 3).

A

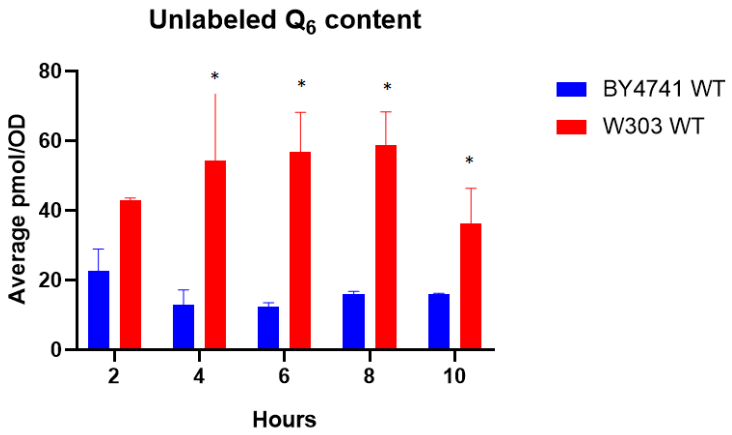

B

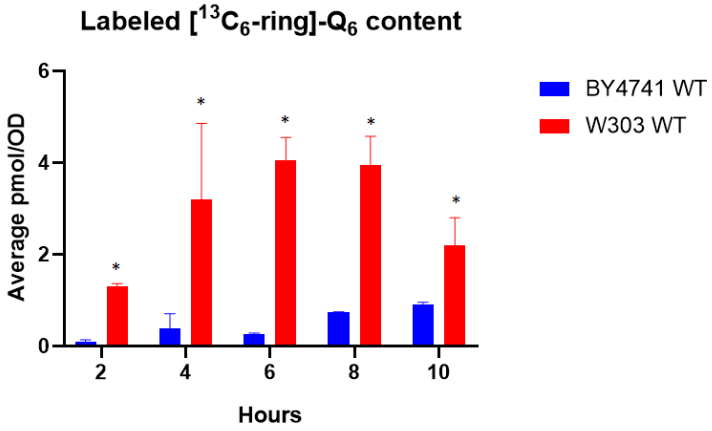

Figure 4. Endogenous unlabeled and *de novo* ^{13}C-labeled Q content in YPG. Q content comparison in the yeast samples labeled with [$^{13}C_6$-ring]-p-coumaric acid and grown in YPG. (A) Unlabeled Q6 in BY4741 WT (blue) and W303 WT (red). (B) Labeled [$^{13}C_6$-ring]-Q6 in BY4741 WT (blue) and W303 WT (red). Statistical significance was calculated by Student's T-test (two tailed unequal variance) between red and blue bars for each time point, single asterisk represents p value < 0.05. Error bars represent S.D. (n = 3).

A

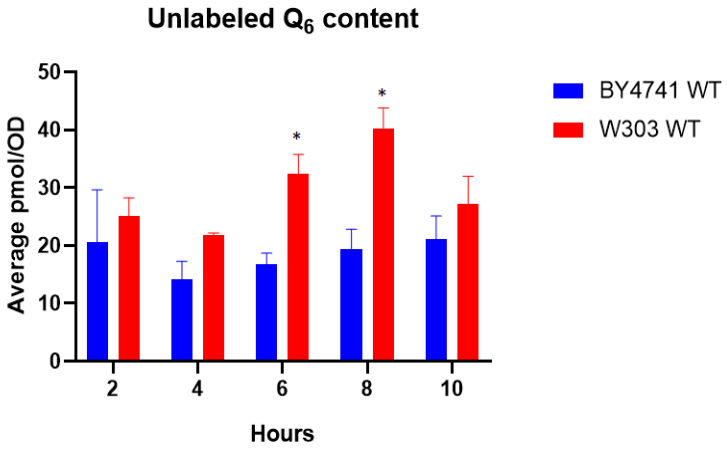

B

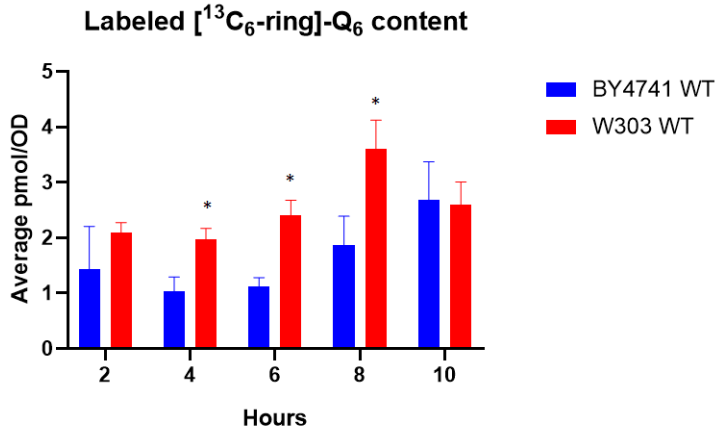

Figure 5. Endogenous unlabeled and *de novo* ^{13}C-labeled Q content in SD-complete. Q content comparison in the yeast samples labeled with [$^{13}C_6$-ring]-p-coumaric acid and grown in SD-complete. (A) Unlabeled Q6 in BY4741 WT (blue) and W303 WT (red). (B) Labeled [$^{13}C_6$-ring]-Q6 in BY4741 WT (blue) and W303 WT (red). Statistical significance was calculated by Student's T-test (two tailed unequal variance) between red and blue bars for each time point, single asterisk represents p value < 0.05. Error bars represent S.D. (n = 3).

A

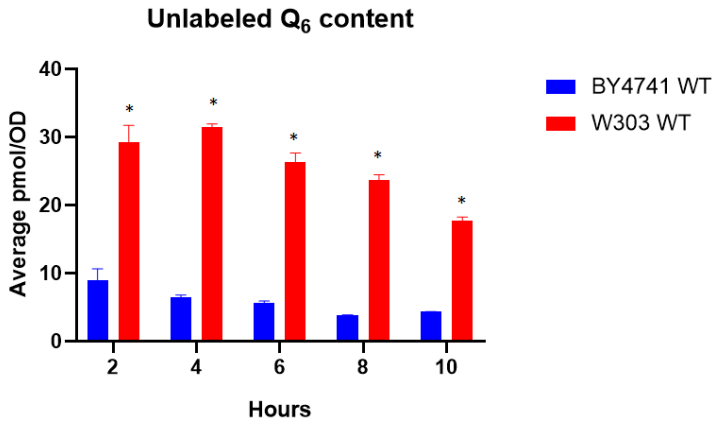

B

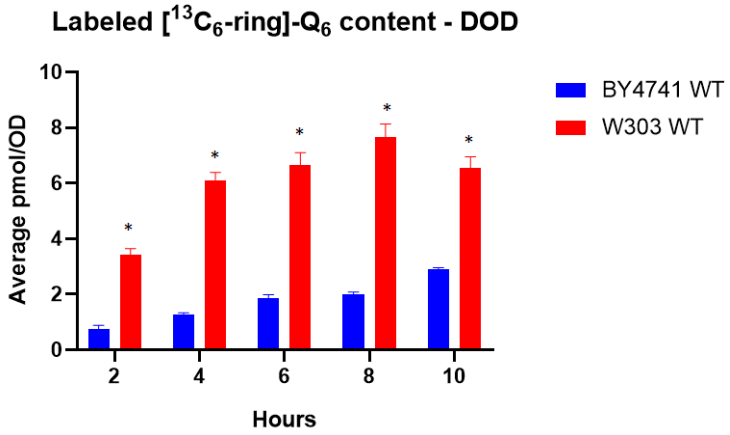

Figure 6. Endogenous unlabeled and *de novo* ^{13}C-labeled Q content in DOD. Q content comparison in the yeast samples labeled with [$^{13}C_6$-ring]-p-coumaric acid and grown in DOD. (A) Unlabeled Q6 in BY4741 WT (blue) and W303 WT (red). (B) Labeled [$^{13}C_6$-ring]-Q6 in BY4741 WT (blue) and W303 WT (red). Statistical significance was calculated by Student's T-test (two tailed unequal variance) between red and blue bars for each time point, single asterisk represents p value < 0.05. Error bars represent S.D. (n = 3).

A

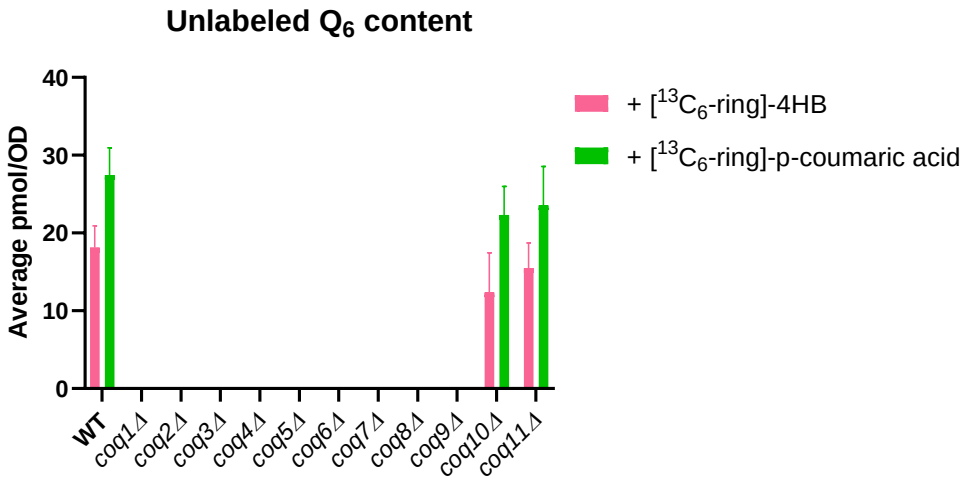

B

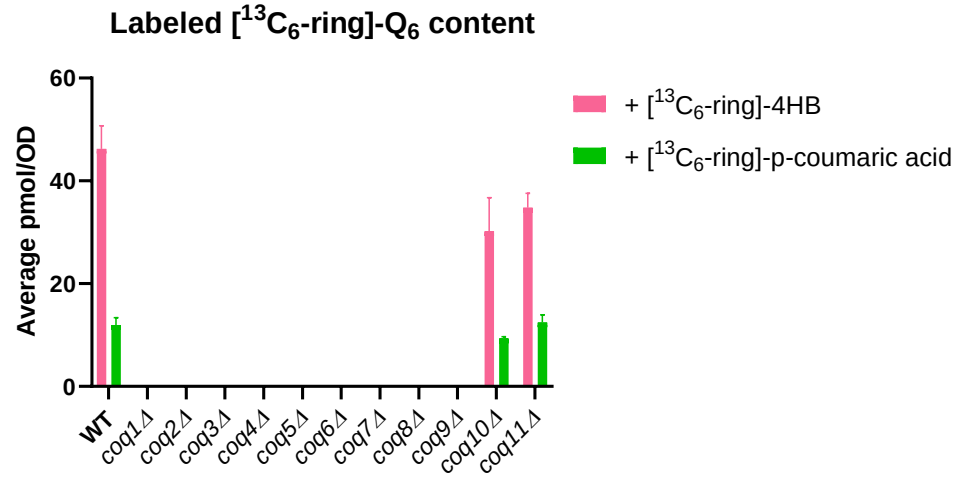

Figure 7. Q content comparison in WT and *Coq nulls* grown in DOD. W303 WT and *Coq nulls* in the W303 background were labeled with [$^{13}C_6$-ring]-4HB (pink) or [$^{13}C_6$-ring]-p-coumaric acid (green). (A) Endogenous unlabeled Q_6 levels, and (B) de novo [$^{13}C_6$-ring]-Q_6 levels. Error bars represent S.D. (n = 3).

A

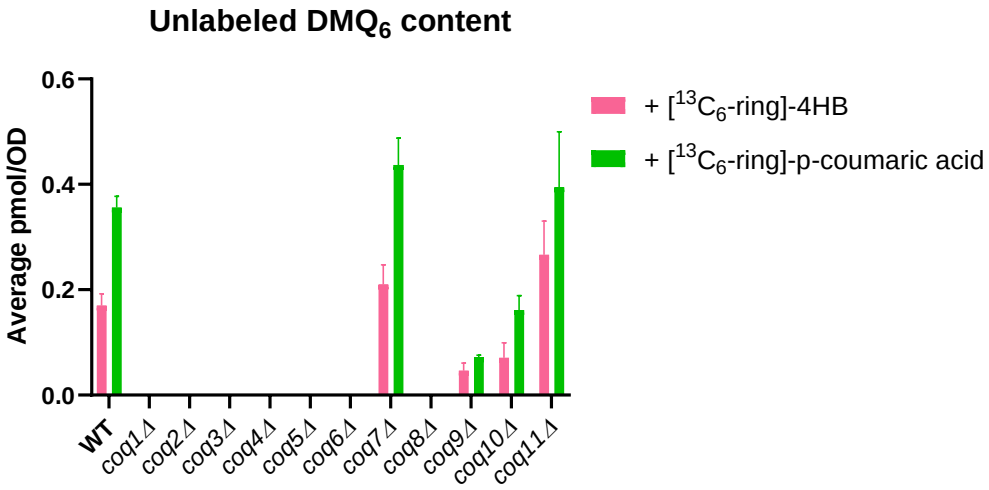

B

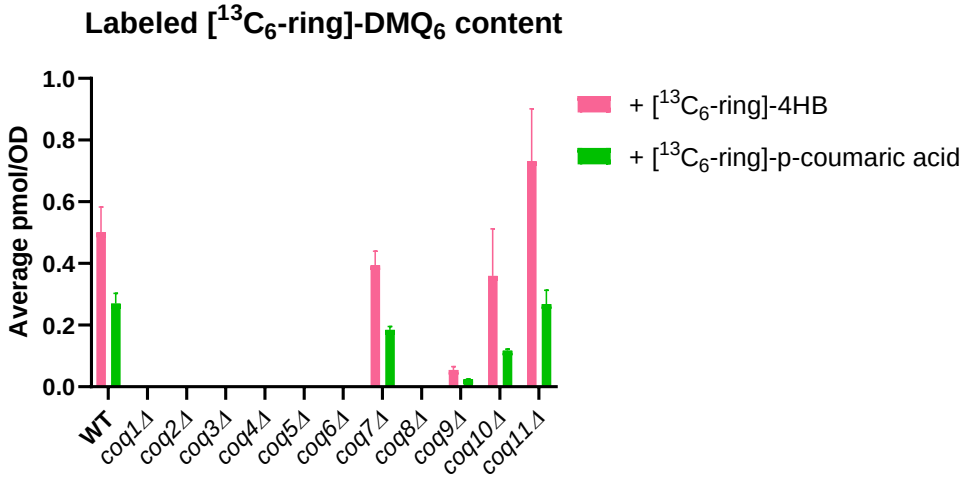

Figure 8. DMQ_6 content comparison in WT and *Coq nulls* grown in DOD. W303 WT and *Coq nulls* in the W303 background were labeled with [$^{13}C_6$-ring]-4HB (pink) or [$^{13}C_6$-ring]-p-coumaric acid (green). (A) Endogenous unlabeled DMQ_6 levels, and (B) de novo [$^{13}C_6$-ring]-DMQ_6 levels. Error bars represent S.D. (n = 3).

A

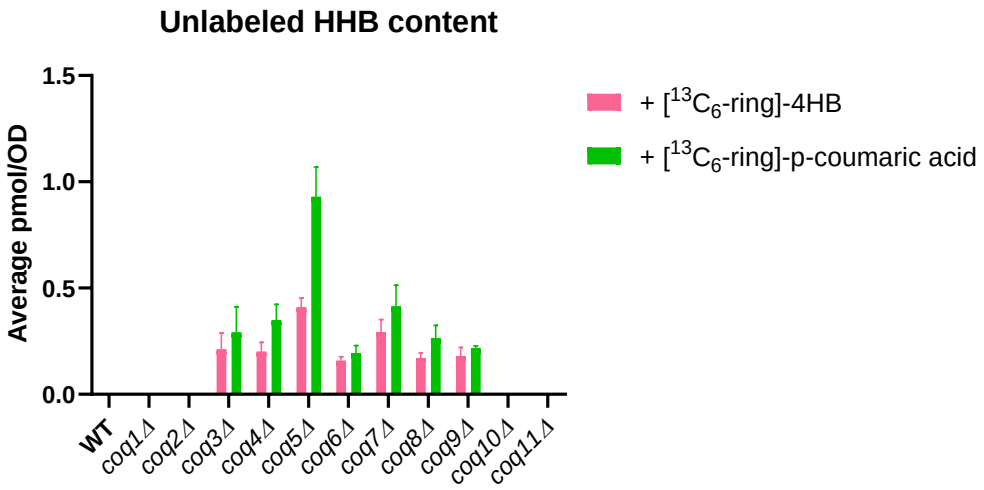

B

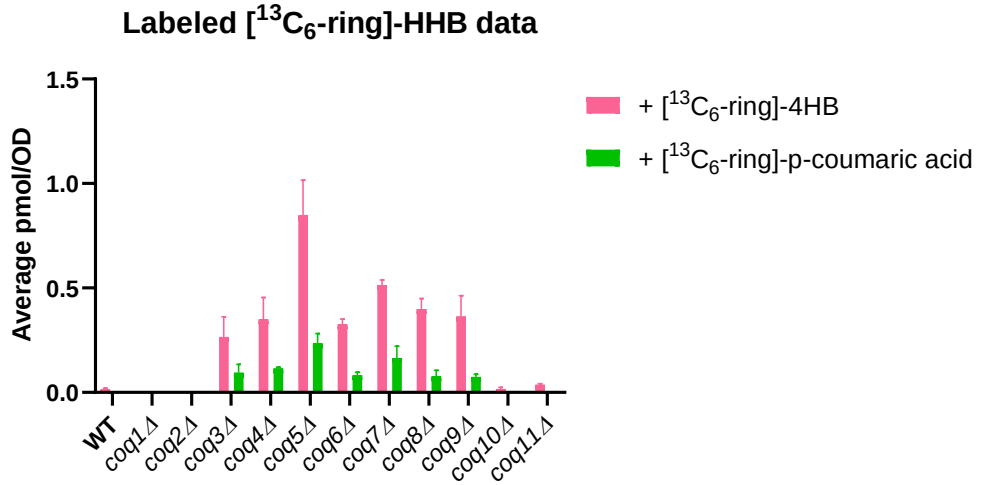

Figure 9. HHB content comparison in WT and *Coq nulls* grown in DOD. W303 WT and *Coq nulls* in the W303 background were labeled with [$^{13}C_6$-ring]-4HB (pink) or [$^{13}C_6$-ring]-p-coumaric acid (green). (A) Endogenous unlabeled HHB levels, and (B) de novo [$^{13}C_6$-ring]-HHB levels. Error bars represent S.D. (n = 3).

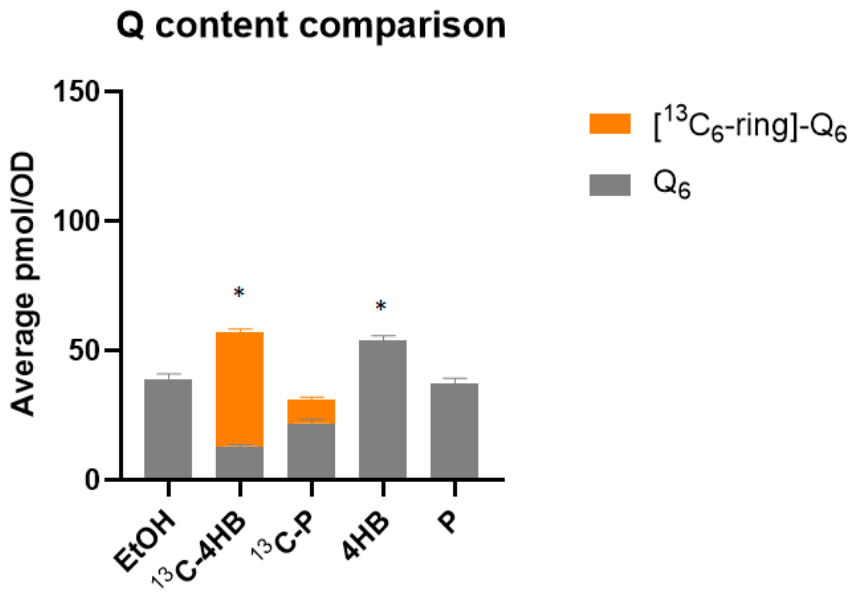

Figure 10. Q content comparison in W303 WT yeast grown in DOD. The yeast samples were treated with [$^{13}C_6$-ring]-4-hydroxybenzoic acid (^{13}C-4HB), [$^{13}C_6$-ring]-p-coumaric acid (^{13}C-P), 4-hydroxybenzoic acid (4HB), and p-coumaric acid. Endogenous unlabeled Q_6 levels (grey) and de novo [$^{13}C_6$-ring]-Q_6 levels (orange) are shown. Statistical significance was calculated by Student's T-test (two tailed unequal variance) between the total Q levels for each treatment compared to EtOH (vehicle control), single asterisk represents p value < 0.05. Error bars represent S.D. (n = 3).

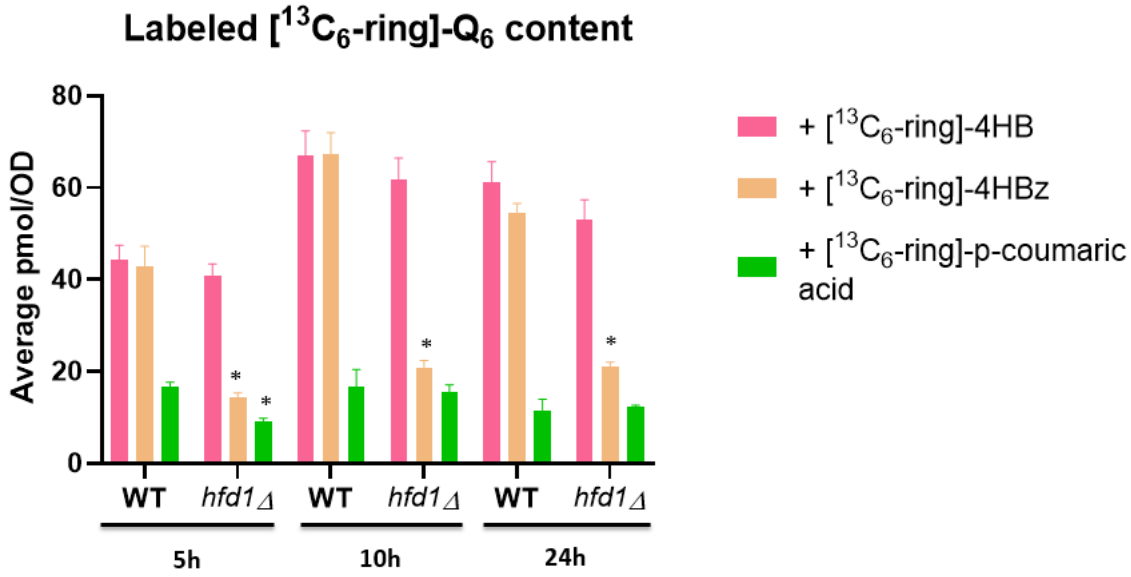

Figure 11. *De novo* stable isotope labeled Q content comparison in WT and *hfd1 null* yeast labeled with different Q precursors. W303 WT and *hfd1Δ* mutant in the W303 background were grown in DOD liquid media for 5, 10, and 24 h and labeled with [$^{13}C_6$-ring]-4HB (pink), with [$^{13}C_6$-ring]-4HBz (orange), or [$^{13}C_6$-ring]-p-coumaric acid (green). Bars show the *de novo* labeled [$^{13}C_6$-ring]-Q_6 content as measured in the yeast under the conditions mentioned (n = 3). Statistical significance was calculated by Student's T-test (two tailed unequal variance) between WT and *hfd1Δ* for each label at each time point, single asterisk represents p value < 0.05. Error bars represent S.D. (n = 3).

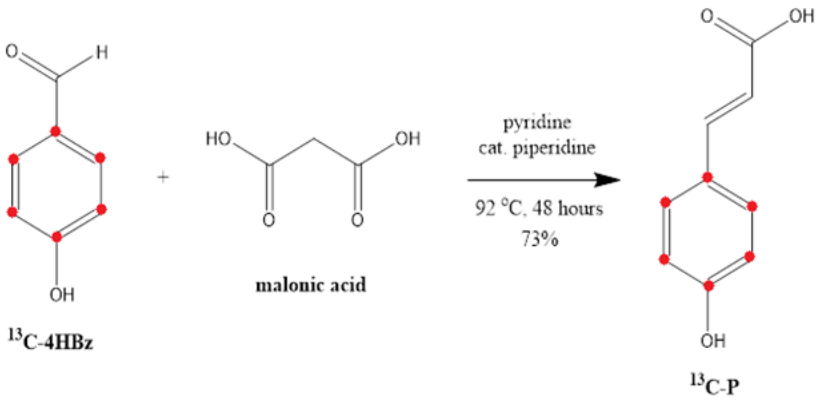

Scheme 1: Synthesis of [$^{13}C_6$-ring]-p-coumaric acid **^{13}C-P**. Atoms with red dots represent stable isotope ^{13}C-carbons.

References:

1) Bentinger, M., M. Tekle, and G. Dallner. (**2010**). *Biochem. Biophys. Res. Commun.* **396,** 74

2) Nowicka, B., and J. Kruk. (**2010**). *Biochim. Biophys. Acta.* **1797,** 1587

3) Turunen, M., J. Olsson, and G. Dallner. (**2004**). *Biochim. Biophys. Acta.* **1660,** 171

4) Pierrel, F., O. Hamelin, T. Douki, S. Kieffer-Jaquinod, U. Muhlenhoff, M. Ozeir, R. Lill, and M. Fontecave. (**2010**). *Chem. Biol.*, **17,** 449

5) Marbois, B., L. X. Xie, S. Choi, K. Hirano, K. Hyman, and C. F. Clarke. (**2010**). *J. Biol. Chem.*, **285,** 27827

6) Xie, L. X., Williams, K. J., He, C. H., Weng, E., Khong, S., Rose, T. E., Kwon, O., Bensinger, S. J., Marbois, B. N., and Clarke, C. F. (**2015**). *J. Lipid Res.*, **67**, 909

7) Block, A. , J. R. Widhalm, A. Fatihi, R. E. Cahoon, Y. Wamboldt, C. Elowsky, S. A. Mackenzie, E. B. Cahoon, C. Chapple, and G. J. Bassett. (**2014**). *The Plant Cell*, **26,** 1938

8) Soubeyrand, E., Johnson, T. S., Latimer, S., Block, A., Kim, J., Colquhoun, T. A., Butelli, E., Martin, C., Wilson, M. A., and Bassett, G. J. (**2018**). *The Plant Cell*, **30**, 2910

9) Clarke, C. F. (**2000**). *Protoplasma*, **213,** 134

10) Olson , R. E., R. Bentley, A. S. Aiyar, G. H. Dialameh, P. H. Gold, V. G. Ramsey, and C. M. Springer. (**1963**). *J. Biol. Chem.*, **238,** 3146

11) Stefley, J. A., and Pagliarini, D. J. (**2017**). *Trends Biochem. Sci*., **42**, 824

12) Payet, L. A., Leroux, M., Willison, J. C., Kihara, A., Pelosi, L., and Pierrel, F. (**2016).** *Cell Chemical Biology*, **23**, 1241

13) Allan, C. M., Awad, A. M., Johnson, J. S., Shirasaki, D. I., Wang, C., Blaby-Haas C. E., Merchant, S. S., Loo, J. A., and Clarke, C. F. (**2015**). *J. Biol. Chem.*, **290**, 7517

14) Gnügge, R., Liphardt, T., and Rudolf, F. (**2016**). *Yeast*, **33,** 83.

15) Brachmann, C. B., Davies, A., Cost, G. J., Caputo, E., Li J., Hieter, P., and Boeke, J. D. (**1998**). *Yeast*, **14**, 115

16) Gin P., and Clarke C. F. (**2005**). *J. Biol. Chem.*, **280**, 2676

17) Ashby, M. N., Kutsunai, S. Y., Ackerman, S., Tzagoloff, A., and Edwards, P. A. (**1992**). *J. Biol. Chem.*, **267**, 4128

18) Do, T. Q., Schultz, J. R., and Clarke, C. F. (**1996**). *Proc. Natl. Acad. Sci. U.S.A.*, **93**, 7534

19) Hsu, A. Y., Do, T. Q., Lee, P. T., and Clarke, C. F. (**2000**). *Biochim. Biophys. Acta.*, **1484**, 287

20) Barkovich, R. J., Shtanko, A., Shepherd, J. A., Lee, P. T., Myles, D. C., Tzagoloff, A., and Clarke, C. F. (**1997**). *J. Biol. Chem.*, **272**, 9182

21) Gin, P., Hsu, A. Y., Rothman, S. C., Jonassen, T., Lee, P. T., Tzagoloff, A., and Clarke, C. F. (**2003**). *J. Biol. Chem.*, **278**, 25308

22) Marbois, B. N., and Clarke, C. F. (**1996**). *J. Biol. Chem.*, **271**, 2995

23) Johnson, A., Gin, P., Marbois, B. N., Hsieh, E. J., Wu, M., Barros, M. H., Clarke, C. F., and Tzagoloff, A. (**2005**). *J. Biol. Chem.*, 280, 31397

24) Barros *et. al*., (**2005**). *J. Biol. Chem.*, **280**, 42627

CHAPTER 5

Discussion of ongoing project and future directions

Author contributions: Anish Nag, Lucía Fernández-del-Río, and Catherine F. Clarke contributed to the intellectual development of the project. Gilles Bassett provided reagents. Lucía Fernández-del-Río performed the cell culture assays. Anish Nag developed the 4HB derivatization strategy. Anish Nag and Yu Chen contributed to setting up the HPLC-MS/MS methodology. Anish Nag and Catherine F. Clarke contributed to the writing and revision of this chapter.

Introduction:

As shown in previous chapters, Coenzyme Q (Ubiquinone, CoQ, or Q) is a vital molecule made up of a redox-active benzoquinone ring and a lipophilic polyprenyl tail. It serves a critical role as an electron carrier in cellular respiration, and is ubiquitous in eukaryotes and prokrayotes as well as in the photosynthetic reaction center of purple bacteria (1, 2). Ubiquinone also doubles as a liposomal chain terminating antioxidant that is capable of protecting neighboring membrane bound lipids and proteins from oxidative damage caused by hydroxyl, peroxide and other reactive oxygen species (ROS) (3, 4). Furthermore, besides its roles as an electron carrier and an antioxidant, evidence has been recently gathered that demonstrates that Q can also serve a solely mechanical function by increasing the thickness of biological membranes in response to osmotic stress (5).

In most organisms the benzenoid ring precursor of Q is 4-hydroxybenzoic acid (4HB); the only exception to date is the yeast *Saccharomyces cerevisiae*, which can also utilize p-aminobenzoic acid (pABA) to generate Q, through a series of prenylation and demination steps that converge with the primary Q biosynthetic pathway stemming from 4HB (6). Chapter 3 illustrated the discovery of a novel Q ring precursor kaempferol, which belongs to the flavonol class of molecules (7). However, the exact metabolic pathway by which kaempferol increases Q levels in mammalian cells and gets incorporated into Q biosynthesis was not established. It was postulated that kaempferol acts as a Q ring precursor either via cleavage of its structure resulting in metabolites that are structurally similar to 4HB, or directly by itself acting as a substrate for the Coq2 polyprenyl transferase (Figure 1). The first theory was recently proven to be valid in

Arabidopsis thaliana by Dr. Gilles Bassett, who showed that plant peroxidases are responsible for the cleavage of kaempferol and the generation of 4HB as a consequence (8). More specifically, it was confirmed that the B-ring of kaempferol actually serves as the ring moiety of Q via intermediary conversion to 4HB.

We are currently further investigating the metabolism of kaempferol in mammalian cells in order to verify whether the B-ring of kaempferol is incorporated into Q, via cleavage and conversion of the former into 4HB catalyzed by mammalian peroxidases. Dr. Bassett used a combination of *in vitro* peroxidase assays with plant extracts as well as stable isotope labeling assays to study the production of 4HB and Q respectively from kaempferol. Our efforts are being directed at developing similar methods to detect and quantify 4HB and Q generated from kaempferol in mammalian cells and cell extracts.

Results and discussions:

We first tested whether the B-ring of kaempferol is indeed incorporated as the benzenoid ring of Q in mammalian cells. We achieved this by incubating mouse kidney cells (TKPTS) in presence of stable isotope labeled [$^{13}C_6$-B-ring]-kaempferol (Figure 2, A). Cellular lipid contents were subsequently extracted and subjected to HPLC-MS/MS analysis to quantify endogenous unlabeled Q and *de novo* stable isotope labeled Q levels. It was observed that the TKPTS cells grown in presence of [$^{13}C_6$-B-ring]-kaempferol (generated by Dr. Gilles Bassett), successfully generated [$^{13}C_6$-ring]-Q_9 and [$^{13}C_6$-ring]-Q_{10}, the major and minor isoforms of Q in murine cells

respectively (Figure 2, B and C). As expected, the total Q content was also increased when the cells were treated with unlabeled kaempferol, [$^{13}C_u$]-kaempferol, [$^{13}C_6$-B-ring]-kaempferol, and [$^{13}C_6$-ring]-4HB. Untreated cells and those treated with unlabeled kaempferol showed no [$^{13}C_6$-ring]-Q_9 and [$^{13}C_6$-ring]-Q_{10}. All of these results established that it is indeed the B-ring of kaempferol that gets converted to Q in mammalian cells as previously hypothesized. The incorporation of the stable isotope label of [$^{13}C_6$-B-ring]-kaempferol into Q was lower than that of [$^{13}C_u$]-kaempferol and [$^{13}C_6$-ring]-4HB. One possibility for this observation could be due to the method by which the [$^{13}C_6$-B-ring]-kaempferol was isolated through an *in vivo* strategy from *A. thaliana* fed with [$^{13}C_6$-ring]-phenylalanine by Dr. Gilles Bassett. As a consequence, the actual concentration of [$^{13}C_6$-B-ring]-kaempferol might potentially be lower than the measured concentration due to the possibility of the stable isotope label from [$^{13}C_6$-ring]-phenylalanine not getting completely incorporated into [$^{13}C_6$-B-ring]-kaempferol by the plants.

With the confirmation of the B-ring of kaempferol being responsible for generating the benzenoid head group of Q murine cells, we wanted to further investigate the potential pathway by which this process occurs. In particular, we are interested in verifying whether mammalian peroxidases are responsible for cleavage of the kaempferol molecule, akin to that observed in plants. In order to set up such an in vitro peroxidase assay with mammalian cell extracts to analyze the conversion of kaempferol to 4HB, we needed to develop a method for detection and quantification of 4HB. We attempted to detect and quantify 4HB directly via HPLC-MS/MS methods using negative ion detection mode. However, these attempts proved to be inconsistent and unsuccessful, possibly due to the inherent difficulty of 4HB detection via HPLC-MS/MS analysis. Thus, we shifted our efforts into developing a method of chemically derivatizing 4HB,

followed by subsequent analysis of the derivatized 4HB via HPLC-MS/MS. The derivatization of 4HB was performed utilizing a strategy highlighted in a recent study (12). Specifically, dansyl chloride (**dansyl-Cl**) was used as the derivatizing reagent, which is attached on 4HB through a base catalyzed S_N2 reaction highlighted in **Scheme 1**, to obtain the derivatized product to be used in our HPLC-MS/MS analysis (**dansyl-4HB**).

With the derivatization of 4HB and generation of dansyl-4HB, the HPLC-MS/MS parameters for detecting and quantifying the latter were developed. The precursor (Figure 3) and product ions (Figure 4) were selected and optimized along with the elution solvent gradient. Subsequently a set of dansyl-4HB standards resuspended in methanol with concentrations ranging from 10 pg/mL to 10 µg/mL were created using a serial dilution strategy. Figure 5 shows a representative chromatogram obtained from the calibration standard sample with concentration 1 ng/mL dansyl-Cl run through the HPLC-MS/MS method optimized for dansyl-4HB detection and quantification. It was also observed that the sample with the highest concentration of 10 µg/mL, fell beyond the linear range of quantification, and was therefore omitted from the calibration curve. The curve consequently obtained showed a high degree of linearity (Figure 6). However, chromatograms of methanol blanks injected in between each standard sample, started showing the peak corresponding to dansyl-4HB when the standard concentration exceeded 100 ng/mL. This was attributed to the possible tendency of the dansyl-4HB to adhere to the HPLC column and the tubing at higher concentrations. Thus a second set of standards were also created via serial dilutions, ranging from 10 pg/mL to 100 ng/mL instead of 10 µg/mL. The calibration curve thus obtained had a slightly improved linear regression value (Figure 7), without creating the problem of the dansyl-4HB adhering to the HPLC system.

With the establishment of the methodology to consistently derivatize 4HB followed by the detection, quantification and analysis of the derivatized product dansyl-4HB through HPLC-MS/MS, we are now at a position to set up *in vitro* peroxidase assays using mouse kidney cell extracts and kaempferol. Currently efforts are being taken to incorporate the *in vitro* peroxidase assay methods used by Dr. Gilles Bassett on plants and set up a similar assay that would be compatible with tests on mammalian cells, as well as our derivatization strategy of the product(s) of the assay which we are postulating to primarily be 4HB.

Materials and methods:

Chemicals and reagents

All chemicals required for the derivatization of 4HB were obtained commercially from Sigma-Aldrich. [$^{13}C_6$-B-ring]-kaempferol was obtained from Dr. Gilles Bassett (University of Florida, Gainesville). Other stable isotope labeled compounds were ordered from Cambridge Isotopes Inc. Media and other reagents required for mammalian cell cultures and HPLC-MS/MS studies were obtained from Thermo-Fischer Scientific.

Cell cultures

Mouse kidney proximal tubule epithelial (Tkpts) cells (13), were provided by Dr. Elsa Bello-Reuss (Texas Tech University Health Science Center) and Dr. Judit K. Magyesi (University of Arkansas for Medical Sciences, Little Rock, AR). The cells were grown and cultured according to conditions listed in our previous study (7). Briefly, the cells were grown in DMEM/F12 with

4.5 g/L glucose supplemented with 10% FBS, 2 mM L-glutamine, and gentamicin-amphotericin B (125 µg/ml and 5 mg/ml, respectively). The cultures were maintained at 37 °C in a humidified atmosphere with 5% CO_2.

Treatment of Tkpts cells with stable isotope labeled compounds

The same experimental conditions were used for all compounds when tested in the Tkpts cells. Assays were performed as highlighted in (7) with minor modifications. Briefly, twelve-well plates with an initial amount of 50,000–100,000 cells/well were used. Cells were incubated with the tested compounds for 48 hours under standard culture conditions (37 °C, 5% CO_2). Once the treatment was completed, cells were detached from culture plates and pelleted by low-speed centrifugation (approximately 1,000 g). Cell pellets were collected and stored at −80 °C until use. Final concentrations of each compound in assays to determine Q content and biosynthesis were kept at 5 µM, except for [$^{13}C_6$-ring]-4HB which was added at a final concentration of 1 µM.

Lipid extractions for HPLC-MS/MS measurements

The Tkpts cell pellets collected after 48 hours of incubation in presence of the compounds selected for treatment, were subjected to the lipid extraction protocol described in (7). Briefly, dipropoxy-Q_{10} was added to the pellets as an internal standard. Cell pellets were vortexed in 1 ml of methanol and 1 ml of petroleum ether. The organic upper layer was transferred to a new tube. Another 1 ml of petroleum ether was added to the original methanol layer, and samples were vortexed again. The organic phase was removed, and the combined organic phase was dried under a stream of nitrogen gas.

HPLC-MS/MS quantification of Q species

Lipid extracts were measured by HPLC-tandem mass spectrometry (MS/MS) analyses as previously described (7). Briefly, the samples were resuspended in 200 µL of ethanol containing 1 mg/ml benzoquinone in order to oxidize all the lipids. Chromatographic separation was achieved through a reverse phase Luna 5µM PFP(2) column (Phenomenex) with a mobile phase composed of 90% solvent A (95:5 mixture of methanol:isopropanol containing 2.5 mM ammonium formate) and 10% solvent B (isopropanol containing 2.5 mM ammonium formate) at a constant flow rate of 1 ml/min. Transitions monitored are described in Table 1. The area value of each peak, was normalized with the corresponding standard curve and internal standard, with a reference to the total protein content of the cells serving as the denominator.

Derivatization of 4HB by dansyl-Cl

The derivatization of 4HB by dansyl-Cl was performed as described in (12), with minor modifications. Briefly, stock solutions of 4HB (1mg/mL in acetone), dansyl-Cl (0.5mg/mL in acetone) and $NaHCO_3$ (200 µM in water) were first prepared. The stock solution of 4HB was serially diluted to achieve the required final concentration (10 µg/mL or 1 µg/mL in acetone). To 100 µL of this solution of 4HB in a 1.5 mL Eppendorf tube was added 200 µL of the dansyl-Cl stock solution, followed by 200 µL of the $NaHCO_3$ stock solution. The tube was vortexed at high speed for 30 seconds, followed by incubation in a water bath maintained at 60 ^oC for 20 minutes, at which point discoloration of the solution showed completion of the reaction (quantitative yield of dansyl-4HB was assumed). After that, 500 µL of ethyl acetate was added, the tube was vortexed at maximum speed for 1 minute, centrifuged at 10,000 g for 30 seconds, and the upper ethyl acetate layer pipetted out into a fresh centrifuge tube. The step above was repeated for a total of two consecutive ethyl acetate extractions. The extracts were combined in the fresh

centrifuge tube and dried by passing a stream of N_2 gas. The dried extract was resuspended in 1 mL methanol and serially diluted to obtain a linear range of dansyl-4HB concentrations, with an upper limit of 10 µg/mL or 100 ng/mL to a lower limit of 10 pg/mL.

Detection and quantification of dansyl-4HB by HPLC-MS/MS

An API 4000 linear MS/MS spectrometer from Applied Biosystems (Foster City, CA) was used. Applied Biosystem software, Analyst version 1.4.5, was used for data acquisition and processing. An Agilent 1100 series binary HPLC solvent delivery system was used with a reverse phase Gemini-NX 5µ C18 column (particle size 5 µm, 100 × 3 mm; Phenomenex) for analyzing the dansyl-4HB standards. The mobile phase consisted of solvent A (H_20, with 0.1% formic acid) and solvent B (acetonitrile, with 0.1% formic acid). The solvent flow rate was kept constant at 200 µL/ min, with a total run time of 7 minutes and the injection volume for the samples was set at 10 µL. From 0 to 0.5 minutes, solvent A was used at 90% and solvent B at 10%. The percentage of solvent B increased linearly from 10 to 99% over from 0.5 to 3 minutes, and was kept constant from 3 to 4.5 minutes. Then the percentage of Solvent A was increased linearly from 1% to 90% and that of solvent B decreased back down to 10% from 4.5 to 5 minutes. This ratio of the two solvents was maintained from 5 to 7 minutes. The samples were analyzed in multiple reaction monitoring mode with the detection set for *m/z* 372.3/171.2. The values for the MS detection parameters were optimized by direction injection of dansyl-4HB in positive ion mode, and were set at the following values: declustering potential (DP) - 131 v, entrance potential (EP) - 10 v, collision energy (CE) - 37 v, and cell collision exit potential (CXP) - 12 v.

Table 1. Summary of all the Q analytes and the corresponding precursor-product ion masses detected during the HPLC-MS/MS quantification of cellular lipid extracts

Molecule	***m/z* (+ H)**	***m/z* (+ NH3)**
Q_9	795.6/197.08	812.6/197.08
[$^{13}C_6$-ring]-Q_9	801.6/203.08	818.6/203.08
Q_{10}	863.6/197.08	880.6/197.08
[$^{13}C_6$-ring]-Q_9	869.6/203.08	886.6/203.08
Dipropoxy-Q_{10}	919.7/253.1	936.7/253.1

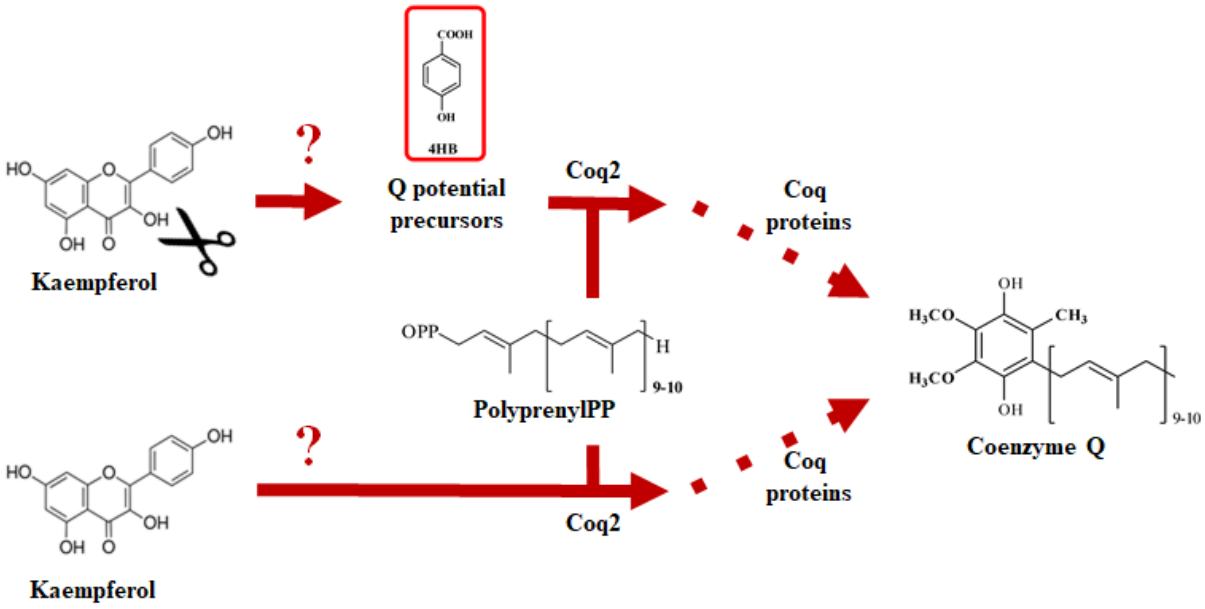

Figure 1. Possible routes for conversion of kaempferol to Q. Kaempferol can undergo molecular cleavage (represented by the black scissors) to yield potential Q precursors that may include 4-hydroxybenzoic acid (4HB), which can get prenylated by Coq2 and enter the Q biosynthetic pathway catalyzed by the Coq proteins (represented by the red dotted arrows). Conversely, kaempferol might get directly prenylated by Coq2 and undergo other transformations to yield Q. Red question marks represent potential steps catalyzed by unknown enzymes.

A

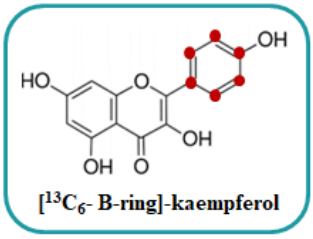

B

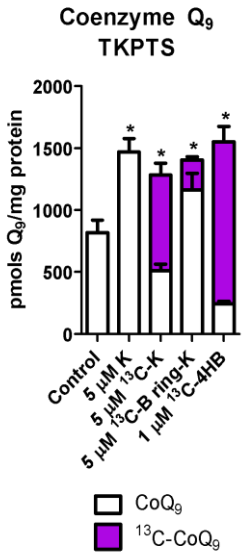

C

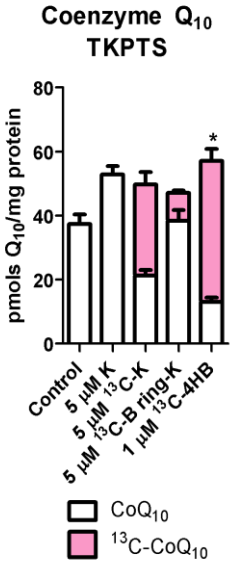

Figure 2. Effect of [$^{13}C_6$-B-ring]-kaempferol treatment on mouse Tkpts cells. Mouse Tkpts cells were grown in presence of (A) [$^{13}C_6$-B-ring]-kaempferol (^{13}C-B ring-K). Untreated cells served as negative control, along with cells treated with unlabeled kaempferol (K). [$^{13}C_u$]-kaempferol (^{13}C-K) and [$^{13}C_6$-ring]-4-hydroxybenzoic acid (^{13}C-4HB) served as positive controls. (B) Unlabeled (white bars) and labeled [$^{13}C_6$-ring]-Q_9 (purple bars), and (C) unlabeled (white bars) and labeled [$^{13}C_6$-ring]-Q_{10} (pink bars) content is shown. Statistical significance was calculated using Student's T-test (two tailed, unequal variance). Asterisks represent p value < 0.05. Error bars represent S.D. (n = 6).

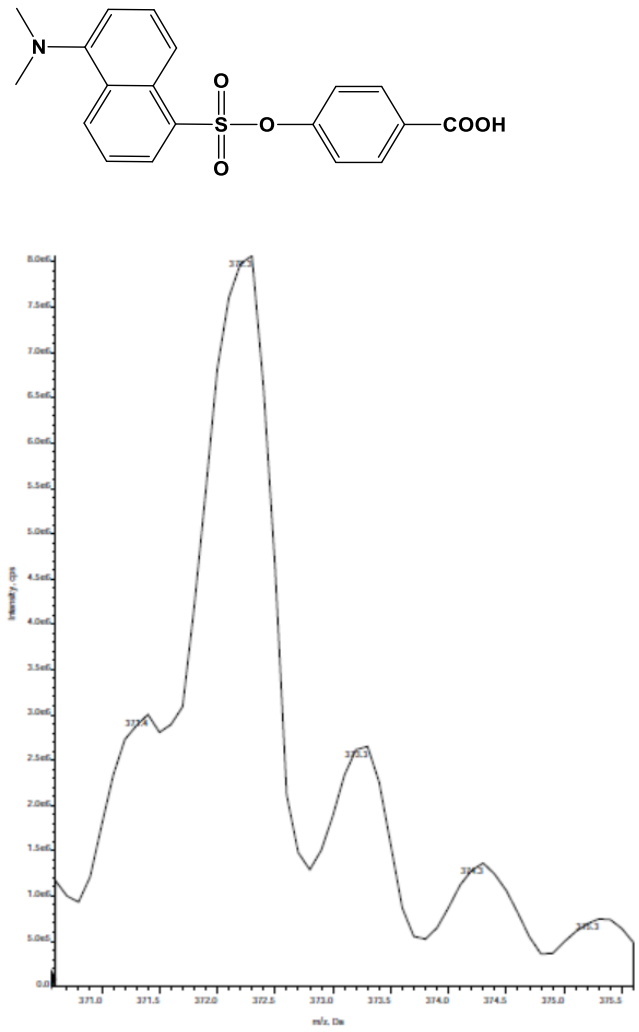

Figure 3. Precursor ion chromatogram of dansyl-4HB. Direct injection of dansyl-4HB to optimize the HPLC-MS/MS parameters produced corresponding precursor ion peak at [*m/z* + 1] = 372.3.

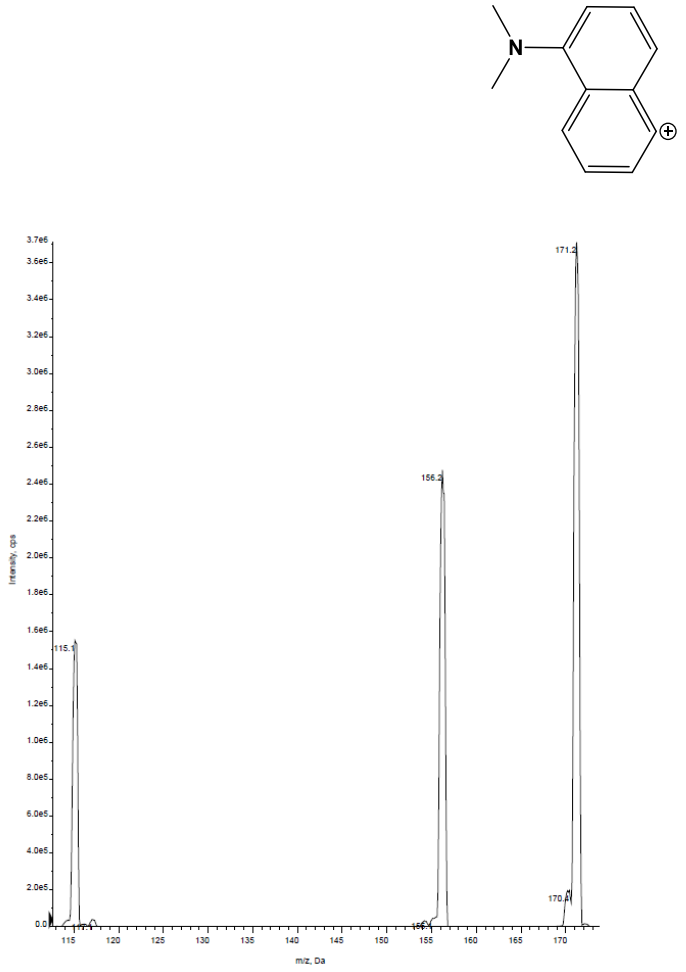

Figure 4. Product ion chromatogram of dansyl-4HB. Direct injection of dansyl-4HB to optimize the HPLC-MS/MS parameters produced the the major product ion peak at [*m/z* + 1] = 171.2.

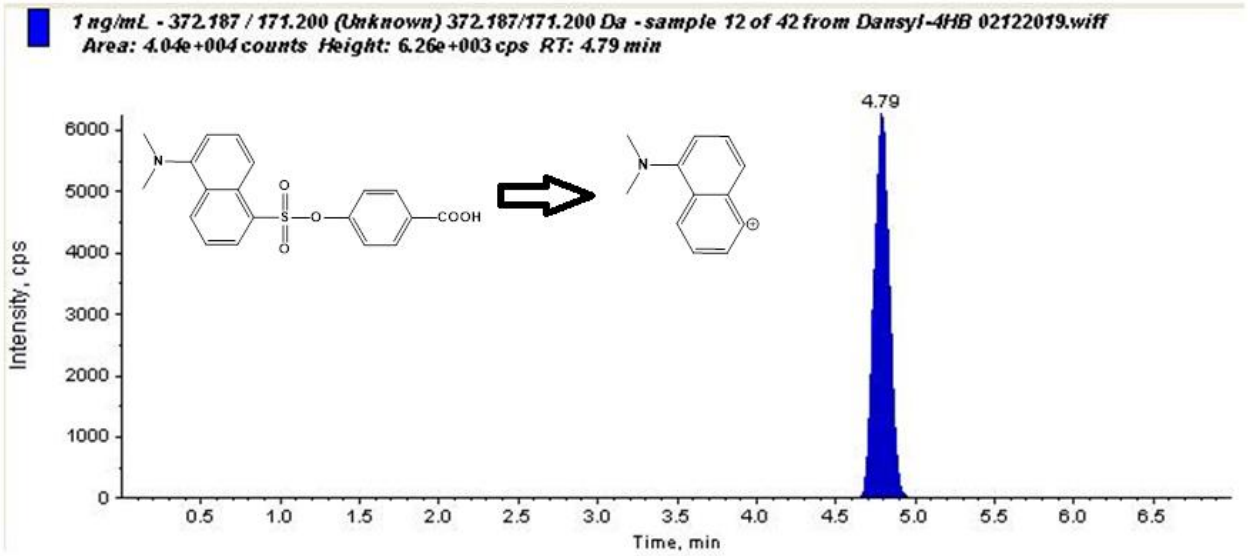

Figure 5. Representative chromatogram of dansyl-Cl standard sample with concentration 1 ng/mL. The corresponding transition being monitored from the precursor to the product ion is shown.

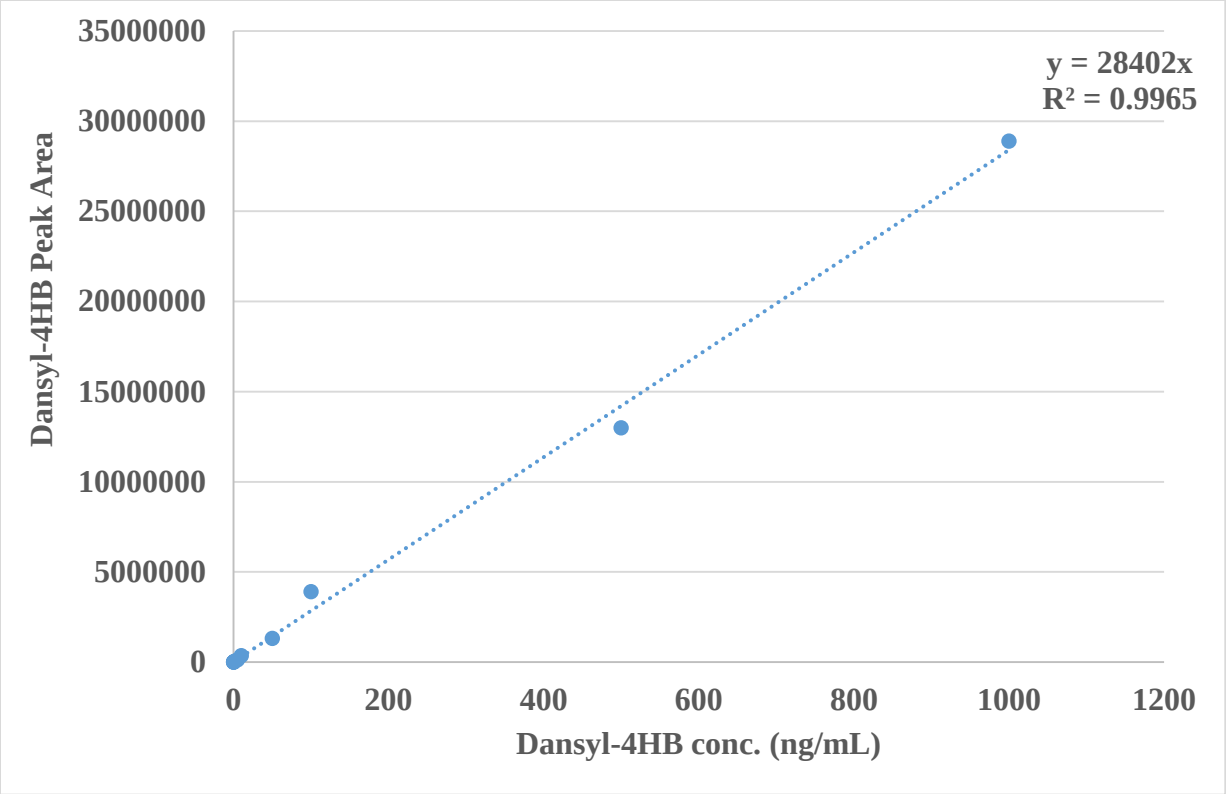

Figure 6. Dansyl-Cl standard calibration curve 1. The concentration of the standards plotted on the curve ranged from 10 pg/mL to 1 µg/mL.

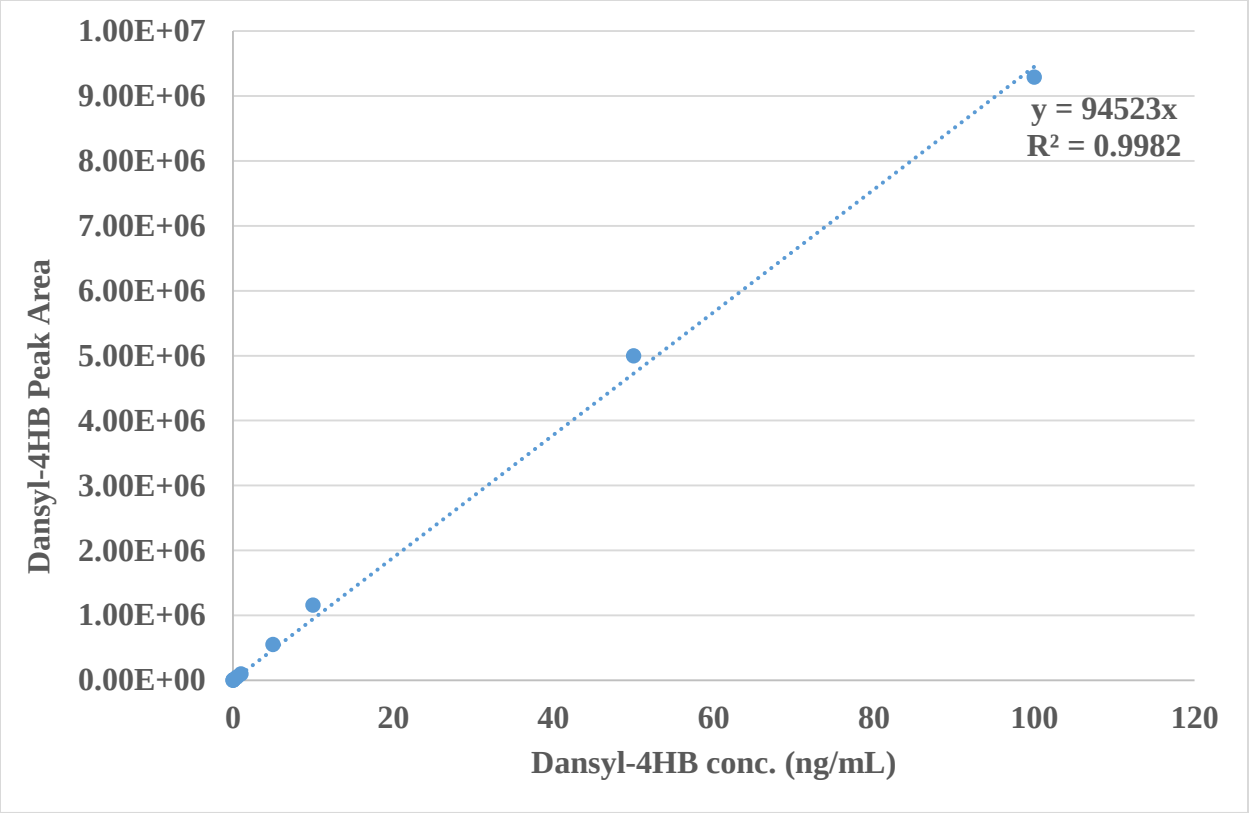

Figure 7. Dansyl-Cl standard calibration curve 2. The concentration of the standards plotted on the curve ranged from 10 pg/mL to 100 ng/mL.

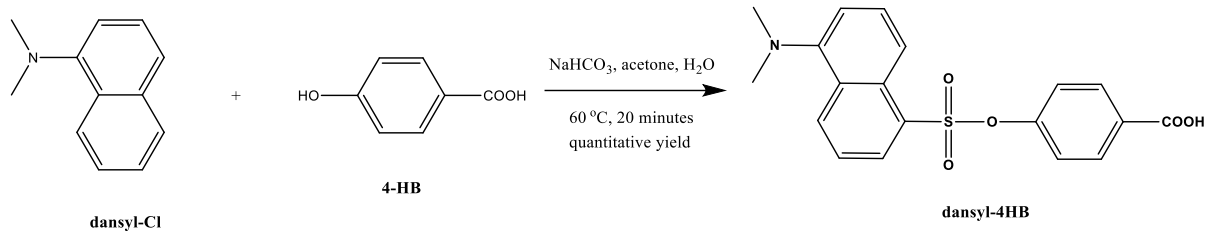

dansyl-Cl

4-HB

dansyl-4HB

Scheme 1. Synthesis of dansyl-4-hydroxybenzoic acid (**dansyl-4HB**).

References:

1) Lenaz, G., and Genova, M.L. (**2009**). *Biochim. Biophys. Acta.*, **1787**, 563

2) Nowicka, B., and Kruk, J. (2010). *Biochim. Biophys. Acta.*, **1797,** 1587

3) Bentinger, M., Tekle, M., and Dallner, G. (**2001**). *Biochem. Biophys. Res. Commun.*, **396,** 74

4) Allan, C. M., Awad, A. M., Johnson, J. S., Shirasaki, D. I., Wang, C., Blaby-Haas C. E., Merchant, S. S., Loo, J. A., and Clarke, C. F. (**2015**). *J. Biol. Chem.*, **290**, 7517

5) Sévin, D.C., and Sauer, U. (**2014**). *Nat. Chem. Biol.*, **10**, 266

6) Marbois, B., Xie, L.X., Choi, S., Hirano, K., Hyman, K., and Clarke, C.F. (**2010**). *J. Biol. Chem.*, **285**, 27827

7) Fernández-del-Río, L., Nag, A., Casado, E. G., Ariza, J., Awad, A. M., Joseph, A. I., Kwon, O., Verdin, E., de Cabo, R., Schneider, C., Torres, J. Z., Burón, M. I., Clarke, C. F., and Villalba, J. M. (**2017**). *Free Radic. Biol. Med.*, **110**, 176

8) Soubeyrand, E., Johnson, T. S., Latimer, S., Block, A., Kim, J., Colquhoun, T. A., Butelli, E., Martin, C., Wilson, M. A., and Basseta, G. J. (**2018**). *The Plant Cell*, **30**, 2910

9) Tzagoloff, A., and Dieckmann, C. L. (**1990**). *Microbiol. Rev.*, **54**, 211

10) He, C. H., Xie, L. X., Allan, C. M., Tran, U. P. C., and Clarke, C. F. (**2014**). *Biochim. E. Biophys. Acta*, **1841**, 630

11) Letian X., Ozeir, M., Tang, J. Y., Chen, J. Y., Jaquinod, S-K., Fontecave, M., Clarke, C. F., and Pierrel. F. (**2012**). *J. Biol. Chem.*, **287**, 23571

12) Lee, Y-H., Lin, Y-C., Feng, C-H., Tseng, W-L., and Lu, C-Y. (**2017**). *Scientific Reports*, **7**, 39907

13) Ernest, S., and Bello-Reuss, E. (**1995**). *The American journal of physiology*, **269**, 323

Appendix I

Chromatin-remodeling SWI/SNF complex regulates Coenzyme Q_6 synthesis and a metabolic shift to respiration in yeast

Author contributions: Agape M. Awad, Srivats Venkataramanan, Catherine F. Clarke and Tracy L. Johnson contributed to the intellectual development of the project. Agape M. Awad, Anish Nag, Michelle C. Bradley, and Catherine F. Clarke contributed to the yeast assays and the HPLC/MS-MS studies. Srivats Venkataramanan, Lauren T. Neves, Anoop Raj Galivanche, Stephen Douglas, and Tracy L. Johnson contributed to the protein and RNA work. Agape M. Awad, Srivats Venkataramanan, Anish Nag, Catherine F. Clarke, and Tracy L. Johnson contributed to the writing and revision of the manuscript.

JBC ARTICLE

Chromatin-remodeling SWI/SNF complex regulates coenzyme Q_6 synthesis and a metabolic shift to respiration in yeast

Received for publication, May 23, 2017, and in revised form, July 17, 2017 Published, Papers in Press, July 24, 2017, DOI 10.1074/jbc.M117.798397

Agape M. Awad[‡§1], Srivats Venkataramanan[§¶1], Anish Nag[‡§], Anoop Raj Galivanche[¶], Michelle C. Bradley[‡§], Lauren T. Neves[§¶], Stephen Douglass[¶], Catherine F. Clarke[‡§2], and Tracy L. Johnson[§¶3]

From the [‡]Department of Chemistry and Biochemistry, the [§]Molecular Biology Institute, and the [¶]Department of Molecular Cell and Developmental Biology, UCLA, Los Angeles, California 90095

Edited by Dennis R. Voelker

Despite its relatively streamlined genome, there are many important examples of regulated RNA splicing in *Saccharomyces cerevisiae*. Here, we report a role for the chromatin remodeler SWI/SNF in respiration, partially via the regulation of splicing. We find that a nutrient-dependent decrease in Snf2 leads to an increase in splicing of the *PTC7* transcript. The spliced *PTC7* transcript encodes a mitochondrial phosphatase regulator of biosynthesis of coenzyme Q_6 (ubiquinone or CoQ_6) and a mitochondrial redox-active lipid essential for electron and proton transport in respiration. Increased splicing of *PTC7* increases CoQ_6 levels. The increase in *PTC7* splicing occurs at least in part due to down-regulation of ribosomal protein gene expression, leading to the redistribution of spliceosomes from this abundant class of intron-containing RNAs to otherwise poorly spliced transcripts. In contrast, a protein encoded by the non-spliced isoform of *PTC7* represses CoQ_6 biosynthesis. Taken together, these findings uncover a link between Snf2 expression and the splicing of *PTC7* and establish a previously unknown role for the SWI/SNF complex in the transition of yeast cells from fermentative to respiratory modes of metabolism.

Similar to other eukaryotic genomes, genes in *Saccharomyces cerevisiae* may be interrupted by non-coding sequences, called introns. Introns are removed from the pre-mRNA through the action of the spliceosome, a macromolecular machine composed of five small nuclear ribonucleoproteins. The spliceosome recognizes consensus sequence signals on the pre-mRNA, termed splice sites, by which it subsequently binds to the intron and catalyzes its removal via two transesterification reactions (1). Pre-mRNA splicing is critical for accurate gene expression in all eukaryotes, and there is significant evidence that alterations in microenvironments, such as changes in the chromatin state or chromatin-modifying factors, can affect splicing outcomes (1). However, the mechanisms for how chromatin and chromatin factors influence splicing are not completely understood.

Although the genome of *S. cerevisiae* contains a smaller number of introns than metazoan genomes, there are, nonetheless, numerous examples of intron-dependent gene regulation (2). The largest functional class of intron-containing genes (ICGs)[4] in budding yeast is ribosomal protein genes (RPGs) that encode the protein components of the ribosome. Therefore, the energy-intensive process of translation is under the heavy regulatory control of the spliceosome, such that splicing of RPGs can be finely tuned to the cells' environmental conditions and to nutrient availability (3).

Interestingly, this enrichment of introns within RPGs impacts the splicing of, as well as provides an opportunity for the regulation of, other ICGs within the yeast genome. About a third of yeast introns occur in RPGs, and the high transcription levels of these genes means that about 90% of the intron load encountered by the spliceosome is from this one functional class of genes (4). Indeed, the prevalence of RPG introns functions to titrate spliceosomes away from other introns, especially those containing suboptimal splice sites. Conversely, down-regulating RPG expression promotes the splicing of transcripts harboring suboptimal splice sites. This effect is perhaps best described during the process of yeast meiosis. Under conditions of vegetative growth, a number of meiosis-specific ICGs are expressed, but they possess suboptimal splice sites and are therefore poorly recognized by the spliceosome and suboptimally spliced. However, upon the down-regulation of RPGs during meiosis, increased availability of the previously limiting pool of spliceosomes leads to improved splicing efficiency of introns in meiosis-specific transcripts (5, 6).

This work was supported by National Science Foundation Grants MCB-1330803 and 1518316, and by NIGMS, National Institutes of Health, Grant GM-085474; the Whitcome Pre-doctoral Fellowship in Molecular Biology (to S. V.); and Ruth L. Kirschstein National Service Award GM-007185 (to M. B). The authors declare that they have no conflicts of interest with the contents of this article. The content is solely the responsibility of the authors and does not necessarily represent the official views of the National Institutes of Health.

RNA-seq data are available in the Gene Expression Omnibus (GEO) under accession number GSE94404.

[1] Both authors contributed equally to this work.

[2] To whom correspondence may be addressed: UCLA Dept. of Chemistry and Biochemistry, 607 Charles E. Young Dr. E., Box 156905, Los Angeles, CA 90095. Tel. 310-825-0771; Fax: 310-206-5213; E-mail: cathy@chem.ucla.edu.

[3] To whom correspondence may be addressed: UCLA Dept. of Molecular Cell and Developmental Biology, 610 Charles E. Young Dr. S., Los Angeles, CA 90095. Tel.: 310-206-2416; E-mail: tljohnson@ucla.edu.

[4] The abbreviations used are: ICG, intron-containing gene; RPG, ribosomal protein gene; ns, non-spliced; s, spliced; CoQ, coenzyme Q; DMQ_6, 5-demethoxy-Q_6; 4HB, 4-hydroxybenzoic acid; HHB, 3-hexaprenyl-4-hydroxybenzoic acid; qPCR, quantitative PCR; TOR, target of rapamycin.

There are other important examples of intron-based regulation in *S. cerevisiae*, especially among ICGs with non-consensus splice sites (7, 8). One such gene is *PTC7*, which encodes a Mg^{2+}/Mn^{2+}-dependent, type 2C serine/threonine protein phosphatase (9). The intron within *PTC7* is particularly intriguing because it contains a non-consensus branch-point sequence, rendering its splicing relatively inefficient under logarithmic growth conditions. The *PTC7* intron lacks a premature termination codon and is translated in-frame. The longer, non-spliced (ns) form of the *PTC7* RNA encodes a longer protein ($Ptc7_{ns}$) that contains a single trans-membrane helix located near the N terminus but is otherwise identical to the protein isoform derived from the spliced *PTC7* RNA ($Ptc7_s$). The read-through nature of the *PTC7* intron is conserved across yeast species, indicating potential functionality for both $Ptc7_s$ and $Ptc7_{ns}$ protein isoforms (10). $Ptc7_{ns}$ has been localized to the nuclear membrane, whereas $Ptc7_s$ is located within mitochondria (10). $Ptc7_s$ has been implicated in regulation of coenzyme Q (also termed ubiquinone or CoQ) biosynthesis via its phosphatase activity (11, 12). However, mechanisms of regulation of Ptc7 itself and the role of the evolutionarily conserved $Ptc7_{ns}$ isoform remain outstanding questions.

CoQ is a redox-active lipid composed of a fully substituted benzoquinone ring and a polyisoprenoid tail and is required for mitochondrial electron transport. The length of the polyisoprenoid group is species-specific; humans produce CoQ_{10}, and *S. cerevisiae* produce CoQ_6, with 10 and 6 isoprene units, respectively. The primary role of CoQ in the inner mitochondrial membrane is to accept the electrons from complex I and complex II and pass those electrons to complex III. Several other metabolic pathways, such as pyrimidine synthesis, sulfide oxidation, and fatty acid β-oxidation, rely on CoQ as an electron carrier (13). CoQ is present in all intracellular membranes, where it may function as a lipid-soluble antioxidant. Several human syndromes, including encephalomyopathy, ataxia, cerebellar atrophy, myopathy, and steroid-resistant nephrotic syndrome, are linked to primary deficiencies in CoQ biosynthesis (14–17).

Mitochondrial proteins are responsible for facilitating the biosynthesis of CoQ_6 in *S. cerevisiae* and include Coq1–Coq11 (18). Many of the Coq proteins necessary for the biosynthesis of CoQ_6 associate in a high-molecular weight complex (termed the "CoQ-synthome"), a multisubunit complex that is peripherally associated with the inner mitochondrial membrane on the matrix side (18). $Ptc7_s$ has been shown to localize to the mitochondria, where it is thought to regulate the phosphorylation state of Coq7 (11) and/or influence mitochondrial respiratory metabolism (12). In the former case, Ptc7s is believed to control, at least in part, the phosphorylation state of the Coq7 polypeptide, which modulates its hydroxylase activity. Coq7 catalyzes the hydroxylation of 5-demethoxy-Q_6 (DMQ_6), the penultimate step in the biosynthesis of CoQ_6 in yeast (19, 20).

The conserved SWI/SNF complex utilizes ATP hydrolysis by Snf2, the catalytic subunit, to disrupt specific histone–DNA contacts, resulting in the sliding or eviction of nucleosomes from the locus. As a result, Snf2 activity contributes to transcriptional regulation (21, 22). The genome-wide distribution of SWI/SNF is responsive to conditions of stress, and the complex is required for transcription of a number of stress response genes (23, 24). We have previously reported that levels of Snf2 change in response to nutrient conditions. We have also reported that the change in Snf2 leads to changes in levels of RPG transcripts, thereby regulating splicing outcomes (6). Here, we show that changes in levels of Snf2 modulate the CoQ_6 biosynthetic pathway in *S. cerevisiae*. First, we show that deletion of Snf2 alters the relative levels of $Ptc7_s$ and $Ptc7_{ns}$ isoforms in yeast and increases both the rate of synthesis and steady-state levels of CoQ_6. This is due to down-regulation of RPG transcripts and an increase in the available pool of spliceosomes. Moreover, we find that the Snf2 protein is down-regulated over time under batch growth conditions and nutrient depletion, and together with a concomitant increase in the splicing of *PTC7*, this leads to higher CoQ_6 levels in preparation for the transition from a fermentative mode of metabolism to a respiratory mode. Furthermore, we show that the two Ptc7 isoforms have opposing effects on the CoQ_6 biosynthetic pathway, which may explain contradictory reports in the literature about the effects of Ptc7 on CoQ_6 levels (11, 12). Importantly, although Snf2 is down-regulated in response to nutrient-depleted conditions, it is nonetheless required for growth on nonfermentable carbon sources, suggesting that dynamic control of Snf2 levels is crucial for the transition from fermentation to respiration.

Results

Deletion of Snf2 leads to enhanced splicing of PTC7 and a shift in the ratios of Ptc7 protein isoforms

Previously published RNA sequencing data for yeast lacking Snf2, the core ATPase component of the SWI/SNF complex (GEO accession number GSE94404), revealed an increase in splicing of a number of introns (6). Satisfyingly, the greatest improvement in splicing upon deletion of Snf2 is experienced by *RPL22B*, via a previously described mechanism consistent with down-regulation of RPG expression (25). The next two largest improvements in splicing efficiency are experienced by *YBR062C* (an ORF of unknown function) and *PTC7*, a previously described type 2C serine-threonine mitochondrial phosphatase that contains all 11 canonical motifs of the PPM family (type 2C) protein phosphatases, previously reported to play a role in CoQ_6 biosynthesis in yeast (11) (Fig. 1*A*). This increase in splicing of *PTC7* RNA was verified by RT-PCR (Fig. 1*B*). In addition, the results from the RNA-seq and RT-PCR were also independently verified by qPCR (data not shown). It has previously been demonstrated that increased splicing of poorly recognized introns can be achieved by decreased expression of competing, highly expressed RPGs (5). Furthermore, we have shown that deletion of Snf2 causes *en masse* down-regulation of RPGs and consequent improvement in splicing of a large number of introns (6). RPG down-regulation in the absence of Snf2 was validated by RT-PCR analysis. For example, expression of RPS16A and RPL34B, two intron-containing RPGs, is down-regulated in *snf2*Δ yeast compared with WT (Fig. 1*C*).

The *PTC7* transcript makes two distinct protein isoforms, one from the nonspliced and one from the spliced RNA. The spliced isoform ($Ptc7_s$) localizes to the mitochondria, whereas

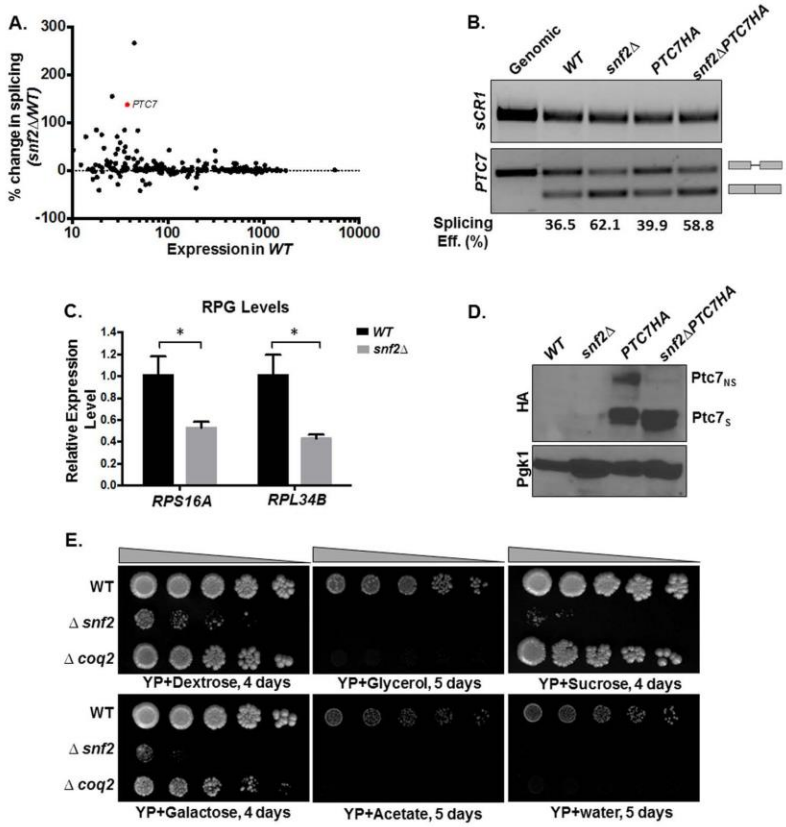

Figure 1. Deletion of *SNF2* enhances splicing of *PTC7* and the steady-state levels of the short Ptc7 protein isoform. *A*, deletion of *SNF2* enhances splicing of a subset of yeast RNAs, including *PTC7*. The scatter plot shows changes in splicing of individual introns in *snf2*Δ yeast over WT plotted against expression in WT. Percentage change in splicing is calculated as 100 × (S.E. in *snf2*Δ − S.E. in WT)/(S.E. in WT). *PTC7* is represented by the *red dot*. *B*, expression and splicing of *PTC7* in *WT* and *snf2*Δ yeast with HA-tagged and untagged Ptc7. Semiquantitative analysis of splicing efficiency of *PTC7* mRNA is indicated *below* each *lane*. *sCR1* served as an internal control. *Gray bars*, exons of the RNA; *thin gray line*, intron. *C*, RT-qPCR measurement of selected intron-containing RPG transcripts between WT and *snf2*Δ yeast strains. Shown is the mean of three biological replicates (unpaired Student's *t* test; *, $p < 0.05$). *Error bars*, S.D. *D*, deletion of *SNF2* affects steady-state levels of HA-tagged Ptc7 proteins. Proteins derived from the nonspliced and spliced forms of the *PTC7*-HA RNA are denoted as $Ptc7_{ns}HA$ and $Ptc7_sHA$, respectively. Pgk1 (phosphoglycerate kinase 1) served as a loading control. *E*, serial dilutions (5-fold) of WT BY4741, *snf2*Δ, and *coq2*Δ (negative respiratory-deficient control; W303 background, because the deletion is unstable in the BY background) on YP agar plates with the indicated carbon sources.

the nonspliced isoform ($Ptc7_{ns}$) has been reported to localize to the nuclear envelope (10). The *PTC7* gene was endogenously HA-tagged, and Western blot analysis demonstrated that deletion of Snf2 leads to an increase in the levels of $Ptc7_s$ compared with $Ptc7_{ns}$ (Fig. 1*D*). It is noteworthy that the increase in the ratio of $Ptc7_s/Ptc7_{ns}$ polypeptides in the WT and *snf2*Δ cells appears to be greater than the increased ratio of spliced/unspliced RNA.

It has previously been demonstrated that yeast strains lacking Snf2 fail to grow on non-fermentable carbon sources, such as glycerol or acetate (26). However, *snf2*Δ mutants frequently incur secondary mutations, and the growth of such strains can resemble WT. Therefore, growth on fermentable and non-fermentable carbon sources was used as a quality control for the assessment of the *bona fide* phenotype (24) of *snf2*Δ prior to each experiment (Fig. 1*E*).

Deletion of Snf2 leads to increased CoQ_6 synthesis in yeast and improves the flux from DMQ_6 to CoQ_6

$Ptc7_s$ has previously been described as playing a role in regulating CoQ_6 synthesis in *S. cerevisiae* (11). A schematic of the entire CoQ_6 biosynthetic pathway with 4-hydroxybenzoic acid as the ring precursor and the role of Ptc7 is detailed in Fig. 2*A*. $Ptc7_s$ is thought to enhance CoQ_6 biosynthesis via its activation of Coq7 and subsequent catalysis of the hydroxylation of DMQ_6, the penultimate step of CoQ_6 biosynthesis (Fig. 2*B*) (11, 27).

$^{13}C_6$-Labeled 4-hydroxybenzoic acid ($^{13}C_6$-4HB), a ring precursor for Q biosynthesis, was used to determine the levels of $^{13}C_6$-CoQ_6 biosynthesis in WT *versus* *snf2*Δ yeast grown to similar culture densities. The absence of Snf2 causes increased steady-state levels of CoQ_6 and increased *de novo* biogenesis of $^{13}C_6$-CoQ_6 (Fig. 3*A*). Additionally, there are significant changes in the levels of *de novo* synthesized DMQ_6, as well as 3-hexa-

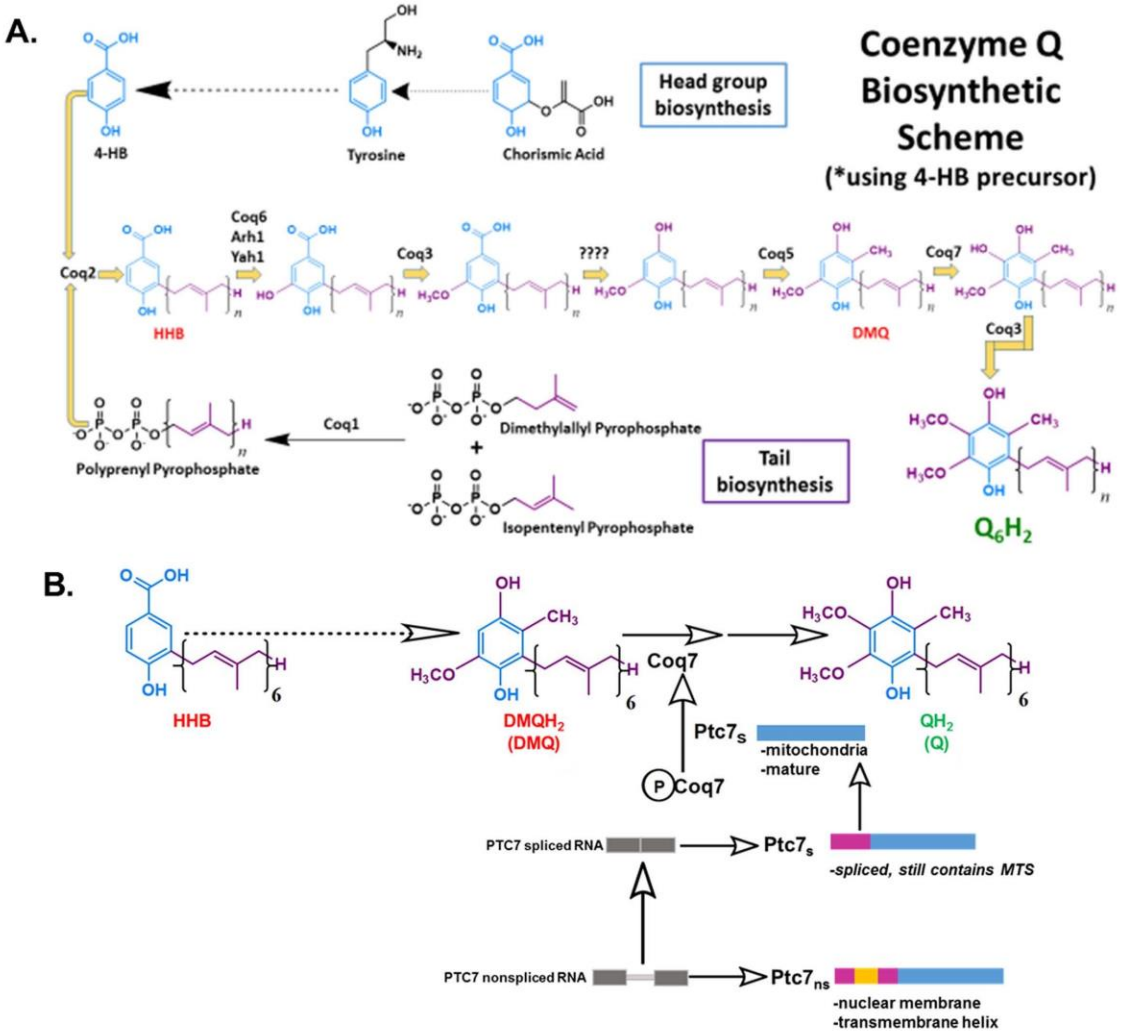

Figure 2. CoQ_6 biosynthetic pathway in *S. cerevisiae* and role of $Ptc7_s$ isoform on Coq7 phosphorylation and function. *A*, schematic of CoQ_6 biosynthetic pathway in yeast using 4HB as a ring precursor, ultimately forming the reduced CoQ_6H_2 product *in vivo*. The *question marks above* the decarboxylation and second hydroxylation steps denote that the enzyme(s) responsible is still unknown. *B*, schematic of the CoQ_6 biosynthetic pathway in yeast. The proposed function of $Ptc7_s$ as a mitochondrial phosphatase modulating Coq7 activity is indicated. $Ptc7_{ns}$ has been localized to nuclear membrane. The *gray bars* represent the exon regions of the RNA, and the *thin gray line* represents the intron region of the RNA. The *pink-colored regions* represent the predicted 38-amino acid mitochondrial targeting sequence (*MTS*) of the protein, the *yellow region* represents the 31-amino acid intron of the protein (which interrupts the MTS after amino acid 19, hence spanning from amino acid 20 to 50), and the *blue region* depicts the mature and spliced polypeptide, which spans from amino acid 51 to 374 (47).

prenyl-4-hydroxybenzoic acid (HHB), an early CoQ_6 biosynthetic intermediate (Fig. 3, *B* and *D*). Consistent with the increased synthesis of CoQ_6 being a consequence of Ptc7 action, the *snf2*Δ yeast show significantly lower ratios of $^{13}C_6$-DMQ_6 level to $^{13}C_6$-CoQ_6 content, indicating a significant increase in the efficiency of conversion of DMQ_6 to CoQ_6, namely the step catalyzed by Coq7, a target of $Ptc7_s$ (Fig. 3*C*) (11). Strikingly, we also observe that the levels of both steady-state and *de novo* synthesized HHB are significantly lower in *snf2*Δ than in the WT yeast (Fig. 3*D*). This suggests that the deletion of Snf2 not only causes higher CoQ_6 production by regulating catalysis from DMQ_6 but that it also funnels the early precursors more efficiently than WT, thus allowing a more streamlined conversion of intermediates of the pathway to the overall product of CoQ_6. This is reinforced by the observation that *snf2*Δ yeast show significantly lower ratios of $^{13}C_6$-HHB to $^{13}C_6$-CoQ_6 content (Fig. 3*E*).

Depletion of Snf2 during batch growth is associated with increased PTC7 splicing and increased CoQ_6 production

Because *snf2*Δ yeast have a significantly slower growth rate than WT, we considered the possibility that the increased CoQ_6

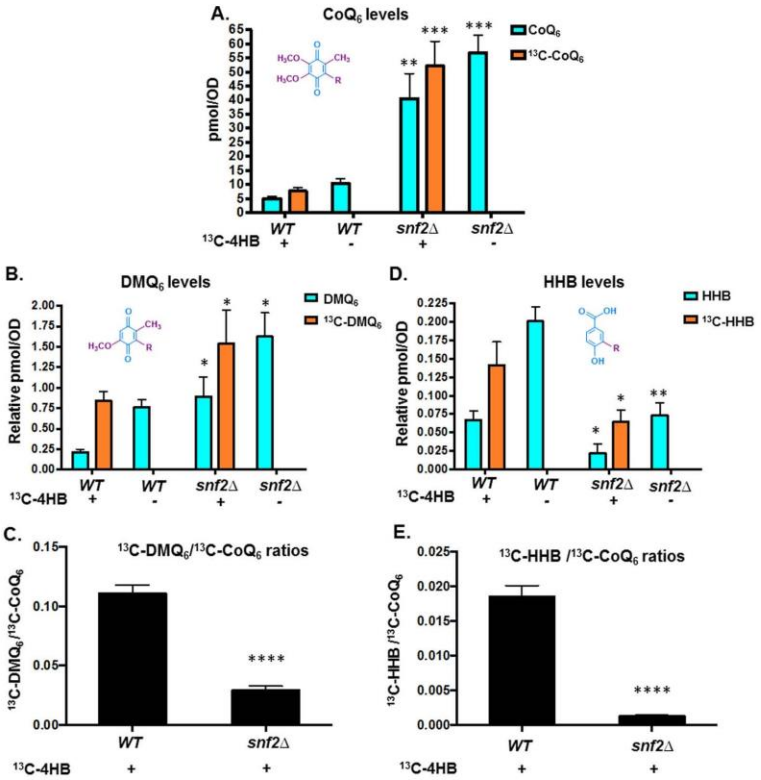

Figure 3. Deletion of *SNF2* leads to increased steady state levels and *de novo* CoQ_6 biosynthesis in yeast and improves the flux from DMQ_6 to CoQ_6. *A*, levels of steady-state CoQ_6 (^{12}C-CoQ_6, *blue bars*) and *de novo* synthesized CoQ_6 ($^{13}C_6$-CoQ_6, *orange bars*) were determined in WT and *snf2*Δ yeast. $^{13}C_6$-4HB was added during midlog phase (A_{600} = 0.5), and labeling was allowed to proceed until a cell density of A_{600} ~1.75 was reached by both strains. ^{12}C-CoQ_6 and $^{13}C_6$-CoQ_6 present in yeast cell pellets were quantified by HPLC-MS/MS, as described under "Experimental procedures." *Error bars*, S.D. of $n = 3$ biological replicates (unpaired Student's *t* test between *corresponding bars* for *snf2*Δ and WT; **, $p < 0.005$; ***, $p < 0.0005$). *B*, levels of steady-state (^{12}C-DMQ_6, *blue bars*) and *de novo* synthesized DMQ_6 ($^{13}C_6$-DMQ_6, *orange bars*) were determined in WT and *snf2*Δ yeast. DMQ_6 was determined from the same cultures as in *A*. *Error bars*, S.D. of $n = 3$ biological replicates (unpaired Student's *t* test between corresponding bars for *snf2*Δ and *WT*; *, $p < 0.05$). *C*, ratios of $^{13}C_6$-DMQ_6/$^{13}C_6$-CoQ_6 in WT and *snf2*Δ yeast, depicting flux of conversion of $^{13}C_6$-DMQ_6 to $^{13}C_6$-CoQ_6. *Error bars*, S.D. of $n = 3$ biological replicates (unpaired Student's *t* test between corresponding bars for *snf2*Δ and WT; ****, $p < 0.00005$). *D*, levels of steady-state HHB (^{12}C-HHB, *blue bars*) and *de novo* synthesized HHB ($^{13}C_6$-HHB, *orange bars*) were determined in WT and *snf2*Δ yeast. HHB was determined from the same cultures as in *A*. *Error bars*, S.D. of $n = 3$ biological replicates (unpaired Student's *t* test between *corresponding bars* for *snf2*Δ and WT; *, $p < 0.05$; **, $p < 0.005$). *E*, ratios of ^{13}C-HHB/^{13}C-CoQ_6 in WT and *snf2*Δ yeast, depicting flux of conversion of $^{13}C_6$-HHBto $^{13}C_6$-CoQ_6. *Error bars*, S.D. of $n = 3$ biological replicates (unpaired Student's *t* test between *corresponding bars* for *snf2*Δ and WT; ****, $p < 0.00005$).

synthesis was a consequence of the increased time in culture required to achieve equal cell density. To address this, rates of CoQ_6 biosynthesis in WT and *snf2*Δ yeast were determined at timed intervals of culture. First, measurements of steady-state and *de novo* synthesis rates of CoQ_6 between 2 and 12 h of batch growth in YPD revealed that whereas there is indeed an increased rate of synthesis in the *snf2*Δ yeast strain, the steady-state levels of CoQ_6 plateau within 4–6 h of labeling (Fig. 4*A*). We also observe decreasing levels of Snf2 as the time course progresses and nutrients are depleted (Fig. 4*B*). Consistent with the role of Snf2 in RPG transcription, RPG levels decrease with time in batch cultures of yeast, in a manner that tracks well with decreasing levels of Snf2 (Fig. 4*C*). This decrease also coincides with a concomitant increase in the splicing of *PTC7* (Fig. 4, *D* and *E*). Notably, splicing of the *PTC7* transcript in *snf2*Δ yeast starts off higher than in WT yeast, but as Snf2 is depleted from the WT strain, splicing of the *PTC7* transcript approaches the levels of splicing in the *snf2*Δ strain (Fig. 4*F*).

To better understand the kinetics of CoQ_6 synthesis, a shorter time course was performed to capture points preceding the plateau, between 0 and 5 h of labeling. Within 4 h after labeling with ^{13}C-4HB precursor, significant down-regulation in the levels of Snf2 protein is evident (Fig. 5*A*). The decrease in the level of Snf2 protein is mirrored in the increase in splicing efficiency of *PTC7* transcript in the WT strain (Fig. 5, *B–E*). It is interesting to note that the *PTC7* transcript is initially better spliced in the *snf2*Δ strain than in WT, but as the levels of Snf2 in the WT yeast decrease, splicing improves to a degree comparable with the *snf2*Δ strain (Fig. 5, *D* and compare *C* and *F*).

Additionally, there is a striking increase in the overall CoQ_6 product and its *de novo* biosynthesis in the *snf2*Δ yeast within 0–5 h of labeling, as compared with CoQ_6 levels of the WT

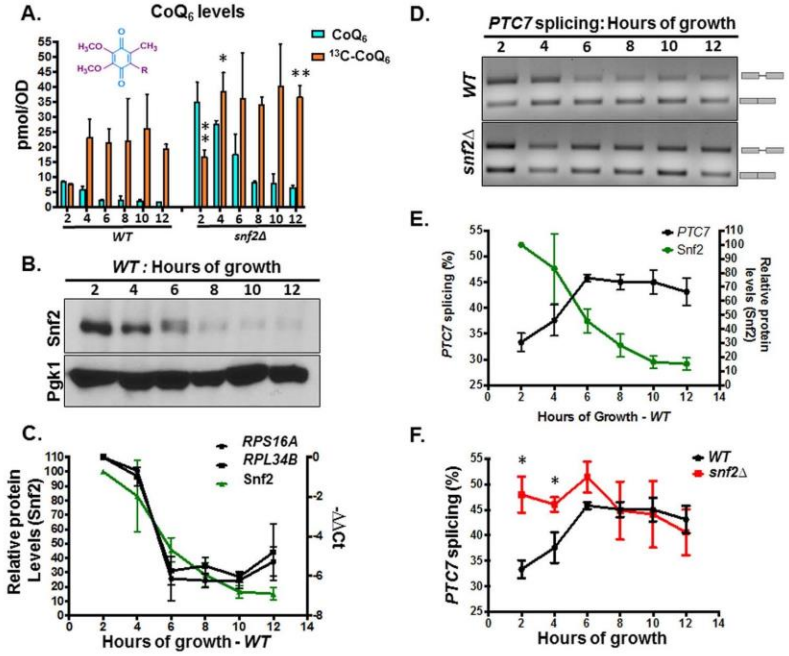

Figure 4. Snf2 levels decrease during batch growth, coinciding with increased *PTC7* splicing and increased CoQ_6 synthesis. *A*, levels of steady-state CoQ_6 (^{12}C-CoQ_6, *blue bars*) and *de novo* synthesized CoQ_6 ($^{13}C_6$-CoQ_6, *orange bars*) in WT and *snf2*Δ yeast were determined at the designated hours after labeling with $^{13}C_6$-4HB. *Error bars*, S.D. of $n = 3$ biological replicates (unpaired Student's *t* test between *corresponding bars* for *snf2*Δ and WT; *, $p < 0.05$; **, $p < 0.005$). *B*, steady-state levels of Snf2 protein in WT cells corresponding to samples from *A* were determined by immunoblot. Pgk1 served as a loading control. *C*, RT-qPCR measurement of selected intron-containing RPG transcripts (*black lines*) and Snf2 protein levels (*green line*) in WT yeast cells were determined at the designated hours after labeling with $^{13}C_6$-4HB as indicated in *A*. Shown is the mean of three biological replicates. *Error bars*, S.D. *D*, expression and splicing of *PTC7* in WT and *snf2*Δ yeast cells corresponding to samples from *A*. PCR products representing the spliced and nonspliced forms are indicated. *E*, quantification of splicing of *PTC7* transcript (*black line*) and Snf2 protein levels (*green line*) in WT yeast cells corresponding to samples from *D*. Snf2 protein levels were previously depicted in *C* and are shown here again for purposes of comparison. Shown is the mean of three biological replicates. *Error bars*, S.D. *F*, quantification of splicing of *PTC7* transcripts in WT and *snf2*Δ yeast cells corresponding to samples from *D*. The splicing of WT *PTC7* shown in *D* is depicted again here for purposes of comparison. Shown is the mean of three biological replicates. *Error bars*, S.D. (unpaired Student's *t* test; *, $p < 0.05$.

during the same time course (Fig. 6, compare *A* and *F*). Furthermore, the gradual increase in CoQ_6 biosynthesis observed in the WT strain plateaus at 3–4 h after labeling (Fig. 6*A*), by which point the significant down-regulation in the levels of Snf2 protein is also evident (Fig. 5*A*). The steady-state and *de novo* synthesized levels of DMQ_6 and HHB were also measured in the 5-h time course of WT and *snf2*Δ yeast (Fig. 6, *B*, *C*, *G*, and *H*). Strikingly, the conversion of *de novo* DMQ_6 to CoQ_6 increases (as shown by the decreased ratio of $^{13}C_6$-DMQ_6 to $^{13}C_6$-CoQ_6) in a manner concurrent with the decrease in Snf2 levels and increase in *PTC7* splicing in WT (compare Fig. 6*D* with Fig. 5 (*A* and *B*)). In fact, as the levels of Snf2 in WT yeast decrease, the conversion efficiency of DMQ_6 to CoQ_6 approaches the low ratio of DMQ_6 to CoQ_6 in *snf2*Δ yeast (Fig. 6, compare *D* and *I*). The role of $Ptc7_s$ in the increased synthesis of CoQ_6 in the absence of Snf2 can be inferred from the observation that whereas the conversion efficiency from DMQ_6 to CoQ_6 is higher in the absence of Snf2, the level of DMQ_6 itself does not change appreciably between WT and *snf2*Δ yeast over the 5-h time course (Fig. 6, compare *B* and *G*). However, the *snf2*Δ cells also show significantly lower rates of HHB synthesis (Fig. 6, compare *C* and *H*), as well as lower ratios of $^{13}C_6$-HHB to $^{13}C_6$-CoQ_6 content (Fig. 6, compare *E* and *J*), consistent with the observation that deletion of Snf2 markedly accelerates the synthesis of CoQ_6, presumably by expediting the conversion of these intermediates to the final product.

RPG down-regulation in general leads to increased PTC7 splicing

Our previous work showed that Snf2-dependent down-regulation of ribosomal protein genes enhances splicing, particularly of genes with nonconsensus splice sites. To determine whether the observed increase in *PTC7* splicing is a consequence of RPG down-regulation *per se*, rapamycin was used to inhibit target of rapamycin (TOR)-dependent RPG transcription in a Snf2-independent manner (28) (Fig. 7*A*). It has also been previously published that rapamycin mitigates certain mitochondrial disorders in *Drosophila* and improves lifespan in response to TOR inhibition, purportedly by modulating carbon metabolism (29). In our work, rapamycin treatment led to a significant increase in the splicing of the *PTC7* transcript (Fig. 7, *B* and *C*). As previously observed, the change in the ratio of $Ptc7_s$/$Ptc7_{ns}$ protein (Fig. 1*D*) is greater than the change in the ratio of spliced to nonspliced transcript upon the deletion of Snf2 (Fig. 1*B*). This suggests that whereas Snf2-dependent RPG down-regulation changes the splicing of the *PTC7* transcript,

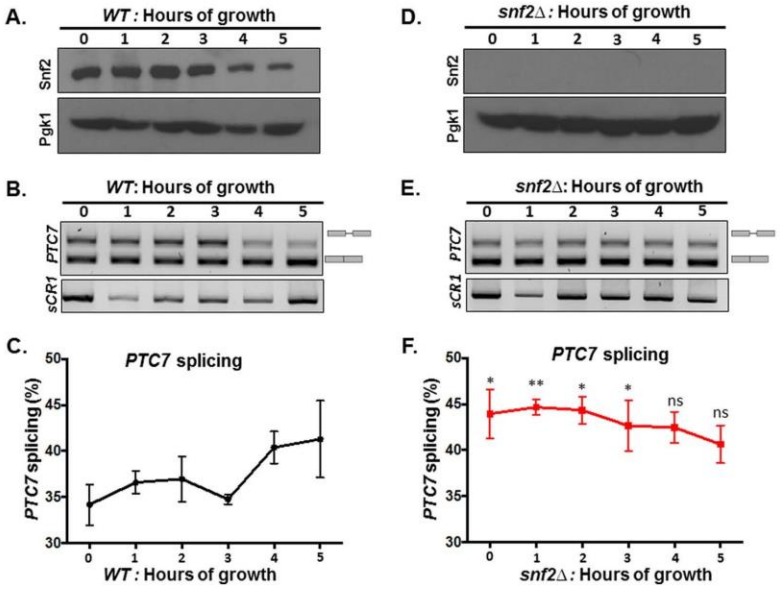

Figure 5. The decrease in Snf2 levels over time in batch cultures of WT yeast correlates with enhanced splicing of *PTC7* RNA. *A*, steady-state levels of Snf2 protein in WT cells corresponding to samples from indicated time points were determined by immunoblot. Pgk1 (phosphoglycerate kinase 1) served as a loading control. *B*, expression and splicing of *PTC7* in WT yeast cells corresponding to samples from *A*; PCR products represent the spliced and nonspliced forms, as indicated. *C*, quantification of splicing of *PTC7* transcript (*black line*) in WT yeast cells corresponding to samples from *B*. Shown is the mean of three biological replicates. *Error bars*, S.D. *D*, the Snf2 protein is absent in *snf2*Δ cells corresponding to samples from the indicated time points as determined by immunoblot. Pgk1 served as a loading control. *E*, expression and splicing of *PTC7* in *snf2*Δ yeast cells corresponding to samples from *D*; PCR products representing the spliced and nonspliced forms are indicated. *F*, quantification of splicing of *PTC7* transcript (*red line*) in *snf2*Δ yeast cells corresponding to samples from *E*. Shown is the mean of three biological replicates. *Error bars*, S.D. (unpaired Student's *t* test between *corresponding bars* for *snf2*Δ and WT in *C*; *, $p < 0.05$; **, $p < 0.005$).

there are probably additional layers of gene regulation that control the relative levels of the $Ptc7_s$ and $Ptc7_{ns}$ protein isoforms. Experiments probing these mechanisms are currently ongoing. Nonetheless, these results are consistent with a model whereby down-regulation of RPG expression redirects spliceosomes from these abundant transcripts to otherwise poorly spliced transcripts, such as *PTC7* (5, 6). In light of the role of Snf2 in RPG expression, changes in Snf2 levels allow fine-tuning of splicing in response to the cell's metabolic needs.

Ptc7 isoforms have differing and opposing effects on CoQ_6 synthesis

The predicted structures of the two isoforms of Ptc7, $Ptc7_s$ and $Ptc7_{ns}$, have been modeled (Fig. 8, *A* and *B*). In fact, the $Ptc7_{ns}$ contains a transmembrane helix, encoded for by the *PTC7* intron, which is capable of spanning the nuclear membrane. Overall, the presence of this transmembrane helix is not predicted to influence the folding of the rest of the protein, thus potentially retaining its phosphatase activity (Fig. 8).

To determine the effect of each Ptc7 isoform on CoQ_6 synthesis, we assayed CoQ_6 levels in cells expressing both forms of Ptc7, $Ptc7_s$ only, $Ptc7_{ns}$ only, or neither (*ptc7*Δ). As reported previously, there is no significant change in CoQ_6 synthesis levels in the *ptc7*Δ mutant (12, 30). However, exclusive expression of $Ptc7_s$ leads to an increase in CoQ_6 synthesis, whereas exclusive expression of $Ptc7_{ns}$ leads to a decrease in CoQ_6 synthesis (Fig. 9*A*). The relative RNA levels from each strain are shown (Fig. 9*B*). Moreover, there are no significant changes observed in the protein levels of Snf2 or Coq7, the target of Ptc7 activity (Fig. 9*C*), in these strains. Whereas each of these isoforms was expressed within the endogenous context and from the endogenous *PTC7* promoter, protein levels of the $Ptc7_{ns}$ appeared to be increased relative to the other isoforms (Fig. 9, *B* and *C*), perhaps due to a cellular feedback mechanism that increases expression or enhances stability of $Ptc7_{ns}$.

The steady-state and *de novo* synthesized levels of CoQ_6 were also measured in a 5-h time course with the yeast strains expressing either $Ptc7_{ns}$ or $Ptc7_s$. Both steady-state and *de novo* CoQ_6 biosynthesis are significantly lower in $Ptc7_{ns}$ strain than in the $Ptc7_s$ and in fact appear to be actively repressed, suggesting that the two isoforms of Ptc7 have differing and opposing effects on CoQ_6 biosynthesis (Fig. 9*D*). In addition, the exclusive presence of $Ptc7_s$ causes increased *de novo* biogenesis of ^{13}C-CoQ_6 as compared with the exclusive presence $Ptc7_{ns}$ (Fig. 9*D*). Whereas the positive effect of $Ptc7_s$ on CoQ_6 biosynthesis is consistent with the mechanisms of Ptc7 action described previously, it is clear that $Ptc7_{ns}$ has a repressive effect on CoQ_6 biosynthesis (compare $Ptc7_{ns}$ and *ptc7*Δ in Fig. 9*A*). To begin to elucidate the mechanism of this repression, we assayed the mRNA transcript levels of genes encoding components of the CoQ_6 biosynthetic complex (*viz. COQ1–11* and *PTC7*). On average, there is little change in the expression of the complex upon deletion of Snf2 (Fig. 9, *G* and *H*) or with the exclusive expression of $Ptc7_s$ or *ptc7*Δ. However, exclusive expression of $Ptc7_{ns}$ is associated with pronounced down-regulation of every

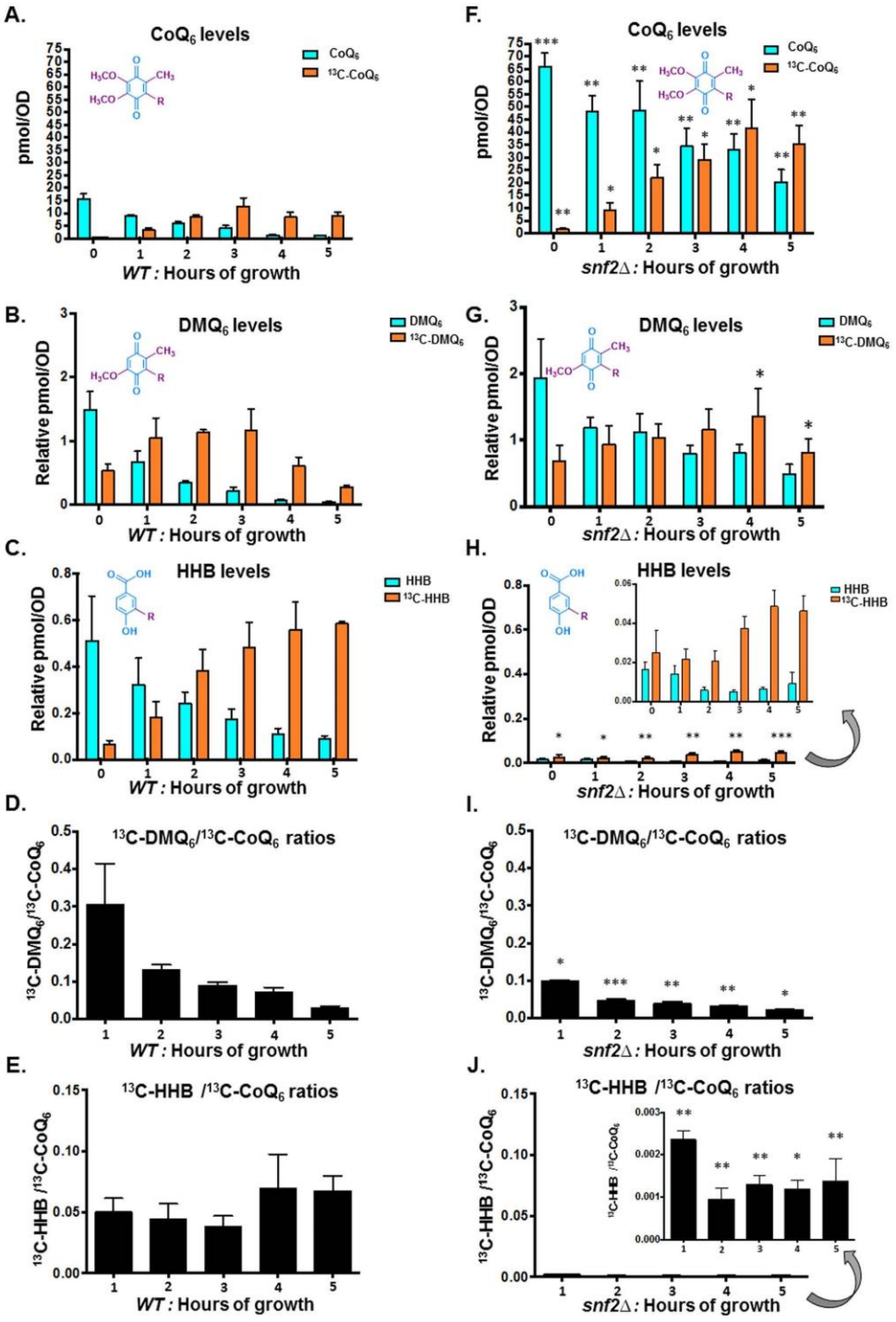

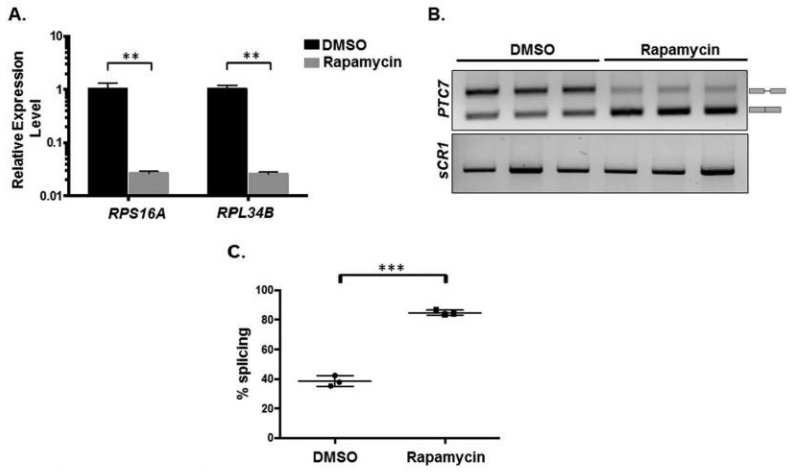

Figure 7. RPG down-regulation and redistribution of spliceosomes result in increased *PTC7* splicing. *A*, RT-qPCR measurement of selected intron-containing RPG transcripts between WT yeast treated with rapamycin and a vehicle control. Mean of three biological replicates (unpaired Student's *t* test, $^{**}p < 0.005$). *Error bars*, S.D. *B*, expression and splicing of *PTC7* in WT yeast treated with rapamycin and a vehicle control (DMSO). PCR products representing the spliced and nonspliced forms are indicated. *C*, quantification of three independent biological replicates of *B* (unpaired Student's *t* test; ***, $p < 0.0005$). *Error bars*, S.D.

member of the CoQ-synthome (Fig. 9, *E* and *F*). Although the mechanism by which these components are down-regulated is unclear, it is interesting that $Ptc7_{ns}$ has previously been localized to the nuclear membrane (10), hinting at a novel role for this isoform in expression of the RNAs encoding the CoQ-synthome. Two possible mechanisms by which nucleus-localized $Ptc7_{ns}$ may affect synthesis of the CoQ-synthome are via direct action on nucleus-localized Coq7 or via indirect effects on gene expression. It is important to mention here that to the best of our knowledge, no reports have demonstrated nuclear localization of, or a nuclear role for, Coq7 in *S. cerevisiae*.

Interestingly, yeast strains engineered to express either $Ptc7_s$ or $Ptc7_{ns}$ still retain the ability to grow on medium containing a non-fermentable carbon source, as do *ptc7*Δ null mutants (data not shown). This is consistent with our prior observations that ~1–10% of CoQ_6 levels are sufficient for comparable growth on medium containing a nonfermentable carbon source. It has been postulated that residual CoQ_6 levels are observed due to the overlapping activities of Ptc5 and/or Ptc6, and in fact the *ptc5*Δ*ptc7*Δ double null mutant has impaired growth under conditions of temperature stress (11, 31). It is also worth noting that unlike the deletion of *SNF2*, the conversion efficiencies or ratios between the early components of the pathway (DMQ_6 or HHB) and CoQ_6 do not vary between strains exclusively expressing either Ptc7 isoform (Fig. 10, *C* and *D*). This is because although there are significant changes in the levels of *de novo* synthesized DMQ_6 as well as HHB when comparing $Ptc7_s$ to $Ptc7_{ns}$ (Fig. 10, *A* and *B*), $Ptc7_s$ is synthesizing higher levels of *de novo* CoQ_6, DMQ_6, and HHB, compared with overall lower levels of these same lipids in $Ptc7_{ns}$ (Fig. 10, *C* and *D*). Thus, the overall conversion efficiencies (ratios) between both isoforms are comparable (Fig. 10, *C* and *D*). This is consistent with our interpretation that the absence of Snf2 contributes to the metabolic state of the cell in other ways in addition to its role in regulation of the Ptc7 isoforms.

Figure 6. Overall conversion efficiency of the CoQ_6 biosynthetic pathway increases upon depletion of Snf2, with increased conversions of both DMQ_6 to Q_6 and HHB to Q_6. *A*, levels of steady-state CoQ_6 (^{12}C-CoQ_6, *blue bars*) and *de novo* synthesized CoQ_6 ($^{13}C_6$-CoQ_6, *orange bars*) in WT yeast cells were determined at the designated hours after labeling with $^{13}C_6$-4HB. *Error bars*, S.D. of $n = 3$ biological replicates. *B*, levels of steady-state DMQ_6 (^{12}C-DMQ_6, *blue bars*) and *de novo* synthesized DMQ_6 ($^{13}C_6$-DMQ_6, *orange bars*) in WT yeast were determined at the designated hours after labeling with $^{13}C_6$-4HB. *Error bars*, S.D. of $n = 3$ biological replicates. *C*, levels of steady-state HHB (^{12}C-HHB, *blue bars*) and *de novo* synthesized ($^{13}C_6$-HHB, *orange bars*) in WT and *snf2*Δ yeast were determined at the designated hours after labeling with $^{13}C_6$-4HB. *Error bars*, S.D. of $n = 3$ biological replicates. *D*, the ratio of $^{13}C_6$-DMQ_6/$^{13}C_6$-CoQ_6 in WT yeast was determined at the designated hours after labeling with $^{13}C_6$-4HB. *Error bars*, S.D. of $n = 3$ biological replicates. The 0-h time point is excluded, because the ratio is not indicative of pathway conversion. *E*, the ratio of $^{13}C_6$-HHB/$^{13}C_6$-CoQ_6 in WT yeast was determined at the designated hours after labeling with $^{13}C_6$-4HB. *Error bars*, S.D. of $n = 3$ biological replicates. The 0-h time point is excluded, because the ratio is not indicative of pathway conversion. *F*, levels of steady-state CoQ_6 (^{12}C-CoQ_6, *blue bars*) and *de novo* synthesized ($^{13}C_6$-CoQ_6, *orange bars*) in *snf2*Δ yeast cells were determined at the designated hours after labeling with $^{13}C_6$-4HB. *Error bars*, S.D. of $n = 3$ biological replicates (unpaired Student's *t* test between *corresponding bars* for *snf2*Δ and WT in *A*; *, $p < 0.05$; **, $p < 0.005$; ***, $p < 0.0005$). *G*, levels of steady-state DMQ_6 (^{12}C-DMQ_6, *blue bars*) and *de novo* synthesized DMQ_6 ($^{13}C_6$-DMQ_6, *orange bars*) in *snf2*Δ yeast were determined at the designated hours after labeling with $^{13}C_6$-4HB. *Error bars*, S.D. of $n = 3$ biological replicates. (unpaired Student's *t* test between *corresponding bars* for *snf2*Δ and WT in *B*; *, $p < 0.05$). *H*, levels of steady-state HHB (^{12}C-HHB, *blue bars*) and *de novo* synthesized HHB ($^{13}C_6$-HHB, *orange bars*) in *snf2*Δ yeast were determined at the designated hours after labeling with ^{13}C-4HB. *Error bars*, S.D. of $n = 3$ biological replicates (unpaired Student's *t* test between corresponding bars for *snf2*Δ and WT in *C*; *, $p < 0.05$; **, $p < 0.005$; ***, $p < 0.0005$). *I*, the ratio of $^{13}C_6$-DMQ_6/$^{13}C_6$-CoQ_6 in *snf2*Δ yeast cells was determined at the designated hours after labeling with $^{13}C_6$-4HB. *Error bars*, S.D. of $n = 3$ biological replicates (unpaired Student's *t* test between corresponding bars for *snf2*Δ and WT in *D*; *, $p < 0.05$; **, $p < 0.005$; ***, $p < 0.0005$). The 0-h time point is excluded, because the ratio is not indicative of pathway conversion. *J*, the ratio of $^{13}C_6$-HHB/$^{13}C_6$-CoQ_6 in *snf2*Δ yeast cells was determined at the designated hours after labeling with $^{13}C_6$-4HB. *Error bars*, S.D. of $n = 3$ biological replicates (unpaired Student's *t* test between *corresponding bars* for *snf2*Δ and WT in *E*; *, $p < 0.05$; **, $p < 0.005$). The 0-h time point is excluded, because the ratio is not indicative of pathway conversion.

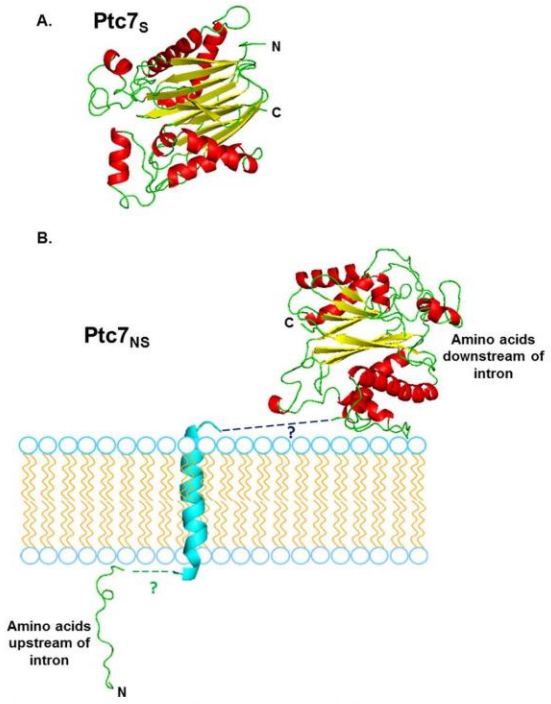

Figure 8. Structural predictions of mitochondrial $Ptc7_s$ and nuclear membrane traversing $Ptc7_{ns}$. *A*, PHYRE2 homology modeling of mature mitochondrial $Ptc7_s$, which is experimentally determined to start at amino acid Gly^{39} (46). 85% of residues modeled at >90% confidence (15% of residues modeled *ab initio*). The N terminus and C terminus of the protein are shown. *B*, PHYRE2 homology modeling of nuclear membrane $Ptc7_{ns}$. The predicted trans-membrane helix encoded by the intron is shown in *cyan*. 86% of residues modeled at >90% confidence (14% of residues modeled *ab initio*. To show the interaction with the nuclear membrane, the N-terminal loop residing on the one side of the nuclear membrane is proposed to be linked to the modeled transmembrane helix, which is then proposed to be linked to the rest of the Ptc7 protein that is predicted to reside on the alternate side of the nuclear membrane. The *nine black dashes* connecting the helix to the larger portion of the protein represent nine amino acids in the intron that were in an unmodeled region.

These data reveal a novel role for Snf2 in respiration and specifically in the transition from a largely fermentative mode of metabolism to a largely respiratory one in *S. cerevisiae*, as shown by the model in Fig. 11. Under conditions of high nutrient availability, Snf2-dependent transcription of intron-rich RPGs sequesters spliceosomes away from transcripts with weak splice sites, such as *PTC7*. As a consequence, both isoforms of the Ptc7 protein are expressed at appreciable levels, and their opposing effects on CoQ_6 synthesis ensure that CoQ_6 is maintained at a relatively low level. As the nutrients in the medium are depleted, the levels of Snf2 and, consequently, RPG transcripts, decrease concurrently, freeing up spliceosomes to act on *PTC7*. This leads to better splicing of *PTC7* and a shift in the relative abundances of the two protein isoforms, which eventually leads to an increase in CoQ_6 synthesis.

Discussion

Whereas it has been broadly acknowledged that chromatin states and chromatin factors influence splicing outcomes in various organisms, identifying the functional importance of such regulation under biologically relevant conditions remains a challenge. We have shown previously that down-regulation of Snf2, the core ATPase component of the SWI/SNF chromatin-remodeling complex, in response to nutrient depletion leads to a change in cellular splicing outcomes due to down-regulation of RPGs and subsequent redistribution of spliceosomes (5, 6). We show here that Snf2-dependent changes in splicing of *PTC7* during yeast growth, combined with the general conditions in the cell in the absence of Snf2, causes a shift in the ratio of two distinct isoforms of the Ptc7 protein that have distinct and opposing effects on CoQ_6 biosynthesis. This change in the ratio of the isoforms is concomitant with an increase in CoQ_6 levels in the cell, preparing for the transition from a largely fermentative to a respiratory mode of metabolism.

Previous studies have presented contradictory evidence regarding the involvement of *PTC7* in CoQ_6 biosynthesis. Ptc7 is required for the dephosphorylation of Coq7, thus transitioning Coq7 to its "active" form, which is able to catalyze the penultimate step of the CoQ_6 pathway. This led to the prediction that the *ptc7*Δ strain would demonstrate decreased CoQ_6 synthesis, as assayed by quantification of lipids from purified mitochondria (11). Surprisingly, although Ptc7 supports general respiratory function, the absence of *PTC7* does not lead to a deficiency in CoQ_6 levels, as assayed in lipid extracts of whole cells (12) (Fig. 9*A*). The studies here help to resolve this apparent contradiction. Studies with the *ptc7*Δ cells fail to address the opposing roles that the two Ptc7 isoforms have in the cell under WT conditions. Only cells with the capacity to express both $Ptc7_s$ and $Ptc7_{ns}$ can accurately reflect the full extent of Ptc7 function. We demonstrate that exclusive expression of $Ptc7_{ns}$ has a significant repressive effect on CoQ_6 biosynthesis (Fig. 9, *A* and *D*). Notably, the rates of conversions from precursors in the pathway to the final product remained unchanged, indicating down-regulation of the entire pathway (Fig. 10, *C* and *D*). Consistent with this, we observe down-regulation of almost all of the components of the CoQ_6 biosynthetic complex upon exclusive expression of $Ptc7_{ns}$ (Fig. 9*F*). The mechanism by which $Ptc7_{ns}$ affects RNA expression is as yet unknown, and investigations to understand the same are ongoing.

PTC7 is not the only known example of a gene in *S. cerevisiae* encoding functional proteins from both the nonspliced pre-mRNA as well as the "mature" spliced mRNA (10). We recently reported translation of unspliced *GCR1* pre-mRNA leading to a functional Gcr1 protein, although in this case, translation starts from within the retained intron (7). Whereas the read-through nature of the intron is conserved across most *Saccharomycetaceae* species, the intron is excised in the same species (analysis of publicly available RNA-seq data sets; data not shown), rendering it likely that both forms of the protein are necessary and functional. This is illustrated in the case of *Tetrapisispora blattae*, which, like *S. cerevisiae*, underwent a whole genome duplication event; but unlike *S. cerevisiae*, which lost the duplications of most of its genes, *T. blattae* retains two copies of the *PTC7* gene. Interestingly, the two *PTC7* genes in *T. blattae* subfunctionalized into a gene that encodes a mitochondrial PP2C ($Ptc7_b$, from a spliced transcript of *PTC7b* con-

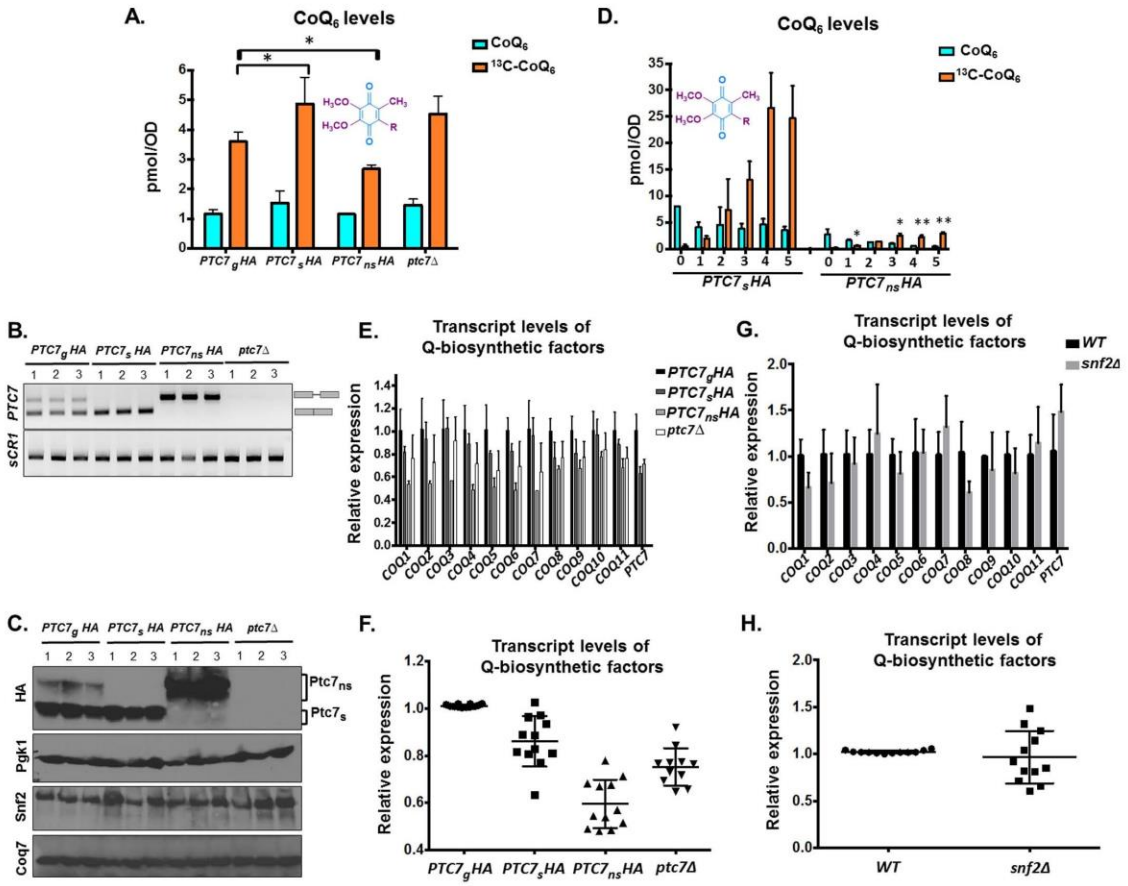

Figure 9. Ptc7 isoforms have differing and opposing effects on CoQ_6 synthesis. *A*, levels of steady-state CoQ_6 (^{12}C-CoQ_6, *blue bars*) and *de novo* synthesized CoQ_6 ($^{13}C_6$-CoQ_6, *orange bars*) in strains expressing distinct Ptc7 isoforms (*PTC7$_g$HA*, genomic, both isoforms expressed; *PTC7$_s$HA*, exclusively expresses the isoform from spliced mRNA; *PTC7$_{ns}$HA*, exclusively expresses the isoform from nonspliced pre-mRNA) and *ptc7*Δ. Labeling with $^{13}C_6$-4HB was allowed to proceed for 3 h. *Error bars*, S.D. of $n = 3$ biological replicates (unpaired Student's *t* test; *, $p < 0.05$). *B*, expression and splicing of *PTC7* for samples corresponding to *A*. PCR products representing the spliced and nonspliced forms are indicated. *C*, steady-state levels of HA-tagged Ptc7 proteins were determined by immunoblotting for samples corresponding to *A*. Proteins derived from the nonspliced and spliced forms of the *PTC7* RNA are denoted as Ptc7$_{ns}$ and Ptc7$_s$, respectively. Pgk1 (phosphoglycerate kinase 1) served as a loading control. Immunoblots for Snf2 and Coq7 are also included. *D*, levels of steady-state (^{12}C-CoQ_6, *blue bars*) and *de novo* synthesized ($^{13}C_6$-CoQ_6, *orange bars*) CoQ_6 in *PTC7$_s$HA* and *PTC7$_{ns}$HA* yeast cells were determined at the designated hours after labeling with $^{13}C_6$-4HB. *Error bars*, S.D. of $n = 3$ biological replicates (unpaired Student's *t* test between corresponding bars for *PTC7$_s$HA* and *PTC7$_{ns}$HA*; *, $p < 0.05$; **, $p < 0.005$). *E*, RT-qPCR measurement of *COQ1–COQ11* and *PTC7* transcript levels between strains expressing different Ptc7 isoforms (*PTC7$_g$HA*, genomic, both isoforms expressed; *PTC7$_s$HA*, exclusively expresses the isoform from spliced mRNA; *PTC7$_{ns}$HA*, exclusively expresses the isoform from nonspliced pre-mRNA) and *ptc7*Δ. Shown is the mean of three biological replicates. *Error bars*, S.D. *F*, summary analysis of transcript levels of Q-biosynthetic factors from *E*. *G*, RT-qPCR measurement of *COQ1-COQ11* and *PTC7* transcript levels between WT and *snf2*Δ yeast. Shown is the mean of three biological replicates. *Error bars*, S.D. *H*, summary analysis of transcript levels of Q-biosynthetic factors from *G*.

taining a stop codon within its intron) and a second gene encoding a PP2C predicted to localize to the nuclear envelope (Ptc7$_a$, from an nonspliced transcript of *PTC7a* (32). This conservation further suggests that both protein isoforms derived from the *PTC7* transcript in *S. cerevisiae* are functional. Cells lacking Ptc7$_{ns}$ show increased sensitivity to latrunculin A treatment, compared with strains expressing both isoforms of Ptc7 or lacking Ptc7$_s$ (10). Such sensitivity might suggest a distinct role for Ptc7$_{ns}$ in actin filament formation.

It is noteworthy that nuclear roles for numerous metabolic enzymes have been described previously. The ability of metabolic enzymes to "moonlight" in the nucleus, affecting gene regulation at various steps, appears to be crucial for the ability of cells to sense and adapt to their potentially distinct nutrient environments (33). Numerous mitochondrial enzymes, such as succinate dehydrogenase, fumarase, aconitase, and malate dehydrogenase (all components of the Krebs cycle), have been shown to have significant nuclear roles in the regulation of gene expression (34–38). In some of these cases, enzymatic activity of these enzymes has been shown to be crucial to their nuclear roles (39). This precedence, combined with the evolutionarily conserved presence of an isoform of Ptc7 in the nuclear membrane, raises the possibility that a nucleus-localized phosphatase is crucial to regulation of components of the CoQ_6 biosyn-

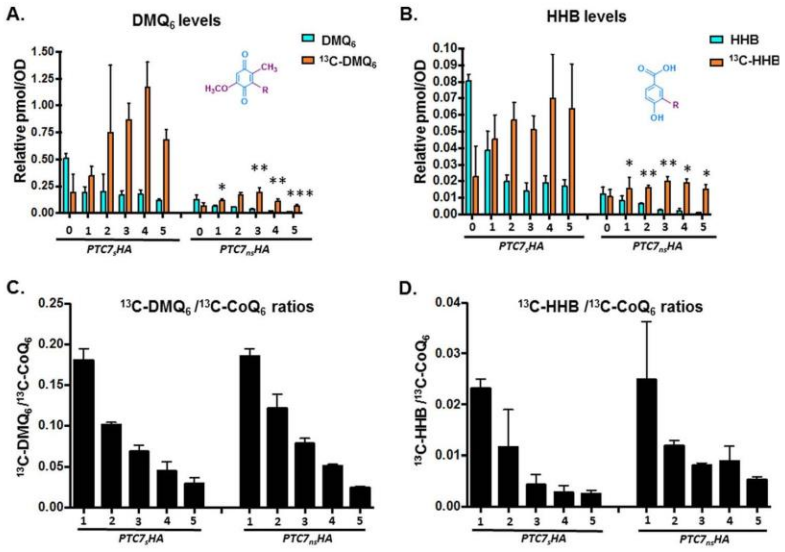

Figure 10. Exclusive expression of Ptc7 isoforms dramatically alters levels of CoQ_6 biosynthetic pathway intermediates DMQ_6 and HHB, yet overall conversion efficiency between both isoforms is comparable. *A*, levels of steady-state DMQ_6 (^{12}C-DMQ_6, *blue bars*) and *de novo* synthesized DMQ_6 ($^{13}C_6$-DMQ_6, *orange bars*) in *PTC7$_s$HA* and *PTC7$_{ns}$HA* yeast cells were determined at the designated hours after labeling with $^{13}C_6$-4HB. *Error bars*, S.D. of $n = 3$ biological replicates (unpaired Student's *t* test between *corresponding bars* for *PTC7$_s$HA* and *PTC7$_{ns}$HA*; *, $p < 0.05$; **, $p < 0.005$; ***, $p < 0.0005$). *B*, levels of steady-state HHB (^{12}C-HHB, *blue bars*) and *de novo* synthesized HHB ($^{13}C_6$-HHB, *orange bars*) in *PTC7$_s$HA* and *PTC7$_{ns}$HA* yeast cells were determined at the designated hours after labeling with $^{13}C_6$-4HB. *Error bars*, S.D. of $n = 3$ biological replicates (unpaired Student's *t* test between *corresponding bars* for *PTC7$_s$HA* and *PTC7$_{ns}$HA*; *, $p < 0.05$; **, $p < 0.005$). *C*, ratio of $^{13}C_6$-DMQ_6/$^{13}C_6$-CoQ_6 in *PTC7$_s$HA* and *PTC7$_{ns}$HA* yeast cells were determined at the designated hours after labeling with $^{13}C_6$-4HB. Ratios were derived from levels of $^{13}C_6$-CoQ_6, as shown in Fig. 7*D*. *Error bars*, S.D. of $n = 3$ biological replicates. The 0-h time point is excluded, because the ratio is not indicative of pathway conversion. *D*, ratio of $^{13}C_6$-HHB/$^{13}C_6$-CoQ_6 in *PTC7$_s$HA* and *PTC7$_{ns}$HA* yeast cells were determined at the designated hours after labeling with $^{13}C_6$-4HB. Ratios were derived from levels of $^{13}C_6$-CoQ_6, as shown in Fig. 7*D*. *Error bars*, S.D. of $n = 3$ biological replicates. The 0-h time point is excluded, because the ratio is not indicative of pathway conversion.

thetic pathway. Intriguingly, CLK-1 and COQ7, the *C. elegans* and human homologs of Coq7, which is a target for Ptc7 in *S. cerevisiae* (11), have been demonstrated to localize to the nucleus and are postulated to have roles independent of CoQ biosynthesis (40). COQ7 has also been shown to associate with chromatin in HeLa cells (40), although recently this has been attributed to a transformed cell phenomenon (41). Whereas nuclear localization of Coq7 in *S. cerevisiae* has not been demonstrated, we suggest a potential role in nuclear gene regulation for Ptc7 via phosphatase activity on Coq7 or other unidentified targets, including conventionally nuclear and other "moonlighting" mitochondrial enzymes.

It is also possible that Ptc7 has a substrate other than Coq7 that affects expression of the CoQ_6-synthome. In fact, a recent study identified with high confidence numerous differentially phosphorylated proteins in a *ptc7*Δ strain (12). Notably, this proteomic analysis does not distinguish between the potential effects of the two Ptc7 isoforms globally. In fact, rescue using plasmid-based expression of *PTC7* (full-length) does not restore dephosphorylation levels for a number of nuclear proteins, although the increased phosphorylation of mitochondrial proteins upon deletion of *PTC7* is almost completely reversed by exogenous expression of Ptc7 (12). Furthermore, it is possible that the mitochondrial role for $Ptc7_s$ is in fact covered by multiple redundancies. Ptc5 and Ptc6, two other PP2C protein phosphatases, also localize to the mitochondrial membrane, and *PTC5* demonstrates a negative genetic interaction with *PTC7*, indicating the possibility of overlapping functions (11, 31).

Interestingly, the effect of Snf2 deletion on CoQ_6 biosynthesis does not perfectly mirror the exclusive expression of $Ptc7_s$. We postulate that this is partially due to the Snf2 affecting the flux of the entire CoQ_6 biosynthetic pathway, as demonstrated by the increased conversion of early precursors. Whereas deletion of Snf2 does not, on average, change the expression of the components of the CoQ_6-synthome (Fig. 9, *G* and *H*), it is possible the Snf2 may have other effects of CoQ_6 flux. We are exploring these possibilities.

Intriguingly, although the absence of Snf2 enhances levels of CoQ_6, yeast strains lacking Snf2 have a severe growth defect on non-fermentable carbon sources, such as glycerol or acetate (26) (Fig. 1*E*). However, Snf2 protein is undetectable by immunoblotting during growth in medium containing glycerol or acetate as the only carbon source (data not shown). This leads us to hypothesize that before Snf2 protein is down-regulated in response to glucose depletion, it is required for the transition from a fermentative metabolic state to one that is predominantly respiratory in nature. The molecular details of the requirement for Snf2 in this transition are the subject of ongoing investigation. However, it is probably at least in part due to its reported role in the activation (de-repression) of genes whose transcription had previously been subject to glucose-mediated catabolite repression. This activation occurs once the glucose has been depleted or the yeast have been shifted to a

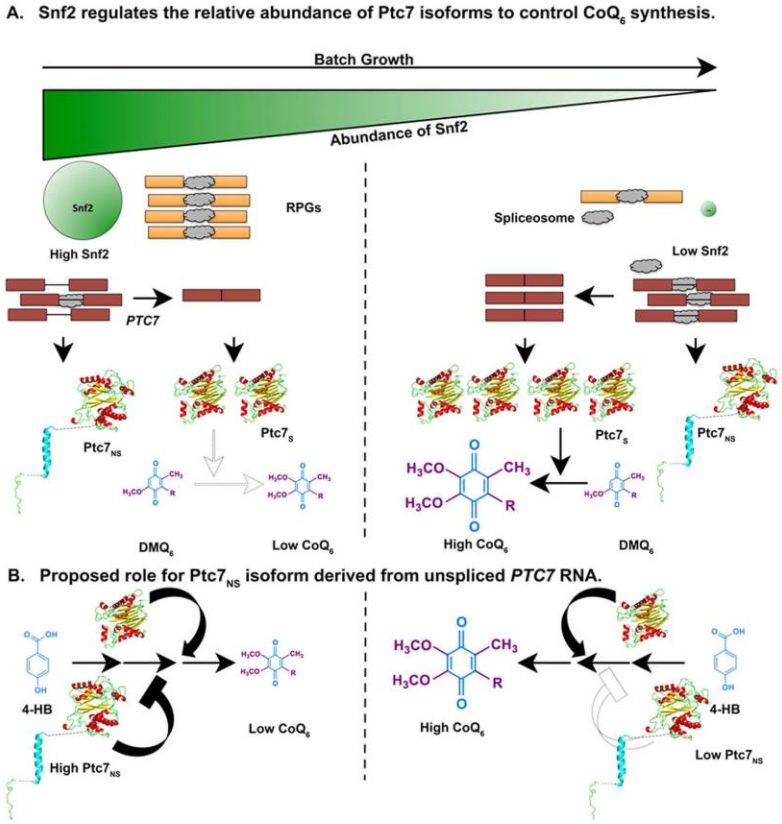

Figure 11. Model for a novel role for Snf2 in respiration, and in the transition from a primarily fermentative mode of metabolism to a primarily respiratory mode of metabolism. *A*, during *S. cerevisiae* batch growth, the abundance of Snf2 decreases in conjunction with depletion of nutrients in the medium. RPGs under the control of Snf2 are down-regulated, allowing redistribution of spliceosomes to other poorly spliced transcripts. Splicing of the *PTC7* transcript increases, enhancing the ratio of $Ptc7_s/Ptc7_{ns}$ and overall levels of $Ptc7_s$. These changes in Ptc7 isoform levels lead to increased conversion of DMQ_6 and increased synthesis of CoQ_6. The *darker arrow* represents a greater effect or reaction conversion, whereas a *lighter arrow* represents a smaller effect or reaction conversion. *B*, $Ptc7_{ns}$ has a repressive effect on CoQ_6 biosynthesis. CoQ_6 levels are low or high, depending on the levels of the $Ptc7_{ns}$ isoform relative to $Ptc7_s$. Similar to *A*, *darker arrows* and *bars* denote a larger effect, whereas *lighter arrows* and *bars* denote a smaller effect.

different, non-fermentable carbon source (26). We postulate that once the gene expression profile required for adaptation to the new nutrient environment has been initiated and/or established, the requirement for Snf2 is relieved, and in fact, the down-regulation of Snf2 enhances splicing of *PTC7*. This transient requirement for Snf2 bears striking similarities to a previous report detailing the role of Snf2 in reversing Ume6-mediated repression at certain meiotic genes early in meiosis, before it is itself down-regulated to enable splicing of meiotic transcripts (6).

This work reveals a mechanism by which SWI/SNF acts as a nexus point in the fermentation–respiratory transition in *S. cerevisiae*. We also demonstrate opposing effects of isoforms of a single gene, *PTC7*, on the process of CoQ_6 biosynthesis, via distinct mechanisms. Numerous aspects of these mechanisms remain to be studied, as well as their potential roles in the gene regulation response to other physiological conditions that yeast might experience.

Experimental procedures

Yeast strains and culture conditions

The yeast strains used in this study are listed in Table 1. All strains except W303Δcoq2 are derived from the BY background. Yeast strains were grown in YPD (1% yeast extract, 2% peptone, 2% dextrose) medium at 30 °C. Snf2 and Ptc7 null strains were maintained with a backup expression plasmid (pRS316 backbone harboring either *SNF2* or *PTC7*). The plasmid was shuffled out by growth on 5-fluoroorotic acid before using the strains in experiments. Strains with tagged isoforms of Ptc7 were a kind gift from Dr. Ron Davis (10). These strains were back-crossed against WT or *snf2*Δ strains, and daughter strains used for this study are listed in Table 1. The *snf2*Δ strain was observed to spontaneously mutate if grown on YPD for longer than 7–8 days, acquiring suppressor mutations that made it difficult to distinguish from WT. Hence, for all experiments with *snf2*Δ, the plasmid contain-

Table 1
Genotype and source of yeast strains

Strain number	Name	Genotype	Source/reference
TJY6724	WT	*MATa his3Δ leu2Δ LYS2 met15Δ ura3Δ*	Ref. 6
TJY6727	*snf2Δ*	*MATα his3Δ leu2Δ ura3Δ snf2Δ::NatMX*	Ref. 6
TJY7114	*PTC7$_s$HA*	*MATa his3Δ leu2Δ ura3Δ PTC7$_s$HA:KanMX*	This study
TJY7115	*snf2ΔPTC7$_s$HA*	*MATa his3Δ leu2Δ ura3Δ snf2Δ::NatMX PTC7$_s$HA:KanMX*	This study
W303Δ*coq2*	*coq2Δ*	*MATa ade2-1 his3-1,15 leu2-3,112 trp1-1 ura3-1 coq2::HIS3*	Ref. 47
TJY7116	*PTC7$_s$HA*	*MATa his3Δ leu2Δ ura3Δ PTC7$_s$HA:KanMX*	This study
TJY7118	*PTC7$_{ns}$HA*	*MATa his3Δ leu2Δ ura3Δ PTC7$_{ns}$HA:KanMX*	This study
TJY7142	*ptc7Δ*	*MATa his3Δ leu2Δ ura3Δ ptc7Δ:KanMX*	This study
BY4741Δ*coq9*	*coq9Δ*	*MATα his3Δ0 leu2Δ0 met15Δ0 ura3Δ0 coq9::KANMX4*	Ref. 48

ing *SNF2* was shuffled out prior to each experiment, allowing a fresh *snf2Δ* strain with each experiment, to avoid these suppressor mutants. We found that this was absolutely instrumental to observe the proper phenotype and behavior of the *snf2Δ* strain.

RNA-sequencing analyses

The RNA-sequencing data reported in this study were generated previously (6). Briefly, RNA sequencing libraries were prepared using the Illumina Truseq® V3 kit and ribosomal RNA depletion (Ribo-Zero, Illumina). Single-end, 50-nucleotide sequence reads (HiSeq 2000) were aligned to SacCer3 and spliced transcripts from the Ares Lab Yeast Intron Database version 3 (42) in a single step using STAR (43). Only the highest scoring alignments for each read were kept, allowing for at most a single tie. Reads/kb/million were computed for each gene by dividing the total number of reads that aligned entirely within the gene's exon boundaries by the gene's total exon length in kilobase pairs per million mapped reads. Reads within ICGs were categorized as exonic, spliced, or unspliced. Exonic reads map entirely within an exon, as defined by the Ares Lab Yeast Intron Database. Introns with annotated small nucleolar RNAs within the defined intron boundaries were disregarded in this analysis. Spliced reads are those that align with a gap that corresponds to an annotated intron, and unspliced reads map partially within an exon and partially within an intron with no gap. Spliced and unspliced read counts were normalized by dividing total spliced counts by the number of potential unique alignment positions that contribute to the total. For spliced reads, this is read length minus one for every intron. For unspliced read counts, this is the length of the intron plus the read length minus one. Splicing efficiency for each intron was calculated as normalized spliced counts divided by the sum of the normalized spliced and normalized unspliced counts. Changes in splicing efficiency were calculated as percentage difference over WT efficiency and plotted against expression levels (reads/kb/million) in WT. Data are available under GEO accession number GSE94404, and detailed methods were described previously (6).

RT-PCR and real-time PCR analysis

RNA was isolated from a 5-ml aliquot of cell culture corresponding to time points described in each experiment. After DNase treatment (Roche Applied Science), equal quantities of total RNA from each sample were used to make cDNA using a cDNA synthesis kit (Fermentas). To detect *PTC7* splicing isoforms, primers flanking the intronic sequences were used for PCR using 1 μl of cDNA diluted 1:20. PCR products were then separated on a 2% agarose gel and imaged. RT-qPCR was done in a 10-μl reaction volume with gene-specific primers using 1 μl of cDNA diluted 1:20 using Perfecta SYBR Green Fastmix (Quanta Biosciences) and a CFX96 Touch System (Bio-Rad). All samples were analyzed in triplicate for each independent experiment. RT-qPCR was also performed for the *scR1* (cytoplasmic signal recognition particle RNA subunit) RNA from each cDNA sample. Gene expression analysis was done by $2^{-\Delta Ct}$ methods using *scR1* as a reference. -Fold expression of mRNA was measured compared with WT by $2^{-\Delta\Delta Ct}$ methods (44).

Immunoblots

Protein was isolated from cell pellets with FA-1 lysis buffer (50 mM HEPES, pH 7.5, 150 mM NaCl, 1 mM EDTA, 1% Triton X-100, 0.1% sodium deoxycholate, 1 mM PMSF, and protease inhibitors) with bead beating. The buffer was supplemented with protease inhibitor mixture tablet (Roche Applied Science). Total protein was resolved by SDS-PAGE. The gel was transferred to PVDF membrane, and proteins were detected with the following antibodies at the stated dilutions: anti-SNF2 antibody (yN-20, Santa Cruz Biotechnology) at a 1:200 dilution in 2% milk, anti-HA antibody (901514, BioLegend) at a 1:2000 dilution in 5% milk, anti-Pgk1 antibody (459250, Invitrogen) at a 1:3000 dilution in 5% milk, or anti-Coq7 antibody (described previously (16) at a 1:2000 dilution in 3% milk. Signal was detected with enhanced chemiluminescence (Thermo Scientific) as described by the manufacturer.

Metabolic labeling of CoQ_6 with $^{13}C_6$-labeled precursors

Yeast strains were grown overnight in 25 ml of YPD in a shaking incubator (30 °C, 250 rpm) and diluted to an A_{600} of 0.1 in 60 ml of fresh YPD the next morning. The cultures were incubated as before to an A_{600} of 0.5 (midlog phase) and subsequently treated with $^{13}C_6$-4HB at 10 μg/ml (600 μg total) or ethanol vehicle control (0.015%, v/v). At designated time periods, cells were harvested by centrifugation at 3000 $\times$ *g* for 5 min, from 50-ml aliquots (used for lipid extraction) or 10-ml aliquots (used for RNA and protein analysis). Cell pellets were stored at −20 °C.

Analysis of CoQ_6 and CoQ_6 intermediates

Lipid extraction of cell pellets was conducted as described (18) with methanol and petroleum ether and CoQ_4 as the internal standard. Lipid measurements were performed by HPLC-

MS/MS and normalized to total OD. Prior to mass spectrometry analysis, all samples were treated with 1.0 mg/ml benzoquinone to oxidize hydroquinones to quinones. Mass spectrometry analyses utilized a 4000 QTRAP linear MS/MS spectrometer (Applied Biosystems), and data were acquired and analyzed using Analyst version 1.4.2 and 1.5.2 software (Applied Biosystems). Separation of lipid quinones was performed with a binary HPLC delivery system and a Luna 5μ phenyl-hexyl column (100 $\times$ 4.6 mm, 5 μm; Phenomenex). The mobile phase consisted of a 95:5 methanol/isopropyl alcohol solution with 2.5 mM ammonium formate as solution A and a 100% isopropyl alcohol solution with 2.5 mM ammonium formate as solution B. The percentage of solution B was increased linearly from 0 to 5% over 6 min, whereby the flow rate was increased from 600 to 800 μl. Initial flow rate and mobile phase conditions were changed back to initial phase conditions linearly over 3.5 min. Each sample was analyzed using multiple-reaction monitoring mode. The following precursor-to-product ion transitions were detected as well as the +17 *m/z* ammoniated adducts for each of the metabolic products: $^{13}C_6$-HHB *m/z* 553.4/157.0 (ammoniated: 570.4/157.0), ^{12}C-HHB *m/z* 547.4/151.0 (ammoniated: 564.4/151.0), $^{13}C_6$-DMQ_6 *m/z* 567.6/173.0 (ammoniated: 584.6/173.0), ^{12}C-DMQ_6 *m/z* 561.6/167.0 (ammoniated: 578.6/167.0), $^{13}C_6$-CoQ_6 *m/z* 597.4/203.1 (ammoniated: 614.4/203.1), ^{12}C-CoQ_6 *m/z* 591.4/197.1 (ammoniated: 608.4/197.1), and ^{12}C-CoQ_4 *m/z* 455.4/197.0 (ammoniated: 472.4/197.0).

Plate dilution assays

Strains were grown overnight in 5 ml of YPD and diluted to an A_{600} of 0.2 in sterile PBS. A 5-fold serial dilution in PBS was performed, after which 2 μl of each dilution (1$\times$, 5$\times$, 25$\times$, 125$\times$, and 625$\times$) were spotted onto the designated carbon sources. The final A_{600} of the aforementioned dilution series are 0.2, 0.04, 0.008, 0.0016, and 0.00032, respectively.

PHYRE homology modeling

Phyre2 is a modeling program designed to analyze protein structure, function, and mutations (45). It is used to analyze the primary sequence of a protein and, with homology detection methods, constructs a structure that compares the protein of interest with other proteins (or motifs of proteins) with known structure. In regard to Ptc7, the full nonspliced version of the protein ($Ptc7_{ns}$), which is composed of 374 amino acids and retains its 31-amino acid intron (amino acids 19–50), was analyzed. The resulting structure and alignment coverage contained 86% of residues modeled at >90% confidence, with 14% of residues modeled *ab initio*. Additionally, the spliced isoform of Ptc7 ($Ptc7_s$), which is localized and processed in the mitochondria, comprised of 305 amino acids, resulting from the removal of the 31-amino acid intron and the excision of the predicted mitochondrial targeting sequence (the 38 N-terminal amino acids of $Ptc7_s$) (46), was also modeled using the PHYRE2 intensive modeling mode. The resulting structure and alignment coverage contains 85% of residues modeled at >90% confidence, with 15% of residues modeled *ab initio*.

Author contributions—A. M. A. and S. V. contributed equally to this work (both conducted the majority of the experiments, analyzed the results, and wrote the paper together). A. N. and M. C. B. assisted A. M. A. in conducting experiments; A. N. assisted A. M. A. in analyzing mass spectrometry results. A. R. G. and L. N. assisted S. V. in experiments, with A. R. G. also having assisted in the background research relating to PTC7 differential splicing in the snf2Δ strain shown in Fig. 1*A*. S. D. aligned the RNA-sequencing data and calculated splicing efficiencies. M. C. B. and L. N. thoroughly read and edited the working draft of the paper. C. F. C. and T. L. J. oversaw all details related to the project and provided guidance on experiments, data analysis, and the writing of this paper.

Acknowledgments—We thank Dr. James Bowie (UCLA) for advice and guidance in generating the PHYRE models and in the depiction of the spliced and nonspliced versions of Ptc7. We acknowledge the UCLA Molecular Instrumentation Core proteomics facility for the use of the QTRAP4000. We thank the laboratory of Dr. Ronald W. Davis (Stanford) for generously providing the Ptc7 spliced and nonspliced isoforms.

References

1. Naftelberg, S., Schor, I. E., Ast, G., and Kornblihtt, A. R. (2015) Regulation of alternative splicing through coupling with transcription and chromatin structure. *Annu. Rev. Biochem.* **84,** 165–198
2. Johnson, T. L., and Vilardell, J. (2012) Regulated pre-mRNA splicing: the ghostwriter of the eukaryotic genome. *Biochim. Biophys. Acta* **1819,** 538–545
3. Pleiss, J. A., Whitworth, G. B., Bergkessel, M., and Guthrie, C. (2007) Rapid, transcript-specific changes in splicing in response to environmental stress. *Mol. Cell* **27,** 928–937
4. Ares, M., Jr., Grate, L., and Pauling, M. H. (1999) An handful of intron-containing genes produces the lion's share of yeast mRNA. *RNA* **5,** 1138–1139
5. Munding, E. M., Shiue, L., Katzman, S., Donohue, J. P., and Ares, M., Jr. (2013) Competition between pre-mRNAs for the splicing machinery drives global regulation of splicing. *Mol. Cell* **51,** 338–348
6. Venkataramanan, S., Douglass, S., Galivanche, A. R., and Johnson, T. L. (2017) The chromatin remodeling complex Swi/Snf regulates splicing of meiotic transcripts in *Saccharomyces cerevisiae*. *Nucleic Acids Res.* 10.1093/nar/gkx373
7. Hossain, M. A., Claggett, J. M., Edwards, S. R., Shi, A., Pennebaker, S. L., Cheng, M. Y., Hasty, J., and Johnson, T. L. (2016) Posttranscriptional regulation of Gcr1 expression and activity is crucial for metabolic adjustment in response to glucose availability. *Mol. Cell* **62,** 346–358
8. Hossain, M. A., Rodriguez, C. M., and Johnson, T. L. (2011) Key features of the two-intron *Saccharomyces cerevisiae* gene *SUS1* contribute to its alternative splicing. *Nucleic Acids Res.* **39,** 8612–8627
9. Jiang, L., Whiteway, M., Ramos, C. W., Rodriguez-Medina, J. R., and Shen, S.-H. (2002) The YHR076W gene encodes a type 2C protein phosphatase and represents the seventh PP2C gene in budding yeast. *FEBS Lett.* **527,** 323–325
10. Juneau, K., Nislow, C., and Davis, R. W. (2009) Alternative splicing of *PTC7* in *Saccharomyces cerevisiae* determines protein localization. *Genetics* **183,** 185–194
11. Martín-Montalvo, A., González-Mariscal, I., Pomares-Viciana, T., Padilla-López, S., Ballesteros, M., Vazquez-Fonseca, L., Gandolfo, P., Brautigan, D. L., Navas, P., and Santos-Ocaña, C. (2013) The phosphatase Ptc7 induces coenzyme Q biosynthesis by activating the hydroxylase Coq7 in yeast. *J. Biol. Chem.* **288,** 28126–28137
12. Guo, X., Niemi, N. M., Hutchins, P. D., Condon, S. G., Jochem, A., Ulbrich, A., Higbee, A. J., Russell, J. D., Senes, A., Coon, J. J., and Pagliarini, D. J. (2017) Ptc7p dephosphorylates select mitochondrial proteins to enhance metabolic function. *Cell Rep.* **18,** 307–313

13. Turunen, M., Olsson, J., and Dallner, G. (2004) Metabolism and function of coenzyme Q. *Biochim. Biophys. Acta* **1660,** 171–199
14. Doimo, M., Desbats, M. A., Cerqua, C., Cassina, M., Trevisson, E., and Salviati, L. (2014) Genetics of coenzyme Q10 deficiency. *Mol. Syndromol.* **5,** 156–162
15. Quinzii, C. M., Emmanuele, V., and Hirano, M. (2014) Clinical presentations of coenzyme Q10 deficiency syndrome. *Mol. Syndromol.* **5,** 141–146
16. Tran, U. C., and Clarke, C. F. (2007) Endogenous synthesis of coenzyme Q in eukaryotes. *Mitochondrion* **7,** S62–S71
17. González-Mariscal, I., García-Testón, E., Padilla, S., Martín-Montalvo, A., Pomares Viciana, T., Vazquez-Fonseca, L., Gandolfo Domínguez, P., and Santos-Ocaña, C. (2014) The regulation of coenzyme Q biosynthesis in eukaryotic cells: all that yeast can tell us. *Mol. Syndromol.* **5,** 107–118
18. Allan, C. M., Awad, A. M., Johnson, J. S., Shirasaki, D. I., Wang, C., Blaby-Haas, C. E., Merchant, S. S., Loo, J. A., and Clarke, C. F. (2015) Identification of Coq11, a new coenzyme Q biosynthetic protein in the CoQ-synthome in *Saccharomyces cerevisiae*. *J. Biol. Chem.* **290,** 7517–7534
19. Padilla, S., Jonassen, T., Jiménez-Hidalgo, M. A., Fernández-Ayala, D. J., López-Lluch, G., Marbois, B., Navas, P., Clarke, C. F., and Santos-Ocaña, C. (2004) Demethoxy-Q, an intermediate of coenzyme Q biosynthesis, fails to support respiration in Saccharomyces cerevisiae and lacks antioxidant activity. *J. Biol. Chem.* **279,** 25995–26004
20. Padilla, S., Tran, U. C., Jiménez-Hidalgo, M., López-Martín, J. M., Martín-Montalvo, A., Clarke, C. F., Navas, P., and Santos-Ocaña, C. (2009) Hydroxylation of demethoxy-Q6 constitutes a control point in yeast coenzyme Q6 biosynthesis. *Cell Mol. Life Sci.* **66,** 173–186
21. Whitehouse, I., Flaus, A., Cairns, B. R., White, M. F., Workman, J. L., and Owen-Hughes, T. (1999) Nucleosome mobilization catalysed by the yeast SWI/SNF complex. *Nature* **400,** 784–787
22. Liu, X., Li, M., Xia, X., Li, X., and Chen, Z. (2017) Mechanism of chromatin remodelling revealed by the Snf2-nucleosome structure. *Nature* **544,** 440–445
23. Dutta, A., Gogol, M., Kim, J. H., Smolle, M., Venkatesh, S., Gilmore, J., Florens, L., Washburn, M. P., and Workman, J. L. (2014) Swi/Snf dynamics on stress-responsive genes is governed by competitive bromodomain interactions. *Genes Dev.* **28,** 2314–2330
24. Dutta, A., Sardiu, M., Gogol, M., Gilmore, J., Zhang, D., Florens, L., Abmayr, S. M., Washburn, M. P., and Workman, J. L. (2017) Composition and function of mutant Swi/Snf complexes. *Cell Rep.* **18,** 2124–2134
25. Gabunilas, J., and Chanfreau, G. (2016) Splicing-mediated autoregulation modulates Rpl22p expression in *Saccharomyces cerevisiae*. *PLoS Genet.* **12,** e1005999
26. Neigeborn, L., and Carlson, M. (1984) Genes affecting the regulation of SUC2 gene expression by glucose repression in *Saccharomyces cerevisiae*. *Genetics* **108,** 845–858
27. Martín-Montalvo, A., González-Mariscal, I., Padilla, S., Ballesteros, M., Brautigan, D. L., Navas, P., and Santos-Ocaña, C. (2011) Respiratory-induced coenzyme Q biosynthesis is regulated by a phosphorylation cycle of Cat5p/Coq7p. *Biochem. J.* **440,** 107–114
28. Martin, D. E., Soulard, A., and Hall, M. N. (2004) TOR regulates ribosomal protein gene expression via PKA and the Forkhead transcription factor FHL1. *Cell* **119,** 969–979
29. Wang, A., Mouser, J., Pitt, J., Promislow, D., and Kaeberlein, M. (2016) Rapamycin enhances survival in a *Drosophila* model of mitochondrial disease. *Oncotarget* **7,** 80131–80139
30. González-Mariscal, I., Martín-Montalvo, A., Ojeda-González, C., Rodríguez-Eguren, A., Gutiérrez-Ríos, P., Navas, P., and Santos-Ocaña, C. (2017) Balanced CoQ6 biosynthesis is required for lifespan and mitophagy in yeast. *Microb. Cell* **4,** 38–51
31. Sharmin, D., Sasano, Y., Sugiyama, M., and Harashima, S. (2014) Effects of deletion of different PP2C protein phosphatase genes on stress responses in *Saccharomyces cerevisiae*. *Yeast* **31,** 393–409
32. Marshall, A. N., Montealegre, M. C., Jiménez-Lopez, C., Lorenz, M. C., and van Hoof, A. (2013) Alternative splicing and subfunctionalization generates functional diversity in fungal proteomes. *PLoS Genet.* **9,** e1003376
33. Boukouris, A. E., Zervopoulos, S. D., and Michelakis, E. D. (2016) Metabolic enzymes moonlighting in the nucleus: metabolic regulation of gene transcription. *Trends Biochem. Sci.* **41,** 712–730
34. De, P., and Chatterjee, R. (1962) Evidence of nucleolar succinic dehydrogenase activity. *Exp. Cell Res.* **27,** 172–173
35. De, P., and Chatterjee, R. (1962) Nucleolar localization of succinic dehydrogenase in human malignant cells with MTT. *Experientia* **18,** 562
36. Yogev, O., Yogev, O., Singer, E., Shaulian, E., Goldberg, M., Fox, T. D., and Pines, O. (2010) Fumarase: a mitochondrial metabolic enzyme and a cytosolic/nuclear component of the DNA damage response. *PLoS Biol.* **8,** e1000328
37. Jung, S. J., Seo, Y., Lee, K. C., Lee, D., and Roe, J. H. (2015) Essential function of Aco2, a fusion protein of aconitase and mitochondrial ribosomal protein bL21, in mitochondrial translation in fission yeast. *FEBS Lett.* **589,** 822–828
38. Lee, S. M., Kim, J. H., Cho, E. J., and Youn, H. D. (2009) A nucleocytoplasmic malate dehydrogenase regulates p53 transcriptional activity in response to metabolic stress. *Cell Death Differ.* **16,** 738–748
39. McEwen, B. S., Allfrey, V. G., and Mirsky, A. E. (1963) Studies on energy-yielding reactions in thymus nuclei. *J. Biol. Chem.* **238,** 2571–2578
40. Monaghan, R. M., Barnes, R. G., Fisher, K., Andreou, T., Rooney, N., Poulin, G. B., and Whitmarsh, A. J. (2015) A nuclear role for the respiratory enzyme CLK-1 in regulating mitochondrial stress responses and longevity. *Nat Cell Biol.* **17,** 782–792
41. Liu, J. L., Yee, C., Wang, Y., and Hekimi, S. (2017) A single biochemical activity underlies the pleiotropy of the aging-related protein CLK-1. *Sci. Rep.* **7,** 859
42. Grate, L., and Ares, M., Jr. (2002) Searching yeast intron data at Ares lab Web site. *Methods Enzymol.* **350,** 380–392
43. Dobin, A., Davis, C. A., Schlesinger, F., Drenkow, J., Zaleski, C., Jha, S., Batut, P., Chaisson, M., and Gingeras, T. R. (2013) STAR: ultrafast universal RNA-seq aligner. *Bioinformatics* **29,** 15–21
44. Livak, K. J., and Schmittgen, T. D. (2001) Analysis of relative gene expression data using real-time quantitative PCR and the $2(-\Delta\Delta C(T))$ method. *Methods* **25,** 402–408
45. Kelley, L. A., Mezulis, S., Yates, C. M., Wass, M. N., and Sternberg, M. J. (2015) The Phyre2 web portal for protein modeling, prediction and analysis. *Nat. Protoc.* **10,** 845–858
46. Vögtle, F. N., Wortelkamp, S., Zahedi, R. P., Becker, D., Leidhold, C., Gevaert, K., Kellermann, J., Voos, W., Sickmann, A., Pfanner, N., and Meisinger, C. (2009) Global analysis of the mitochondrial N-proteome identifies a processing peptidase critical for protein stability. *Cell* **139,** 428–439
47. Ashby, M. N., Kutsunai, S. Y., Ackerman, S., Tzagoloff, A., and Edwards, P. A. (1992) COQ2 is a candidate for the structural gene encoding para-hydroxybenzoate:polyprenyltransferase. *J. Biol. Chem.* **267,** 4128–4136
48. Winzeler, E. A., Shoemaker, D. D., Astromoff, A., Liang, H., Anderson, K., Andre, B., Bangham, R., Benito, R., Boeke, J. D., Bussey, H., Chu, A. M., Connelly, C., Davis, K., Dietrich, F., Dow, S. W., *et al.* (1999) Functional characterization of the *S. cerevisiae* genome by gene deletion and parallel analysis. *Science* **285,** 901–906

Appendix II

Treatment with 2,4-dihydroxybenzoic acid prevents progression of FSGS and renal fibrosis in podocyte-specific Coq6 knockout mice

Author contributions: The author contributions are listed on page 142.

BASIC RESEARCH www.jasn.org

Treatment with 2,4-Dihydroxybenzoic Acid Prevents FSGS Progression and Renal Fibrosis in Podocyte-Specific *Coq6* Knockout Mice

Eugen Widmeier,[1,2] Merlin Airik,[3] Hannah Hugo,[1] David Schapiro,[1] Johannes Wedel,[1] Chandra C. Ghosh,[1] Makiko Nakayama,[1] Ronen Schneider,[1] Agape M. Awad,[4] Anish Nag,[4] Jang Cho,[1] Markus Schueler,[1] Catherine F. Clarke,[4] Rannar Airik,[3] and Friedhelm Hildebrandt[1]

Due to the number of contributing authors, the affiliations are listed at the end of this article.

ABSTRACT

Background Although studies have identified >55 genes as causing steroid-resistant nephrotic syndrome (SRNS) and localized its pathogenesis to glomerular podocytes, the disease mechanisms of SRNS remain largely enigmatic. We recently reported that individuals with mutations in COQ6, a coenzyme Q (also called CoQ_{10}, CoQ, or ubiquinone) biosynthesis pathway enzyme, develop SRNS with sensorineural deafness, and demonstrated the beneficial effect of CoQ for maintenace of kidney function.

Methods To study *COQ6* function in podocytes, we generated a podocyte-specific *Coq6* knockout mouse ($Coq6^{podKO}$) model and a transient siRNA-based *COQ6* knockdown in a human podocyte cell line. Mice were monitored for development of proteinuria and assessed for development of glomerular sclerosis. Using a podocyte migration assay, we compared motility in *COQ6* knockdown podocytes and control podocytes. We also randomly assigned 5-month-old $Coq6^{podKO}$ mice and controls to receive no treatment or 2,4-dihydroxybenzoic acid (2,4-diHB), an analog of a CoQ precursor molecule that is classified as a food additive by health authorities in Europe and the United States.

Results Abrogation of *Coq6* in mouse podocytes caused FSGS and proteinuria (>46-fold increases in albuminuria). *In vitro* studies revealed an impaired podocyte migration rate in *COQ6* knockdown human podocytes. Treating $Coq6^{podKO}$ mice or cells with 2,4-diHB prevented renal dysfunction and reversed podocyte migration rate impairment. Survival of $Coq6^{podKO}$ mice given 2,4diHB was comparable to that of control mice and significantly higher than that of untreated $Coq6^{podKO}$ mice, half of which died by 10 months of age.

Conclusions These findings reveal a potential novel treatment strategy for those cases of human nephrotic syndrome that are caused by a primary dysfunction in the CoQ_{10} biosynthesis pathway.

J Am Soc Nephrol 30: ●●●–●●●, 2019. doi: https://doi.org/10.1681/ASN.2018060625

Steroid-resistant nephrotic syndrome (SRNS) is a genetically heterogeneous, incurable renal disease that is the second most frequent cause of ESRD in the first two decades of life.[1] Mutations in >55 genes have been identified as causing SRNS,[2] which is clinically defined as nephrotic syndrome that is resistant to standard steroid treatment.[3,4] FSGS appears to be most frequent histological feature of SRNS.[5] Although the blood-filtrating component of the glomerulus consists of three cell types (endothelium, mesangium, and podocytes), identification of

Received June 18, 2018. Accepted December 29, 2018.

R.A. and F.H. contributed equally to this work.

Published online ahead of print. Publication date available at www.jasn.org.

Correspondence: Dr. Friedhelm Hildebrandt, Division of Nephrology, Boston Children's Hospital, EN561, 300 Longwood Avenue, Boston, MA 02115, or Dr. Rannar Airik, Department of Pediatrics, Children's Hospital of Pittsburgh of UPMC, 4401 Penn Avenue, Pittsburgh, PA 15224. E-mail: Friedhelm.Hildebrandt@childrens.harvard.edu or airikr@pitt.edu

>55 monogenic causes of SRNS[6] has revealed that podocytes are the primary cell type affected in SRNS.[7,8] Podocytes are specialized epithelial cells with a complex structure that have elaborate interdigitating foot processes, which form the slit diaphragm, a filtration barrier that consists of various cytoskeletal proteins. Maintenance of podocyte structure and function requires a highly regulated amount of energy, suggesting a high sensitivity to alteration of oxidative metabolism.[9,10] Gene identification has revealed that mutations in genes encoding cytoskeletal components[11–17] and components of the mitochondrial enzymes[18–24] cause SRNS. Coenzyme Q (CoQ), or ubiquinone, is a redox-active lipophilic molecule and a critical component of the mitochondrial inner membrane, where it functions in the electron transport chain by transferring electrons from complexes I and II to complex III.[25,26] CoQ acts also in nucleotide biosynthesis.[25] It displays a potent antioxidant activity in its reduced form, thus protecting cellular membranes from lipid peroxidation.[27,28] *De novo* CoQ production involves a complex but poorly understood biochemical pathway, depending on the activity of at least ten different enzymes. Recently, mutations in genes encoding CoQ biosynthesis pathway enzymes PDSS2, COQ2, COQ6, and ADCK4 have been reported to cause SRNS.[21–23,29] Discovery of monogenic forms of SRNS that represent primary mitochondrial diseases due to deficiency in CoQ_{10} levels has identified a subpopulation of patients with SRNS, who may benefit from treatment with dietary CoQ_{10} or its precursor analogs. In order to test this hypothesis, we generated a podocyte-specific knockout *Coq6* mouse line and a transient human podocyte knockdown cell line.

Significance Statement

Studies have identified mutations in >55 genes that cause steroid-resistant nephrotic syndrome (SRNS) and localized SRNS pathogenesis to podocytes. The authors previously reported that individuals with mutations in COQ6, a coenzyme Q (CoQ_{10}, CoQ, or ubiquinone) biosynthesis pathway enzyme, develop SRNS, and demonstrated that CoQ can reduce kidney dysfunction. In this study, they generated a podocyte-specific *Coq6* knockout mouse and showed that abrogating Coq6 in mouse podocytes caused FSGS and proteinuria. *In vitro* studies revealed an impaired podocyte migration rate in *COQ6* knockdown human podocytes. Treating affected mice or cells with 2,4-dihydroxybenzoic acid, an analog of a CoQ precursor molecule, prevented renal dysfunction and reversed migration rate impairment. This suggests a potential therapeutic approach for those cases of human nephrotic syndrome that result from a primary dysfunction in the CoQ_{10} biosynthesis pathway.

METHODS

Mouse Breeding and Maintenance

The *Nphs2.Cre*$^{+}$;*Coq6*$^{loxP/loxP}$ mouse model on C57BL/6 genetic background used in this study was generated from targeted *Coq6* ES cells obtained from the Knockout Mouse Project (EUCOMM) Repository. *Coq6* ES cells were injected into blastocysts to generate *Coq6*-transgenic mice. *Coq6*$^{+/loxP}$ mice were crossed with *Nphs2.Cre*$^{+}$ mice[30] and double heterozygous mice were backcrossed to generate podocyte-specific *Nphs2.Cre*$^{+}$;*Coq6*$^{loxP/loxP}$ knockout mice and littermate controls (Supplemental Figure 1A). Genotypes of animals were assessed by PCR (Supplemental Figure 1, B and C). Genotyping primer sequences are available upon request. *Nphs2.Cre*$^{+}$ mice were kindly provided by Dr. Holzman (University of Pennsylvania). The experimental protocol was reviewed and approved by the Animal Care Committee of the Boston Children's Hospital. All animals were housed in pathogen-free conditions with lights on at 7:00 AM and off at 7:00 PM. Mice had unlimited access to water and rodent chow. Animals were randomly assigned to experimental groups.

Urine Analysis

Urine was collected by housing the mice overnight (12 hours) in metabolic cages. All samples were frozen straight away and stored at −80°C. The samples were thawed on ice before performing the urine albumin and creatinine measurements. Urinary albumin and urinary creatinine were measured using a fluorometric albumin kit (Progen) and a colorimetric creatinine kit (R&D Systems) per manufacturer instructions. Proteinuria was expressed as milligrams of albumin per milligram of creatinine.

Histologic and Ultrastructural Analyses

Kidneys were harvested immediately after euthanasia and submerged in fixative—4% paraformaldehyde for histology, or 2.5% glutaraldehyde, 1.25% paraformaldehyde, and 0.03% picric acid in 0.1 M sodium cacodylate buffer (pH 7.4) for transmission electron microscopy (TEM) and scanning electron microscopy (SEM). Kidney serial sections were subjected to staining with hematoxylin and eosin, periodic acid–Schiff, Masson's trichrome, and Jones' methenamine silver following standard protocols, as well as histologic analyses. TEM and SEM were carried out using standard techniques.

Immunofluorescence Analyses

Mice kidneys were frozen in optimal cutting temperature compound and sectioned at 5 μm. These sections were fixed with PBS containing 4% paraformaldehyde, blocked with PBS containing 10% donkey serum and 1% BSA for 90 minutes at room temperature, then incubated with primary antibody at 4°C overnight. Sections were washed several times with PBS and incubated with fluorophore-conjugated secondary antibodies (Invitrogen) for 45 minutes at room temperature. A Leica SP5X confocal microscope was used for imaging. Image processing was done using Leica AF, ImageJ, and Adobe Photoshop CS6 software.

Isolation and Characterization of Mouse Glomeruli

Mouse glomeruli were isolated as described previously in a modified fashion due to perfusion.[31] Briefly, kidneys were harvested immediatly after euthanasia and perfused via renal artery with HBSS containing Dynabeads M-450, digested in Collagenase 1A and DNAse I solution, glomeruli were separated on DynaMag-2 magnet and glass-glass homogenized in

Pierce RIPA lysis buffer containing Halt Protease Inhibitor and Halt Phosphatase Inhibitor cocktails. Protein concentration was determined by DC Protein assay (Bio-Rad). An equal amount of protein was subjected to SDS–PAGE followed by western blotting. Band intensity was assessed with Image Lab software.

Mouse Drinking Water Supplementation with 2,4-Dihydroxybenzoic Acid

2,4-Dihydroxybenzoic acid (2,4-diHB) was administered to the mice in the drinking water at 25-mM concentration and changed twice a week. The treatment was started at 5 months of age and continued up to 10.5 months of age.

Cell Lines and Cell Culture

Experiments shown in this publication were performed in HEK293T cells and immortalized human podocytes. HEK293T cells were purchased from the ATCC biologic resource center. Human immortalized podocytes were a kind gift from Moin Saleem, University of Bristol, Bristol, UK, and were cultured as previously described.[32] HEK293T cells were maintained in DMEM supplemented with 10% FBS, 50 IU/ml penicillin, and 50 μg/ml streptomycin. Podocytes were maintained in RPMI plus GlutaMAX-I (Gibco) supplemented with 10% FBS, 50 IU/ml penicillin/50 μg/ml streptomycin, and 1% insulin-transferrin-selenium-X. Cell lines were tested for mycoplasma contamination on a biweekly basis.

RNAi Knockdown in Human Podocyte Cell Line

To achieve a transient knockdown human, podocytes were transfected with siRNA using RNAiMAX per manufacturer instructions.

Gene	siRNA targets	siRNA target sequence
COQ6 (NM_182476.2)	siRNA# 9	GGACUUAGGUUCCGUGAGC
	siRNA# 10	GAGCAAAGCCAUUCGCUAU
	siRNA# 11	CCACAGAGUCCAUCCGCUU
	siRNA# 12	CCUAAAGAAAGAUUACGUU

Isolation of Mitochondria

Mitochondria from HEK293T and human podocyte cell lines were isolated using a mitochondria isolation kit (ThermoFisher) per manufacturer instructions. Isolated mitochondria were lysed in Pierce RIPA lysis buffer containing Halt Protease Inhibitor and Halt Phosphatase Inhibitor cocktails. Equal amounts of isolated mitochondria were subjected to SDS–PAGE and western blotting. Band intensity was assessed with Image Lab software.

Podocyte Migration Assays

The podocyte migration assay using xCELLigence system was performed as previously described.[33] Briefly, real-time migration assays were performed using the xCELLigence system (Roche Applied Science) with CIM-plate 16 per manufacturer instructions. Immortalized human podocytes were transfected either with scrambled siRNA or with siRNAs targeting human *COQ6*. Thirty-six hours after transfection, 4×10^4 cells were seeded in serum-free medium in the upper chambers of the migration plate. The lower chambers were filled with medium containing 10% FBS as chemo attractant, or with serum-free medium as control. Indicated supplements were added to the media in the lower and upper chambers before the assay was started. Changes in impedance were analyzed using the RTCA software. Results were plotted as cell index (relative podocyte migration) versus time.

Gene Expression Analyses

Total cellular RNA from immortalized human podocytes was extracted using the RNeasy Plus kit following manufacturer instructions. Total RNA was quantified and an equal amount of 1 μg was subjected to RT-PCR using the iScript cDNA synthesis kit. Gene expression was assessed using TaqMan probes and normalized to expression of *GAPDH*.

Primary Antibodies

Target protein	Company	Catalogue #	Species
COQ6	Santa Cruz Biotechnology	sc-393932	Mouse
αTubulin	Abcam	ab15246	Rabbit
CoxIV	Cell Signaling	4850	Rabbit
βActin	Abcam	ab20272	Mouse
Podocin	Sigma Aldrich	P0372	Rabbit
Nephrin	Progen	GP-N2	Guinea pig
WT1	Cell Signaling	83535	Rabbit
Synaptopodin	ThermoFisher	PA5–56997	Rabbit
Nidogen	Novus Biologicals	NBP1–97701	Rat
Desmin	Cell Signaling	5332	Rabbit
αSMA	Cell Signaling	19245	Rabbit
CollV	Abcam	ab6586	Rabbit
58K	Abcam	ab27043	Mouse

Statistical Analyses

Statistical analyses were performed using Graph Pad Prism 7 software. Significance was determined at $P<0.05$. Particular tests performed in the experiments are indicated in the figure legends.

RESULTS

Podocyte-Specific Knockout of *Coq6* Leads to Increased Mortality in Adult Mice

To study the role of Coq6 in normal kidney function, we generated a transgenic *Coq6* ($Coq6^{tm1a}$) mouse line using embryonic stem cells from EUCOMM (Supplemental Figure 1A). Proper targeting of the *Coq6* gene was confirmed by gene-specific genotyping (Supplemental Figure 1B). Whole body loss of *Coq6* in $Coq6^{tm1a}$ mice was found by us to be not compatible with life. To circumvent $Coq6^{tm1a}$ embryonic lethality, we generated podocyte-specific *Coq6* knockout mice *Nphs2.* Cre^{+};$Coq6^{flox/flox}$ (hereafter referred to as $Coq6^{podKO}$), by

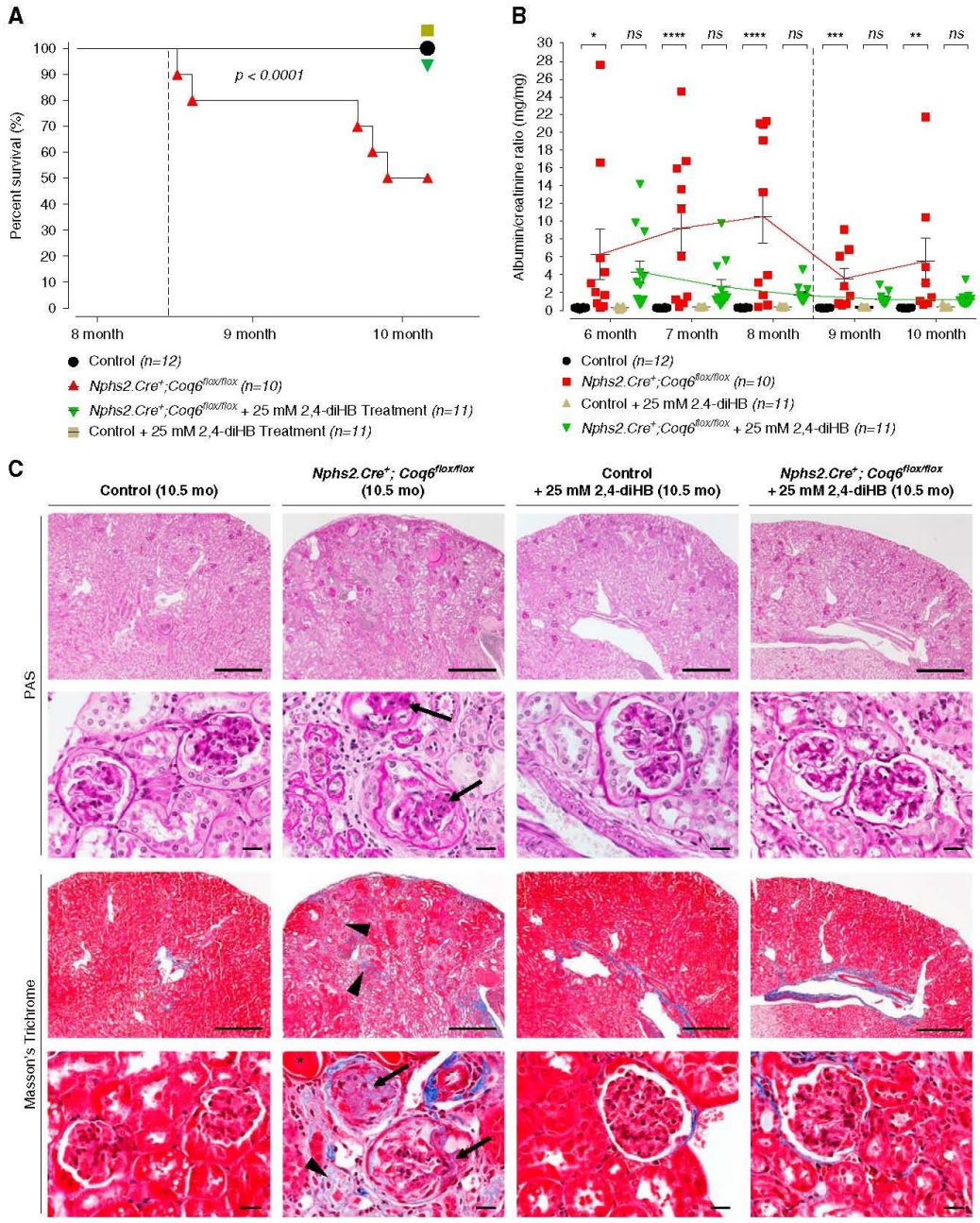

Figure 1. *Nphs2.Cre*$^{+}$*;Coq6*$^{flox/flox}$ mice develop severe progressive proteinuria and consecutive death in adulthood. Treatment with 2,4-diHB prevents disease progression, resulting in normal survival range. (A) *Nphs2.Cre*$^{+}$*;Coq6*$^{flox/flox}$ mutant mice exhibit reduced life span with a median survival of 306 days, whereas *Nphs2.Cre*$^{+}$*;Coq6*$^{flox/flox}$ mutant mice under treatment with 2,4-diHB have similar survival to healthy and healthy treated littermate controls. Dotted line displays onset of renal failure. n=10–12 animals in each group. Log-rank (Mantel–Cox) test, P<0.001. (B) Urinary albumin-to-creatinine ratio serial analysis at indicated ages and genotypes (n=10–12 animals in each group) reveals progressive proteinuria

crossing Podocin-Cre mice with $Coq6^{floxlflox}$ mice in which two *loxP* sites surround exon 6 in the *Coq6* gene. We confirmed by PCR that Podocin-Cre–dependent *Coq6* inactivation occurs only in the kidneys, and not in other organs (Supplemental Figure 1C). Successful deletion of *Coq6* expression in podocytes was confirmed by western blotting of glomerular lysates from $Coq6^{podKO}$ kidneys, where Coq6 protein levels were reduced compared with Podocin-Cre controls (Supplemental Figure 2A). Although $Coq6^{podKO}$ mice appeared grossly normal, we noticed increased morbidity (hunched posture, scruffy fur) (Supplemental Figure 3A) and increased mortality (Figure 1A) in older (>10-month-old) $Coq6^{podKO}$ mice, features that were not observed in littermate controls. Necropsy of 10-month-old $Coq6^{podKO}$ mice revealed that the mutant kidneys were pale and smaller than normal (Supplemental Figure 3B), indicating that podocyte-specific deletion of *Coq6* leads to structural and functional kidney defects in $Coq6^{podKO}$ mice.

$Coq6^{podKO}$ Mice Develop Progressive Glomerular Sclerosis and Proteinuria

To characterize the progression of kidney functional decline we followed $Coq6^{podKO}$ mice by monthly urinalysis for 10 months (Figure 1B). The first significant increase in the albumin-to-creatinine ratio (7.4-fold, $P<0.04$) in $Coq6^{podKO}$ mice was observed at 5 months of age (Supplemental Figure 2B). The onset of kidney functional decline in $Coq6^{podKO}$ mice was associated with mild focal glomerular sclerosis and occasional protein casts in the proximal tubule (Supplemental Figure 2C). Staining with Jones' methenamine silver stain did not reveal drastic alterations in the glomerular basement membrane at this stage (Supplemental Figure 2C). However, kidney histologic analysis in 10-month-old $Coq6^{podKO}$ mice using periodic acid–Schiff and Masson's trichrome staining revealed progressive and more pronounced focal glomerular sclerosis, obliteration of capillary lumens, and thickening of the basement membrane (Figure 1C). In addition, Masson's trichrome staining revealed extensive tubulointerstitial fibrosis in the mutant kidneys (Figure 1C). Interestingly, male $Coq6^{podKO}$ mice were more susceptible to proteinuria compared with female mice. The increase over time in albuminuria was up to 46.9-fold in $Coq6^{podKO}$ mice compared with littermate controls (Figure 1B).

Recently, 2,4-diHB, a metabolic intermediate of CoQ_{10}, has been successfully applied to ameliorate disparate phenotypes in mouse models caused by heterogeneous enzymatic defects in the CoQ_{10} biosynthesis pathway.[34,35] Given that renal structural abnormalities and functional decline manifest only relatively late in $Coq6^{podKO}$ mice, we decided to initiate the treatment in 5-month-old mice. Mice were randomly assigned to study groups. Administration of 2,4-diHB led to significantly increased survival of $Coq6^{podKO}$ mice compared with untreated $Coq6^{podKO}$ mice ($P<0.001$), who presented with 50% mortality by 10 months of age (Figure 1A). Decline in mortality was associated with significantly improved kidney function and normal glomerular histology in 10-month-old treated $Coq6^{podKO}$ mice (Figure 1, B and C, Supplemental Figure 4). Supplementing 2,4-diHB did not have any effect on control mouse kidney function or histology (Figure 1, B and C, Supplemental Figure 4) and ameliorated the physical condition of $Coq6^{podKO}$ mice (Supplemental Figure 3C), revealing normal appearance of kidneys in $Coq6^{podKO}$ mice after necroscopy (Supplemental Figure 3D). To characterize the glomerular phenotype in $Coq6^{podKO}$ mice we quantified the number of sclerotic glomeruli in the treated and nontreated mutant mice and found that, although nontreated $Coq6^{podKO}$ mice had significantly increased numbers of sclerotic glomeruli (93.87%), treatment with 2,4-diHB effectively mitigated the sclerotic phenotype in $Coq6^{podKO}$ (4.95%) kidneys (Figure 2).

Loss of *Coq6* Leads to Podocyte Foot Process Effacement

To characterize the architectural changes in $Coq6^{podKO}$ glomeruli at the ultrastructural level we performed TEM and SEM studies in 5-month-old and 10-month-old $Coq6^{podKO}$ kidneys. Changes in $Coq6^{podKO}$ mouse glomeruli were first observed in 5-month-old mice, with TEM revealing podocyte foot process effacement and SEM demonstrating simplified morphology of the podocytes in $Coq6^{podKO}$ glomeruli (Supplemental Figure 5, A and B). The podocyte architecture became progressively more abnormal in $Coq6^{podKO}$ kidneys by 10 months of age, characterized by lack of primary and foot processes, whereas treatment with 2,4-diHB helped to maintain the normal podocyte configuration in $Coq6^{podKO}$ glomeruli (Figures 3A and 4). To characterize the architectural changes in $Coq6^{podKO}$ glomeruli we compared the number of filtration slit units per micrometer of basement membrane in $Coq6^{podKO}$ and wild-type glomeruli. Whereas filtration slit frequency was significantly diminished in $Coq6^{podKO}$ mice, treatment with 2,4-diHB preserved the normal filtration slit

in $Nphs2.Cre^{+};Coq6^{flox/flox}$ mutant mice (red square) but not in littermate controls (black circle). $Nphs2.Cre^{+};Coq6^{flox/flox}$ mutant mice under treatment with 2,4-diHB (green triangles) are protected from developing proteinuria. Dotted line displays onset of renal failure. Note that once chronic renal failure ensues, urinary albumin excretion is reduced as is known to occur in SRNS. One-way ANOVA *P* values, calculated using Tukey's multiple comparisons test, are shown in the figure; $*P<0.05$, $**P<0.01$, $***P<0.001$, $****P<0.001$; each data point represents mean value of technical duplicates, error bars represent SEM. (C) Kidney serial sections and representative images of 10.5-month-old mice with indicated genotypes were stained according to indicated conditions. The $Nphs2.Cre^{+};Coq6^{flox/flox}$ mutant mice exhibit FSGS (arrow) with focal interstitial fibrosis, tubular atrophy (arrow heads), and proteinaceous casts in dilated tubules (asterisks). In contrast, wild-type littermate control mice and $Nphs2.Cre^{+};Coq6^{flox/flox}$ mutant mice under treatment with 2,4-diHB display normal histologic kidney morphology. Scale bars, upper rows 500 μm and lower rows 20 μm. PAS, periodic acid–Schiff.

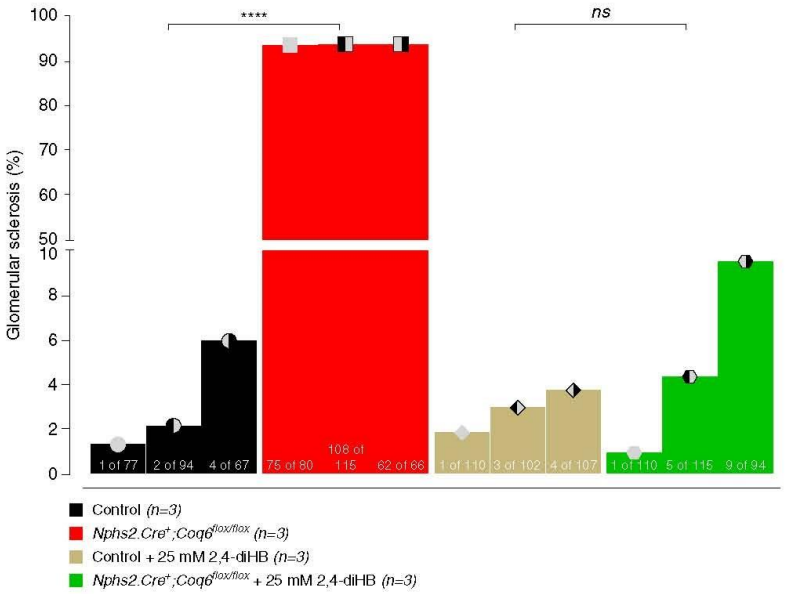

Figure 2. Development of FSGS is abrogated by treatment with 2,4-diHB in *Nphs2.Cre*$^{+}$;*Coq6*$^{flox/flox}$ mutant mice. Kidney serial sections of 10.5-month-old mice with indicated genotypes were stained with Masson's trichrome and analyzed to determine the severity of glomerular sclerosis. The *Nphs2.Cre*$^{+}$;*Coq6*$^{flox/flox}$ mutant mice show FSGS, whereas *Nphs2.Cre*$^{+}$;*Coq6*$^{flox/flox}$ mutant mice under treatment with 2,4-diHB displayed virtually no (<10% of glomeruli) abnormal histologic findings (n=3 animals in each group; each graph bar indicates an single animal, numbers inside the bar graphs indicate number of sclerosed glomeruli per total glomeruli counted in one section. Two-way ANOVA P values calculated using Tukey's multiple comparisons test are shown in the figure. ****P<0.001.

morphology in *Coq6*^{podKO} glomeruli (Figure 3B). Overall, the glomerular phenotype of podocyte-specific loss of *Coq6* recapitulates the human pathology of FSGS of COQ6-deficient individuals.[21]

Abrogation of *Coq6* Expression Leads to Podocytopathy

To characterize the molecular abnormalities in *Coq6*^{podKO} glomeruli, we next analyzed the expression patterns of the slit diaphragm proteins nephrin and podocin, the basement membrane marker nidogen, and the primary process marker synaptopodin by confocal microscopy in 10.5-month-old kidneys (Figure 5). A staining pattern for various podocyte markers was significantly reduced in *Coq6*^{podKO} glomeruli (Figure 5, A and C, Supplemental Figure 6), whereas the basement membrane marker nidogen showed a wider expression than normal, demonstrating that *Coq6* function is required for podocyte maintenance and homeostasis. Because glomerular sclerosis is associated with increased expression of fibrotic markers, we next analyzed the expression of fibrotic markers αSMA, collagen IV, and Desmin in *Coq6*^{podKO} kidneys by confocal microscopy. Indeed, *Coq6*^{podKO} kidneys had significantly increased expression of αSMA, Desmin, and collagen IV in the glomeruli, characteristic of mesangial fibrosis (Supplemental Figures 7–9). We also studied the expression of WT1, a podocyte-specific transcription factor, which is critical for maintaining podocyte differentiation and maturation.[36,37] In contrast to control glomeruli, the number of WT1^{+} podocytes was reduced in *Coq6*^{podKO} glomeruli, suggesting that loss of Coq6 expression either leads to progressive depletion of podocytes (Supplemental Figure 10) or causes their dedifferentiation. Together, our data show that treatment of *Coq6*^{podKO} mice with 2,4-diHB protects from disease progression and ameliorates the outcome regarding renal histology.

Mitochondrial Deficiency Underlies the Glomerular Abnormalities in *Coq6*^{podKO} Mice

Although Coq6 function is associated with the mitochondrial CoQ_{10} biosynthesis pathway, the subcellular localization of Coq6 has remained controversial.[21] Using cellular fractionation of HEK293 and human podocyte cell lysates, we now demonstrate that endogenous Coq6 localizes to the mitochondria (Figure 6, A and B). Consistent with Coq6's localization and function in the mitochondria, the podocytes in *Coq6*^{podKO} glomeruli appeared to contain abnormal mitochondria (characterized by hyperproliferation and increased size), presumably to compensate for defective energy metabolism (Figure 6C, Supplemental Figure 11).

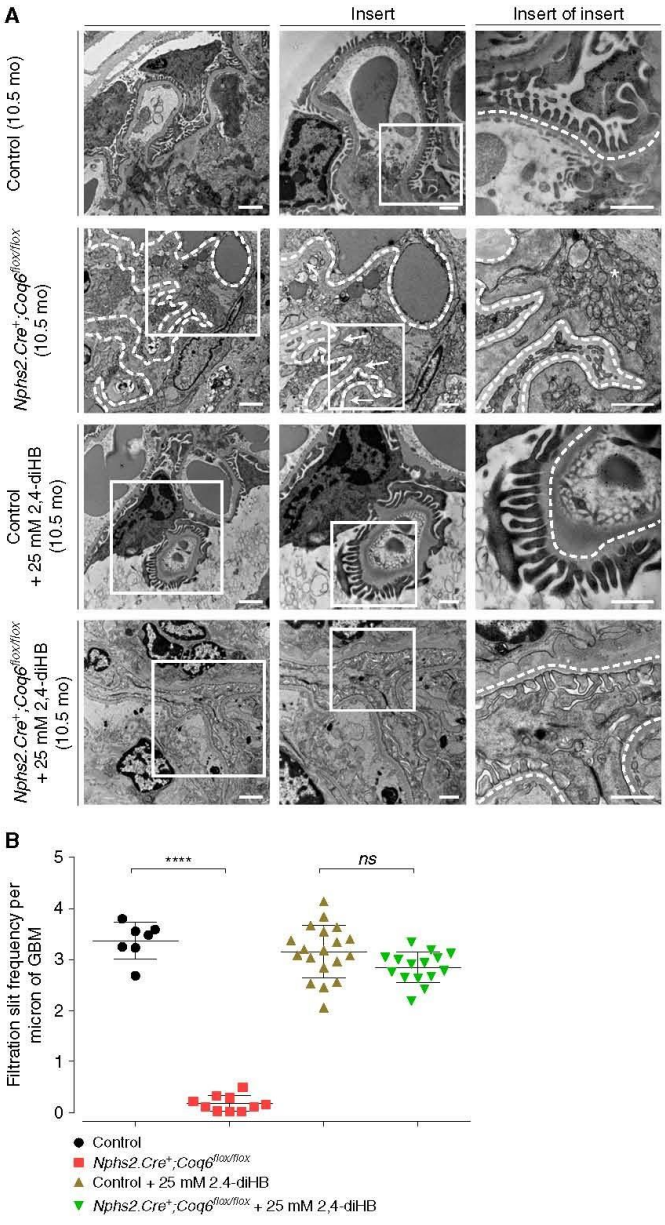

Figure 3. Glomerular structure is disrupted in *Nphs2.Cre*$^{+}$;*Coq6*$^{flox/flox}$ mutant mice and is preserved by 2,4-diHB treatment. (A) TEM representative images at age 10.5 months. *Nphs2.Cre*$^{+}$;*Coq6*$^{flox/flox}$ mutant mice reveal podocyte foot process effacement (arrows) and an increased number of mitochondria (asterisks). Glomerular basement membrane is highlighted by a dotted line. In contrast, *Nphs2.Cre*$^{+}$;*Coq6*$^{flox/flox}$ mutant 2,4-diHB–treated mice display normal foot process morphology. Scale bars, 2 μm left panel, 1 μm middle and right panels. (B) TEM images of 10.5-month-old mice with indicated genotypes (see A) were analyzed to determine the severity of podocyte foot process effacement. The *Nphs2.Cre*$^{+}$;*Coq6*$^{flox/flox}$ mutant mice show significantly reduced frequency of filtration slits per micron of glomerular basement membrane, whereas *Nphs2.Cre*$^{+}$;*Coq6*$^{flox/flox}$ mutant mice under treatment with 2,4-diHB display normal ultrastructural findings compared with littermate controls under treatment. n=2 animals in each group; two glomeruli per animal were analyzed. One-way ANOVA P values calculated using Tukey's multiple comparisons test are shown in the figure. ****P<0.001; error bars represent mean± SD. GBM, glomerular basement membrane.

To further characterize the role of COQ6 in podocyte function, we employed *COQ6* knockdown human podocytes in a cellular migration assay that we recently established to identify compounds that modulate podocyte mobility.[38] Using transient, siRNA-based *COQ6* knockdown in human podocytes (Supplemental Figure 12), we observed reduced migration rate in *COQ6*-depleted cells compared with control podocytes (Supplemental Figure 12B), emphasizing the role of COQ6 in normal podocyte function. Supplementing 2,4-diHB to the culture medium mitigated the migration defect (Supplemental Figure 12B). Having shown that the defect in podocyte migration rate is a functional and specific readout of *COQ6* deficiency, we decided to use this cellular model to test the effects of two other 4-dihydroxybenzoic acid (4-HB) analogs, 4-Hydroxy-3-methoxybenzoic acid (vanillic acid) and 3,4-Dihydroxybenzoic acid (3,4-diHB), in rescuing *COQ6* deficiency. Similar to 2,4-diHB, these compounds are all highly similar to 4-HB, a precursor molecule of CoQ_{10} biosynthesis. Previously, it has been demonstrated that treatment with vanillic acid or 3,4-diHB improved the biosynthesis of COQ6 in a yeast model.[39,40] Indeed, using vanillic acid we saw a partial reversal of the migratory defect in *COQ6* knockdown cells (Supplemental Figure 12C); however, treatment with 3,4-diHB showed no positive effect to the *siCOQ6* podocyte migration phenotype (Supplemental Figure 12D). Together, these data demonstrate that loss of COQ6 function in podocytes can be partially reversed by vanillic acid and fully reversed by 2,4-diHB of the tested

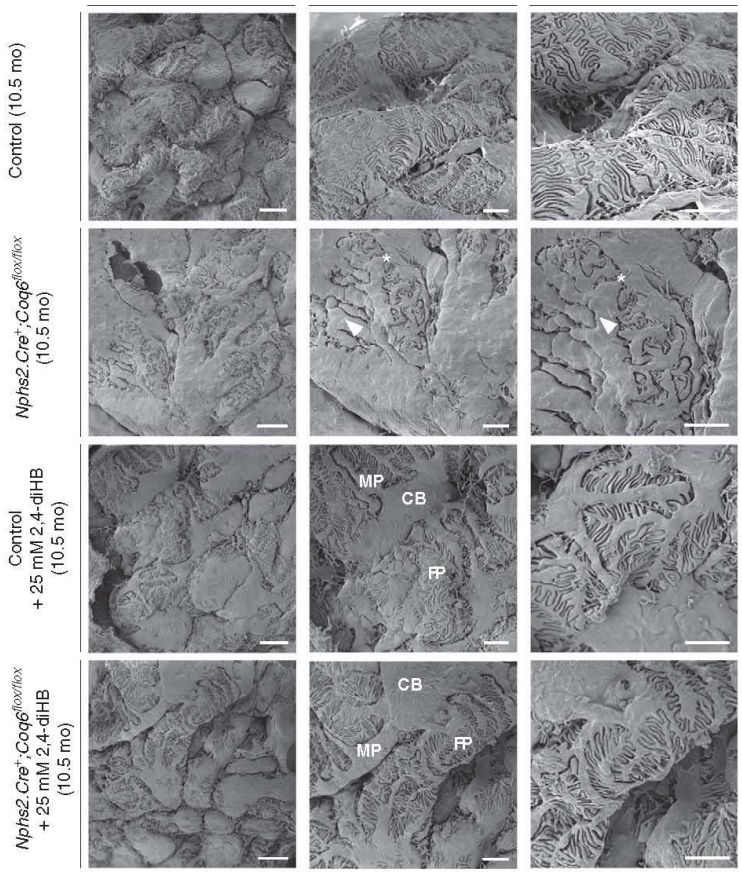

Figure 4. Severely impaired podocyte foot process (FP) structure of *Nphs2.Cre*$^{+}$;*Coq6*$^{flox/flox}$ mutant mice can be preserved by 2,4-diHB administration. SEM representative images in 10.5-month-old mice. *Nphs2.Cre*$^{+}$;*Coq6*$^{flox/flox}$ mutant mice reveal severely impaired podocytic morphology with coarsened cell bodies (CBs) and major processes (MPs; arrow heads) as well as effaced FPs (asterisks). In contrast, *Nphs2.Cre*$^{+}$;*Coq6*$^{flox/flox}$ mutant mice under treatment with 2,4-diHB display normal three-dimensional podocyte morphology, slightly enlarged MPs, and FPs retaining their normal morphology. Scale bars, 4 μm left panel, 2 μm middle and right panels.

CoQ_{10} intermediate precursors, at least under *in vitro* conditions.

DISCUSSION

The CoQ_{10} biosynthesis pathway is thought to consist of sequential enzymatic steps.[41] Moreover, studies in yeast have demonstrated that CoQ biosynthesis pathway enzymes assemble into a high molecular mass protein complexes, whose stability is dependent on the presence of individual peptides.[42,43]

There is a wide spectrum of clinical symptoms, including neurologic disorders, myopathy, and SRNS, in patients caused by deficiency of CoQ_{10} in consequence of mutations in a variety of genes involved in the CoQ_{10} biosynthesis process.[18,20–23,29,44–50] On the basis of these data, it is very important to accurately identify these treatable patients as early as possible.

Several recent *in vitro* and *in vivo* studies, including ours, have demonstrated the beneficial effect of CoQ_{10} in improving the outcome of primary mitochondrial diseases due to CoQ_{10} deficiency.[51,52] Because CoQ_{10} requires high-dose use and is not water soluble, limiting its use in cell culture systems, we decided to examine the effect of its more soluble and hydrophilic 4-HB analogs—2,4-diHB, 3,4-diHB, and vanillic acid—on podocyte function.

There are controversial data in the literature regarding the efficacy of using oral CoQ_{10} in patients with primary CoQ_{10}

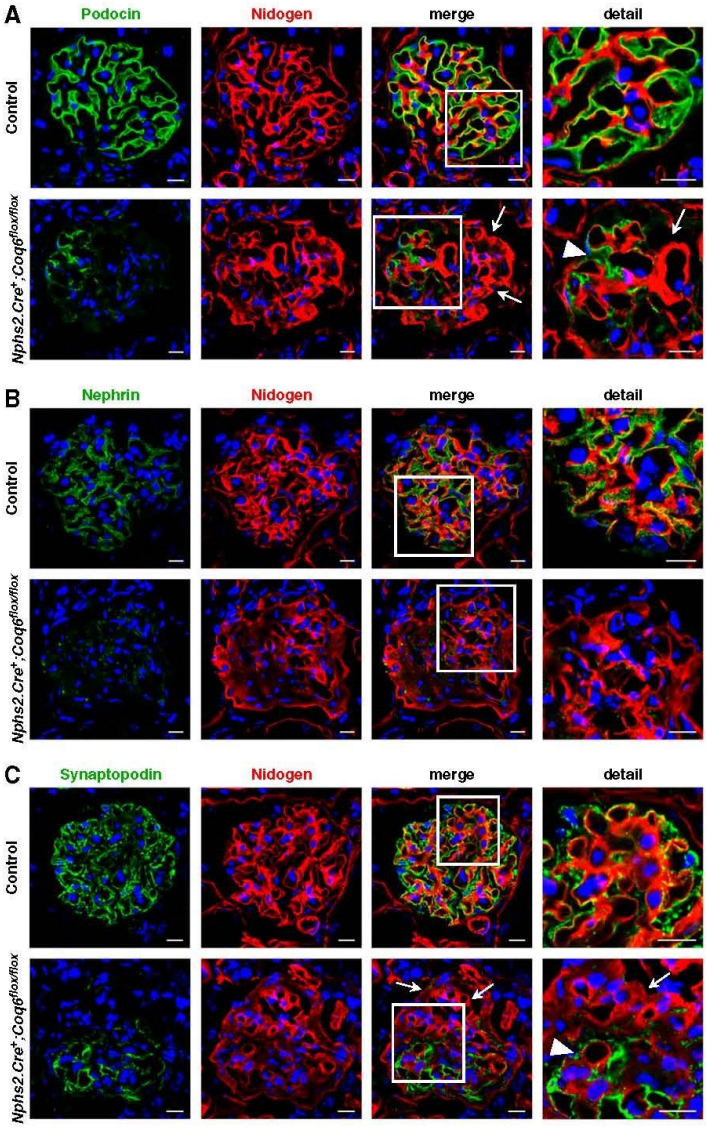

Figure 5. *Nphs2.Cre*$^{+}$*;Coq6*$^{flox/flox}$ mutant mice show reduced expression of podocyte-specific proteins. (A and B) Immunofluorescence staining of frozen kidney sections and representative images in 10.5-month-old mice for the slit diaphragm proteins (green) (A) podocin and (B) nephrin and the basement membrane marker nidogen (red). A normal expression pattern of podocin and nephrin is seen in wild-type littermate control mice. *Nphs2.Cre*$^{+}$*;Coq6*$^{flox/flox}$ mutant mice show (A) reduced podocin staining (arrows) appearing only on a few capillary loops (arrow head), whereas (B) nephrin expression is globally reduced. Scale bars, 10 μm. (C) Staining of frozen kidney sections and representative images in 10.5-month-old mice for the podocytic foot process marker synaptopodin (green) and the basement membrane marker nidogen (red). A normal expression pattern of synaptopodin is seen in wild-type littermate control mice. *Nphs2.Cre*$^{+}$*;Coq6*$^{flox/flox}$ mutant mice show reduced synaptopodin (green) staining (arrows) with a signal appearing only on a few capillary loops (arrow head). Scale bars, 10 μm.

mitochondriopathy, likely stemming from CoQ_{10} tissue-specific bioavailability, its limited delivery to mitochondria, and gene-specific mutations. For example, previous studies have demonstrated the beneficial effect of oral CoQ_{10} for neural improvements, and in some cases partially for renal dysfunction.[19,53,54] After we had demonstrated the beneficial effect of CoQ_{10} precursor compounds for podocyte functional improvement by migration assay we decided to investigate whether the compounds can attenuate proteinuria in *Coq6*^{podKO} mice. On the basis of our data and data in the literature we selected 2,4-diHB to answer this question.[55]

Coq6^{podKO} mice appeared to be normal in development and body condition. Upon the onset of significant proteinuria at age 5 months, *Coq6*^{podKO} mice appeared to deteriorate gradually and became moribund at 10 months of age with advanced decline of renal function. Histologic analysis of 10-month-old *Coq6*^{podKO} mice revealed progressive FSGS associated with simplified morphology of podocytes and foot process effacement. Immunofluorescence studies showed decreased expression of podocyte markers and increased expression of fibrotic markers. *Coq6*^{podKO} mice treated with 2,4-diHB were protected from disease progression, and survival, proteinuria, and renal histology improved dramatically. Studies in cultured human podocytes with transient knockdown of *COQ6* showed reduction in podocyte migration rate that could be completely reversed to control levels by treating the podocytes with 2,4-diHB.

Together, our data demonstrate that 2,4-diHB, an analog of 4-HB that functions to bypass certain deficiencies of the CoQ_{10} biosynthesis pathway, efficiently ameliorates proteinuria and prevents FSGS in *Coq6*^{podKO} mice. There was a sex-specific susceptibility to proteinuria in *Coq6*^{podKO} mice, with female mice being more resistant, and male mice more susceptible to proteinuria after deletion of *Coq6*. The

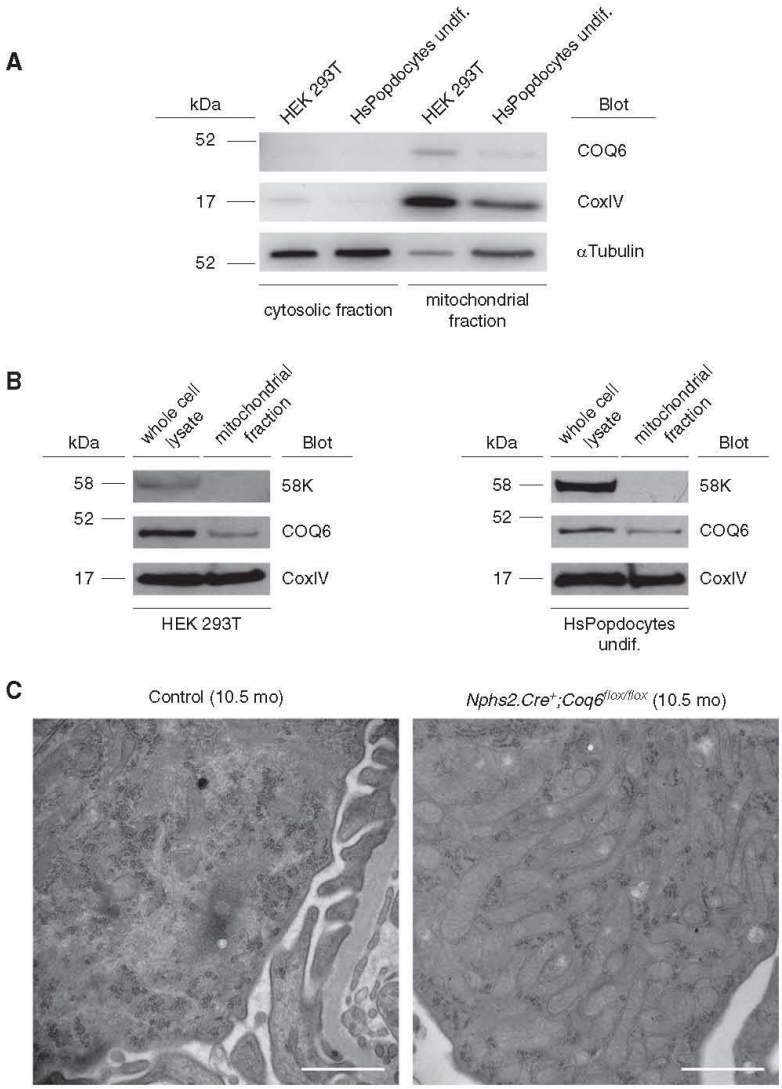

Figure 6. COQ6 localizes to mitochondria and its loss from glomerular podocytes causes mitochondrial intumescence. (A) Subcellular fractions of wild-type HEK293T cell line and of wild-type undifferentiated human podocyte cell line were subjected to western blot analysis. COQ6 was detected in both cell lines, predominantly in the mitochondrial fraction. CoxIV and α-Tubulin were used as markers for mitochondrial and cytosolic subcellular fractions, respectively. Representative image of two independent experiments. (B) Mitochondrial fraction does not contain Golgi complex proteins. Whole cell lysates and the mitochondrial fraction from HEK293T and human podocytes were analyzed using antibodies against the Golgi complex protein 58K, mitochondrial protein CoxIV, and COQ6. 58K was not detected in the mitochondrial fraction, confirming that COQ6 is a mitochondrial protein. (C) TEM of podocytes in 10.5-month-old mice. Compared with the number and morphology of mitochondria in wild-type podocytes, the mitochondria in *Nphs2.Cre*$^{+}$;*Coq6*$^{flox/flox}$ podocytes are enlarged and increased in number indicating impairment of mitochondrial function. Scale bars, 1 μm. Undif, undifferentiated.

reason for this is unclear. However, several aspects of *siCOQ6* podocyte physiology were rescued with 4-HB analogs, with 2,4-diHB having the most robust effect. It is surprising that 2,4-diHB was most effective in the $Coq6^{podKO}$ mice, because this 4-HB analog was originally shown to restore CoQ biosynthesis in a *coq7* yeast mutant and is designed to bypass the final hydroxylation step in CoQ biosynthesis.[56]

In conclusion, we report that 2,4-diHB administration markedly improves proteinuria and podocyte morphology in our $Coq6^{podKO}$ model of SRNS caused by primary mitochondrial dysfunction. This effect is elicited without the risk of adverse effects, because several "hydroxybenzoic acid compounds" and especially 2,4-diHB are FDA- (EAF 3045, CAS RN 89–86–1) and EFSA- (Ref. no. 00910) approved food additives. In addition, 2,4-diHB is widely present as a by-product of food processing in a variety of food products, such as snack foods, beverages, and fish products, as well as being used as an additive in some drugs, *e.g.*, Nicardipine (NDC: 0143–9542–01). Moreover, animal studies revealed high safety of use for 2,4-diHB with LD_{50} of >800 mg/kg body wt,[57] and there is one case report of 2,4-diHB administration to a patient with rheumatic fever in a dose of up to 6 g per day without observation of any severe side effects of treatment.[58] Because of the apparent safety in preclinical and clinical use, it is very likely that patients would very well tolerate treatment with 2,4-diHB. The translational relevance of this discovery is heightened by the feasibility of therapeutic delivery. Translational studies are warranted to determine whether this type of strategy may be used to promote proteinuria remission. It would be useful to perform animal studies with a human mutation using a knock-in strategy. Growing evidence suggests that impaired mitochondrial function causes podocyte damage and leads to proteinuria. Given the present lack of effective therapies of this disease entity and the apparent safety of CoQ_{10}, clinical trials of these compounds in genetically identified cases of SRNS seem appropriate.

ACKNOWLEDGMENTS

The authors thank Maria Ericsson, Louis Trakimas, Elizabeth Benecchi, and Peg Coughlin from the Electron Microscope Core Facility, Harvard Medical School, for excellent transmission electron microscopy services. We also thank Evelyn Flynn for her outstanding technical assistance and Eliso Nudelman for providing mouse cartoon illustrations. This work was performed in part at the Center for Nanoscale Systems (CNS), a member of the National Nanotechnology Coordinated Infrastructure Network, which is supported by the National Science Foundation (NSF) under NSF award no. 1541959. CNS is part of Harvard University.

This study was supported by National Institutes of Health grants to F.H. (DK076683) and R.A. (R00DK099434 and RO1DK115403), and by the National Science Foundation Grant MCB-1330803 (to C.F.C.). F.H. is the William E. Harmon Professor. E.W. is supported by the Leopoldina Fellowship Program, German National Academy of Sciences Leopoldina (LPDS 2015-07)

E.W., M.A., H.H., D.S., J.W., C.C.G., R.S., J.C., and M.S. carried out the animal experiments. E.W., M.A., A.M.A., A.N., C.F.C., and R.A. carried out the cell experiments. E.W., R.A., and F.H. conceived of and directed the project. E.W. and R.A. wrote the paper with help from F.H. The manuscript was critically reviewed by all of the authors.

DISCLOSURES

F.H. is a cofounder of Goldfinch-Bio. No other authors have competing financial interests.

SUPPLEMENTAL MATERIAL

This article contains the following supplemental material online at http://jasn.asnjournals.org/lookup/suppl/doi:10.1681/ASN.2018060625/-/DCSupplemental.

Supplemental Figure 1. Generation and genotyping strategy for $Nphs2.Cre^{+};Coq6^{flox/flox}$ mouse model.

Supplemental Figure 2. At 5 months of age $Nphs2.Cre^{+};Coq6^{flox/flox}$ mice exhibit proteinuria and renal histopathologic changes consistent with FSGS.

Supplemental Figure 3. *Coq6* knockout in $Nphs2.Cre^{+};Coq6^{flox/flox}$ mutant mice leads to reduced physical condition and macroscopic morphologic changes of kidneys.

Supplemental Figure 4. *Coq6* knockout in $Nphs2.Cre^{+};Coq6^{flox/flox}$ mutant mice causes FSGS. Treatment with 2.4-diHB prevents disease progression, resulting in normal histologic findings.

Supplemental Figure 5. Electron microscopy reveals podocyte foot process effacement in $Nphs2.Cre^{+};Coq6^{flox/flox}$ mutant mice at 5 months of age.

Supplemental Figure 6. Quantitative analysis of the expression of podocyte-specific proteins in $Nphs2.Cre^{+};Coq6^{flox/flox}$ glomeruli.

Supplemental Figure 7. $Nphs2.Cre^{+};Coq6^{flox/flox}$ mice show increased glomerular fibrosis and staining for mesangial markers.

Supplemental Figure 8. Quantitative analysis of the expression of the fibrotic markers αSMA and Desmin in $Nphs2.Cre^{+};Coq6^{flox/flox}$ glomeruli.

Supplemental Figure 9. $Nphs2.Cre^{+};Coq6^{flox/flox}$ mice develop renal fibrosis.

Supplemental Figure 10. $Nphs2.Cre^{+};Coq6^{flox/flox}$ mice show a reduced staining of podocyte-specific markers.

Supplemental Figure 11. Deletion of Coq6 leads to morphologic abnormalities in podocyte mitochondria.

Supplemental Figure 12. *COQ6* siRNA-mediated transient knockdown reduces podocyte migration rate of cultured human podocytes with full rescue by 2,4-diHB, partial rescue by vanillic acid, and absent rescue by 3,4-diHB.

REFERENCES

1. Smith JM, Stablein DM, Munoz R, Hebert D, McDonald RA: Contributions of the transplant registry: The 2006 annual report of the North American pediatric Renal Trials and collaborative Studies (NAPRTCS). *Pediatr Transplant* 11: 366–373, 2007

2. Lovric S, Ashraf S, Tan W, Hildebrandt F: Genetic testing in steroid-resistant nephrotic syndrome: When and how? *Nephrol Dial Transplant* 31: 1802–1813, 2016
3. Kim JS, Bellew CA, Silverstein DM, Aviles DH, Boineau FG, Vehaskari VM: High incidence of initial and late steroid resistance in childhood nephrotic syndrome. *Kidney Int* 68: 1275–1281, 2005
4. Benoit G, Machuca E, Antignac C: Hereditary nephrotic syndrome: A systematic approach for genetic testing and a review of associated podocyte gene mutations. *Pediatr Nephrol* 25: 1621–1632, 2010
5. Trautmann A, Bodria M, Ozaltin F, Gheisari A, Melk A, Azocar M, et al.: PodoNet Consortium: Spectrum of steroid-resistant and congenital nephrotic syndrome in children: The PodoNet registry cohort. *Clin J Am Soc Nephrol* 10: 592–600, 2015
6. Vivante A, Hildebrandt F: Exploring the genetic basis of early-onset chronic kidney disease. *Nat Rev Nephrol* 12: 133–146, 2016
7. Somlo S, Mundel P: Getting a foothold in nephrotic syndrome. *Nat Genet* 24: 333–335, 2000
8. Zenker M, Machuca E, Antignac C: Genetics of nephrotic syndrome: New insights into molecules acting at the glomerular filtration barrier. *J Mol Med (Berl)* 87: 849–857, 2009
9. Imasawa T, Rossignol R: Podocyte energy metabolism and glomerular diseases. *Int J Biochem Cell Biol* 45: 2109–2118, 2013
10. Abe Y, Sakairi T, Kajiyama H, Shrivastav S, Beeson C, Kopp JB: Bioenergetic characterization of mouse podocytes. *Am J Physiol Cell Physiol* 299: C464–C476, 2010
11. Mele C, Iatropoulos P, Donadelli R, Calabria A, Maranta R, Cassis P, et al.: PodoNet Consortium: MYO1E mutations and childhood familial focal segmental glomerulosclerosis. *N Engl J Med* 365: 295–306, 2011
12. Brown EJ, Schlöndorff JS, Becker DJ, Tsukaguchi H, Tonna SJ, Uscinski AL, et al.: Mutations in the formin gene INF2 cause focal segmental glomerulosclerosis. *Nat Genet* 42: 72–76, 2010
13. Kaplan JM, Kim SH, North KN, Rennke H, Correia LA, Tong HQ, et al.: Mutations in ACTN4, encoding alpha-actinin-4, cause familial focal segmental glomerulosclerosis. *Nat Genet* 24: 251–256, 2000
14. Heath KE, Campos-Barros A, Toren A, Rozenfeld-Granot G, Carlsson LE, Savige J, et al.: Nonmuscle myosin heavy chain IIA mutations define a spectrum of autosomal dominant macrothrombocytopenias: May-Hegglin anomaly and Fechtner, Sebastian, Epstein, and Alport-like syndromes. *Am J Hum Genet* 69: 1033–1045, 2001
15. Zenker M, Aigner T, Wendler O, Tralau T, Müntefering H, Fenski R, et al.: Human laminin beta2 deficiency causes congenital nephrosis with mesangial sclerosis and distinct eye abnormalities. *Hum Mol Genet* 13: 2625–2632, 2004
16. Has C, Spartà G, Kiritsi D, Weibel L, Moeller A, Vega-Warner V, et al.: Integrin α3 mutations with kidney, lung, and skin disease. *N Engl J Med* 366: 1508–1514, 2012
17. Kambham N, Tanji N, Seigle RL, Markowitz GS, Pulkkinen L, Uitto J, et al.: Congenital focal segmental glomerulosclerosis associated with beta4 integrin mutation and epidermolysis bullosa. *Am J Kidney Dis* 36: 190–196, 2000
18. Rötig A, Appelkvist EL, Geromel V, Chretien D, Kadhom N, Edery P, et al.: Quinone-responsive multiple respiratory-chain dysfunction due to widespread coenzyme Q10 deficiency. *Lancet* 356: 391–395, 2000
19. Salviati L, Sacconi S, Murer L, Zacchello G, Franceschini L, Laverda AM, et al.: Infantile encephalomyopathy and nephropathy with CoQ10 deficiency: A CoQ10-responsive condition. *Neurology* 65: 606–608, 2005
20. Quinzii C, Naini A, Salviati L, Trevisson E, Navas P, Dimauro S, et al.: A mutation in para-hydroxybenzoate-polyprenyl transferase (COQ2) causes primary coenzyme Q10 deficiency. *Am J Hum Genet* 78: 345–349, 2006
21. Heeringa SF, Chernin G, Chaki M, Zhou W, Sloan AJ, Ji Z, et al.: COQ6 mutations in human patients produce nephrotic syndrome with sensorineural deafness. *J Clin Invest* 121: 2013–2024, 2011
22. Diomedi-Camassei F, Di Giandomenico S, Santorelli FM, Caridi G, Piemonte F, Montini G, et al.: COQ2 nephropathy: A newly described inherited mitochondriopathy with primary renal involvement. *J Am Soc Nephrol* 18: 2773–2780, 2007
23. Ashraf S, Gee HY, Woerner S, Xie LX, Vega-Warner V, Lovric S, et al.: ADCK4 mutations promote steroid-resistant nephrotic syndrome through CoQ10 biosynthesis disruption. *J Clin Invest* 123: 5179–5189, 2013
24. Peng M, Falk MJ, Haase VH, King R, Polyak E, Selak M, et al.: Primary coenzyme Q deficiency in Pdss2 mutant mice causes isolated renal disease. *PLoS Genet* 4: e1000061, 2008
25. Ernster L, Dallner G: Biochemical, physiological and medical aspects of ubiquinone function. *Biochim Biophys Acta* 1271: 195–204, 1995
26. Lenaz G, Genova ML: Mobility and function of coenzyme Q (ubiquinone) in the mitochondrial respiratory chain. *Biochim Biophys Acta* 1787: 563–573, 2009
27. Quinzii CM, López LC, Gilkerson RW, Dorado B, Coku J, Naini AB, et al.: Reactive oxygen species, oxidative stress, and cell death correlate with level of CoQ10 deficiency. *FASEB J* 24: 3733–3743, 2010
28. Bentinger M, Brismar K, Dallner G: The antioxidant role of coenzyme Q. *Mitochondrion* 7[Suppl]: S41–S50, 2007
29. López LC, Schuelke M, Quinzii CM, Kanki T, Rodenburg RJ, Naini A, et al.: Leigh syndrome with nephropathy and CoQ10 deficiency due to decaprenyl diphosphate synthase subunit 2 (PDSS2) mutations. *Am J Hum Genet* 79: 1125–1129, 2006
30. Moeller MJ, Sanden SK, Soofi A, Wiggins RC, Holzman LB: Podocyte-specific expression of cre recombinase in transgenic mice. *Genesis* 35: 39–42, 2003
31. Takemoto M, Asker N, Gerhardt H, Lundkvist A, Johansson BR, Saito Y, et al.: A new method for large scale isolation of kidney glomeruli from mice. *Am J Pathol* 161: 799–805, 2002
32. Saleem MA, O'Hare MJ, Reiser J, Coward RJ, Inward CD, Farren T, et al.: A conditionally immortalized human podocyte cell line demonstrating nephrin and podocin expression. *J Am Soc Nephrol* 13: 630–638, 2002
33. Gee HY, Saisawat P, Ashraf S, Hurd TW, Vega-Warner V, Fang H, et al.: ARHGDIA mutations cause nephrotic syndrome via defective RHO GTPase signaling. *J Clin Invest* 123: 3243–3253, 2013
34. Luna-Sánchez M, Díaz-Casado E, Barca E, Tejada MA, Montilla-García Á, Cobos EJ, et al.: The clinical heterogeneity of coenzyme Q10 deficiency results from genotypic differences in the Coq9 gene. *EMBO Mol Med* 7: 670–687, 2015
35. Wang Y, Oxer D, Hekimi S: Mitochondrial function and lifespan of mice with controlled ubiquinone biosynthesis. *Nat Commun* 6: 6393, 2015
36. Mundlos S, Pelletier J, Darveau A, Bachmann M, Winterpacht A, Zabel B: Nuclear localization of the protein encoded by the Wilms' tumor-gene WT1 in embryonic and adult tissues. *Development* 119: 1329–1341, 1993
37. Kreidberg JA, Sariola H, Loring JM, Maeda M, Pelletier J, Housman D, et al.: WT-1 is required for early kidney development. *Cell* 74: 679–691, 1993
38. Widmeier E, Tan W, Airik M, Hildebrandt F: A small molecule screening to detect potential therapeutic targets in human podocytes. *Am J Physiol Renal Physiol* 312: F157–F171, 2017
39. Doimo M, Trevisson E, Airik R, Bergdoll M, Santos-Ocaña C, Hildebrandt F, et al.: Effect of vanillic acid on COQ6 mutants identified in patients with coenzyme Q10 deficiency. *Biochim Biophys Acta* 1842: 1–6, 2014
40. Ozeir M, Mühlenhoff U, Webert H, Lill R, Fontecave M, Pierrel F: Coenzyme Q biosynthesis: Coq6 is required for the C5-hydroxylation reaction and substrate analogs rescue Coq6 deficiency. *Chem Biol* 18: 1134–1142, 2011
41. Yen HC, Liu YC, Kan CC, Wei HJ, Lee SH, Wei YH, et al.: Disruption of the human COQ5-containing protein complex is associated with diminished coenzyme Q10 levels under two different conditions of mitochondrial energy deficiency. *Biochim Biophys Acta* 1860: 1864–1876, 2016

42. Tran UC, Clarke CF: Endogenous synthesis of coenzyme Q in eukaryotes. *Mitochondrion* 7[Suppl]: S62–S71, 2007
43. Hsieh EJ, Gin P, Gulmezian M, Tran UC, Saiki R, Marbois BN, et al.: *Saccharomyces cerevisiae* Coq9 polypeptide is a subunit of the mitochondrial coenzyme Q biosynthetic complex. *Arch Biochem Biophys* 463: 19–26, 2007
44. Wang Y, Hekimi S: Molecular genetics of ubiquinone biosynthesis in animals. *Crit Rev Biochem Mol Biol* 48: 69–88, 2013
45. Salviati L, Trevisson E, Rodriguez Hernandez MA, Casarin A, Pertegato V, Doimo M, et al.: Haploinsufficiency of COQ4 causes coenzyme Q10 deficiency. *J Med Genet* 49: 187–191, 2012
46. Mollet J, Giurgea I, Schlemmer D, Dallner G, Chretien D, Delahodde A, et al.: Prenyldiphosphate synthase, subunit 1 (PDSS1) and OH-benzoate polyprenyltransferase (COQ2) mutations in ubiquinone deficiency and oxidative phosphorylation disorders. *J Clin Invest* 117: 765–772, 2007
47. Mollet J, Delahodde A, Serre V, Chretien D, Schlemmer D, Lombes A, et al.: CABC1 gene mutations cause ubiquinone deficiency with cerebellar ataxia and seizures. *Am J Hum Genet* 82: 623–630, 2008
48. Lagier-Tourenne C, Tazir M, López LC, Quinzii CM, Assoum M, Drouot N, et al.: ADCK3, an ancestral kinase, is mutated in a form of recessive ataxia associated with coenzyme Q10 deficiency. *Am J Hum Genet* 82: 661–672, 2008
49. Duncan AJ, Bitner-Glindzicz M, Meunier B, Costello H, Hargreaves IP, López LC, et al.: A nonsense mutation in COQ9 causes autosomal-recessive neonatal-onset primary coenzyme Q10 deficiency: A potentially treatable form of mitochondrial disease. *Am J Hum Genet* 84: 558–566, 2009
50. Hirano M, Garone C, Quinzii CM: CoQ(10) deficiencies and MNGIE: Two treatable mitochondrial disorders. *Biochim Biophys Acta* 1820: 625–631, 2012
51. Saiki R, Lunceford AL, Shi Y, Marbois B, King R, Pachuski J, et al.: Coenzyme Q10 supplementation rescues renal disease in Pdss2kd/kd mice with mutations in prenyl diphosphate synthase subunit 2. *Am J Physiol Renal Physiol* 295: F1535–F1544, 2008
52. Vazquez Fonseca L, Doimo M, Calderan C, Desbats MA, Acosta MJ, Cerqua C, et al.: Mutations in COQ8B (ADCK4) found in patients with steroid-resistant nephrotic syndrome alter COQ8B function. *Hum Mutat* 39: 406–414, 2018
53. Montini G, Malaventura C, Salviati L: Early coenzyme Q10 supplementation in primary coenzyme Q10 deficiency. *N Engl J Med* 358: 2849–2850, 2008
54. Atmaca M, Gulhan B, Korkmaz E, Inozu M, Soylemezoglu O, Candan C, et al.: Follow-up results of patients with ADCK4 mutations and the efficacy of CoQ10 treatment. *Pediatr Nephrol* 32: 1369–1375, 2017
55. Freyer C, Stranneheim H, Naess K, Mourier A, Felser A, Maffezzini C, et al.: Rescue of primary ubiquinone deficiency due to a novel COQ7 defect using 2,4-dihydroxybensoic acid. *J Med Genet* 52: 779–783, 2015
56. Xie LX, Ozeir M, Tang JY, Chen JY, Jaquinod SK, Fontecave M, et al: Overexpression of the Coq8 kinase in *Saccharomyces cerevisiae* coq null mutants allows for accumulation of diagnostic intermediates of the coenzyme Q6 biosynthetic pathway. *J Biol Chem* 287: 23571–23581, 2012
57. Grady RW, Graziano JH, Akers HA, Cerami A: The development of new iron-chelating drugs. *J Pharmacol Exp Ther* 196: 478–485, 1976
58. Clarke NE, Clarke CN, Mosher RE: Phenolic compounds in chemotherapy of rheumatic fever. *Am J Med Sci* 235: 7–22, 1958

AFFILIATIONS

[1]Division of Nephrology, Boston Children's Hospital, Harvard Medical School, Boston, Massachusetts; [2]Department of Medicine IV, Medical Center–University of Freiburg, Faculty of Medicine, University of Freiburg, Freiburg, Germany; [3]Department of Pediatrics, University of Pittsburgh, Pittsburgh, Pennsylvania; and [4]Department of Chemistry and Biochemistry and Molecular Biology Institute, University of California, Los Angeles, Los Angeles, California